COLLECTED PAPERS on
Dressed Photon Science and Technology

Vol. 32

January 2017 – December 2017

Prof. Emeritus
Motoichi OHTSU

The University of Tokyo

MEMBERS
(From April 1, 2017)

[I] THE UNIVERSITY OF TOKYO*

Professor Emeritus

    Motoichi OHTSU[a]   (Dr. Eng.)

Post-doctoral Researcher

    B. Thubthimthong   (Dr. Eng.)

Technical Manager

    Teruo MURAKAMI

Secretaries

    Mamiko ITABASHI
    Naoko SEKIMUKAI

a) Also a chief director, NPO- Nanophotonics Engineering Organization

(*) Institute of Engineering Innovation, School of Engineering,
    The University of Tokyo
    Room 219, Bldg. Eng. 9, 2-11-16 Yayoi, Bunkyo-ku, Tokyo 113-8656, Japan
    Phone: +81-3-5841-6758
    E-mail: ohtsu@nanophotonics.t.u-tokyo.ac.jp
    URL: http://www.rodrep.or. jp

東京大学大学院 工学系研究科 総合研究機構
〒113-8656　東京都文京区弥生 2-11-16　工学部 9 号館 219 号室
電話: 03-5841-6758
    E-mail: ohtsu@nanophotonics.t.u-tokyo.ac.jp
    URL: http://www.rodrep.or. jp

[II] RESEARCH ORIGIN FOR DRESSED PHOTON (RODREP) *

Chief Director

Motoichi OHTSU   (Dr. Eng.)

Director

Hidefumi HORI   (Dr. Eng.)

Masayuki NAYA   (Dr. Eng.)

Hirofumi SAKUMA   (PhD.)

Teruo MURAKAMI

Auditor

Satoshi SUGIURA

Advisor

Izumi OJIMA   (Dr. Sci.)

Junji MIYAHARA   (Dr. Eng.)

日亜化学工業（株）　横浜技術センター　１階

（事務局）

一般財団法人　総合研究奨励会

〒113-8656　東京都文京区弥生 2-11-16　東京大学大学院工学系研究科
総合研究機構内

一般社団法人ドレスト光子研究起点設立記念シンポジウム
「ドレスト光子をどう攻めるか、使うか?」

<div align="right">

開催日　2017 年 11 月 6 日(月)

開催場所　日亜化学工業(株)横浜技術センター

</div>

時間	内容
13：30〜13：50	開会の辞：　RODreP が今日にいたるまで 宮原諄二　　RODreP 顧問、イノベーションファクター研究会
13：50〜14：15	これまでの DP 研究と将来：RODreP がめざすこと 大津元一　　RODreP 代表理事、東京大学
14：15〜14：40	（招待講演）CG で可視化・映像化することの意義 　　　　　　－自然現象からドレスト光子まで－ 菊池司　　　東京工科大学　准教授
14：40〜15：05	ドレスト光子と社会の接点 納谷昌之　　RODreP 理事、富士フイルム株式会社
≪休憩≫(15 分)	
15：20〜15：45	（招待講演）ドレスト光子のための応答理論 　　　　　　－非共鳴条件、光学フォノンの大切さ－ 坂野斎　　　山梨大学
15：45〜16：10	ドレスト光子の理解にむけて 　　　　　　”時空の渦力学“が導く仮想光子モデル 佐久間弘文　RODreP 理事
16：10〜16：50	共同研究の所信講演（オフシェル科学共同研究補助金受賞者） ・量子確率論および量子ウォークの数理を活用したドレスト光子研究・オフシェル科学の構築　（西郷甲矢人） ・ドレスト光子への代数的量子場的・測定理論アプローチ（岡村和弥） ・作用素環論、スペクトル理論に基づくドレスト光子（安藤浩志）
16：50〜17：15	（総括講演）量子場として見たドレスト光子：運動量空間での特徴づけ 小嶋泉　　　RODreP 顧問
17：15〜17：20	閉会の辞 大津元一　　RODreP 代表理事、東京大学

<div align="center">

●終了後、立食形式の懇親会（無料）を予定しています。

</div>

LIST OF PAPERS

[(pp. XX-XX); pages in this issue of the COLLECTED PAPERS**]**

[I] ORIGINAL PAPERS

[1] H. Sakuma, I. Ojima, and M. Ohtsu, "Gauge symmetry breaking and emergence of Clebsch-dual electromagnetic field as a model of dressed photons," Appl. Phys.A (2017) 123:750.

(pp. 1-5)

[2] H.Saigo, I. Ojima, and M. Ohtsu, "Dressed photons from the viewpoint of photon localization: the entrance to the off-shell science," Appl. Phys.A (2017) 123:724.

(pp. 7-12)

[3] J.H. Kim, T. Kawazoe, and M.Ohtsu, "Dependences of emission intensity of Si light-emitting diodes on dressed-photon—phonon-assisted annealing conditions," Appl. Phys.A (2017) 123:606.

(pp. 13-17)

[II] PRESENTATIONS IN INTERNATIONAL CONFERENCES

[1] B. Thubthimthong, T. Kawazoe, and M. Ohtsu, "Spectral Analysis of a High-Power Infrared Silicon Light Emitting Diode of Dressed Photons," Abstracts of the OSA Laser Congress: Advanced Solid State Laser Conference, October 1 – 5, 2017, Nagoya, Japan, paper number JTh2A

(pp.19-21)

[2] H. Sakuma, I. Ojima, and M. Ohtsu, "Novel Attempt in Formulating a Theory of Near-field Optics Beyond the Framework of On-shell Dynamics", Abstracts of the 24th Congress of the International Commission for Optics, August 21-25, 2017, Tokyo, Japan, paper number W1H.

(pp.23-24)

[3] H. Sakuma, I. Ojima, and M. Ohtsu, "Novel View Towards Gauge Condition as a Conceptual Basis of Dressed Photons", Abstracts of the 11th Asia-Pacific Conference on Near-Field Optics, July 10-13, 2017 , Tainan, Taiwan, p.32.

(p.25)

[4] I. Banno and M. Ohtsu, "Irrationality of the Permittivity in Non-resonant Near-field Optics", Abstracts of the 11th Asia-Pacific Conference on Near-Field Optics, July 10-13, 2017, Tainan, Taiwan, p.35.

(p.26)

[5] M. Ohtsu, "New Routes to Future Studies of Dressed Photons", Abstracts of the 11th Asia-Pacific Conference on Near-Field Optics, July 10-13, 2017 , Tainan, Taiwan, p.37.
[Plenary Presentation]

(p.27)

[6] M. Ohtsu, I. Ojima, and H. Saigo, "Who Has Seen A Free Photon? ---From Mathematical Physics to Light-Matter Fusion Technologies---", Abstracts of the 11th Asia-Pacific Conference on Near-Field Optics, July 10-13, 2017, Tainan, Taiwan, p.54.

(p.28)

[7] J.H. Kim, T. Kawazoe, and M. Ohtsu, "The study on the principle of light emission of Si LED using dressed-photon-phonon", Abstracts of the 11th Asia-Pacific Conference on Near-Field Optics, July 10-13, 2017, Tainan, Taiwan, p.55.

(p.29)

[8] I. Banno and M. Ohtsu, "The Nonlinear Response Theory for Near-field Optics and Application to Non-resonant Effect", Abstracts of the 11th Asia-Pacific Conference

II

on Near-Field Optics, July 10-13, 2017, Tainan, Taiwan, p.62.
(p.30)

[III] REVIEW PAPERS

[1] H.Sakuma, I. Ojima and M. Ohtsu, "Dressed photons in a new paradigm of off-shell quantum fields," Progress in Quantum Electronics Vol.55, September 2017, pp.74-87.

(pp. 31-44)

[2] M. Ohtsu, "Complex System of Dressed Photons and Applications", The Review of Laser Engineering, Vol.54, No.3, March 2017, pp.139-143 (in Japanese).
【大津元一、「複雑系としてのドレスト光子とその応用」、レーザー研究、第 45 巻、第 3 号、2017 年 3 月、pp. 139-143】

(pp.45-49)

[IV] Off-SHELL ARCHIVE

[1] M. Ohtsu and H. Sakuma, "Creation and Measurement of Dressed Photons: A Link to Novel Theories," Offshell:1712R.001.v1.
  [Review paper]

  (p.51-67)

[2] M. Ohtsu, T. Kawazoe, and H. Saigo, "Spatial and Temporal Evolutions of Dressed Photon Energy Transfer," Offshell:1710R.001.v1.
  [Review paper]

  (p.69-92)

[3] M. Ohtsu, "New Routes to Studying the Dressed Photon," Offshell:1709R.001.v1.
  [Review paper]

  (p.93-124)

[V] PUBLISHED BOOKS

[1] M. Ohtsu, Future Optics, Asakura-shoten, Tokyo, October 2017 (167 pages).
【大津元一、「これからの光学」、朝倉書店、東京、2017 年 10 月　（167 ページ）】

(pp.125-128)

[2] M. Ohtsu and T. Yatsui (ed.), Progress in Nanophotonics 4, Springer, Heidelberg, Janurary 2017 (146 pages).

(pp.129-132)

[VI] PRESENTATIONS IN DOMESTIC CONFERENCES

[1] B. Thubthimthong, T. Kawazoe, and M. Ohtsu, "Spectral Analysis of a High-Power Infrared Silicon Light Emitting Diode," Abstracts of the 78th Jpn. Soc. Appl. Phys. Annual Meeting, September 2017, Fukuoka, Japan, paper number 7a-A405-4.
【B. Thubthimthong, T. Kawazoe, and M. Ohtsu, "Spectral Analysis of a High-Power Infrared Silicon Light Emitting Diode," 第 78 回応用物理学会秋季学術講演会予稿集（福岡、2017 年 9 月）、講演番号 7a-A405-4】
(p.133)

[2] T. Kawazoe, S. Sugiura, K. Hashimoto, and M. Ohtsu, "Fabrication of a High Power Homojunction Silicon Laser (2)," Abstracts of the 78th Jpn. Soc. Appl. Phys. Annual Meeting, September 2017, Fukuoka, Japan, paper number 7a-A405-5.
【川添正、杉浦聡、橋本和信、大津元一、「高出力ホモ接合シリコンレーザーの作製
(2)」、第 78 回応用物理学会秋季学術講演会予稿集（福岡、2017 年 9 月）、講演
番号 7a-A405-5】
(p.134)

[3] I Banno and M. Ohtsu, "Theory of Non-resonant Effect in Near-field Optics II: Approach to a Base of Dressed Photon Employing Non-linear Response Theory," Abstracts of the 78th Jpn. Soc. Appl. Phys. Annual Meeting, September 2017, Fukuoka, Japan, paper number 7a-A405-9.
【坂野斎、大津元一、「近接場光学における非線形共鳴効果の理論Ⅱ：非線形応答理論によるドレスト光子の基礎づけの試み」、第 78 回応用物理学会秋季学術講演会予稿集（福岡、2017 年 9 月）、講演番号 7a-A405-9】
(p.135)

[4] H. Sakuma, I. Ojima, and M. Ohtsu, "New initiative of understanding the dynamics of dressed photons as virtual ones," Abstracts of the 78th Jpn. Soc. Appl. Phys. Annual Meeting, September 2017, Fukuoka, Japan, paper number 7a-A405-10.
【佐久間弘文、小嶋泉、大津元一、「仮想光子としてのドレスト光子理解に向けての新たな試み」、第 78 回応用物理学会秋季学術講演会予稿集（福岡、2017 年 9 月）、講演番号 7a-A405-10】
(p.136)

[VII] APPENDIX
Publications and Presentations by NPO Nanophotonics Eng. Org.

[1] T. Kawazoe, "High power Silicon laser based on the dressed photon technology," Extended Abstracts of the 2017 International Conference on Solid State Devices and Materials, Septermber 19-22, 2017, Sendai, Japan, paper number H-7-01.
   [Invited Presentation]

   (pp.137-138)

[2] T. Kawazoe and S. Sugiura, "High Power Silicon Lasers via Dressed Photon", Abstracts of the 11th Asia-Pacific Conference on Near-Field Optics, July 10-13, 2017 , Tainan, Taiwan, p.53.
   [Invited Presentation]

   (p.139)

[I] ORIGINAL PAPERS

Gauge symmetry breaking and emergence of Clebsch-dual electromagnetic field as a model of dressed photons

Hirofumi Sakuma[1,2] · Izumi Ojima[1] · Motoichi Ohtsu[1,3]

Abstract A new model of dressed photons (DPs) as photons in virtual modes is presented by extending conventional electromagnetic field into the one with full energy–momentum support. At first glance, such an extension of electromagnetic field seems to be quite unfamiliar, but, according to one of the fundamental results in mathematical theory on quantum fields, the energy–momentum support covering the whole p-space including timelike, lightlike, and spacelike domains is indispensable for describing their interactions. Virtual photons as mediators of electromagnetic field interactions would be a familiar example: in perturbative calculations of quantum electrodynamics, the concept of virtual photons emerges as photon modes with four polarization vectors, since the theory of virtual photons necessarily involves longitudinal and scalar modes. We show that a new model presented here can be formulated on the basis of vortex (or spin) dynamics and we call Clebsch-dual electromagnetic field which is similar to twistor theory from the group theoretical viewpoint. Since Clebsch-dual vortex dynamics is closely related to scalar photon dynamics, we show here how scalar photons can be interpreted from the viewpoint of micro–macro duality proposed by Ojima in combination with a new interpretation of gauge condition which becomes important in formulating Clebsch-dual vortex dynamics as an extended electromagnetic field in a spacelike domain.

✉ Hirofumi Sakuma
  sakuma@rodrep.or.jp

1 Research Origin for Dressed Photon, Yokohama, Japan

2 Graduate School of Mathematical Sciences, The University of Tokyo, Yokohama, Japan

3 Institute of Engineering Innovation, School of Engineering, The University of Tokyo, Yokohama, Japan

1 Introduction

The main issue addressed here is to develop further the content of a new model of dressed photons (DPs) described by Sakuma et al. [1] (hereafter SOO). The problem of interaction between a given nano-scale material field and incident light in a typical setting of near-field optical researches has been widely investigated in the framework of nanophotonics based on the conventional theory of electromagnetism. We cannot deny, however, that the mystery of elusive phenomenon in optical engineering, termed DPs by Ohtsu [2], seems to have always escaped from being examined in the mainstream researches of nanophotonics within such approaches. By a variety of intriguing applications of DPs showing up now on the central stage in near-field optical engineering and by the ever increasing impetus to move further forward, we are forced to be serious about the problem of deepening of theoretical understanding of DP. Otherwise, it will become impossible for us to meet the growing technological needs in near-field optics.

A theoretical study on DP due to SOO is one of the initiative projects aiming at the formulation of a theoretical basis of the dynamics of DPs as off-shell virtual photons. To understand the dynamics of off-shell photons, we first need to know the essential difference between usual "real" photons and virtual ones. The clue to understand the difference lies in the perturbative calculations of QED in which virtual photons are introduced as dynamical mediators of electromagnetic interactions between charged particles. Unlike "real" photons in the transverse modes, the polarizations of virtual photons cover not only transverse but also the longitudinal as well as "temporal" (as the fourth direction in spacetime) modes, both of which are totally neglected as "unphysical modes" in the usual approaches. In other words, we should say that these "unphysical modes" play crucial roles in understanding the difference between "real"

Springer

1

and virtual photons, which clearly distinguish our present work from a previously proposed off-shell model by Kobayashi et al. [3] in which those "unphysical modes" are not included. While the seemingly contradictory gap between the quantum and classical explanations on these latter modes has already been resolved by a consistent bridge found in [4] in a theoretical framework, serious confusions are persistent in the understanding of the mutual relations between real and virtual photons. In such situations, we start our discussion from reviewing this issue in Sect. 2, since Clebsch duality of electromagnetic field discussed in SOO essentially depends on the existence of above-mentioned "unphysical modes". In the context of Clebsch duality, a new interpretation of the gauge condition is introduced, and for lack of its full explanations in SOO from the standpoint of the longitudinal mode, Sect. 3 will be allotted for this discussion. In Sect. 4, we show, as a new central result of this paper, how DPs as virtual modes manifest themselves in our model. A brief summary of this paper is given in Sect. 5.

2 On Clebsch duality and longitudinal wave mode

Since the explanation of Clebsch duality of electromagnetic field is already given in SOO, we recapitulate here its main ingredients to make this short paper self-contained. Motivated by a celebrated experimental result by Tonomura et al. [5] which has justified the accessibility of electromagnetic four vector potential A^μ, let us consider the case, where A^μ is parallel to Robinson congruence: i.e., a field of null geodesics defined on a four-dimensional pseudo-Riemannian manifold $\mathfrak{R}$, like one of a four Poynting vector field on it associated with free electromagnetic waves. To distinguish this "electromagnetic" field from the conventional one, we denote it by U^μ, instead of the usual A^μ. We see that it would allow such a hydrodynamic interpretation of electromagnetic field that U^μ corresponds to the velocity field and that the associated vorticity field defined by

$$S_{\mu\nu} = \nabla_\nu U_\mu - \nabla_\mu U_\nu, \tag{1}$$

describes the field strength. In Eq. (1), ∇_μ denotes the covariant derivative defined on $\mathfrak{R}$. Since we assume that U^μ is parallel to a null geodesic, it satisfies

$$U^\nu \nabla_\nu U_\mu = U^\nu (\nabla_\nu U_\mu - \nabla_\mu U_\nu) + \nabla_\mu (U^\nu U_\nu / 2) = U^\nu S_{\mu\nu} = 0. \tag{2}$$

Introducing a couple of Clebsch variables (λ, φ) arising from the study of Hamiltonian structure of barotropic flows [6], we parameterize U_μ here as

$$U_\mu = \lambda \nabla_\mu \varphi, \text{ where } \varphi \text{ and } \lambda \text{ satisfy, respectively,}$$

$$\nabla^\nu \nabla_\nu \varphi = 0 \text{ and } \nabla^\nu \nabla_\nu \lambda - (\kappa_0)^2 \lambda = 0, \tag{3a, b, c}$$

where κ_0 in (3c) is a constant parameter to be discussed later. Note that U_μ of the form: $U_\mu = \nabla_\mu \chi$ automatically satisfies Eq. (2), since $S_{\mu\nu}$ vanishes for such an irrotational U_μ field. The reason why we introduce Clebsch-parameterized flow (3a) is that, as is the case for free electromagnetic waves, we are interested in a rotational vector field tangent to Robinson congruence. Actually, from (1) and (3a), we readily derive

$$S_{\mu\nu} = C_\mu L_\nu - L_\mu C_\nu, \text{ where } C_\mu \equiv \nabla_\mu \varphi \text{ and } L_\mu \equiv \nabla_\mu \lambda. \tag{4a, b, c}$$

A couple of Eqs. (3b, c) are scalar ones, so that we can impose a directional constraint $C^\nu L_\nu = 0$ on them, from which we can show that L_ν is necessarily spacelike, i.e., $L^\nu L_\nu < 0$, since C^ν is lightlike. Using this orthogonality relation together with $C^\nu C_\nu = 0$, we see that Clebsch-parameterized flow (3a) in fact satisfies geodesic equation (2), because we have $U^\nu S_{\mu\nu} = (L_\nu C^\nu) \lambda C_\mu = 0$.

An intriguing aspect of Clebsch-parameterized flow comes out when we consider the energy–momentum tensor $\hat{T}^\nu_\mu$ of Clebsch-parameterized vortex dynamics which is defined similar to that of free electromagnetic field in such a form as $T^\nu_\mu = -F_{\mu\sigma} F^{\nu\sigma}$, namely

$$\hat{T}^\nu_\mu = -S_{\mu\sigma} S^{\nu\sigma}. \tag{5a}$$

It can be shown that (5a) actually satisfies the energy–momentum conservation $\nabla_\nu \hat{T}^\nu_\mu = 0$ (for details, see SOO) and possesses a dual representation of the form:

$$\hat{T}^\nu_\mu = -S_{\mu\sigma} S^{\nu\sigma} = \rho C_\mu C^\nu, \text{ where } \rho \equiv -L^\nu L_\nu. \tag{5b}$$

This clearly shows that $\hat{T}^\nu_\mu$ corresponds to the free motion of continuous medium, whose "momentum" field is represented by ρC^ν. The essential difference between the conventional Maxwell theory and the Clebsch-parameterized vortex dynamics can be seen through the comparison between $\nabla_\nu T^\nu_\mu = 0$ and $\nabla_\nu \hat{T}^\nu_\mu = 0$ in such forms as

$$\nabla_\nu T^\nu_\mu = -F_{\mu\sigma} \nabla_\nu F^{\nu\sigma} = 0, \ \nabla_\nu \hat{T}^\nu_\mu = -S_{\mu\sigma} \nabla_\nu S^{\nu\sigma} = 0. \tag{6a, b}$$

In the vacuum situation with no electric current j^σ, Eq. (6a) vanishes because of $j^\sigma = \nabla_\nu F^{\nu\sigma} = 0$. On the other hand, using Eq. (3c), we have

$$\nabla_\nu S^{\nu\sigma} = -(\nabla_\nu L^\nu) C^\sigma = -(\kappa_0)^2 \lambda C^\sigma = -(\kappa_0)^2 U^\sigma. \tag{7}$$

In spite of the above difference, Eq. (6b) holds owing to Eq. (2), since $\nabla_\nu \hat{T}^\nu_\mu = -S_{\mu\sigma} \nabla_\nu S^{\nu\sigma} = (\kappa_0)^2 S_{\mu\sigma} U^\sigma = 0$.

To see the meaning of this difference, we first look into the vector identity of $\nabla_\nu F^{\nu\sigma}$, namely

$$\nabla_\nu F^{\nu\sigma} = -g^{\sigma\nu} \nabla_\nu (\nabla_\tau A^\tau) + [g^{\nu\tau} \nabla_\nu \nabla_\tau A^\sigma + R^\sigma_\nu A^\nu], \tag{8a}$$

where R^σ_ν denotes Ricci tensor. For the reason explained shortly, we keep the term $R^\sigma_\nu A^\nu$ except for the discussions in Sect. 3, although it must be quite small being neglected in

the usual discussion of electromagnetism. If we decompose A^σ into $A^\sigma = \alpha^\sigma + g^{\sigma\tau}\nabla_\tau\chi$, where $\nabla_\sigma\alpha^\sigma = 0$, then (8a) is rewritten as

$$\nabla_\nu F^{\nu\sigma} = -g^{\sigma\nu}\nabla_\nu(\nabla_\tau A^\tau) + [g^{\nu\tau}\nabla_\nu\nabla_\tau A^\sigma + R^\sigma_\nu A^\nu]$$
$$= g^{\nu\tau}\nabla_\nu\nabla_\tau\alpha^\sigma + R^\sigma_\nu\alpha^\nu. \qquad (8b)$$

The last expression simply says that $\nabla_\nu F^{\nu\sigma}$ is expressed in terms of gauge independent α^σ and it reduces to $g^{\nu\tau}\nabla_\nu\nabla_\tau\alpha^\sigma + R^\sigma_\nu\alpha^\nu = 0$ in the absence of electric current $j^\sigma(= \nabla_\nu F^{\nu\sigma}) = 0$. In conventional electromagnetic theory, where $\nabla_\tau A^\tau$ causes no physical effects, it can safely be eliminated by Lorenz-type gauge condition. In Sect. 3, however, we show that there is a case for which $-g^{\sigma\nu}\nabla_\nu(\nabla_\tau A^\tau)$ in (8a) can be reinterpreted as an electric field associated with longitudinal mode of electromagnetic field.

As to scalar modes $\nabla_\tau A^\tau$ in electromagnetic field, there still seems to be a prevailing confusion on their interpretation. It is well known that if we try to recover the microscopic quantum gauge field A_μ from the gauge invariant $F_{\mu\nu}$ alone, then we have a mathematical difficulty. As far as microscopic particle-excitation modes are concerned, the difficulty can be avoided by eliminating longitudinal photon with negative norm and by giving null probability to scalar photon $\nabla_\tau A^\tau$. As briefly touched upon in Introduction, however, Ojima [4] showed that we need the gauge dependent A_μ on the macroscopic side, where the longitudinal photons and Goldstone mode in the Higgs phase are physical in condensed non-particle modes. In addition, in the context outside of Ojima's micro–macro duality, the coexistence of a longitudinal electric field and transverse modes of free electromagnetic waves was reported in classical electromagnetism in such theoretical and experimental papers (see, e.g., Cicchitelli et al. [7]). In Sect. 3, we show that a longitudinal electric field is directly related to $\nabla_\tau A^\tau$, so that the result of Ojima and those of classical electromagnetism are mutually consistent, while they are derived in separate studies. In this sense, it is meaningful to look into the following equations:

$$g^{\nu\tau}\nabla_\nu\nabla_\tau A^\sigma + R^\sigma_\nu A^\nu = 0; \quad \nabla_\nu F^{\nu\sigma} = -g^{\sigma\nu}\nabla_\nu(\nabla_\tau A^\tau)$$
$$\text{with } g^{\mu\nu}\nabla_\mu\nabla_\nu(\nabla_\tau A^\tau) = 0. \qquad (9a, b, c)$$

Note that Clebsch-parameterized vortex dynamics discussed above corresponds to the case in which we have $\varphi = \nabla_\tau A^\tau$ that satisfies the energy–momentum conservation law $F_{\mu\sigma}\nabla_\nu F^{\nu\sigma} = 0$. The fact that Clebsch-parameterized vortex dynamics with lightlike $U^\mu = \lambda\nabla_\mu\varphi = \lambda C^\mu$ involves spacelike Klein–Gordon (KG) equation (3c) is reflected in the following spacelike "Proca equation" in Clebsch-parameterized vortex dynamics:

$$\nabla_\nu(\nabla^\nu U^\sigma - \nabla^\sigma U^\nu) - (\kappa_0)^2 U^\sigma = 0, \qquad (10a)$$

which directly follows from Eq. (7). Since the conventional Proca equation has the form:

$$\nabla_\nu(\nabla^\nu A^\sigma - \nabla^\sigma A^\nu) + m^2 A^\sigma = 0, \qquad (10b)$$

we can say that U^μ is an extended electromagnetic field in the spacelike domain and the detailed discussion on the extension from a lightlike case to a spacelike one is given in SOO and the major outcomes on this extension will be briefly touched on in the beginning of Sect. 4. In the context of group representation theory, the sharp differences involving $\partial_\tau A^\tau$ between massive and massless vector fields obeying the Proca equation (10b) have historically been well known. In the present discussion, we have also encountered the Proca equation (10a) with negative mass term $-(\kappa_0)^2$, and we will see at the end of Sect. 3, as to how the meaning of $\partial_\tau A^\tau$ will change according to these different contexts.

3 Novel view on "gauge condition" in the context of Clebsch duality

Going back to Eq. (9a), let us look into it from the viewpoint of a balance equation between the rotational (α^σ) and irrotational ($\nabla^\sigma\chi \equiv g^{\sigma\tau}\nabla_\tau\chi$) parts of A^σ. For simplicity, we consider the balance in a flat Minkowski space $\{x^\mu\}$, where the operator ∇_μ is replaced by ∂_μ and $R^\sigma_\nu = 0$. Then, the balance equation (9a) for A_σ becomes

$$\partial^\tau\partial_\tau\alpha_\sigma + \partial_\sigma(\partial_\tau A^\tau) = 0. \qquad (11a)$$

Note first that, for a given non-zero $\partial_\tau A^\tau$, the solution α_σ to (11a) consists of a homogeneous solution satisfying $\partial^\tau\partial_\tau\alpha^{(h)}_\sigma = 0$ and an inhomogeneous one $\alpha^{(i)}_\sigma$:

$$\partial^\tau\partial_\tau\alpha^{(i)}_\sigma + \partial_\sigma(\partial_\tau A^\tau) = 0. \qquad (11b)$$

Since $\alpha^{(h)}_\sigma$ is a well-known solution in transverse modes, what we are actually interested in is $\alpha^{(i)}_\sigma$.

A well-known example of such a balance equation is seen in two-dimensional irrotational motion of an incompressible fluid. Let (u, v) be a Cartesian velocity field of the fluid. The incompressibility of fluid means that its motion is non-divergent in the sense of $\partial_x u + \partial_y v = 0$, while the vorticity must vanish, since its motion is irrotational, i.e., $\partial_x v - \partial_y u = 0$. As a result of these two constraints, the velocity field (u, v) must have dual expression, namely

$$u = \partial_x\phi = \partial_y\psi, \quad v = \partial_y\phi = -\partial_x\psi, \qquad (12a, b)$$

where ϕ and ψ are velocity potential and stream function, respectively. Since (12a, b) are equivalent to the famous Cauchy–Riemann equations, ϕ and ψ are the real and imaginary parts of a certain analytic function satisfying $\nabla^2\phi = 0$ and $\nabla^2\psi = 0$. In addition, since $\partial_x\phi\,\partial_x\psi + \partial_y\phi\,\partial_y\psi = 0$, they are called conjugate harmonics.

In what follows, we will show that, owing to (11b) and a relation similar to (12a, b), $\partial_\tau A^\tau$ can be related to a

longitudinal electric field. In (11b), we can assume without loss of generality that non-zero components are those with subscript σ taking values $\sigma = 0\,(x^0)$ and $\sigma = 1\,(x^1)$. Corresponding to this specification of propagation direction, we can also assume that

$$\partial_\tau A^\tau = \partial_0 A^0 + \partial_1 A^1. \tag{13}$$

For the sake of simplicity of notation, let us introduce new notations: $\beta_\sigma \equiv \partial^\tau \partial_\tau \alpha_\sigma^{(i)}$ and $\xi \equiv \partial_\tau A^\tau$. Then, (11b) is rewritten as

$$\beta_\sigma + \partial_\sigma \xi = 0. \tag{14}$$

Since β^σ is divergence free by definition, i.e., $\partial_\sigma \beta^\sigma = 0$, there exists ϖ satisfying

$$\beta^0 = \beta_0 = \partial_1 \varpi, \quad \beta^1 = -\beta_1 = -\partial_0 \varpi. \tag{15a, b}$$

Combining (14) and (15a, b), we obtain

$$\partial_1 \varpi + \partial_0 \xi = 0, \quad \partial_0 \varpi + \partial_1 \xi = 0. \tag{16a, b}$$

Note that $F^{\nu\sigma}$ in Maxwell equation $j^\sigma = \nabla_\nu F^{\nu\sigma}$ can be considered mathematically as a sort of extended "stream functions" for non-divergent vector j^σ. Since the dimension of β^σ is the same as that of j^σ, we can use this relation to redefine ϖ in (15a, b), whose consistency in the present context will be checked shortly. Thus, we have

$$\beta^0 = \partial_1(-F^{01}), \quad \beta^1 = \partial_0(-F^{10}) = \partial_0 F^{01}, \tag{16c, d}$$

where $j^\sigma = \nabla_\nu(-F^{\nu\sigma})$ is used instead of $j^\sigma = \nabla_\nu F^{\nu\sigma}$, in view of the irrelevance of the sign in the equation to determine "stream functions", in contrast to the situation in Maxwell equation: the reason why we only use F^{01} here is because $\xi = \partial_\tau A^\tau$ in (13) is expressed solely in terms of A^0 and A^1. Substitution of $\varpi = -F^{01} = F_{01} = \partial_0 A_1 - \partial_1 A_0$ and $\xi = \partial_0 A^0 + \partial_1 A^1 = \partial_0 A_0 - \partial_1 A_1$ into (16a, b) yields

$$(\partial_{00}^2 - \partial_{11}^2)A_0 = 0, \quad (\partial_{00}^2 - \partial_{11}^2)A_1 = 0, \tag{17a, b}$$

which is an expected property of A_σ for propagating waves and justifies our choice of $\varpi = -F^{01}$. Similarly, by cross differentiating (16a, b), we get

$$(\partial_{00}^2 - \partial_{11}^2)\varpi = 0, \quad (\partial_{00}^2 - \partial_{11}^2)\xi = 0. \tag{18a, b}$$

For a simple plane wave solution of $A_0 = A_1 = \exp i\,(kx^0 - kx^1)$, we get $\varpi = \xi = 2ik \exp i\,(kx^0 - kx^1)$ which shows that $\partial_\tau A^\tau$ in this case is equal to the electric field F_{01} of a longitudinal mode.

Concerning the physical reality of vector potential A_σ, what has actually been verified in the experiments performed by Tonomura et al. [4] is the presence of the rotational component of A_σ and the irrotational one was left untouched. The analysis presented above, however, shows that the irrotational part of A_σ also has a physical meaning and should not be treated as a simple mathematical device. If we accept this, then Lorenz gauge condition $\partial_\tau A^\tau = 0$ can be regarded as a "ground" or unexcited state of the divergence of a physically

meaningful vector A_σ. According to Proca equation (10b), in a timelike domain in which $m^2 > 0$, we must have $\partial_\tau A^\tau = 0$. In this section, we have shown that the constraint $\partial_\tau A^\tau = 0$ does not necessarily hold any more for lightlike solutions, and in Sect. 2, we discussed "Proca equation" (10a) as a candidate to extend (10b) naturally into spacelike domain by the help of Clebsch-parameterized vortex dynamics in which an excited state of $\partial_\tau A^\tau$ plays a key role. In the following section, we start from explaining briefly how this extension is achieved to obtain a new model of off-shell virtual photons.

4 Dressed photons in off-shell virtual modes

In Sect. 2, we have discussed Clebsch-parameterized vortex dynamics in the case of lightlike C^μ which corresponds to free electromagnetic waves in vacuum. Mathematically, as we see from (5b), a lightlike case is shown in such a form that the trace of $\hat{T}_\mu^\nu$ vanishes, namely, $\hat{T}_\nu^\nu = -S_{\nu\sigma}S^{\nu\sigma} = \rho\,C_\nu C^\nu = 0$, which suggests that a spacelike case would be realized by replacing a null vector C^μ by a spacelike one. Actually, this conjecture turns out to be correct and by repeating similar procedures starting from the geodesic equation (2), we can eventually obtain the energy–momentum tensor $\hat{T}_\mu^\nu$ for a spacelike C^μ (see SOO for the details of derivations). In terms of a new notation $\hat{S}_{\mu\nu\sigma\rho} = S_{\mu\nu}S_{\sigma\rho}$, $\hat{T}_\mu^\nu$ can be expressed as

$$\hat{T}_\mu^\nu = -\hat{S}_{\mu\sigma}^{\ \ \nu\sigma} + \frac{1}{2}\hat{S}_{\alpha\beta}^{\ \ \alpha\beta}g_\mu^\nu, \tag{19a}$$

which satisfies $\nabla_\nu \hat{T}_\mu^\nu = 0$. Since Eq. (19a) is isomorphic to the l.h.s. of Einstein equation which represents Ricci curvature of the spacetime:

$$G_\mu^\nu = -R_{\mu\sigma}^{\ \ \nu\sigma} + \frac{1}{2}R_{\alpha\beta}^{\ \ \alpha\beta}g_\mu^\nu, \tag{19b}$$

with Riemann curvature tensor $R_{\mu\nu\sigma\rho}$ satisfying $\nabla_\nu G_\mu^\nu = 0$, we can say that (19a) describes an inherent spacetime structure of the extended electromagnetic field. The trace of (19a) becomes as $\hat{S}_{\alpha\beta}^{\ \ \alpha\beta}$ and it can be shown that $\hat{S}_{\alpha\beta}^{\ \ \alpha\beta} = 8(\kappa_0)^2 U^\nu U_\nu$ which is negative, since U^μ is spacelike.

Equations (3b, c) for a spacelike case now become a couple of KG equations:

$$\nabla^\nu \nabla_\nu \varphi - (\kappa_0)^2 \varphi = 0, \quad \nabla^\nu \nabla_\nu \lambda - (\kappa_0)^2 \lambda = 0 \text{ with } g^{\mu\nu}\nabla_\mu \varphi\,\nabla_\nu \lambda = 0. \tag{20a, b, c}$$

Since DPs tend to manifest themselves at a sharp end in an open space as the simplest setting for such a configuration, let us consider λ field in a spherical coordinates system (r, θ, ϕ). Utilizing the method of separation of variables, we assume $\lambda = \exp(ik_0 x^0)\tilde{\lambda}(r, \theta, \phi) = \exp(ik_0 x^0)R(r)\Theta(\theta)\Phi(\phi)$ and get from (20b):

$$\Delta \tilde{\lambda} + [(\kappa_0)^2 + (k_0)^2]\tilde{\lambda} = 0, \tag{21}$$

where Δ denotes the Laplacian in terms of spherical coordinates. For simplicity, let us consider a solution dependent only on r. Then, (21) reduces to

$$\frac{d^2 R}{dr^2} + \frac{2}{r}\frac{dR}{dr} + [(\kappa_0)^2 + (k_0)^2]R = 0. \tag{22}$$

Recall that a timelike KG equation having the form of $\nabla^\nu \nabla_\nu \lambda + m^2 \lambda = 0$ is formally transformed into a spacelike one of (20b) if we replace the rest mass m by $i\kappa_0$. Quantum theoretically speaking, k_0 in the time dependent part of λ is proportional to the energy of a given state. In parallel to the case of transformation of m into $i\kappa_0$, we consider the case of $k_0 \rightarrow ie$. The behavior of spacelike KG equation is explained, for instance, by [8], and it is shown that non-localized wave-like solutions are stable, while localized ones are always unstable (either amplifying or damping). The reason why we consider the case of $k_0 \rightarrow ie$ is because DPs are spatially localized. Replacing k_0 by ie in (22), we obtain

$$\frac{d^2 R}{dr^2} + \frac{2}{r}\frac{dR}{dr} - [e^2 - (\kappa_0)^2]R = 0, \tag{23}$$

which yields a spatially localized Yukawa-potential-type solution of

$$R(r) = \frac{1}{r}\exp\left[-\sqrt{e^2 - (\kappa_0)^2}\, r\right]. \tag{24}$$

The significance of this solution is that when the magnitude of energy fluctuation arising from incident light–matter interactions combined presumably with a quantum mechanical effect of the uncertainty principle exceeds a certain threshold value of κ_0 which is basically determined by the scale of nano-materials involved, an unstable (temporally damping and spatially localized) solution $\lambda = \exp(-et)R(r)$ of a spacelike KG equation pops up into a timelike domain. Given the above-mentioned incident light–matter interactions as a background "forcing", the incessant process of excitation of the field (19a) and resultant damping looks similar to "vacuum fluctuation" in which modeled DP field plays a role of virtual photons. A spatially localized feature of (19a) shows that it is asymptotically flat and is continuously connected to a far field. In the above argument, we exclude growing-up modes with negative e, because we are interested in a solution which is bounded both spatially as well as temporally for $t > 0$.

5 Summary

A new interpretation of gauge condition has been proposed by looking at the balance between the rotational and irrotational parts of vector potential A^μ. Our analysis shows that $\nabla_\nu A^\nu$ has a physical meaning and it can be regarded as longitudinal electric field. As a supporting justification of this result, we refer to theoretical interpretations made by Ojima on longitudinal and scalar photons from the viewpoint of micro–macro duality. On the basis of physical reality of $\nabla_\nu A^\nu$, we have extended conventional electromagnetic field A^μ into spacelike domain by introducing Clebsch-dual electromagnetic field. As quantum field theory tells, spacelike energy–momentum support is a necessary ingredient to describe field interactions mathematically as is the case for Coulomb interaction in which virtual photons play key roles, so that Clebsch-dual field yielding spacelike energy–momentum supports can be regarded as a natural approach to construct a model of DPs as virtual photons. A newly introduced model of Clebsch-dual can explain extreme localization as well as ephemerality of the field, which seems to make this model a promising candidate for the model of DP as virtual photon.

References

1. H. Sakuma, I. Ojima, M. Ohtsu, Dressed photons in a new paradigm of off-shell quantum fields. Progr. Quantum Electron. **55**, 74–87 (2017)
2. M. Ohtsu, From classical to modern near-field optics and the future. Opt. Rev. **21**, 905–910 (2014)
3. K. Kobayashi, S. Sangu, H. Ito, M. Ohtsu, Near-field optical potential for a neutral atom. Phys. Rev. A **63**, 013806 (2000)
4. I. Ojima, B. Nakanishi-Lautrup, *Field, crossed product and duality, RIMS workshop: research on quantum field theory* (American Physical Society, College Park, 2006), pp. 29–37
5. A. Tonomura, N. Osakabe, T. Matsuda, T. Kawasaki, J. Endo, S. Yano, H. Yamada, Evidence for Aharanov-Bohm effect with magnetic field completely shielded from electron wave. Phys. Rev. Lett. **56**, 792–795 (1986)
6. H. Lamb, *Hydrodynamics*, 6th edn (Cambridge University Press, Cambridge, 1932), pp. 248–249
7. L. Cicchitelli, H. Hora, R. Postle, Longitudinal field components for laser beams in vacuum. Phys. Rev. A **41**, 3727–3732 (1990)
8. A. Bers, R. Fox, C.G. Kuper, S.G. Lipton, in *The impossibility of free tachyons, relativity and gravitation*, ed. by C.G. Kuper, A. Peres (Gordon and Breach Science Publishers, New York, 1971), pp. 41–46

Applied Physics A
Materials Science & Processing

CrossMark

Dressed photons from the viewpoint of photon localization: the entrance to the off-shell science

Hayato Saigo[1] · Izumi Ojima[2] · Motoichi Ohtsu[2,3]

Abstract In the present paper, a new aspect of the interplay is examined between mathematical–physical arguments and light–matter fusion technologies in terms of the concept of "effective mass", starting from a question: Who has seen a free photon? Owing to the general results due to Newton–Wigner and to Wightman, a position operator is absent for massless free particles with non-zero finite spins, and hence, we cannot observe free photons in any local space regions. To solve this paradox of "photon localization", the effective mass of a photon needs to be generated through the couplings of photons with matter. Here "polaritons" picture as a basic notion in optical and solid physics is shown to verify this viewpoint, which is seen to apply also to more general settings . Focusing on the role played by nanoparticles, we reach a new look at the notion of "dressed photons" as off-shell particles. The perspective above shows that essential mathematical structure of quantum field theory for the so-called elementary particles in subatomic scale can also be applied to certain phenomena in the nano-scale.

✉ Hayato Saigo
  h_saigoh@nagahama-i-bio.ac.jp

1   Nagahama Institute of Bio-Science and Technology, 1266
    Tamura-Cho, Nagahama 526-0829, Japan

2   Research Origin for Dressed Photon, c/o the University
    of Tokyo, Bdg. Eng-9, 2-11-16 Yayoi, Bunkyo-ku,
    Tokyo 113-8656, Japan

3   Institute of Engineering Innovation, Graduate School
    of Engineering, The University of Tokyo, 2-11-16 Yayoi,
    Bunkyo-ku, Tokyo 113-8656, Japan

1 Introduction

In this paper, we examine a new aspect of the interplay between mathematical–physical arguments and light–matter fusion technologies in terms of the concept of "effective mass", starting from a fundamental (and seemingly naive) question: who has seen a free photon?

Since the argument by Newton and Wigner [8] and the theorem by Wightman [13], it has been known in mathematical physics that any position operator cannot be defined for a massless free particle with a non-zero finite spin, in sharp contrast to the cases of massive particles which can be localized.

This statement is clearly in contradiction to the intuition of almost all physicists and engineers who have used the concept of "position of a photon" as one of the basic ingredients of theory and application of quantum mechanics. Without specifying its position who can see a free photon?

This dilemma is resolved by introducing the "effective mass" of a photon due to the interaction with material systems. As we will discuss later, the validity of this interpretation is confirmed in reference to the picture of "polariton", a basic notion in optical and solid physics [3, 4].

The scenario can be applied to more general settings. As a striking example, we focus on the roles played by nanoparticles in the context of "dressed photons" [9], which open the door to the "off-shell" sciences and technologies.

2 On-shell vs. off-shell

Toward introducing the notion of "dressed photons" and "off-shell" sciences and technologies, let us begin with reviewing the concepts of on-shell/off-shell. The equation

$$E = mc^2, \tag{1}$$

🙏 Springer

is probably one of the most well-known formulas in physics.

The right-hand side is the product of the mass and the square of the light speed, and the left one it represents is the so-called "static energy". It is an expression symbolizing the striking recognition of mass–energy equivalence, and the impact of this formula will not be diminished.

One should be aware, however, that this expression does not cover the whole world. The equality $E = mc^2$ belongs to a more general expression of the relation between energy, momentum and mass

$$E^2 - c^2p^2 = m^2c^4, \tag{2}$$

which is called the "(on-the-)mass-shell" condition or "on-shell" condition (for short). Its Fourier-transformed version is the free Klein–Gordon equation:

$$\left(\frac{1}{c^2} \frac{\partial^2}{\partial t^2} - \nabla^2 + \left(\frac{mc}{\hbar} \right)^2 \right) \psi = 0. \tag{3}$$

This condition universally characterizes macroscopically identifiable particles and each of such particles is all thought to fulfill this condition with some specific value of m.

In quantum field theory that has been built with the aim of integrating the theory of relativity and quantum theory (which was another revolution in physics), however, it is known that the world cannot be described satisfactorily only in terms of on-shell entities [10].

To describe actual physical phenomena, it is absolutely necessary to have "agents" that do not satisfy the on-shell condition. These agents usually called "virtual particles" represent crucial characteristics of quantum fields which cannot be explained by classical particle description.

The mode of existence deviating from the on-shell condition is called "off-shell" (aspects of quantum fields). In the naive common-sense knowledge among physicists, it is believed that only in the subatomic scale the consideration of this kind of off-shell becomes practically necessary.

From the mathematical viewpoint, however, a quantum field becomes a free field without interactions if its energy–momentum spectrum does not cover the total dual space of the spacetime [10].

The experimental manifestation of this mathematical consequence can be found in the phenomena described by the concept of "dressed photons" [9] which should constitute exactly the "off-shell science" in the nano-scale. Taking the interaction with nanomaterials into account, the "aspects as a quantum field" of the light becomes significant.

In what follows we introduce the notion of dressed photons from the viewpoint of mathematical physics, especially from the so-called "localization problem" of a photon.

3 Photon localization problem

It is often said that "light is a wave and a particle". Here, light as a particle is a particle with zero mass, that is,

$$E_{\text{free}}^2 - c^2 p_{\text{free}}^2 = 0. \tag{4}$$

Hence, it is considered as a particle which satisfies the on-shell condition in the form mentioned above. Later on, we will call light as particle in this sense as "free photon".

It should be noted here that "particle" notion as used herein refers to the digital behavior of exchanging energy and momentum. It is not considered as being spatially localized.

In fact, this picture is never compatible with the concept of free photon. Newton and Wigner [8] and Wightman [13] showed that a mathematical result meaning

> Particles with mass 0 (spin is not 0) cannot be localized under the standard and general formulation of particle and localization.

More precisely, Wightman proved the result based on the argument by Newton–Wigner by formulating the general notion of localization. The "general notion of localization" can be summarized as follows [11–13]:

(i)   The spectral resolution of position operators: it is defined by a family $\mathcal{B}(\mathbb{R}^3) \ni \Delta \longmapsto E(\Delta) \in \text{Proj}(\mathfrak{H})$ of projection-valued measures $E(\Delta)$ in a Hilbert space $\mathfrak{H}$ defined for each Borel subset Δ of $\mathbb{R}^3$, characterized by the following properties (ia), (ib), (ic):

(ia) $E(\Delta_1 \cap \Delta_2) = E(\Delta_1)E(\Delta_2)$;
(ib) $E(\Delta_1 \cup \Delta_2) = E(\Delta_1) + E(\Delta_2)$, if $\Delta_1 \cap \Delta_2 = \phi$;
(ic) $E(\mathbb{R}^3) = 1$;

(ii) Physical interpretation of $E(\Delta)$: when the system is prepared in a state ω, the expectation value $\omega(E(\Delta))$ of a spectral measure $E(\Delta)$ gives the probability for the system to be found in a localized region Δ;

(iii) Covariance of the spectral resolution: under a transformation $(\mathbf{a}, \mathcal{R})$ with a spatial rotation $\mathcal{R}$ followed by a spatial translation $\mathbf{a}$, a Borel subset Δ is transformed into $\mathcal{R}\Delta + \mathbf{a}$. Corresponding to this, we have its unitary implementer $U(\mathbf{a}, \mathcal{R})$ in $\mathfrak{H}$, which represents $(\mathbf{a}, \mathcal{R})$ covariantly on E in such a way that

$$E(\Delta) \to E(\mathcal{R}\Delta + \mathbf{a}) = U(\mathbf{a}, \mathcal{R})E(\Delta)U(\mathbf{a}, \mathcal{R})^{-1}.$$

To see why the system defined above can be considered as a basis for localization, we give a sketch in a conventional quantum mechanical manner: let Δ be a region, for example, a closed volume in $\mathbb{R}^3$,

$$E(\Delta) = \int_\Delta d^3r |r> < r|,$$

and

$$\omega(E(\Delta)) = \int_\Delta d^3r < \Psi|r><r|\Psi > .$$

Then, the position operator is defined as $\hat{r}|r> = r|r>$.

The difference between the massive case and the massless case comes from the difference of the Wigner little groups, i.e. the stabilizer subgroups of standard four momenta. From the system in the axioms corresponding to the position operator, we can construct a covariant representation under the action of three-dimensional Euclidean group, which generates an induced representation from its little group. In the massless case, however, we can prove by purely representation–theoretic method that there is no such covariant representation for the massless case whose little group is the two-dimensional Euclidean group, in sharp contrast to the massive case whose little group is the three-dimensional rotational group.

According to the above concept of localization, the position operator can be defined consistently. It is important to note that this concept is concerned with *localization of states in space at a given time* formulated in terms of *spatial* translations **a** and rotations $\mathcal{R}$, respectively. If we considered the axioms like (i)–(iii) on the whole *space-time*, it would imply the validity of the canonical commutation relations between four momenta p_μ and spacetime coordinates x^ν, which would imply the Lebesgue spectrum covering the whole $\mathbb{R}^4$ for both observables $\hat{p}_\mu$ and $\hat{x}^\nu$. Then, any such physical requirements as the spectrum condition or as the mass spectrum cannot be imposed on the energy–momentum spectrum $\hat{p}_\mu$, and hence, the concept of localizability in space–time does not make sense.

From this point of view, position should not be considered the "a priori" observables. It is defined with respect to some fixed reference system (some chosen inertial system). Then the problem is whether we can construct the position operator consistently or not. Wightman proved the following mathematical results:

Theorem 1 ([13], excerpt from theorem 6 and 7) *A Lorentz or Galilei covariant massive system is always localizable. For the Lorentz case, the only localizable massless elementary system (i.e. irreducible representation) has spin zero. For the Galilei case, no massless elementary system is localizable.*

Corollary 1 *A free photon is not localizable.*

The fact that a free photon cannot be localized here means that "position" for a free photon is not well defined as a physical quantity for any reference system (reference inertial system).

But, if it is so in reality, can we say nothing about "the position of photons"? This does not seem to match our intuition about many real optical situations (including quantum optics). How can we solve this paradox anyway?

4 Effective mass generation

Our strategy for the photon localization problem can be summarized as follows [11, 12]:

- Photons are coupled with a material system into a composite system with a coupled dynamics.
- Positive effective mass emerges in the composite system as a result of the interaction between the photons and the matter.
- Once the positive effective mass is generated, Wightman's theorem based on Newton–Wigner arguments itself provides the "basis" for the localization of a photon.

From our point of view, therefore, this theorem of Wightman, which is interpreted traditionally as a no-go theorem against the localizability, becomes actually an affirmative support for it. It simply means:

Whenever a photon is localized, it should carry a nonzero effective mass.

As a first typical example of our scheme, we focus first on a photon interacting with a homogeneous medium, in the case of the monochromatic light with angular frequency ω as a classical light wave. For simplicity of the argument, we neglect here the effect of absorption, that is, the imaginary part of refractive index.

When a photon interacting with the homogeneous medium can be treated as a single particle, it is natural to identify its velocity **v** with the "signal velocity" of light in the medium. The relativistic total energy E of the particle should be related to the absolute value of the velocity $v := \sqrt{\mathbf{v} \cdot \mathbf{v}}$ by its effective mass m_{eff}:

$$E = \frac{m_{\text{eff}} c^2}{\sqrt{1 - \frac{v^2}{c^2}}}. \tag{5}$$

Since v is well known to be smaller than the light velocity c in vacuum, m_{eff} should be positive, as far as the particle picture above is valid.

Then we consider m_{eff} as the relativistic (rest) mass, and identify its momentum **p** with

$$\mathbf{p} = \frac{m_{\text{eff}} \mathbf{v}}{\sqrt{1 - \frac{v^2}{c^2}}}. \tag{6}$$

Hence, as long as "an interacting photon" can be well approximated by a single particle, it should have positive mass. Then its "localization problem" is resolved.

Although the concrete forms of energy/momentum are related to the Abraham–Minkowski controversy [1, 2, 6, 7] and modified versions of Einstein/de Broglie formulae [11], our argument itself does not depend on the energy/momentum formulae.

The only essential point is that a massless particle can be made massive through interactions with external system. That is, while a free photon satisfies its on-shell condition

$$E_{\text{free}}^2 - c^2 p_{\text{free}}^2 = 0, \tag{7}$$

an "interacting photon" should satisfy the different on-shell condition

$$E^2 - c^2 p^2 = m_{\text{eff}}^2 c^4 > 0. \tag{8}$$

In short, an "interacting photon" can gain a positive effective mass, while a "free photon" remains massless. This is the key for solving the photon localization problem.

We note, however, the present argument is based on the assumption that "a photon dressed with interactions", which itself should be viewed as coupled system of the photon and the material system, can be viewed as a "single particle".

In the next section we proceed to consolidate the validity of this picture, especially the existence of particles whose effective mass is produced by the interactions, which is quite analogous to Higgs mechanism: such a model for photon localization certainly exists, which is based on the concept of "polariton", well known in optical and solid physics.

5 Polaritons

As is well known, the refractive index n microscopically comes from the interaction between the light and the medium. From this viewpoint, it is quite natural to think that photons acquire "effective mass" in the medium.

This simple idea can be justified in the picture of "polariton" [3, 4], which was known in the field of optical properties. Polariton (more precisely, "exciton polariton") is nothing but a synthetic system of free photon and exciton (the excitation of the material field caused by light is regarded as a quantum field).

A polariton satisfies the on-shell condition different from free photon

$$E^2 - c^2 p^2 = m_{\text{eff pol}}^2 c^4 > 0. \tag{9}$$

Here $m_{\text{eff pol}}$ denotes the effective mass of the polariton.

If we consider interacting photons as particles with effective mass, the framework in the Newton–Wigner [8] and Wightman [13] itself gives the way of localization.

As we remarked earlier, the meaning of localizability here means that position at each time as physical quantity depending on some chosen reference inertial system. By taking a stationary coordinate system for a homogeneous medium as a reference system, it becomes possible to define a physical quantity consistent with our intuition as position of photons.

More concretely, photon localization problem for photons in a homogeneous medium can be solved as follows [11, 12]:

Let us consider the chain of processes composed of creation of an "excition (an excited state of polarization field above the Fermi surface)" and annihilation of a photon followed by annihilation of an exciton and creation of a photon.

The chain of processes itself is often considered as the motion of particles called *polaritons* (in this case "exciton–polaritons"), which constitute particles associated with the coupled wave of the polarization wave and electromagnetic wave.

The concept of polariton has been introduced to develop a microscopic theory of electromagnetic interactions in materials, i.e. the behavior of photons in material systems [3, 4].

Photons become polaritons by the interaction with matter. The polariton picture has provided an approximation better than the scenarios without it. Moreover, the velocity of polaritons discussed below gives another confirmation of the presence of an effective mass.

It is well known that the permittivity $\epsilon(\omega)$ is given by

$$\epsilon(\omega) = n^2 = \frac{c^2 k^2}{\omega^2}. \tag{10}$$

Hence, we can determine the dispersion relation (between frequency and wave number), which is nothing but the on-shell condition, of polariton once the formula of permittivity is specified. In general, this dispersion relation implies branching, quite analogous to the Higgs mechanism. The signal pulse corresponding to each branch can also be detected in many optical experiments. For example, see the experiments in [5] cited below.

In the simplest case, the permittivity is given by the transverse frequency ω_T of exciton's as follows:

$$\epsilon(\omega) = \epsilon_\infty + \frac{\omega_T^2(\epsilon_{st} - \epsilon_\infty)}{\omega_T^2 - \omega^2}, \tag{11}$$

where ϵ_∞ denotes $\lim_{\omega \to \infty} \epsilon(\omega)$ and $\epsilon_{st} = \epsilon(0)$ (static permittivity).

With a slight improvement through the wavenumber dependence of the exciton energy, the theoretical result of polariton velocity $\frac{\partial \omega}{\partial \mathbf{k}} < c$ based on the above dispersion

1C

relation, or the on-shell condition, can explain satisfactorily experimental data of the passing time of light in materials (for example, [5]). This strongly supports the validity of the polariton picture, and hence, of our argument for the photon localization problem.

6 Dressed photons

As we have discussed, the arguments of Newton–Wigner [8] and the theorem of Wightman [13] says the following in short: for position to have physical meaning, it must have effective mass.

Then the next question is what will happen if we consider localization possibilities beyond homogeneous media and more general forms.

As a typical example of more general form of localization via interaction, let us consider the system composed of light and nanoparticles. In this context the notion of "dressed photons" [9] is introduced as a universal model for photon localization.

If we focus on the interaction of free photons and excitons as a synthetic system there always remain some aspects not to be covered in on-shell framework alone. In spite of this serious obstruction, all the discussion so far has been done ironically within the on-shell framework.

It should be evident that light in the coupled system with nanoparticles can no longer be captured in the on-shell framework.

Let us consider the coupled system composed of two nanoparticles included in a homogeneous medium. When the light enters the coupled system, photons become polaritons in a uniform medium as we have discussed. Then the polaritons intermediate the interaction between two particles.

By applying the methods of renormalization (see Chapter 2, especially Section 2-2, in [4] and references therein), the main part of interaction can be described by Yukawa-type potential. Microscopically, it means that two nanoparticles exchange the massive off-shell particles (or "virtual particles"), which can be interpreted as "photons dressed by excitation of nanoparticles". We call the off-shell particle as "dressed photon" (DP) [9].

As a Yukawa field, the dressed photon field around a nanoparticle satisfies the (time-independent) Klein–Gordon equation:

$$\left[\nabla^2 - \left(\frac{m_{DP} c}{\hbar} \right)^2 \right] \phi(r) = 0. \tag{12}$$

Here m_{DP} denote the mass of the dressed photon given by the renormalization method (see Chapter 2, especially

Section 2-2, in [9] and references therein), which is dependent on the effective mass of the electrons in the nanoparticles and the effective mass of the polaritons.

The solution for the Klein–Gordon equation is Yukawa type:

$$\phi(r) = \frac{e^{-(\frac{m_{DP} c}{\hbar}) r}}{r}. \tag{13}$$

Hence, the dressed photons are localized around the particle. The scale of the effective radius of the dressed photon field is almost the same as the one of the nanoparticle.

In this paper we have started from the photon localization problem and have clarified the significance of the concept of dressed photon. For free photons, position is not an intrinsic physical quantity, only interaction with matter allows localization. Hence, the simple answer to our original question "Who has seen a free photon ?" is, just "Neither I nor you". But when the matter reacts trembling, interacting photons are there.

If the matter is macroscopically homogeneous, it was possible to solve the localization problem within the on-shell framework in terms of polariton.

As soon as taking the nanoparticles into account, however, it is necessary to think of off-shell particle which we call dressed photon. Unlike the case of a homogeneous medium, here the translational symmetry is broken and the momentum conservation is violated.

Therefore, if we try to think about the interaction between light and matter under such circumstances, we must inevitably get into the off-shell world. The intrinsic energy fluctuation of the light current gives the physical basis for "off-shell" interaction.

In short, dressed photons are nothing but the excitations of the quantum field of composite system of photons and nanoparticles with macro-system based on the nonequilibrium stationary state as a kind of fluctuating "vacuum".

7 Conclusion

The perspective above gives the fundamental insight: the essential mathematical structure of quantum field theory for the so-called elementary particles in subatomic scale can also be applied to certain phenomena in the nanoscale. This insight will actualize completely new interplays between mathematical physics and optical technology.

In the history of modern physics, such a biased idea has been prevailing as a "common sense" that on-shell is fundamental and that off-shell plays role only in the subatomic scale, as has been symbolized by too much emphasis on the "famous formula" $E = mc^2$. The discovery of

dressed photons and its various applications, however, will promote fundamental change in such a biased "common sense".

Here the fundamental is rather off-shell: the possibility to research and apply "light as a quantum field" beyond the on-shell particle picture has already opened up. Speaking more ambitiously, the possibility to construct "off-shell science" that analyzes various phenomena in a wide range of scales not restricted to the combination of light and nanoparticles is open also in the universal framework. In other words, by the discovery of dressed photons the photon localization problem has turned out to be the entrance to the coming off-shell science.

References

1. M. Abraham, Rend. Circ. Mat. Palermo **28**, 1 (1909)
2. S.M. Barnett, Phys. Rev. Lett. **104**, 070401 (2010)
3. U. Fano, Phys. Rev. **103**, 1202 (1956)
4. J.J. Hopfield, Phys. Rev. **112**, 1555 (1958)
5. Y. Masumoto, Y. Unuma, Y. Tanaka, S. Shionoya, J. Phys. Soc. Jpn. **47**, 1844 (1979)
6. H. Minkowski, Nach. Königl. Ges. Wiss. Göttingen **53** (1908)
7. H. Minkowski, Math. Ann. **68** 472 **(Reprinted 1910)**
8. D. Newton, E.P. Wigner, Rev. Mod. Phys. **21**, 400 (1949)
9. M. Ohtsu, *Dressed Photons* (Springer, Berlin, 2013), pp. 11–36
10. I. Ojima, Quantum Probab WNA **26**, 277 (2010)
11. I. Ojima, H. Saigo, Open Syst. Inf. Dyn. **19**, 1250008 (2012)
12. I. Ojima, H. Saigo, Mathematics **2015**(3), 897 (2015)
13. A.S. Wightman, Rev. Mod. Phys. **34**, 845 (1962)

Dependences of emission intensity of Si light-emitting diodes on dressed-photon–phonon-assisted annealing conditions and driving current

Jun Hyoung Kim[1] · Tadashi Kawazoe[2] · Motoichi Ohtsu[1,3]

Abstract We investigated how the injected current and the irradiation light power for dressed-photon–phonon (DPP)-assisted annealing affected the performance of the fabricated device. It was shown that there exists a threshold injection current for DPP-assisted annealing. In the case of the devices we fabricated, the threshold current was about 400 mA: When the injected current was below the threshold, the electroluminescence emission intensity did not change even after DPP-assisted annealing. On the other hand, when the injected current was above the threshold, the emission intensity increased by two orders of magnitude. The role of irradiation light was also examined and it was found that the emission spectral profile varied depending on the intensity of the irradiation light power in DPP-assisted annealing. Furthermore, we confirmed that the emission intensity had a quadratic dependence on the driving current when the driving current was higher than 400 mA. This quadratic dependence was considered to be due to electron–electron scattering.

✉ Motoichi Ohtsu
  ohtsu@nanophotonics.t.u-tokyo.ac.jp

[1] Graduate School of Engineering, Institute of Engineering Innovation, The University of Tokyo, 2-11-16 Yayoi, Bunkyo-ku, Tokyo 113-8656, Japan

[2] Tokyo Denki University, 5 Senju-Asahi-cho, Adachi-ku, Tokyo 120-8551, Japan

[3] Research Origin for Dressed Photon, University of Tokyo, Bdg. Eng-9, 2-11-16 Yayoi, Bunkyo-ku, Tokyo 113-8656, Japan

1 Introduction

Crystalline silicon (Si) has long been a key material supporting the development of technology for more than half a century because of its numerous advantages: Si is an abundant material in the earth's crust, and it is easy to produce high-quality Si substrates. In addition, the rapid development of fine process technology has made Si the most popularly used material for electronics.

However, because Si is an indirect transition-type semiconductor, it has been considered to be unsuitable for light-emitting devices; since the bottom of the conduction band and the top of the valence band in Si are at different positions in reciprocal lattice space, the momentum conservation law requires an interaction between an electron–hole pair and phonons for radiative recombination. However, the probability of this interaction is low. Nevertheless, Si has been the subject of extensive research on the fabrication of Si light-emitting devices because of its excellent compatibility with electronic devices and the merits mentioned above. These include, for example, research using nanoparticles such as quantum dots [1] and porous Si [2], or using the Raman effect [3]. However, the devices fabricated in these research studies have some limitations, such as low efficiency, the need to operate at low temperature, complicated fabrication processes, and the difficulty of current injection.

To solve these problems, a novel method that exploits the dressed-photon (DP) has been invented [4–6]. The DP is a quasi-particle created when a photon couples with an electron–hole pair as a result of a near-field interaction. Theoretical studies have shown that a DP could excite multi-mode coherent phonons and create a coupled state with these multi-mode coherent phonons, called a dressed-photon–phonon (DPP) [4, 7]. The operating principle of a

Springer

light-emitting device based on a DPP is that electron–hole pairs could receive enough momentum from coupled coherent phonons if the spatial distributions of dopants in a p–n homojunction could be optimized for creating DPPs. Therefore, the light emission efficiency would be drastically increased by obeying the momentum conservation law.

In the present paper, first, the principle and method of DPP-assisted annealing for fabricating Si-based LEDs are described (Sects. 2, 3, respectively), and then their light emission features and dependences on the injected current, originating from the DPP-assisted annealing, are presented (Sect. 4).

2 Principle of fabrication

A novel method, named DPP-assisted annealing, has been invented by the authors to fabricate Si light-emitting diodes (LEDs) [4, 5]. The principles of this method are as follows: When a forward current I_{anneal} is injected into a p–n homojunction, it generates Joule energy in the crystal. As a result, dopants (B atoms) diffuse, causing their spatial distribution to vary. As a result of this diffusion, the spatial distribution of B atoms in some regions can become suitable for creating DPPs [8]. In these regions, stimulated emission is brought about because the created DPPs allow the injected carriers to recombine radiatively through interaction with phonons, as described in Sect. 1. Since the emitted light propagates away to the outside of the Si crystal, a part of the Joule energy is dissipated in the form of photons, by which the Si crystal is locally cooled, and consequently, the diffusion rate of B atoms locally decreases. As a result of the balance between the heating by Joule energy and cooling by stimulated emission, the distribution of B atoms tends to reach a stationary state in a self-organized manner [9], and this state can be the optimum state for photon emission. Here, it should be noted that a unique feature, named photon breeding, has been found in the emission process [8, 9]. That is, the photon energy $h\nu_{em}$ of the light emitted from the fabricated device is equivalent to the photon energy $h\nu_{anneal}$ of the light irradiated during the DPP-assisted annealing.

A recent study has found that DPP-assisted annealing varies the distribution of B atoms such that B atom-pairs tend to orient in the <100> direction [8]. Phonons can be strongly confined at these B atom-pairs because the pairs serve as cavity resonators for the lattice vibration [7]. As a result, localized phonons can be created (Fig. 1). Since the <100> direction corresponds to the $\Gamma - X$ direction in reciprocal lattice space and the DP excites localized multimode coherent phonons at the B atom-pairs, DPPs having momenta necessary for radiative recombination are
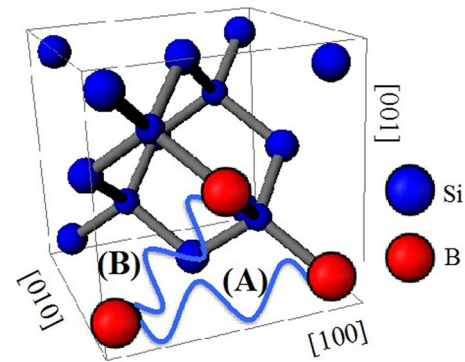
Fig. 1 Schematic explanation of localized phonons. Sinusoidal curves (A) and (B) represent localized phonons created at B atom-pairs oriented in the <100> direction and another direction, respectively

created. Therefore, the more B atom-pairs tend to orient in the <100> direction, the higher the possibility of radiative recombination is. Moreover, a physical model based on a two-level quantum mechanical system has successfully explained the dynamics of DPP-assisted annealing and shown that the optimum spatial distribution of B atoms is formed at a microscopic level by DPP-assisted annealing [9]. More recent studies have shown that the measured positions of phonon sidebands in the emission spectrum agreed well with theoretical calculations that assumed coupling of electron–hole pairs with LO-mode and TO-mode phonons via DPPs [10].

Based on these theoretically and practically sound foundations, LEDs using SiC or GaP, which are indirect transition-type semiconductors [5, 11, 12], and bulk Si crystal-based lasers [6, 13] have also been successfully fabricated.

3 Device fabrication

To fabricate a Si diode, As-doped n-type Si substrates with a thickness of 625 μm were used. The orientation of the substrates was (100), and the electrical resistivity was 10 Ω cm. These substrates were subjected to ion implantation to form a p–n homojunction. That is, B atoms were implanted as donors with energy of 700 keV and a dose of $1.7 \times 10^{14}/cm^2$. The peak concentration of B atoms was $1 \times 10^{19}/cm^3$. We skipped the normally performed subsequent thermal annealing process for two reasons: (1) Activation and recovery of the crystallinity should be accomplished during the DPP-assisted annealing process. (2) Analysis of the acquired Raman spectra showed that they did not contain any spectral components caused by damage due to ion implantation.

An Al thin film with a thickness of 300 nm was deposited by sputtering on the back side (the n-type side) to

serve as an anode. We used a double layer for the front side (the p-type side) by successively depositing an ITO thin film with a thickness of 100 nm and a Pt thin film with a thickness of 150 nm. The Pt layer was patterned into a mesh-like shape by a lift-off process. This double-layered cathode was designed to allow the light to irradiate the device surface during the DPP-assisted annealing and to efficiently extract the electroluminescence (EL) light emitted from the p–n homojunction. Then, the substrate was diced into 1 mm × 1 mm chips, and the chips were fixed to a PCB by soldering. Finally, wire-bonding was performed. Figure 2a shows a photograph of the fabricated Si diode. Figure 2b shows the measured relationship between the forward bias voltage and the driving current I injected into the device. Figure 2c indicates a fine rectification characteristic in the low current region, and a negative resistance at $I > 80$ mA.

After the fabrication above, DPP-assisted annealing was carried out. A Peltier device was used to keep the temperature of the Si diode constant. A forward current was injected into the Si diode. To prevent the device from being damaged by a temperature increase during the DPP-assisted annealing, a triangle-wave current I_{anneal} of 1-Hz repetition frequency was injected. During this injection, the Si diode surface was irradiated with CW light with energy

$hv_{anneal} = 0.943$ eV (wavelength, 1313 nm). The irradiation light power was fixed at 1 W.

4 Results and discussion

We examined the dependences of the EL spectral features on the DPP-assisted annealing conditions. First, we examined the dependence on the injected current I_{anneal}. For the DPP-assisted annealing, the irradiation power was set to 1 W. Figure 3 shows the EL spectral profiles acquired when the DC injection current I for driving the fabricated device was 300 mA. It is clear from Fig. 3a that when the peak value of the triangle-wave current I_{anneal} was 250 mA, the weak EL spectrum did not change its profile or emission intensity even after DPP-assisted annealing for 8 h. On the other hand, Fig. 3b shows that when the peak of the triangle-wave current I_{anneal} was increased to 500 mA, the EL spectral profiles changed significantly, and the emission intensity increased by two orders of magnitude after DPP-assisted annealing for only 2 h. We examined this increase by incrementally increasing I_{anneal} in 50 mA steps. The maximum annealing time was set to 8 h. As a result of this examination, we found that the effect of DPP-assisted annealing (the increase in the emission intensity) was seen only when the peak of the triangle-

Fig. 2 **a** Photograph of the fabricated Si diode. **b**, **c** Measured relationships between the forward bias voltage and the driving current I injected into the device (**b** and **c** are low and high current regions, respectively). In **c**, negative resistance is seen at $I > 80$ mA
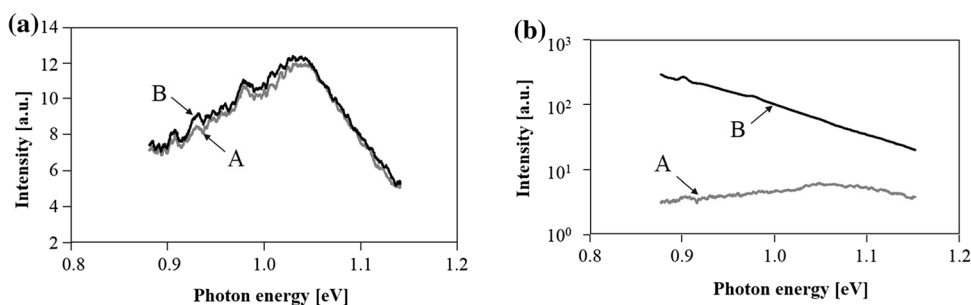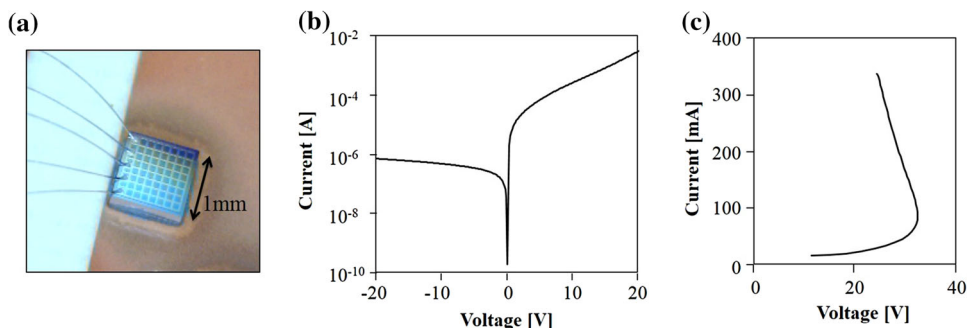
Fig. 3 EL spectral profiles acquired when the DC injection current I for driving the fabricated device was 300 mA. For the DPP-assisted annealing, the irradiation power was set to 1 W. **a** Spectra before DPP-assisted annealing (curve A) and after DPP-assisted annealing for 8 h ($I_{anneal} = 250$ mA) (curve B). **b** Spectra before DPP-assisted annealing (curve A) and after DPP-assisted annealing for 2 h ($I_{anneal} = 500$ mA) (curve B)
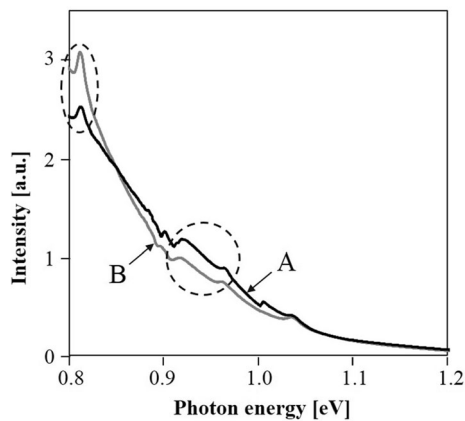
Fig. 4 EL emission spectral profiles at the driving current $I = 300$ mA, which were acquired to examine the contribution of the irradiation power to the DPP-assisted annealing. The current I_{anneal} injected for the DPP-assisted annealing was set to 500 mA. The irradiation power for the DPP-assisted annealing was 1 W for sample 1 (curve A) and 300 mW for sample 2 (curve B). *Broken circle* and *ellipse* represent a bump centered at 0.943 eV (wavelength, 1313 nm) and a narrow peak at 0.815 eV (wavelength, 1520 nm), respectively

wave current I_{anneal} was higher than about 400 mA, which represents the threshold of the injected current I_{anneal} required for DPP-assisted annealing.

Second, we examined how the irradiation light power contributed to the DPP-assisted annealing using two samples: samples 1 and 2 were irradiated with light having powers of 1 W and 300 mW, respectively. The peak of the triangle-wave current I_{anneal} was set to 500 mA. After the DPP-assisted annealing, the EL spectra were acquired with a driving current I of 300 mA. Figure 4 shows the result, which represents two specific features. One is a bump centered at 0.943 eV (wavelength, 1313 nm), which is equal to the energy $h\nu_{anneal}$ of the light irradiated during the DPP-assisted annealing. The height of this bump in the case of sample 1 was higher than that in the case of sample 2, which is because of the photon breeding described in Sect. 2 [8, 9]. The higher the light power, the clearer the photon breeding feature is.

The other feature is a narrow peak at 0.815 eV (wavelength, 1520 nm), whose height in the case of sample 1 was lower than that in the case of sample 2. This was attributed to the distribution characteristics of the B atom-pairs. The number of B atom-pairs as a function of the length d of the pair has been represented by the Weibull distribution

$$p(d) = (3/\beta) \cdot (d/\beta)^2 \cdot \exp\left[-(d/\beta)^3\right] \quad (1)$$

where $\beta = \sqrt[3]{3/4\pi\delta}$ and δ is the concentration of the doped B atoms [8]. By least squares fitting of Eq. (1) to the measured distribution profiles, it was found that $p(d)$ took a maximum at $d = 5a$ (a: the lattice constant of Si) [8]. Here,

to obey the momentum conservation law for radiative recombination, the value of the wave number of the phonon has to be $1/a$ for coupling with an electron–hole pair. This is because the difference in the wave-number at the Γ point and the X point in reciprocal space is $1/a$. When d is equal to $5a$, the value of the wave-number of the lowest localized phonon mode is $1/5a$, and thus, the electron–hole pair requires five phonons to obey the momentum conservation law [14]. Based on this requirement, the emitted photon energy is given by $h\nu_{em} = E_g - 5E_{LO}$, where E_g (= 1.14 eV) and E_{LO} (= 65 meV) are the bandgap energy of Si and the LO phonon energy, respectively. From this equation, $h\nu_{em}$ was found to be 0.815 eV. That is, the narrow peak at 0.815 eV is attributed to the distribution characteristics of B atom-pairs represented by Eq. (1). The height of this peak in the case of sample 1 is lower because the DPP-assisted annealing with higher irradiation power significantly modified the original distribution of B atom-pairs so that photon breeding is clearly manifested at 0.943 eV.

Third, we examined the dependence of the EL emission power on the driving current I. Figure 5a shows the experimental results. The maximum power was 20 mW at $I = 1.0$ A. This figure also shows that the emission power was proportional to I at $I < 400$ mA, which is a known inherent feature of the DPP-assisted process. On the other hand, the emission power was proportional to I^2 at $I > 400$ mA, which may be because the main contribution to the emission was thermal radiation. However, the possibility of this contribution was denied for the following two reasons: (1) Fig. 5b shows the emission spectra acquired over a photon energy range wider than that in Fig. 4. Although the emission intensity in this figure increased with increasing I, the spectral profile does not show any dependence on I. If this emission were due to thermal radiation, they should be blue-shifted with increasing I. (2) No light emission was observed before the DPP-assisted annealing even when I was as high as 1.0 A.

Thus, we concluded that this light emission comes from the momentum transfer between localized phonons and electrons caused by electron–electron scattering, as is schematically explained by Fig. 6. In the case of an LED fabricated with a direct-transition-type semiconductor, electron–electron scattering decreases the light emission efficiency. However, in a DPP-assisted LED, this scattering process plays a different role. As was explained in Sect. 2, the B atom-pairs in the p–n homojunction tend to orient in the <100> direction due to the DPP-assisted annealing. Here, not only phonons but also electrons can be captured by these B atom-pairs because they serve as cavity resonators for creating localized phonons. In other words, electrons can appear due to DPP-assisted annealing even in the area of the energy band structure of Fig. 6 where

Fig. 5 Dependence of the EL emission power and spectral profile on the driving current I. **a** Relation between I and the emission power. **b** Emission spectra acquired for $I = 600$, 800, and 1000 mA (curves A, B, and C, respectively). These spectra were acquired over a photon energy range wider than that in Fig. 4
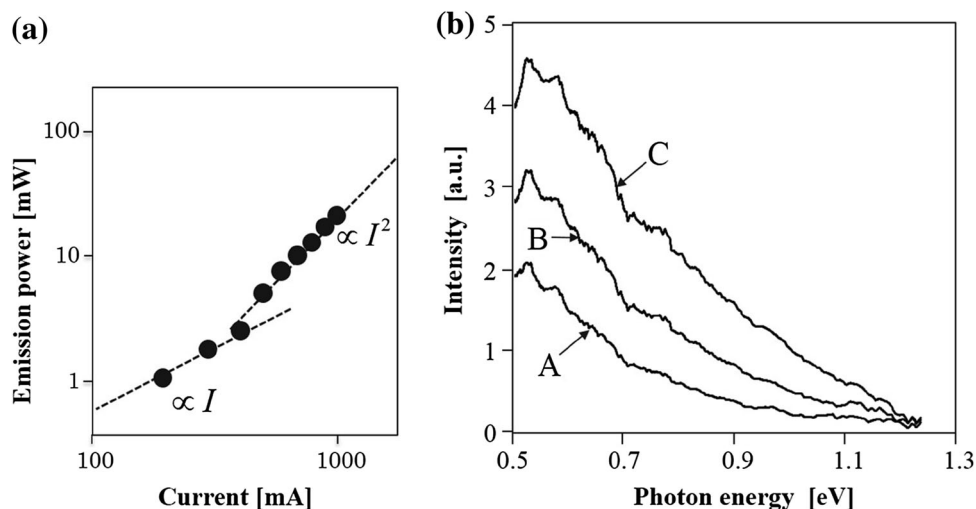
Fig. 6 The energy band structure of Si and schematic explanation of light emission caused by electron–electron scattering. *Black*, *gray*, and *white circles* represent the electrons in the initial, intermediate, and final states of scattering, respectively
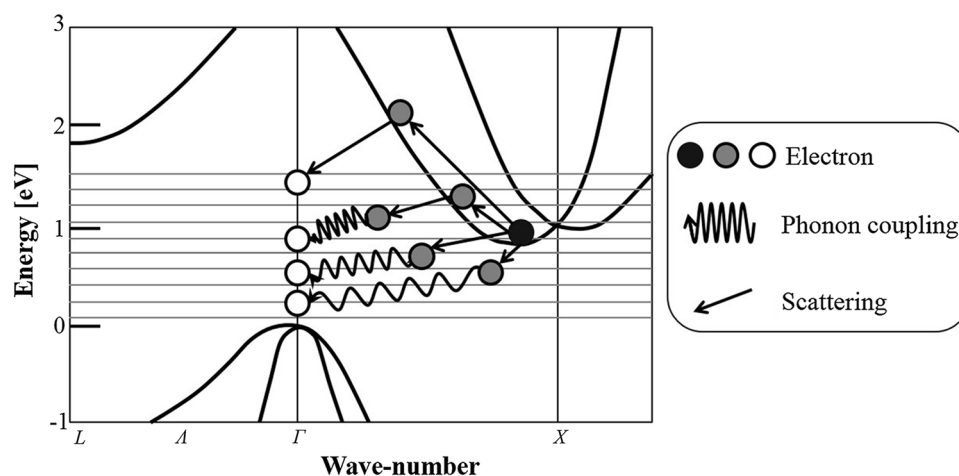
electrons cannot exist originally. Thus, two electrons could couple with localized phonons, leading to light emission by electron–electron scattering and the resulting I^2-dependence of the emission intensity.

5 Conclusion

First, we found that the injection current for generating Joule energy should be higher than a certain threshold in order for DPP-assisted annealing to be effective. In the case of the devices we fabricated, the threshold was about 400 mA. Next, we confirmed the contribution of light irradiation to DPP-assisted annealing: The higher the power of the irradiation light, the higher the emission intensity at the photon energy of the irradiation light (0.943 eV), which represents photon breeding. Finally, we found that the emission power increased in proportion to I^2 ($I > 400$ mA). From this quadratic dependence, light emission at high current was explained by electron–electron scattering.

References

1. N.M. Park, T.S. Kim, S.J. Park, Appl. Phys. Lett. **78**, 2575 (2001)
2. L.T. Canham, Appl. Phys. Lett. **57**, 1046 (1990)
3. H. Rong, R. Jones, A. Liu, O. Cohen, D. Hak, A. Fang, M. Paniccia, Nature **433**, 725 (2005)
4. M. Ohtsu, Nanophotonics **1**, 83 (2012)
5. T. Kawazoe, M. Mueed, M. Ohtsu, Appl. Phys. B **104**, 747 (2011)
6. T. Kawazoe, M. Ohtsu, K. Akahane, N. Yamamoto, Appl. Phys. B **107**, 659 (2012)
7. Y. Tanaka, K. Kobayashi, J. Microsc. **229**, 228 (2008)
8. T. Kawazoe, K. Nishioka, M. Ohtsu, Appl. Phys. A **121**, 1409 (2015)
9. J.H. Kim, T. Kawazoe, M. Ohtsu, Appl. Phys. A **121**, 1395 (2015)
10. M. Yamaguchi, T. Kawazoe, M. Ohtsu, Appl. Phys. A **115**, 119 (2014)
11. T. Kawazoe, M. Ohtsu, Appl. Phys. A **115**, 127 (2014)
12. J.H. Kim, T. Kawazoe, M. Ohtsu, Adv. Opt. Technol. **2015**, Article ID 236014 (2015)
13. H. Tanaka, T. Kawazoe, M. Ohtsu, K. Akahane, N. Yamamoto, Appl. Phys. A **121**, 1377 (2015)
14. M. Ohtsu, *Silicon Light-Emitting Diodes and Lasers* (Springer, Heidelberg, 2016), pp. 35–39

[II] PRESENTATIONS
IN INTERNATIONAL CONFERENCES

Spectral Analysis of a High-Power Infrared Silicon Light Emitting Diode of Dressed Photons

Borriboon Thubthimthong[1], Tadashi Kawazoe[2,3], and Motoichi Ohtsu[1,3,4]

[1]The Institute of Engineering Innovation, School of Engineering, The University of Tokyo, 2-11-16 Yayoi, Bunkyo, Tokyo 113-8656 Japan
[2]Tokyo Denki University, Tokyo, 5 Senju Asahi-cho, Adachi-ku, Tokyo 120-8551, Japan
[3]Nanophotonics Engineering Organization, 1-20-10 Sekiguchi, Bunkyo-ku, Tokyo 120-0014, Japan
[4]Research Origin for Dressed Photon, The University of Tokyo, 2-11-16 Yayoi, Bunkyo-ku, Tokyo 113-8656, Japan
Author e-mail address: borriboon@nanophotonics.t.u-tokyo.ac.jp

Abstract: We investigated infrared photon emission mechanisms in the Si light-emitting diode fabricated by dressed-photon-phonon-assisted annealing. Photoluminescence measurements indicated that triple optical phonons played an important role in the high-power infrared emission of 200 mW.

OCIS codes: (230.3670) Light-emitting diodes; (160.6000) Semiconductor materials; (300.6470) Spectroscopy, semiconductors,

1. Introduction

Recent advances in dressed photon (DP) research have given rise to a new breakthrough in Si light-emitting diodes (LEDs) and Si lasers [1]. Despite being an indirect-band-gap semiconductor, Si can be used as an efficient photon emitters through momentum exchange between conduction-band electrons and dressed photons-phonons (DPP) [1]. The high-power Si LED is possible by engendering special arrangements of borons implanted in Si using the DPP-assisted annealing [2]. Of particular importance is the fact that such DPP-assisted photon emitters show the photon breeding effect where emitted photon energy of the device after the annealing is equal to that of the irradiated photons (at 1.3 μm wavelength) used in the annealing. In this paper, we show the output characteristics of the Si LED. In particular, we investigate, via a photoluminescence study, the effect of the generated DPP states that contribute to the high-power light emissions in the Si LED.

2. Fabrications

The fabricated Si LED is shown in Fig. 1. It consists of a pn homojunction formed by a single-step boron implantation (700 keV acceleration energy, with $10^{19}/cm^3$ concentration) into an As-doped Si substrate (10 Ω-cm). A stable thin-film mesh electrode of Cr/Al compositions was integrated on top of the boron-implanted surface. The back electrode of the LED was fabricated from a Cr/Al/Au triple layer. The fabricated device was soldered onto an AlN printed circuit board. The top thin-film electrode was connected to the circuit board by wire bonding. In order to activate the light emission of the LED, DPP-assisted annealing was performed at atmospheric pressure by irradiating a 1314 nm laser light of a power of 1 W to the upper surface while simultaneously injecting a time-varying electrical current into the device in a forward bias configuration. The time-varying electrical current had a triangular waveform that ramped up and down between 0 A and 1 A at a frequency of 1 Hz. A Peltier temperature controller was used to control the device temperature at 16 ˚C throughout the annealing process that lasted for 2 hours.
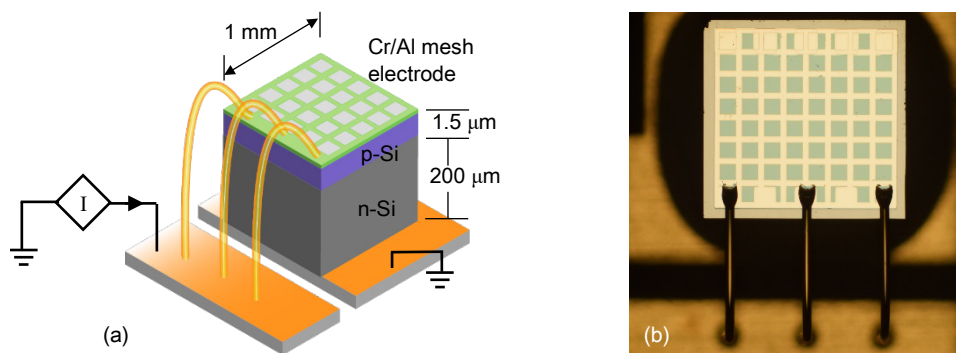

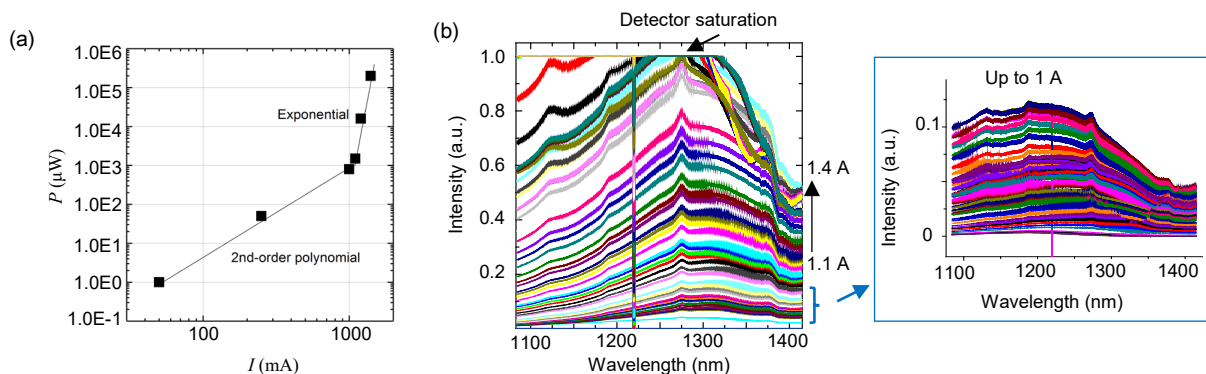Fig. 1. The Si LED. (a) The schematics of the Si LED. (b) The top view photo.

Fig. 2. The measured *P-I* characteristics and EL spectra of the Si LED. (a) The *P-I* characteristics as a function of the forward-biased injected current. (b) The EL spectra at the different injected currents.

3. Characterizations

The optical performance of the fabricated Si LED was evaluated after the fabrication. The characteristics of the total optical output power versus the injected electrical current (*P-I*) of the fabricated Si LED is shown in Fig. 2a. When *I* < 1.0 A, the Auger scattering process dominated, leading to the thermal effect where the optical power is proportional to the square of injected current ($P \propto I^2$). When *I* > 1.0 A, the total optical output power is an exponential function of *I*. In our test, the maximum power as high as 200 mW was obtained at *I* = 1.4 A. This remarkably high optical output power is 100 times as large in comparison with commercially available GaAs LEDs [3]. The external quantum efficiency is as high as 14 %.

To investigate the origin of the high optical output power and the contribution of the DPP, electroluminescence (EL) spectra and photoluminescence (PL) spectra were measured. Fig. 2b shows the EL spectrum obtained from the fabricated Si LED. In the case of *I* < 1.0 A, the EL spectrum shows a broad yet flat emission spectrum below the normalized intensity of 0.2. As shown in the inset of Fig. 2b, the central wavelength was at 1.20 μm (1.03 eV) for *I* < 1.0 A. When *I* > 1.0 A, the emission spectrum shows significantly higher emission intensity for all wavelengths measured. The central wavelength of the spectrum was shifted to 1.28 μm (0.969 eV) which was close to that of annealing laser (1.31 μm or 0.946 eV), indicating the photon breeding effect at high injected current.

Although the contributions of phonons have been discussed previously by the authors [2], clear observations of the emission peaks were difficult because of the broad emission spectrum caused by the Auger scattering process. The PL spectrum analysis can further reveal the electronic structure of the device as well as the contributions of the DPP states at various stages of fabrications. Using a 532 nm laser of a 200 mW output power, we obtained the PL spectra before and after the DPP-assisted annealing. For the PL spectrum before the annealing, we pumped the laser of a large beam spot onto a boron-implanted Si wafer. For the spectrum after the annealing, the laser was focused onto the small device surface. The PL spectra before and after DPP-assisted annealing are shown in Fig. 3a and Fig. 3b, respectively. Figure 3a shows a broad peak centered at 1.104 eV (1123 nm) resulted from the interband transition. No additional PL emission peak were observed. This indicates the lack of DPP states and thus of the DPP contributions before the DPP-assisted annealing. It should be noted that the light intensity in Fig.3a is extremely lower than that in Fig.3b. After the annealing, an emission peaks at 0.924 eV (1342 nm), which was close to that of the annealing laser and that in the EL measurement, were observed. Moreover, the broad emission peak from the band gap transition is shifted to 1.049 eV (1182 nm).

We explain the occurrence of the new emission peaks by using the band diagram of the DPP-assisted Si LED shown in Fig. 3c. The difference in energy of 63 meV between the original broad emission peak of the B-implanted Si before annealing and the red-shifted one from the annealed Si LED is equal to the energy quanta of a single optical phonon (64 meV) [4], indicating the phonon-assisted emission in the Si LED. On the other hand, the 180 meV-shifted energy of the DPP-assisted emission peak appeared at 0.924 eV translates to around 3 phonon energy quanta (3×64 meV), indicating the triple phonon-assisted emission process. We believe that the remarkably high optical output power in the device is contributed also by lesser re-absorptions since the newly created emission peaks around 1.3 μm were not absorbed back by the interband transition.
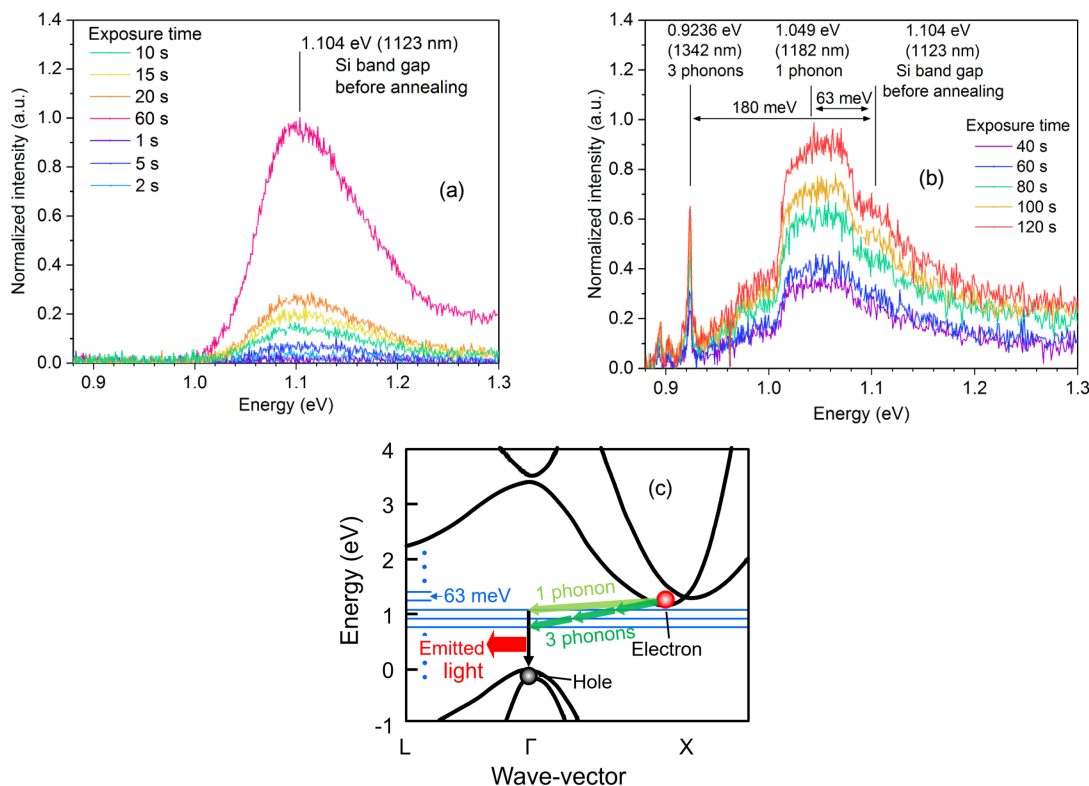
Fig. 3. The PL spectrum measurement results right after the boron implantation (a) and after DPP-assisted annealing (b). The band diagram of the Si LED (c) shows the relaxation process of electrons assisted by the optical phonons. The horizontal blue lines represent the energy levels of the optical phonons equally spaced by 63 meV.

4. Conclusions

The mechanisms of the photon emissions in the Si LED, fabricated by DPP-assisted annealing, was investigated in a PL study by using a 532 nm laser excitation. The *P-I* characteristics together with the EL spectra at different injected currents were measured. We observed the PL emission peaks around 1.3 μm corresponding to those obtained from the EL peaks for high injected current (> 1.0 A) and that of the annealing laser, confirming the photon breeding effect in the Si LED. Photoluminescence measurements indicated coupling between electrons and triple optical phonons played an important role in the high-power infrared emission of 200 mW. Presently, the DPP mechanism has also been applied for a high-power Si laser device that has realized a 14 W optical output power [5].

References
[1] M. Ohtsu, *Silicon Light-Emitting Diodes and Lasers* (Springer, 2016).
[2] T. Kawazoe, M. A. Mueed, and M. Ohtsu. "Highly efficient and broadband Si homojunction structured near-infrared light emitting diodes based on the phonon-assisted optical near-field process." *Applied Physics B: Lasers and Optics* 104.4 (2011): 747-754.
[3] "LED Technical Information." Hamamatsu Photonics K. K. http://www.hamamatsu.com/resources/pdf/ssd/led_kled9001e.pdf. Access: May 29, 2017.
[4] P.M. Amirtharaj and D.G. Seiler, "Optical Properties of Semiconductors" in *Handbook of optics*, M. Bass et al, eds. *Handbook of Optics* (McGraw-Hill, New York, 2001).
[5] T. Kawazoe and S. Sugiura, "High Power Silicon Lasers via Dressed Photon"(invited paper), The 11th Asia-Pacific Conference on Near-field Optics, Tainan, Taiwan, July 10-13, 2017

Novel Attempt in Formulating a Theory of Near-field Optics Beyond the Framework of On-shell Dynamics

Hirofumi Sakuma*, Izumi Ojima* and Motoichi Ohtsu#*

*Research Origin for Dressed Photon, # Institute of Engineering Innovation, School of Engineering, the University of Tokyo
hsakuma1@gmail.com

Abstract: We present here a novel formulation of electromagnetic field in order to make a breakthrough for some longstanding issues in near-field optics and dressed photons. The core guiding principle in our approach is to shed a light on the off-shell aspects in the relevant dynamics, which seems to be unfamiliar yet in many branches of physics, especially including nanophotonics. We discuss a possibility that the elusive natures of optical near-field and dressed photons can successfully be understood by an off-shell view on the phenomena. To provide quantitative explanation of our hypothesis along the above line, we introduce a unified augmented picture of electromagnetic field.

1. Introduction

In contrast to remarkable and plentiful accomplishments made so far in a variety of fields in nanophotonics, the theoretical basis of optical near-field (ONF) and dressed photon (DP) in a quantum theoretical formulation is not firmly consolidated yet. The concepts of ONF and DP were originally introduced by one of the authors, Ohtsu [1], in order to identify anomalous optical phenomena: within the conventional framework of optics these phenomena cannot be explained, because they manifest themselves in a given experimental setting where the core assumptions of the conventional theory are invalidated.

Concerning this point, the prevailing usage of the term DP does not seem to be consistent with its original meaning. It often happens that term DP is used in a wider context including quantized photon-material interactions described by the conventional classical and quantum theories. The issue we are going to address here is to cast a new light on the original meaning of DP from the viewpoint of off-shell dynamics in quantum field theory.

2. Novel model of virtual fluctuating photons

Through our experimental as well as theoretical studies, we are arriving at a conclusion that the elusive features of DP can be attributed to the off-shell natures of the dynamics involved. It is well known that the physical state of a stable free particle is described, as shown in Fig. 1, as a hyperboloid or a mass-shell in the energy-momentum (EM) plane. According to relativistic quantum field theory [2], the description of interaction processes depicted on the EM plane requires quantum fields whose energy-momentum supports are not only timelike and lightlike but also spacelike. Well known examples of spacelike quanta violating the Einstein causality are virtual off-shell photons showing up in Feynman diagrams.
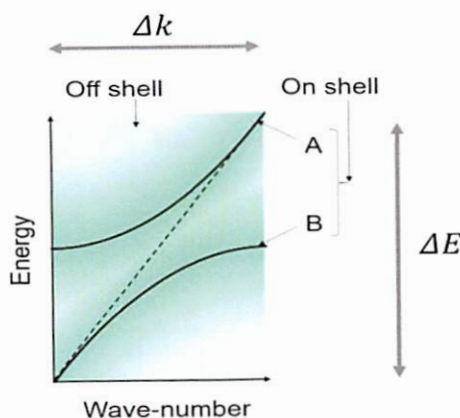

Fig. 1. Dispersion relations in EM (E-k) diagram explaining the difference between on-shell and off-shell states

On the basis of the above arguments we consider that the essential ingredients of a plausible new model of DP are the presence of quantum electromagnetic field whose energy-momentum support involves the timelike as well as spacelike components. We show that such a model construction is actually possible on the basis of Clebsch duality [3] concerning electromagnetic field. That is to say, firstly, we can extend the

conventional electromagnetic theory in such a way that it covers not only timelike and lighlike domain but spacelike one in EM space. In terms of electromagnetic vector potential A^μ, the mutually exclusive two branches respectively corresponding to timelike and spacelike domains can be represented by a twin Proca equations of the following forms

$$\partial_\nu \left(\partial^\nu A^\sigma - \partial^\sigma A^\nu\right) + m^2 A^\sigma = 0, \qquad \partial_\nu \left(\partial^\nu \widetilde{A}^\sigma - \partial^\sigma \widetilde{A}^\nu\right) - l^2 \widetilde{A}^\sigma = 0, \qquad \text{(1a, b)}$$

where $\widetilde{A}^\mu$ denotes extended electromagnetic potential whose energy-momentum is spacelike. Secondly, corresponding to the aforementioned picture of $\widetilde{A}^\mu$, we can show that the energy-momentum tensor $\widetilde{G}_\mu^\nu$ of Clebsch-dual electromagnetic field $\widetilde{F}^{\mu\nu} \equiv \partial_\mu \widetilde{A}^\nu - \partial_\nu \widetilde{A}^\mu$ automatically satisfies the energy-momentum conservation law:

$$\nabla_\nu \widetilde{G}_\mu^\nu = 0, \qquad \widetilde{G}_\mu^\nu \equiv -\widetilde{R}_{\mu\sigma}^{\ \nu\sigma} + \frac{1}{2} \widetilde{R}_{\alpha\beta}^{\ \alpha\beta} g_\mu^\nu, \qquad \widetilde{R}_{\mu\sigma}^{\ \nu\sigma} \equiv \widetilde{F}_{\mu\sigma} \widetilde{F}^{\nu\sigma}, \qquad \text{(2a, b, c)}$$

which is isomorphic to the Einstein equation of the form

$$\nabla_\nu G_\mu^\nu = 0, \qquad G_\mu^\nu \equiv -R_{\mu\sigma}^{\ \nu\sigma} + \frac{1}{2} R_{\alpha\beta}^{\ \alpha\beta} g_\mu^\nu, \qquad G_\mu^\nu = T_\mu^\nu, \qquad \text{(3a, b, c)}$$

where G_μ^ν, $R_{\mu\sigma}^{\ \nu\sigma}$, g_μ^ν respectively denote Einstein, Riemann curvature and metric tensors while T_μ^ν is the energy-momentum tensor of a given physical field and ∇_ν denotes covariant derivative. The above isomorphism between $\widetilde{G}_\mu^\nu$ and G_μ^ν implies that $\widetilde{G}_\mu^\nu$ may represent a part of the energy-momentum of "spacetime" as a physical entity. Recall that the physical property of spacetime was elucidated first by the special theory of relativity in which light field plays a crucial role and it was extended further to a curved spacetime by the general theory of relativity in which (3a,b,c) hold. We believe that our new model based on (1b) leading to the isomorphism is consistent with the abovementioned close relation between light field and spacetime structure. A salient feature of near-field optics and dressed photons is an intense localization of the field under consideration, which suggests that the field accompanies extremely high wavenumber components in the transformed Fourier space. It is obvious that a realization of such a localized field necessarily accompanies high energy (frequency) components if the field possesses a timelike property. On the other hand, if it possesses a spacelike property, then high frequency components are no longer necessary to attain it, which seems to be consistent with experimental results. A quantitative estimate on the degree of localization of DP was given by Sangu et al. [4] showing that the field falls off like Yukawa potential and it can be shown that similar fall-off nature of the field is reproduced by our new model.

3. References

[1] M. Ohtsu, From classical to modern near-field optics and the future, (Opt. Rev. 21 2014, pp. 905-910)

[2] R. F. Streater, A. S. Wightman, PCT, Spin and Statistics, and All That, (Princeton University Press, 2000)

[3] H. Sakuma, I. Ojima, M. Ohtsu, Dressed Photons in a New Paradigm of Off-shell Quantum Field, (To appear in Progr. Q. E. 2017)

[4] S. Sangu, K. Kobayashi, M. Ohtsu, Optical near fields as photon-matter interacting systems, (J. Microscopy, 2001, pp. 279-285)

Novel View Towards Gauge Condition as a Conceptual Basis of Dressed Photons

Hirofumi Sakuma*, Izumi Ojima* and Motoichi Ohtsu#*

*Research Origin for Dressed Photon,
#Institute of Engineering Innovation, School of Engineering, the University of Tokyo
E-mail address: (hsakuma1@gmail.com)

Abstract: Owing to the undue segmentation of disciplines, there have been serious confusions in the physical interpretation of the longitudinal mode of electromagnetic (EM) field, which is directly related to the gauge conditions. Here we discuss this important problem on the basis of the main results of our series of works including updated Clebsch-dual structure of electromagnetic field, which is crucial for understanding the near-field "light" or dressed photons as quasi-particles arising from virtual photons. In the use of the analyticity playing key roles, we show that four divergence of electromagnetic potential associated with wave propagation plays physical roles in dressed photon dynamics.

The concept of dressed photons proposed by Ohtsu [1] arising from the optical technology concerning near-field lights, is now one of the important focus issues actively investigated, since it has opened an entirely new field in nanophotonics whose methodological approaches are substantially different from the conventional ones. As a radically new attempt of understanding the elusive phenomenon at issue, Sakuma et al. [2,3], has proposed a novel model termed as the Clebsch-dual representation (CDR) of electromagnetic (EM) field, which is isomorphic to EM field but whose energy-momentum support covers all the lightlike and spacelike domains complementary to the lightlike and timelike domains covered by the original EM field. To sum up the new model in one word, we can say that Clebsch-parametrised vector (EM) potential in the new (vortex) model leads to a vorticity field quite akin to Lorentzian spinor field on which $SL(2, C)$ acts, thereby the derived vortex dynamics becomes isomorphic to Maxwell's equations. The duality between EM field and CDR can be expressed clearly in terms of Proca equation and its counterpart:

$$\partial_\nu \left(\partial_\nu A^\sigma - \partial^\sigma A^\nu \right) + m^2 A^\sigma = 0 ; \quad \partial_\nu \left(\partial_\nu U^\sigma - \partial^\sigma U^\nu \right) - \kappa^2 U^\sigma = 0 , \qquad \text{(1a, b)}$$

where A^σ and U^σ denote vector potentials in respective systems, m and κ are real constants. Referring to the following Maxwell's equation

$$j^\sigma = \partial_\nu \left(\partial_\nu A^\sigma - \partial^\sigma A^\nu \right) = \partial_\nu \partial_\nu A^\sigma - \partial^\sigma \left(\partial_\nu A^\nu \right) = \partial_\nu \partial_\nu \alpha^\sigma ; \quad A^\sigma = \alpha^\sigma + \partial^\sigma \chi \text{ with } \partial_\sigma \alpha^\sigma = 0 , \quad \text{(2a, b)}$$

we immediately see the well-known result of transverse wave propagation valid in the vacuum: $0 = j^\sigma = \partial_\nu \partial_\nu \alpha^\sigma$. Directly from the conservation of energy-momentum tensor of EM wave field, however, we can show that another solution is physically permissible in the vacuum, namely,

$$\partial_\nu \partial_\nu A^\sigma = 0 \text{ with } j^\sigma = -\partial^\sigma \left(\partial_\nu A^\nu \right) \text{ and } \partial_\sigma \partial^\sigma \left(\partial_\nu A^\nu \right) = 0 . \qquad \text{(3a, b, c)}$$

The solution given above is not new in itself, as the Lagrangian associated with it is acturally the well-known one used in the covariant quantization of EM field in the Feynman-type gauges.

What is new in our discussion is that, contrary to the conventional interpretation of EM vector potential, we claim that $\phi \equiv \partial_\nu A^\nu$ is a physical quantity in the sense that the vector current given in (3b) can be reinterpreted as an electric field current which is longitudinally propagating with the speed of light. This is proved by referring to the well-known correspondence between the Cauchy-Riemann relation and the velocity potential and streamfunction of two dimensional non-divergent and irrotational flows. The important implication of this is that the congruence of shear-free null geodesics given by (3b) provides a key to physically meaningful "basis" vector field of CDR. In our opinion, as to the term "dressed photon", the consensus has not been reached yet and there seems to be a confusion in the usage of the term. As is explained in [1], dressed photons as our target particles are quasi-particle arising from virtual off-shell photons. A salient feature of CDR is that, due to its spacelike characteristics, it can naturally explain Yukawa potential type exponential decay of a dressed photon's amplitude in the radial direction. The present quantum-field theoretical derivation of the exponential decay in a unified scheme should be contrasted with that discussed in Sangu et al. [4] based on the quantum mechanical setting-up.

[1]M. Ohtsu, "From classical to modern near-field optics and the future", Opt. Rev. 21 (2014), pp. 905-910.
[2]H. Sakuma, I. Ojima and M. Ohtsu, "Dressed Photons in a New Paradigm of Off-shell Quantum Fields", to appear in Progress in Q. E.
[3]H. Sakuma, "Note on a novel vortex dynamics of spacetime as a heuristic model of the vacuum energy", (2014), arXiv:1409.2607[gr-qc]
[4] S. Sangu, K. Kobayashi and M. Ohtsu, "Optical near fields as photon-matter interacting systems", J. Microscopy, (2001), pp. 279-285

Irrationality of the Permittivity in Non-resonant Near-field Optics

**Itsuki Banno[1] and Motoichi Ohtsu[2, 3]**

[1] *Interdisciplinary Graduate School of Medicine and Engineering, University of Yamanashi*
banno@yamanashi.ac.jp

[2] *Institute of Engineering Innovation, School of Engineering, the University of Tokyo,* [3] *Research Origin for Dressed Photon*
ohtsu@nanophotonics.t.u-tokyo.ac.jp

Abstract: The present theory shows the irrationality of the macroscopic constitutive equation (MCE) using the permittivity in near-field optics (NFO). This irrationality originates in the fact that the longitudinal and transverse electric fields coexist in NFO and cause different responses under a non-resonant condition. Otherwise, i.e., under the resonant condition or the far-field observation condition, the MCE works soundly. A reasonable CE is suggested for a two-level system in NFO.

1. Introduction: the Longitudinal Incident Characterizing the Near-field Optics

Suppose a small-scale material is placed in the vicinity of the nanostructure, which irradiates the longitudinal and transverse electric fields ($\Delta \mathbf{E}^{(\ell)}$ and $\Delta \mathbf{E}^{(t)}$) simultaneouly (Fig.1). The existence of $\Delta \mathbf{E}^{(\ell)}$ incident distinguishes such the NF optical system from the ordinary optical system. Here, the $\Delta \mathbf{E}^{(\ell)}$ is yielded by the charge density on the nanostructure, obeys Coulomb's law, and has non-radiative nature, while the $\Delta \mathbf{E}^{(t)}$ is yielded by the transverse current density on the nanostructure, obeys Ampere-Maxwell's law and Faraday's law, and has radiative nature accompanied by the magnetic field. The $\Delta \mathbf{E}^{(\ell)}$ and $\Delta \mathbf{E}^{(t)}$ are qualitatively different, so that the responses to those are different as shown in the below.
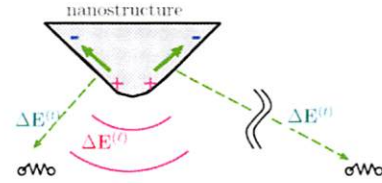
Fig.1: The longitudinal electric field, $\Delta \mathbf{E}^{(\ell)}$ exposes to the material in the NF optical system (the lefthand side), while does not in the ordinary optical system (the righthand side).

2. The Proper Response in a Non-resonant Near-field Optics

Under the Coulomb gauge and the long wave approximation, the $\Delta \mathbf{E}^{(\ell)}$ and $\Delta \mathbf{E}^{(t)}$ are expressed in terms of the scalar and vector potentials, respectively, i.e., $\Delta\varphi(\mathbf{r}, t) = \Delta\varphi(0) - \Delta\mathbf{E}^{(\ell)}(0) \cdot \mathbf{r}\cos\omega t$ and $\Delta\mathbf{A}(\mathbf{r}, t) = -\frac{1}{\omega}\Delta\mathbf{E}^{(t)}(0)\sin(\omega t + \xi)$, where ω is the incident angular frequency, and ξ is the phase difference between the two incidents. Our response theory [1] *treats the* $\Delta \mathbf{E}^{(\ell)}$ *and* $\Delta \mathbf{E}^{(t)}$ *equally* and leads to the induced charge and current density operators as:

$$\Delta\hat{\rho}(\mathbf{r}, t) = \frac{1}{i\hbar}\int_{-\infty}^{t}dt_1\int d^3 r_1 \left\{ \left[\hat{\rho}^{(0)}(\mathbf{r}, t), \hat{\rho}^{(0)}(\mathbf{r}_1, t_1)\right]\Delta\varphi(\mathbf{r}_1, t_1) - \left[\hat{\rho}^{(0)}(\mathbf{r}, t), \hat{j}_{i_1}^{(0)}(\mathbf{r}_1, t_1)\right]\Delta A_{i_1}(\mathbf{r}_1, t_1)\right\},$$

$$= \Delta\hat{\rho}_\varphi(\mathbf{r}, t) + \Delta\hat{\rho}_\mathbf{A}(\mathbf{r}, t), \tag{1}$$

$$\Delta\hat{j}_i(\mathbf{r}, t) = \frac{1}{i\hbar}\int_{-\infty}^{t}dt_1\int d^3 r_1 \left\{ \left[\hat{j}_i^{(0)}(\mathbf{r}, t), \hat{\rho}^{(0)}(\mathbf{r}_1, t_1)\right]\Delta\varphi(\mathbf{r}_1, t_1) - \left[\hat{j}_i^{(0)}(\mathbf{r}, t), \hat{j}_{i_1}^{(0)}(\mathbf{r}_1, t_1)\right]\Delta A_{i_1}(\mathbf{r}_1, t_1)\right\} - \frac{q}{m}\hat{\rho}^{(0)}(\mathbf{r}, t)\Delta A_i(\mathbf{r}, t),$$

$$= \Delta\hat{j}_{\varphi\, i}(\mathbf{r}, t) + \Delta\hat{j}_{\mathbf{A}\, i}(\mathbf{r}, t) + \Delta\hat{j}_{\mathbf{A}\,\text{local}\, i}(\mathbf{r}, t), \tag{2}$$

where $\hat{\rho}^{(0)}, \hat{j}_i^{(0)}$ are the charge and current density operators in the non-perturbed system, respectively. Applying to a two-level spinless system, one obtains the relationships between the response functions to $\Delta \mathbf{E}^{(\ell)}$ and $\Delta \mathbf{E}^{(t)}$:

$$\frac{\Delta\rho_\mathbf{A}(\mathbf{r}, t)}{\Delta E_j^{(t)}(0)\cos(\omega t + \xi)} = \frac{\Delta\rho_\varphi(\mathbf{r}, t)}{\Delta E_j^{(\ell)}(0)\cos\omega t}, \tag{3}$$

$$\frac{\Delta j_{\mathbf{A}\, i}(\mathbf{r}, t)}{\Delta E_j^{(t)}(0)\sin(\omega t + \xi)} = \eta^2 \frac{\Delta j_{\varphi\, i}(\mathbf{r}, t)}{\Delta E_j^{(\ell)}(0)\sin\omega t}, \quad \frac{\Delta j_{\mathbf{A}\,\text{local}\, i}(\mathbf{r}, t)}{\Delta E_j^{(t)}(0)\sin(\omega t + \xi)} = (1 - \eta^2)f_{ij}(\mathbf{r})\frac{\Delta j_{\varphi\, i}(\mathbf{r}, t)}{\Delta E_j^{(\ell)}(0)\sin\omega t}, \tag{4}$$

where $\eta = \frac{\hbar\Delta\omega_1}{\hbar\omega} = \frac{\text{excitation energy}}{\text{photon energy}}$ (the detuning factor), the function $f_{ij}(\mathbf{r})$ is determined by the orbitals of the ground and excitation states and has the order of unity. Under $\eta \simeq 1$(the resonant condition) or $f_{ij}(\mathbf{r}) \simeq 1$ (the far-field observation condition,i.e., the situation insensitive to the profile of the source), Eq.(4) leads to $\frac{\Delta j_{\mathbf{A}\, i}(\mathbf{r}, t) + \Delta j_{\mathbf{A}\,\text{local}\, i}(\mathbf{r}, t)}{\Delta E_j^{(t)}(0)\sin(\omega t + \xi)} = \frac{\Delta j_{\varphi\, i}(\mathbf{r}, t)}{\Delta E_j^{(\ell)}(0)\sin\omega t}$; this and Eq.(3) mean that the responses to the $\Delta \mathbf{E}^{(\ell)}$ and $\Delta \mathbf{E}^{(t)}$ are equivalent. Therefore, the total electric field may be considered as the cause of response and the macroscopic constitutive equation (MCE) using the permittivity works soundly. Otherwise, under the non-resonant and NF observation condition, the two responses are different and should be treated separately. In particular, Eq.(4) in the limit $\eta \to 0$ leads to a specific situation in NFO, i.e., $\left|\frac{\Delta j_{\varphi\, i}(\mathbf{r}, t)}{\Delta E_j^{(\ell)}(0)\sin\omega t}\right| \simeq \left|\frac{\Delta j_{\mathbf{A}\,\text{local}\, i}(\mathbf{r}, t)}{\Delta E_j^{(t)}(0)\sin(\omega t + \xi)}\right| \gg \left|\frac{\Delta j_{\mathbf{A}\, i}(\mathbf{r}, t)}{\Delta E_j^{(t)}(0)\sin(\omega t + \xi)}\right|$. Finally, based on Eq.(4), we will suggest a reasonable substitution of the MCE for a two-level system in NFO.

[1] We will have another presentation in APNFO-11 concerning the nonlinear response functions systematically derived employing Lagrangian formulation, overcoming the many electron problem, and maintaining the charge conservation law and the gauge invariance: Itsuki Banno and Motoichi Ohtsu, *"The Nonlinear Response Theory for Near-field Optics and Application to Non-resonant Effect."*

New Routes to Future Studies of Dressed Photons

Motoichi Ohtsu*#

#*Institute of Engineering Innovation, School of Engineering, the University of Tokyo*
*Research Origin for Dressed Photon
E-mail address: ohtsu@nanophotonics.t.u-tokyo.ac.jp

Abstract: The history of optical near field science is reviewed, and a physical picture of the dressed photon (DP) is presented. Revolutionary technical advances in this field have been demonstrated, such as nanometric optical logic gates, material surface polishing, and high-power lasers and light-emitting diodes (photon breeding devices) made of silicon crystals. Two routes to establishing novel theoretical studies are proposed in order to promote further advances in DP science and technology in the future.

About three decades have passed since the invention of a reliable method for fabricating high-quality fiber probes for generating optical near fields efficiently [1]. The sub-wavelength optical near fields generated by such probes have broken through the diffraction limit of light, which has forever governed the resolution of optical microscopy/spectroscopy and optical information storage [2]. From theoretical studies of the electron–photon interactions in a nanometric material, a detailed physical picture of the optical near field emerged, and its quantum mechanical creation/annihilation operators have been derived. The quasi-particle represented by these operators was named the dressed photon (DP). The spatial profile of the DP field can be represented by a Yukawa function. Furthermore, a novel electric-dipole-forbidden transition process and a DP coherent phonon coupling process have been discovered [3]. Based on these discoveries, revolutionary technologies for operating nanometric optical logic gates, polishing material surfaces, etc. have been realized [3]. Furthermore, high-power lasers and light-emitting diodes have been fabricated by using crystalline silicon, which is an indirect-transition type material, and these devices have been named photon breeding devices [4].

The technical advances reviewed above represent great achievements in experimental studies on DPs. Further discoveries and inventions in optical science and technology can be expected if more advanced theoretical studies are conducted in order to analyze the nature of the DP more precisely. The theoretical model to be developed in these studies should be generic, so that we do not have to be concerned about the detailed nano-material structures in which the DP is generated, or the properties of those structures. We are following two routes for establishing such a novel theoretical model:

[Route 1] Route 1 involves constructing a novel off-shell quantum field theory. By noting that the DP is a quantum field off-shell, its momentum and energy uncertainties are large. This means that the DP is a small virtual photon, and this is the origin of the versatile novel DP technologies reviewed above. By following this route, in the theoretical work conducted so far, the DP was identified as a quantum field with nonzero effective mass. Based on the relativistic electromagnetic theory, theoretical analysis was carried out by analogy with vortex fluid mechanics [5]. Also, by modifying the conventional gauge condition to the electromagnetic field, it was found that the longitudinal electromagnetic component in vacuum contributed to the generation of the DP field. As a result, a novel electromagnetic field was found to exist in the space-like domain of the Minkowski spacetime, and its scalar potential was derived from the Proca equation and was represented by the Yukawa function, which is nothing more than the DP field.

[Route 2] Route 2 involves treating the DP as an elementary particle, i.e., a nanometric Democritus's *atom*, by considering multiple photons and electrons interacting in the nanometric space as a complex system. This route is different from the reductionism that is overwhelmingly prevalent in modern physics. So far, a mathematical science model for this complex system has been developed in order to analyze the diffusion of p-dopant B atoms in a silicon crystal. As a result, the unique features of photon breeding devices were successfully reproduced [6].

By analyzing the micro–macro duality in the quantum field [7], an approach that is consistent with the two routes above, it is expected that a novel process for detecting the DP will be established, and this will promote further advances in DP science and technology in the future.

[1] M. Ohtsu, *Near-Field Nano/Atom Optics and Technology* (Springer, Hidelberg, 1998).
[2] M. Ohtsu (ed.), *Handbook of Nano-Optics and Nanophotonics* (Springer, Heidelberg, 2013).
[3] M. Ohtsu, *Dressed Photons* (Springer, Heidelberg, 2014).
[4] M. Ohtsu, *Silicon Light-Emitting Diodes and Lasers* (Springer, Heidelberg, 2016).
[5] H. Sakuma, I. Ojima, and M. Ohtsu, *Progress in Quantum Electron.* **41** (2017) to be published.
[6] M. Katori, and H. Kobayahi, *Prog. Nanophotonics* 4 (M. Ohtsu and T. Yatsui, eds., Springer, Heidelberg, 2017) pp.19-55.
[7] I. Ojima, *Stochastic Analysis* (T. Hida, ed., World Scientific, Singapore, 2005) pp.143-161.

Who Has Seen A Free Photon?
---From Mathematical Physics To
Light-Matter Fusion Technologies---

Motoichi Ohtsu, Izumi Ojima and Hayato Saigo
RODreP(Research Origin for Dressed Photon), RODreP and Nagahama Institute of Bio-Science and Technology
E-mail address: ohtsu@nanophotonics.t.u-tokyo.ac.jp, u6jic7qh@za.ztv.ne.jp and h_saigoh@nagahama-i-bio.ac.jp

Abstract:
The so-called paradox of "photon localization" is resolved by introducing the "effective mass" of a photon due to the interaction with matter. The validity of this interpretation is confirmed in reference to the picture of "polariton", a basic notion in optical and solid physics.
The scenario also applies to more general settings. Any kinds of boundary conditions with finite volume (like cavity) will make photons heavier and slower, even without a medium. As a striking example, we focus on the role played by nanoparticles in the context of "dressed photons" and also propose a new look at the photon-matter interaction, which will provide a brand new platform for the interplay between mathematical-physical arguments and light-matter fusion technologies.

In this talk a new aspect of the interplay between mathematical-physical arguments and light-matter fusion technologies, making use of the concept of "effective mass", will be introduced, through an investigation of a fundamental (and seemingly naive) question: Who has seen a free photon?

Since the argument by Newton and Wigner in 1949, it has been known in mathematical physics that any position operator cannot be defined for a massless free particle with a non-zero finite spin, in sharp contrast to the cases of massive particles which can be localized [1].

This statement is clearly in contradiction to the above familiar situations where almost all physicists and engineers have used the notion of " position of a photon" as one of the basic ingredients of theory and application of quantum mechanics. Then, who has seen a free photon?

This dilemma is resolved by introducing the "effective mass" of a photon due to the interaction with matter. The validity of this interpretation is confirmed in reference to the picture of "polariton", a basic notion in optical and solid physics [2].

The scenario also applies to more general settings. Any kinds of boundary conditions with finite volume (like cavity) will make photons heavier and slower, even without a medium [3]. As a striking example, we focus on the role played by nanoparticles in the context of "dressed photons" [4].

[1] Newton, T.D. and Wigner, E.P. Localized states for elementary systems. Rev. Mod. Phys. **21**, 400 (1949).
[2] Ojima, I., and Saigo, H., Who has seen a free photon?, Open Sys.Information Dyn. **19**, 1250008 (2012).
[3] Ojima, I., and Saigo, H., Photon Localization Revisited, Mathematics, **2015**, 3, 897-912 (2015).
[4] Ohtsu, M., Dressed Photons, Springer-Verlag, 2013.

The study on the principle of light emission of Si LED using dressed-photon-phonon

Jun Hyoung Kim[1], Tadashi Kawazoe[2], and Motoichi Ohtsu[1]

[1]*Institute of Engineering Innovation, School of Engineering, the University of Tokyo*
[2]*Nanophotonics Engineering Organization (NPEO)*
E-mail address: kimjh@nanophotonics.t.u-tokyo.ac.jp

Abstract: The basic theory of photon breeding effect expects that spectrum of LEDs fabricated by DPP-assisted annealing has sharp peaks. However actual spectrum shows broad peaks. In this paper, we will show that electron-electron scattering plays important role to explain the light emission phenomenon of Si LEDs fabricated by DPP-assisted annealing.

Si has not been considered as suitable material for light-emitting device, because it is indirect transition type semiconductor. However our group has suggested a new approach to fabricating Si-based light-emitting device; Focusing on dressed-photon-phonon (DPP) and photon breeding effect, the limitation from material properties can be overcome [1], and Si-technology is going to enter a new phase.

Recent research has clarified that the above-mentioned light-emitting phenomenon is due to the optimization of spatial distribution of dopants (boron, B) at microscopic level [2]. Generally B atoms are distributed randomly inside crystal. Our group, however, suggested a novel process, DPP-assisted annealing, to optimize the spatial distribution of B atoms. Moreover, physical model based on 2-level system successfully explains the dynamics during DPP-assisted annealing [3], and multiple peaks of spectrum also can be explained by simulation based on phonon coupling [4]. However there still exist unsolved conundrums. One of those is that although the theory expects sharp peaks at spectrum, the real peaks are very broad. And what makes emission peaks broad should be clarified.

Fig. 1 shows the dependence of emitted light intensity on the injected current. From this figure, it seems like the intensity of light emission changes linearly when current is less then 400mA. However the intensity of light emission is proportional to the square of the current when it is higher than 400mA. Let's first discuss about the region less than 400mA. Fig. 2 shows the spectra of two Si LEDs driven at 300mA. The only difference between those 2 LEDs is that the intensity of radiated light (1313nm IR laser) during DPP-assisted annealing. It is clear that the stronger radiated light intensity during DPP-assisted annealing is, the higher peak around 1313nm EL spectrum of LED has. This is what the theory of photon breeding expects.

Next, let's discuss about the region higher than 400mA. Because the intensity of light emission is proportional to the square of the current, light emission phenomenon at this region may be thought to be due to thermal radiation. However Fig. 3 shows that the peak near 0.53eV does not show any dependence on the current. If this light emission phenomenon is due to the thermal radiation, the peak should show blue-shift as the current increases. As a result of consideration, we conclude that this phenomenon comes from the transfer of momentum between localized phonon and electron caused by electron-electron scattering.

In summary, light emission from Si LED fabricated by DPP-assisted annealing consists of two components; Light emission caused by photon breeding effect of which the intensity is proportional to the current, and light emission caused by electron-electron scattering of which the intensity is proportional to the square of the current. And the latter makes the peaks broad.

Contr 6-2
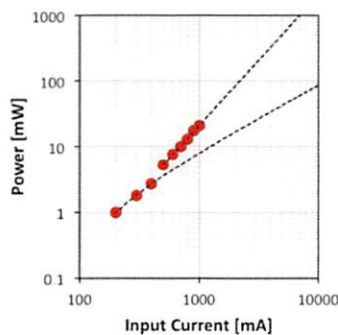
Fig. 1 Dependence of emitted
light intensity on current
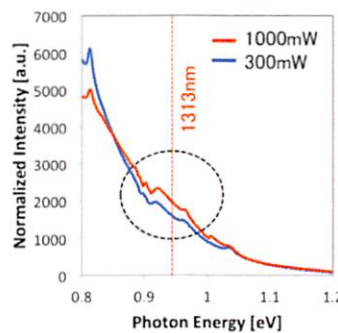
Fig. 2 Effect of radiated light
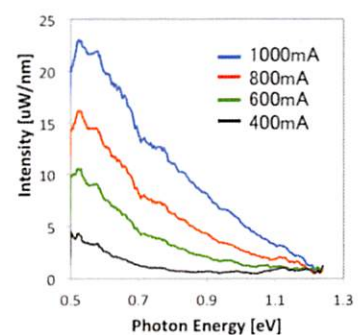during DPP-assisted annealing

Fig. 3 EL spectrum of Si LED

[1] T. Kawazoe et al., Appl. Phys. B **104**(4), 747 (2011).
[2] T. Kawazoe et al., Appl. Phys. A **121**, 1409 (2015)
[3] J. H. Kim et al., Appl. Phys. A **121**, 1395 (2015)
[4] M. Yamaguchi et al., Appl. Phys. A **115**, 119 (2014)

The Nonlinear Response Theory for Near-field Optics and Application to Non-resonant Effect

Itsuki Banno[1] and Motoichi Ohtsu[2,3]

[1] *Interdisciplinary Graduate School of Medicine and Engineering, University of Yamanashi*
banno@yamanashi.ac.jp

[2] *Institute of Engineering Innovation, School of Engineering, the University of Tokyo,* [3] *Research Origin for Dressed Photon*
ohtsu@nanophotonics.t.u-tokyo.ac.jp

Abstract: A nonlinear response theory adequate for near-field optics (NFO) is developed; it treats equally the longitudinal and transverse incident fields, coexisting in the NF optical system. The principle problem is to separate the effect of the longitudinal incident from the effect of the Coulomb interaction between the electron charges, and it is overcome, employing the fundamental idea of the density functional theory. The Lagrangian formulation systematically derives the linear and nonlinear response functions, and promises to maintain the charge conservation law and the gauge invariance. As an application, nonlinear NF optical effect is discussed under the non-resonant condition.

1. Introduction: a Desirable Response Theory in Near-field Optics

We would like to know the optical response of a small-scale material in the vicinity of the nanostructure, which irradiates the longitudinal and transverse electromagnetic (EM) fields or, equivalently, the scalar and vector potentials, φ and $\mathbf{A}$. The existence of the φ incident distinguishes such the near-field (NF) optical system from the ordinary optical system, and a response theory adequate for NFO is desirable to treat φ and $\mathbf{A}$ incidents equally.

2. The Unrecognized Difficulty: the Connection between Near-field Optics and Many-electron Problem

Such the requirement is incompatible with the usual many-electron theory, in which the φ and $\mathbf{A}$ are treated unequally. Actually, under the Coulomb gauge, the φ is expressed in terms of the electron field operators, solving the Poisson equation, and the whole of φ is rewritten to the Coulomb interaction between the charged particles. In doing so, the quantum many-electron effect (the exchange-correlation effect) is taken into account to make the ground and excited states to be the proper bound states. This manner is incompatible with NFO, in which the φ incident survives strongly and its effect is indistinguishable from the effect of the inherent electron charge.

Instead of such the treatment of the φ, one may employ the fundamental ansatz of the density functional theory. That is, the proper many-electron density (so that the proper φ) of the ground state may be reproduced by imposing a suitable auxiliary one-body potential [1]. This auxiliary potential may be included in the action integral as the the Lagrange's undetermined multiplier to incarnate the proper grand state density in the semiclassical theory.

3. Response Functions Guaranteeing the Charge Conservation Law and Gauge Invariance

The Heisenberg operator of the 4-element current density, $\hat{j}^\mu$ may be expanded to the Taylor series with respect to the EM field variation, ΔA^ν, and the expansion coefficients are the linear and nonlinear response function operators:

$$\hat{j}^\mu(x;[A^{(0)\nu}+\Delta A^\nu]) - \hat{j}^\mu(x;[A^{(0)\nu}]) = \int d^4x_1 \hat{\chi}^\mu_{\mu_1}(x,x_1)\Delta A^{\mu_1}(x_1) + \int d^4x_1 \int d^4x_2 \hat{\chi}^\mu_{\mu_1\mu_2}(x,x_1,x_2)\Delta A^{\mu_1}(x_1)\Delta A^{\mu_2}(x_2) + \cdots, \quad (1)$$

$$\hat{\chi}^\mu_{\mu_1\cdots\mu_n}(x,x_1,\cdots,x_n) \equiv \frac{1}{n!}\left.\frac{\delta^n \hat{j}^\mu(x;[A^\nu])}{\delta A^{\mu_1}(x_1)\cdots\delta A^{\mu_n}(x_n)}\right|_{A^\nu=A^{(0)\nu}} = \frac{-c^2}{n!}\left.\frac{\delta^{n+1} I_{mat}}{\delta A_\mu(x)\delta A^{\mu_1}(x_1)\cdots\delta A^{\mu_n}(x_n)}\right|_{A^\nu=A^{(0)\nu}}, \quad (2)$$

where I_{mat} is the action integral of the matter including the interaction with the EM field, and $\hat{j}^\mu = (c\hat{\rho}, \hat{\mathbf{j}})$, $\hat{j}_\mu = (c\hat{\rho}, -\hat{\mathbf{j}})$, $A^\mu = (\varphi, c\mathbf{A})$, $A_\mu = (\varphi, -c\mathbf{A})$. The induced current density or, equivalently, the response functions are determined via the optimization of I_{mat} with respect to the electron field operators of the material under the given scalar and vector potential incidents, ΔA^ν from the nanostructure. This procedure results in the third hand side of Eq.(2), from which one may read the symmetry of the coordinates of the result and cause, i.e., x and x_i. The charge conservation law, $\partial_\mu \hat{j}^\mu(x;[A^\nu]) = 0$ and the symmetry among the coordinates leads to:

$$\partial_\mu \hat{\chi}^\mu_{\mu_1\cdots}(x,x_1,\cdots) = 0, \qquad \partial^{\mu_i}\hat{\chi}^\mu_{\mu_1\cdots}(x,x_1,\cdots) = 0 \quad (i=1,2,\cdots,n). \quad (3)$$

The second equation of Eq.(3) stands for the gauge invariance, that is, the present response theory is gauge free.

4. Recursive Formulae for Non-linear Response Functions and Application to Non-resonant Effect

One may derive a series of recursive formulae for the nonlinear response functions, e.g., the third order one is,

$$\hat{\chi}^\mu_{\mu_1\mu_2\mu_3}(x,x_1,x_2,x_3) = \frac{1}{3}\frac{-q}{mc^2}\left\{\delta^4(x_2-x_3)\bar{\delta}_{\mu_2\mu_3}\hat{\chi}^\mu_{\mu_1 0}(x,x_1,x_2) + \begin{pmatrix}1\,2\,3\\2\,3\,1\end{pmatrix} + \begin{pmatrix}1\,2\,3\\3\,1\,2\end{pmatrix}\right\} \quad (4)$$

$$+ \frac{1}{3}\frac{1}{i\hbar c^2}\left\{\theta(ct_2-ct_3)\left[\hat{\chi}^\mu_{\mu_1\mu_2}(x,x_1,x_2),\hat{j}^{(in0)}_{\mu_3}(x_3)\right] + \begin{pmatrix}1\,2\,3\\2\,3\,1\end{pmatrix} + \begin{pmatrix}1\,2\,3\\3\,1\,2\end{pmatrix}\right\},$$

where $\begin{pmatrix}1\,2\,3\\2\,3\,1\end{pmatrix} + \begin{pmatrix}1\,2\,3\\3\,1\,2\end{pmatrix}$ mean the terms with the replaced indices of the cyclic order and $\bar{\delta}^\mu_{\mu'} = 1$ for $\mu = \mu' = 1,2,3$ or $\bar{\delta}^\mu_{\mu'} = 0$ otherwise. The first term dominates over the second term under the non-resonant condition. Using such the formulae, one may explore a nonlinear NF-specific effect under the non-resonant condition [2].

[1] P. Hohenberg and W. Kohn, Phys. Rev. **136**, 3864 (1964); W. Kohn and L. J. Sham, Phys Rev. **140**, A1133 (1965).
[2] We will have another presentation in APNFO-11 concerning the linear response theory in the non-resonant NF optical system: Itsuki Banno and Motoichi Ohtsu, *"Irrationality of the Permittivity in Non-resonant Near-field Optics."*

[III] REVIEW PAPERS

Review

Dressed photons in a new paradigm of off-shell quantum fields

CrossMark

Hirofumi Sakuma [a,*], Izumi Ojima [a], Motoichi Ohtsu [a,b]

[a] Research Origin for Dressed Photon, c/o Yokohama Technology Center, NICHIA Corporation, 3-13-19 Moriya-cho Kanagawa-ku, Yokohama-shi, 221-0022, Japan
[b] Institute of Engineering Innovation, School of Engineering, The University of Tokyo, 2-11-16 Yayoi Bunkyo-ku, Tokyo, 113-8656, Japan

A R T I C L E   I N F O

A B S T R A C T

This article reviews recent progress in theoretical studies of dressed photons. For providing concrete physical images of dressed photons, several experimental studies are demonstrated. They are applications of dressed photons to novel optical functional devices, nano-fabrication technologies, energy conversion technologies, and photon breeding devices. After these experimental demonstrations, as the main part of this review, quantum-field theoretical formulation of dressed photons is attempted in use of the newly introduced Clebsch-dual variable of electromagnetic field. The reason for introducing the new formulation will be explained in the final section from the viewpoint to exhibit the contrast between free and interacting quantum fields in regard to their energy-momentum supports which are seldom touched upon (or forgotten) in the common physical discussions about quantum fields.

1. Introduction

The aim of the present paper is to clarify the conceptual and mathematical basis of the dynamic behaviors of *dressed photons* discovered by M. Ohtsu, one of the co-authors of this article, from the viewpoint of the duality relations between the usual free photon field and its "*Clebsch-dual* field", the latter of which is to be explained in what follows.

In the context of quantum field theory (QFT), the familiar common language is based on the particle pictures in terms of the creation $a_k^\dagger$ and annihilation a_l operators, $[a_l, a_k^\dagger]_\mp = \delta_{lk}$, acting on a Fock space constructed on the vacuum state $|0\rangle$ as the (symmetric or antisymmetric) tensor powers $V = \bigoplus_{n\geq0} V_n$, $V_0 = \mathbb{C}|0\rangle$, $V_n := V_1^{\otimes n}$ (: symmetric or anti-symmetric tensor product) of 1-particle states $V_1 := Lin\{a_k^\dagger|0\rangle; k : \text{momentum}\}$, $V_n = Lin\{a_{k_1}^\dagger a_{k_2}^\dagger \cdots a_{k_n}^\dagger|0\rangle; k_1, k_2, \cdots, k_n\}$. While this language is very convenient in treating many-body problems in both contexts of relativistic particle physics and of non-relativistic solid state physics, its serious pitfall lies in its "forgetfulness" about the strict restriction on its applicability in physical nature! Since the above simple-minded interpretation of quantum fields in terms of creation and annihilation operators is meaningful *only for free fields without interactions*, the validity of this vocabulary is at most for the *asymptotic fields and states* which describe quantum fields approximately only in the remote past or future regimes, respectively, before or after the actual scattering processes. The serious gap between interacting and free quantum fields in terms of Fock space language can clearly be seen in their totally different *energy-momentum spectral supports*, the latter being restricted to the mass hyperboloid $p^2 := p_\mu p^\mu = m^2$ but the former extending over the whole *p*-space(!!) according to a general result due to the axiomatic QFT

(as a mathematical formulation of quantum fields) [1].

The typical examples of this sort in the relativistic QFT on the vacuum are given by *intermediate states* between in-coming and outgoing states of scattering processes in particle physics, which are described in terms of *off-shell* particles and which cannot be identified with any on-shell free particles described by creation/annihilation operators of asymptotic fields. In solid state physics described by quantum statistical mechanics, another typical non-applicability domain of particle pictures can also be found in the well-known phenomena of *phase transitions* caused by the instability between two stable thermodynamic phases with different particle pictures, through which the same physical system undergoes drastic changes in material configurations: for instance, a phase transition from the *normal* phase with non-vanishing electric resistance to the *superconducting* one characterized by the vanishing resistance. These examples clarify that the *on-shell states* (abbreviation of "states on-the-mass shell") described by the creation and annihilation operators are not eternal invariants of a system but *variables* highly dependent upon the environments in which the relevant physical system is placed. When certain continuous symmetry present in one phase is broken in the other, there arise some *massless* excitation modes in the broken phase, according to a general theorem called Nambu-Goldstone theorem, as is the case of the phase transition from the normal one with unbroken electromagnetic $U(1)$ to the superconducting one with broken $U(1)$ symmetry.

Furthermore, the commitment of electromagnetic field (quantum and/or classical) causes more complications as will be discussed, like the case of *infrared divergences*, where "infrared soft photons" carrying low energies cause serious divergences through the coupling with the "on-shell states" of charged particles. What has been known as a solution to these infrared divergences is the mechanism to generate non-vanishing mass of photons due to the accumulated contacts between charged particles and soft photons which usually take place in continuous media: this kind of coupling mechanism has been found effective [2] in the mechanism involving the polaritons whose non-vanishing mass is directly related with the refractive index of the medium. Namely, the problem is solved in this case by a shift of the mass position of on-shell states, which defines new quasi-particles.

In the phenomena associated with dressed photons (to be abbreviated as DPs), however, this sort of quasi-particle pictures are not sufficient for explaining their dynamic behaviors, because of the strong localization of the associated creation and annihilation processes. To explain the characteristic dynamic behaviors of DPs, therefore, we need to incorporate the effects of interactions in a satisfactory way. Because of the above-mentioned serious differences between interacting and free fields with respect to their support properties in energy-momentum p_μ, this task seems to be quite non-trivial! For this purpose, our strategy is just to look for a free field $S_{\mu\nu}$, which resembles the free electromagnetic field $F_{\mu\nu}$ but whose p_μ-support covers all the spacelike p_μ's complementary to that $p^2 \geq 0$ of $F_{\mu\nu}$. If we succeed in formulating such $S_{\mu\nu}$, then the joint p_μ-support of $F_{\mu\nu}$ and $S_{\mu\nu}$ covers the whole p-space! Thus, we can mimic the essential features of interacting electromagnetic field by the combined use of two free fields $F_{\mu\nu}$ and $S_{\mu\nu}$. To achieve this task, a theoretical reformulation of electromagnetic theory is necessary as presented here from the viewpoint of *Clebsch variables*; corresponding to the free field strength $F_{\mu\nu}$ supported by lightlike energy-momentum $p^2 = 0$, its "*Clebsch-dual*" $S_{\mu\nu}$ can be constructed whose energy-momentum support covers the spacelike region $p^2 < 0$.

To understand the roles of energy-momentum supports in the present context, it may be useful to examine some example cases. For the simplest case, it is convenient to consider a relativistic process of two-body scattering involving four energy-momentum vectors, p_1, p_2 for incoming two particles and p_3, p_4 for outgoing two, in terms of which variable s, t and u are defined by $s := (p_1 + p_2)^2 = (p_3 + p_4)^2$, $t := (p_3 - p_1)^2 = (p_2 - p_4)^2$, $u := (p_4 - p_1)^2 = (p_2 - p_3)^2$ (: so-called Mandelstam variables). s represents essentially the square of conserved energy in the system of center of mass of incoming two particles, t the square of energy transfer from the incoming particle 1 to the outgoing 3 and u corresponds to t in the crossed channel. In these variables, the process is described by *positive* variable s and by *negative* ones t and u, the latter of which are closely related with the *interaction or potential terms* between two particles. The first one is usually called *s*-channel, and the second and the third ones *t*- and *u*-channels. By taking such parallelisms as $F_{\mu\nu} \leftrightarrow s$-channel and $S_{\mu\nu} \leftrightarrow t$- and *u*-channels, one can get some instructive images about "*Clebsch-dual*" $S_{\mu\nu}$.

The organization of this paper is as follows. After reviewing in Section 2, the past and present status of the theoretical description of phenomena involving DPs, we try in Section 3 to show recent progress in experimental studies of DPs [3]. Here, we should point out that there still remain problems to be solved for gaining a deeper understanding of DPs and exploring more applications. For the purpose of solving these problems, we present the Clebsch dual field of electromagnetic field in Section 4. The final section, Section 5, is devoted to the discussion for summarizing the presented concepts and the context formed to clarify the meaning of the key concept of DPs.

2. Dressed photon as a physical picture of an off-shell photon

As mentioned in the previous section, the concept of elementary excitations [4] is working effectively everywhere in solid state physics: namely, excited states of a many-body system can be described in terms of a collection of certain fundamental excited modes called elementary excitations or "quasi-particles" in short. An exciton as a well-known example represents a quasi-particle related to an electron-hole pair in a solid. The interaction between a photon and an exciton forms a new steady state which also represents a quasi-particle called an exciton-polariton. Its dispersion relation between the wavenumber and energy of the exciton-polaritons in macroscopic space is described by curves A and B in Fig. 1. Note that other kinds of quasi-particles also show dispersion relations similar to these curves.

In this figure, we note the presence of a wide space around the curves A and B, as shown by the green shaded rectangle. A quasi-particle is created also in this space whose large size gives the following characteristic features to the created quasi-particle:

(1) As represented by the horizontal double-pointed gray arrow, the wavenumber k of this quasi-particle spans a wide range. This also means that its uncertainty Δk is large, which is related to the non-conservation of momentum $\hbar k$ of the quasi-particle (where
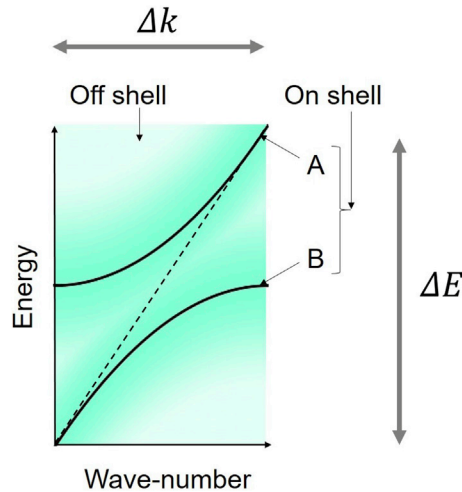
Fig. 1. Dispersion relation between the wave-number k **and the energy** E. The curves A and B represent the dispersion relation of the exciton-polariton. The broken line is for light in free space. The green shaded rectangle is for the dressed photon.

$\hbar = h/2\pi$ and h is the Planck constant) involving a large number of normal modes. At the same time, this implies, according to the Heisenberg uncertainty relation $\Delta(\hbar k) \cdot \Delta x \geq \hbar$, that the uncertainty Δx of position x of the quasi-particle is small, and hence, the size of this quasi-particle is very small.

(2) As is represented by the vertical double-pointed gray arrow, the energy E of this quasi-particle spans a wide range, and hence, its uncertainty ΔE is large, which implies the non-conservation of the energy. Owing to the Heisenberg uncertainty relation $\Delta E \cdot \Delta t \geq \hbar$ with large uncertainty ΔE, the time uncertainty Δt is small. Therefore, this quasi-particle is created and subsequently annihilated within a short time.

The small size in the first feature is due to the small scale of such materials as nanomaterial to create the quasi-particle, where a part of the field generated by this quasi-particle penetrates through the surface of the nanomaterial to the outside. This leaking field has been called optical near field [5]. The second feature of the short lifetime suggests the interpretation of the quasi-particle as a sort of virtual photon. The concept of a DP provides a unified physical picture for describing these two features consistently, including both the large number of normal modes and the spectral sideband features of (1) and (2).

To compare these features with the exciton-polariton represented by the curves A and B in Fig. 1, we note that the latter one represents a quasi-particle in a macroscopic material with the size much larger than the wavelength of light. This quasi-particle propagates into a wide space as a real photon; its momentum and energy are conserved ($\Delta k = 0$, $\Delta E = 0$). The behavior and properties of this real photon have long been studied in the traditional optical science and technology. The situation corresponds to a physical system described by states "on-the-mass shell" (or, on-shell states, in short) in QFT [6–8].

In contrast, the green shaded rectangle corresponds to the situations with "off-shell" photons. While real on-shell photons conserve their momentum and energy, off-shell virtual photons do not. Light-matter couplings in nanometric space can exhibit characteristic distributions in the values of the physical quantities of nanomaterials, such as momentum and energy. To study the off-shell virtual photons, we note that there are such unsolved problems and untouched subjects in analyzing these distributions as

(I) QFT is required to describe the numbers of photons and electron-hole pairs in a many-particle system, which can vary as a result of light-matter couplings in a nanometric space. For this description, creation and annihilation operators have to be defined by quantizing the light and elementary particles. However, a serious problem for off-shell photon is that a virtual cavity cannot be defined in a sub-wavelength sized nanometric space, which makes it difficult to derive the Hamiltonian of the optical energy. In addition, the wavelength (wavenumber) of light and the photon momentum have large uncertainties due to the sub-wavelength size of the space under study.

(II) The off-shell photons are generated and localized on the surface of a nanomaterial under light irradiation. Furthermore, they are virtual photons mediating the interaction between the polarizations induced on the nanomaterial surface. For detecting these photons, therefore, another nanomaterial has to be placed in close proximity to convert them into real photons via multiple scattering of the virtual photons. This conversion makes it possible to detect the virtual photons through the detection of the scattered light in the far field region. Here, the first and the second nanomaterials may be regarded as the source and detector of the virtual photons, respectively. In contrast to the conventional optical phenomena, however, the source and detector are not independent of each other, but are coupled via the virtual photons.

(III) Since the nanomaterials in an actual nanometric subsystem are always surrounded by a macroscopic subsystem composed of macroscopic materials and electromagnetic fields, the contribution from the macroscopic subsystem must be taken into account

in analyzing the interactions between the nanomaterials for estimating the magnitude of the resulting energy transfer and dissipation in the nanometric subsystem.

For solving the above problems (I)-(III), novel theories have been developed and these theories have succeeded in providing a physical picture of the optical near fields and virtual photons consistently, which has been beyond the traditional scope of conventional classical and quantum optics designed only for the on-shell photons in the macroscopic space. Solutions to problems (I)-(III) are as follows:

(i) To solve problem (I), an infinite number of electromagnetic modes with infinite frequencies, polarization states, and energies are assumed, which correspond to the large number of normal modes and the spectral sideband features of (1) and (2) above. An infinite number of energy states are also assumed for the electrons and holes. On these assumptions, the total Hamiltonian is derived to define the creation and annihilation operators of quasi-particles so as to represent the light-matter interactions in the nanometric space [9]. Since these operators are given by the sum of the operators of photons and electron-hole pairs, this quasi-particle is called a DP as a photon dressed in the clothes of material energy of the electron-hole pairs [10]. The DP can also couple with multi-mode coherent phonons in the nanomaterial to create another quasi-particle, named the dressed-photon-phonon (DPP) [11].

(ii) To solve (II), the theoretical approach reviewed in (i) has been used for analyzing the interaction between the two nanomaterials in terms of the annihilation of a DP from the first nanomaterial and of its creation on the second nanomaterial. It has been confirmed by experimental and theoretical studies that the second particle exhibits a characteristic optical response if it absorbs the energy of the modulation sideband described in (i).

(iii) To solve (III), the virtual photon interaction between the nanomaterials in the nanometric subsystem has been analyzed by renormalizing the effects originating from the macroscopic subsystem in a consistent and systematic way [12]. As a result, the spatial distribution of the virtual photon interaction energy can be derived and expressed in terms of a Yukawa potential, which also makes it possible to describe the interaction between the two nanomaterials mediated by the DP (DP-mediated interaction) [13]. This function quantitatively shows that the interaction range is equivalent to the size of the nanomaterial and does not depend on the wavelength of the incident propagating light. Starting from this size-dependent interaction range, novel optical response characteristics have been determined: since the DP is localized in nanometric space, the conventional long-wavelength approximation valid for the light-matter interactions in macroscopic space is not applicable to the DP-mediated interaction. As a result, a transition forbidden via electric dipole becomes an allowed one. Furthermore, size-dependent resonance and spatial hierarchy in the DP-mediated interaction has been found [14].

3. Applications of dressed photons

In this section, recent progress in experimental studies of DP is reviewed. There are four examples of applications that have been developed by using the intrinsic features of the DP-mediated interaction and the resulting DP energy transfer.

(1) Optical functional devices: These devices have been named DP devices by using semiconductor nanomaterials. They enable the transmission and readout of optical signals by the energy transfer and subsequent dissipation of the DP energy [15]. Examples of DP devices developed so far are as follows: a logic gate device for controlling optical signals [16], an energy transmitter for transmitting optical signals between DP devices [17], and an input interface device for converting an incident on-shell photon to a DP [18]. Practical NOT gate and AND gate devices that operate at room temperature have also been fabricated by using InAs nanomaterials [19].

(2) Nano-fabrication technologies: By photochemical etching, bumps on a rough material surface are autonomously removed by using chemically radical atoms. These atoms are created by photo-dissociating gaseous molecules due to DPP energy transfer from the apex of the bump to the molecules under visible light irradiation [20]. Using this method, the surfaces of glass substrates have been smoothed for use as high-power laser mirrors [21], for magnetic storage memory disks [22], for EUV masks [23], and for side walls of densely aligned corrugations of a diffraction grating [24]. This method has been applied to other materials, such as plastic PMMA [25], crystalline GaN [26], and crystalline diamond [27].

(3) Energy conversion:

    (3-1) Optical-to-optical energy conversion: Near infrared light has been converted to visible light by using energy up-conversion in the process of DPP energy transfer between organic dye particles. Red, green, and blue light has been emitted from dye particles by irradiating them with 0.8–1.3 μm wavelength infrared light [28,29].

    (3-2) Optical-to-electrical energy conversion: A photovoltaic device using an organic P3HT film has been developed [30]. The electrode surface conformation of this device was autonomously modified by using novel DPP-assisted deposition of silver particles for efficient DPP generation. A Si photodiode has been also developed, in which the spatial distribution of doped boron (B) atoms was autonomously modified by a novel DPP-assisted annealing method [31]. In these two devices, a phenomenon, "photon breeding", (refer to (4) below) has been confirmed. Furthermore, in the case of the Si photodiode, an optical amplification capability was confirmed, which is due to stimulated emission triggered by the DP.

(4) Photon breeding devices: They are novel LEDs fabricated by using bulk crystals [60–62, Springer Si LED&LD] [32–35] of indirect-transition-type Si semiconductors. The autonomous modification method reviewed in (3-2) above was also used, resulting in efficient momentum transfer between electrons and phonons in Si. Besides Si, an indirect transition-type GaP semiconductor has

been used for fabricating an LED emitting yellow-green light [36,37]. An indirect transition-type SiC semiconductor has also been used for fabricating LED emitting blue-violet light [38], ultraviolet light [39], and white light [40]. In addition to LEDs, an optical and electrical relaxation oscillator [41] and a near infrared laser have been realized by using crystalline Si [42–44]. Furthermore, an LED [45], a light polarization rotator [46], and a light beam deflector [47] have been developed by using ZnO crystal. A light polarization rotator using SiC crystal has been also developed [48].

For simple demonstration, Fig. 2(a) shows the cross-sectional structure of the Si crystal used as the laser medium (1 mm width, 150 μm thickness) [49,50]. The length of the crystal is 15 mm, as seen in the photograph in Fig. 2(b). Closed squares in Fig. 2(c) mean the measured relation between the injection current density J and the optical output power P_{out} of 1.3 μm-wavelength, emitted from one output facet of the fabricated device. The threshold current density J_{th} is 60 A/cm^2. The value of P_{out} takes a maximum value of 13 W at $J = 100 A/cm^2$. This value is more than 10^2-times higher than that of a conventional double heterojunction-structured InGaAsP/InP laser.

Remaining part of this section is devoted to review how to fabricate and operate the photon breeding devices because this review demonstrates characteristic features of DPs and how to gain a deeper understanding of DPs, which will be discussed in next sections.

To realize a device by using a Si bulk crystal, DPPs are used twice: first for device fabrication, and next for device operation.

(4-1) For device fabrication, a p-n homojunction formed in the Si crystal is annealed, via Joule-heat produced by current injection, in order to diffuse B atoms (the p-type dopant). During the annealing, the Si crystal surface is irradiated with light (Fig. 3(a)) to create DPPs on the B atom surface. Driven by the created DPPs, electron-hole recombination takes place, emitting light. Since the energy of the emitted light dissipates from the Si crystal, the efficiency of the Joule-heating decreases. As a result, a characteristic spatial distribution of B atoms is realized, which depends on the created DPP energy. This novel annealing is called DPP-assisted annealing. It has been experimentally confirmed that, in this spatial distribution, neighboring B atoms form a pair, and the resultant B atom-pair orients in a specific direction to efficiently create localized phonons [51].

(4-2) For the operation of the fabricated Si-LED, the light irradiation is not required any more; it is used only during the DPP-assisted annealing. Only forward current that is much lower than that used for annealing is injected, as is the case of the conventional LED operation. By this forward current, an electron is injected into the conduction band at the p-n homojunction and creates a photon by spontaneous emission even though its probability is very low. However, once this photon is created, it subsequently creates a DPP on the surface of the B atom at the p-n homojunction, and this DPP interacts with another electron in the conduction band to exchange momentum so that a secondary photon is created. By repeating these momentum exchange and photon creation processes, the emitted light intensity is amplified and reaches a stationary value within a short period, so that light with a sufficiently high intensity is emitted from the p-n homojunction.

It should be noted that photon breeding occurs during device operation [52]. As a result, the photon energy of the emitted light is equal to the photon energy $h\nu_{annsal}$ of the light irradiated during the annealing (Fig. 3(b)). This is in contrast to a conventional device, where the photon energy of the emitted light is determined by the bandgap energy E_g of the semiconductor material used. This is also because the difference between $h\nu_{annsal}$ and E_g is compensated for by the energy of the created phonons. This means that the photon energy of the light emitted from the device is identical to $h\nu_{annsal}$. This is because the spatial distribution of the B atoms has been controlled by the light irradiated during the DPP-assisted annealing, enabling most efficient stimulated emission and spontaneous emission of photons with identical photon energy. In other words, the light irradiated during the DPP-assisted annealing serves as a "breeder" that creates photons with an energy equivalent to $h\nu_{annsal}$. This is the reason why this novel phenomenon is named photon
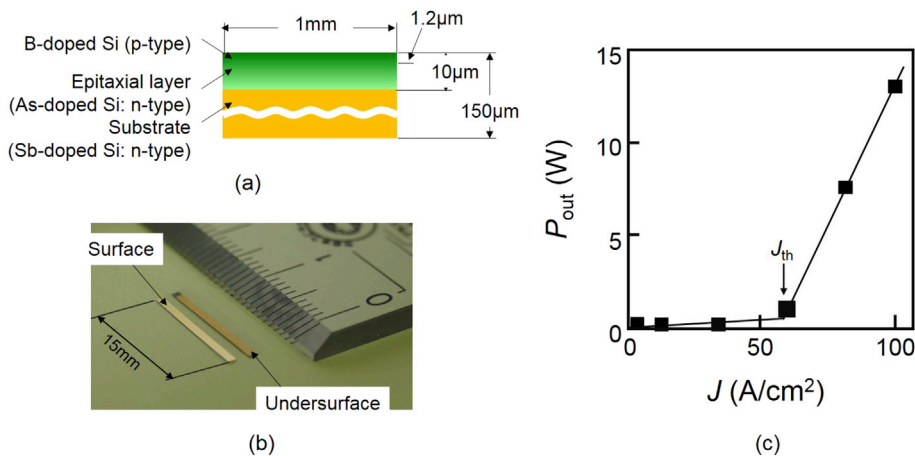

Fig. 2. A near infrared laser. (a) Cross-sectional profile of the Si crystal. (b) Photograph of the laser. (c) Measured relation between the injection current density, $J(A/cm^2)$, and the optical output power, $P_{out}(W)$, emitted from one output facet of the Si crystal.
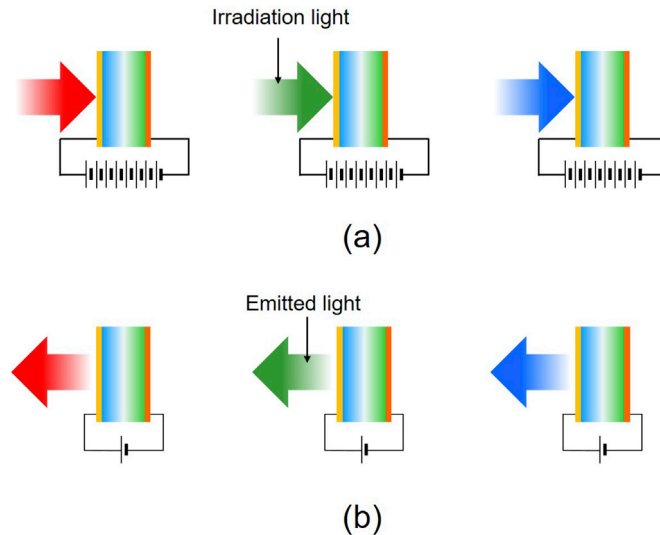
Fig. 3. Fabrication (a) and operation (b) of a photon breeding device.

breeding with respect to photon energy.

Photon breeding has been observed not only for the photon energy but also for the photon spin [51]. For example, linearly polarized light is emitted from the LED if it is fabricated by irradiating linearly polarized light during the annealing step.

At the end of this section, it should be pointed out that there still remain problems to be solved for gaining a deeper understanding of DPs and exploring more applications. These include: (1) Improving the accuracy of the physical picture of the quasi-particle representing the coupled state of a photon, an electron, and a phonon in a nanometric space. (2) Detailed description of energy transfer and dissipation between nanomaterials, mediated by DPs or DPPs. (3) Detailed description of phonon-assisted light-matter interactions in nanometric space. (4) Detailed description of the physical origins of autonomy and hierarchy.

For more advanced methods that will allow us to see the DP and to describe its origin, further studies on the energy transfer from the nano- to macro-systems are required. In particular, as a comment on problem (4) above, the physics of this complex system should be developed on the basis of micro-macro duality in quantum theory [53], which facilitates the formation of micro-macro composite systems consisting of the object physical systems and the probe systems [2]. The specific features that originate from the inherent hierarchy of DPs will be smoothly and conveniently described in this framework with the aid of category-theoretical concepts [54].

4. Novel theoretical attempt on modeling of virtual photon

4.1. Polarization and so far unnoticed duality of electromagnetic field

Since the concept of virtual photons (similarly to that of other particles) has emerged from the perturbative calculations in QFT, its definition may look somewhat loose compared to that of real photons. The present situation lacking a clear picture or clear understanding of DP as a form of virtual photons seems to reflect this vagueness in its definition. Since real and virtual photons are physical entities responsible for the dynamical processes of charged particles, however, they both should be treated on the equal footing.

As we have seen in sections 2 and 3, one of the essential aspects of DP dynamics is its active coupling with other fields generated by materials ubiquitously present in the environment. This feature, however, need not necessarily lead to the absence of a clear physical picture of DP since not all the properties but the intrinsic ones of photons must be preserved in such processes of interactions and since the ground for calling them "photon" would otherwise be lost. An instructive example of such a process is a well-documented mass-acquiring mechanism of a photon as a massless gauge boson in which polarization and longitudinal mode play a significant role.

Motivated by this perspective, we exhibit new aspects about the mutual relations (=duality) between what is dominantly visible and what is invisible in a given domain, from a flexible viewpoint that such mutual relations can easily be changed through a shift from one situation to another. In the specific context of the mathematical description of virtual photons, we show the presence of a duality of electromagnetic field hidden so far. Along this line, we can benefit from the guiding principle of *quantum-classical correspondence* whose importance has been recognized anew in the context of Micro-Macro Duality due to one of the authors [55], aiming at overcoming the drawback of disconnected relations between micro and macro physics caused inadvertently through many twists and turns in the history of quantum mechanics.

4.2. Clebsch parameterized vortex model

It is obvious that an important missing factor in the particle model of geometric optics is the "spin" of a particle. Since we confine

ourselves to the classical physics here, by "spin" we mean rotational field associated with the velocity of a given particle, *i.e.*, vorticity in hydrodynamic terminology. Since the actual spin of photon is closely related to the polarization of associated wave representation, it is relevant to focus on this quantity here. In geometric optics, a light ray is represented as a null geodesic (line) in a four dimensional (4d) pseudo Riemannian manifold *M*. A geodesic is characterized by the property that adjacent tangential vectors on it are connected by parallel displacement, so that velocity field U_μ of (the classical) light particle tangential to a geodesic assumes the form of

$$(\nabla_U U)_\mu = U^\nu \nabla_\nu U_\mu = U^\nu \left(\nabla_\nu U_\mu - \nabla_\mu U_\nu\right) + \nabla_\mu(U^\nu U_\nu/2) = 0, \tag{1}$$

where ∇_X denotes the covariant derivative along a vector field $X = X^\mu \partial_\mu$ associated with the Levi-Civita connection. Since the Levi-Civita connection is torsion-free and since a given geodesic field is null, Eq. (1) is seen to reduce to a simpler form as

$$U^\nu \nabla_\nu U_\mu = U^\nu \left(\partial_\nu U_\mu - \partial_\mu U_\nu\right) = U^\nu S_{\mu\nu} = 0, \tag{2}$$

where $S_{\mu\nu} \equiv \partial_\nu U_\mu - \partial_\mu U_\nu$ is a vorticity field derived from U_μ. Note that a spinless (irrotational) velocity field $U_\mu = \partial_\mu \phi$ automatically satisfies (2), which corresponds to a conventional model of geometric optics.

In order to have a spinning model of the classical "photon", let us consider a Clebsch parameterized (CP) velocity field U_μ [56] defined originally by

$$U_\mu \equiv \lambda \nabla_\mu \phi + \nabla_\mu \chi. \tag{3}$$

While the Clebsch parameterization is well known in the context of the Hamiltonian structure of barotropic fluid [57], to our best knowledge, a preliminary study [58] due to one of the authors' (H. S.) seems to be the only case of its application to a null geodesic field. Since we are concerned with rotational modes of U_μ, we consider in what follows a reduced form of (3), namely,

$$U_\mu = \lambda \nabla_\mu \phi. \tag{4}$$

Notice first that the reduced CP flow field is parameterized by two parameters, in which we must specify differential equations for ϕ and λ. Here, we assume that

$$g^{\mu\nu} \nabla_\mu \nabla_\nu \phi = 0; \quad \left(g^{\mu\nu} \nabla_\nu \phi \nabla_\mu \phi = 0\right), \tag{5}$$

$$g^{\mu\nu} \nabla_\mu \nabla_\nu \lambda - (\kappa_0)^2 \lambda = 0; \quad \left(g^{\mu\nu} \nabla_\nu \lambda \nabla_\mu \lambda = -(\kappa_0)^2 \lambda^2\right), \tag{6}$$

with a certain real constant κ_0. The reason why we select a spacelike Klein-Gordon equation for Eq. (6) will be seen shortly. Since Eqs. (5) and (6) are scalar equations, we can impose a directional constraint on $\nabla_\mu \phi$ and $\nabla_\mu \lambda$. For notational simplicity, let us define covectors (abbreviation of covariant vectors) C_μ, L_μ and a simple bivector $S_{\mu\nu}$ as

$$C_\mu \equiv \nabla_\mu \phi; L_\mu \equiv \nabla_\mu \lambda; S_{\mu\nu} \equiv \nabla_\nu U_\mu - \nabla_\mu U_\nu = C_\mu L_\nu - L_\mu C_\nu. \tag{7}$$

By the last equation in Eq. (7) a skew-symmetric $S_{\mu\nu}$ is given by an exterior product of C_μ and L_μ, according to the definition of a simple bivector which plays an important role in our CP formulation. In our reduced CP, we adopt such a directional constraint as

$$C^\nu \nabla_\nu L_\mu = 0, \tag{8}$$

which simply says that L_μ is advected (or convected) by C^ν. Immediate consequences of this constraint are as follows:

$$L^\mu \left(C^\nu \nabla_\nu L_\mu\right) = 0; \Rightarrow C^\nu \nabla_\nu \left(L^\mu L_\mu\right) = 0; \tag{9}$$

$$\begin{aligned} C^\mu \left(C^\nu \nabla_\nu L_\mu\right) &= 0; \Rightarrow C^\nu \left[\nabla_\nu \left(C^\mu L_\mu\right) - L_\mu \nabla_\nu C^\mu\right] \\ &= C^\nu \nabla_\nu \left(C^\mu L_\mu\right) = 0. \end{aligned} \tag{10}$$

In deriving (10), we have used $C^\nu \nabla_\nu C^\mu = 0$, which says that C^ν itself satisfies the null geodesic equation. By (10), the following orthogonality can be assumed between the two vectors L^μ and C^μ as an initial condition for (8):

$$L_\nu C^\nu = 0. \tag{11}$$

Since any vector perpendicular to a given null vector is either the same null vector or a spacelike one, we can choose L_ν such that it is a spacelike vector satisfying (11), namely,

$$\rho \equiv -L^\nu L_\nu > 0. \tag{12}$$

With the orthogonality relation given in Eqs. (11) and (2) becomes

$$U^\nu \nabla_\nu U_\mu = S_{\mu\nu}(\lambda C^\nu) = \left(C_\mu L_\nu - L_\mu C_\nu\right)(\lambda C^\nu) = (L_\nu C^\nu)\lambda C_\mu = 0, \tag{13}$$

according to which CP flow represented by Eq. (4) satisfies a null geodesic equation. We note here the similarity between Eq. (13) and

the following equation for the electromagnetic field:

$$F_{\mu\nu}P^{\nu} = 0, \tag{14}$$

where $F_{\mu\nu}$ and P^{ν} denote, respectively, the electromagnetic skew-symmetric tensor and Poynting 4-vector. The latter one is parallel to a null geodesic perpendicular to both the electric $\overrightarrow{E} = (F_{01}, F_{02}, F_{03})$ and the magnetic $\overrightarrow{H} = -(F_{23}, F_{31}, F_{12})$ vectors. The difference in form between Eqs. (13) and (14) is that the skew-symmetric tensor $F_{\mu\nu}$ is not defined as the curl of P_{μ} while $S_{\mu\nu}$ is derived by the curl of U_{μ}.

One of the direct consequences of Eq. (4) is the following identity:

$$D \equiv S_{01}S_{23} + S_{02}S_{31} + S_{03}S_{12} = 0, \tag{15}$$

where $D = Pf(S)$ is the Pfaffian of the anti-symmetric matrix $S_{\mu\nu}$: $D^2 = Det(S_{\mu\nu})$. Similarly to $\overrightarrow{E} \cdot \overrightarrow{H} = 0$ for the electromagnetic field $F_{\mu\nu}$, the orthogonality between (S_{01}, S_{02}, S_{03}) and (S_{23}, S_{31}, S_{12}) follows from the existence of non-zero vector U^{ν} satisfying the matrix Eq. (13) because of $Det(S_{\mu\nu}) = D^2$.

4.3. Lightlike field with an embedded classical wave-particle duality

Corresponding to the energy-momentum tensor T_{μ}^{ν} (in the mixed tensor form) associated with electromagnetic field given by

$$T_{\mu}^{\nu} = -F_{\mu\sigma}F^{\nu\sigma}, \tag{16}$$

we have the similar quantity $\widehat{T}_{\mu}^{\nu}$ for $S_{\mu\nu}$ defined by

$$\begin{aligned}
\widehat{T}_{\mu}^{\nu} = -S_{\mu\sigma}S^{\nu\sigma} &= -\left(C_{\mu}L_{\sigma} - L_{\mu}C_{\sigma}\right)\left(C^{\nu}L^{\sigma} - L^{\nu}C^{\sigma}\right) \\
&= -\left(L_{\sigma}L^{\sigma}\right)C_{\mu}C^{\nu} = \rho C_{\mu}C^{\nu},
\end{aligned} \tag{17}$$

where use has been made of equations (5), (11) and (12). While C^{μ} is lightlike, (17) is identical in form to the energy-momentum tensor of freely moving (fluid) particles. Actually, from $C^{\nu}\nabla_{\nu}C_{\mu} = 0$, $\nabla_{\nu}C^{\nu} = 0$ and $C^{\nu}\nabla_{\nu}\rho = 0$, owing to (5), (9) and (12), we get

$$\nabla_{\nu}\widehat{T}_{\mu}^{\nu} = 0. \tag{18}$$

Since (17) has dual representations, (18) can also be expressed in terms of $S_{\mu\nu}$ as

$$\nabla_{\nu}\widehat{T}_{\mu}^{\nu} = -\nabla_{\nu}\left(S_{\mu\sigma}S^{\nu\sigma}\right) = -S_{\mu\sigma}\nabla_{\nu}S^{\nu\sigma} = 0. \tag{19}$$

In deriving the above equation, the well-known Bianchi identity $\nabla_{\nu}S_{\rho\sigma} + \nabla_{\rho}S_{\sigma\nu} + \nabla_{\sigma}S_{\nu\rho} = 0$ is used in combination with the condition $S_{\nu\rho}S^{\nu\rho} = 0$ corresponding to massless property of electromagnetic field. An intriguing consequence of the dual representation (17) is that we readily get the classical version of Einstein - de Broglie relation which cannot be recovered by the conventional classical electromagnetic theory. In fact, we have, on the basis of (17),

$$\widehat{T}_{0}^{\nu} = -S_{0\sigma}S^{\nu\sigma} = \rho C_{0}C^{\nu}, \tag{20}$$

which is the Poynting four vector representing the flux of energy density. The hydrodynamic representation on r.h.s. readily allows us to regard this as the advection of energy density ρC_{0} by a given "velocity" field C^{ν}. In addition, since ρ can be regarded as density, namely, the number of "molecules" per unit volume, the energy associated with one "molecule" is proportional to the frequency of ϕ field.

Going back to (19), we see that the corresponding quantity $\nabla_{\nu}T_{\mu}^{\nu} = -F_{\mu\sigma}\nabla_{\nu}F^{\nu\sigma}$ in Maxwell's theory of electromagnetism vanishes under the following condition of no electric current:

$$\nabla_{\nu}F^{\nu\sigma} = 0, \tag{21}$$

which yields the electromagnetic wave equation in the vacuum. Note, however, that $\nabla_{\nu}S^{\nu\sigma} = 0$ is sufficient for (19) but not necessary, and, in the case of CP flow under consideration, simple manipulations on (6) yields

$$\nabla_{\nu}S^{\nu\sigma} = -(\nabla_{\nu}L^{\nu})C^{\sigma} = -(\kappa_{0})^{2}\lambda C^{\sigma} = -(\kappa_{0})^{2}U^{\sigma}. \tag{22}$$

By virtue of (13), therefore, Eq. (19) holds whether $\nabla_{\nu}S^{\nu\sigma} = 0$ holds or not. Note that, because of $\nabla_{\nu}S^{\nu\sigma} = \nabla_{\nu}(\nabla^{\sigma}U^{\nu} - \nabla^{\nu}U^{\sigma})$, Eq. (22) can be rewritten as

$$\nabla_{\nu}(\nabla^{\nu}U^{\sigma} - \nabla^{\sigma}U^{\nu}) - (\kappa_{0})^{2}U^{\sigma} = 0, \tag{23}$$

which can be regarded as "Proca equation" in our CP vortex dynamics. The original Proca equation for electromagnetic theory takes the form:

$$\nabla_{\nu}(\nabla^{\nu}A^{\sigma} - \nabla^{\sigma}A^{\nu}) + m^{2}A^{\sigma} = 0, \tag{24}$$

in terms of the electromagnetic vector potential A^μ and the mass m^2. Eq. (24) clearly shows that lightlike solutions to $\nabla_\nu(\nabla^\nu A^\sigma - \nabla^\sigma A^\nu) = 0$ are gauge invariant, while solutions to (24) must have a gauge fixing $\nabla_\nu A^\nu = 0$. In other words, the massless property of a real photon described by the rotational part of A^μ is directly related to the gauge invariance. A peculiar feature of (23) is that it is valid even for lightlike U^σ with a fixed "gauge" of $\nabla_\nu U^\nu = 0$, which is assured by the orthogonality condition of (11).

A polarization vector represents an important aspect of electromagnetic waves, since electric and magnetic vectors $\vec{E}, \vec{H}$ are a couple of elemental physical factors, at least in the classical electromagnetic theory, in terms of which other physical quantities are expressed. In Fig. 4, we illustrate a plane-polarized electromagnetic wave whose $\vec{E}$ and $\vec{H}$ are parallel (or anti-parallel) to x^3 and x^2 axes, respectively. Then we can readily construct the corresponding wave in the CP model: $\phi = \hat{\phi}sin(kx^0 - kx^1)$ and $\lambda = \hat{\lambda}cos(kx^0 - kx^1 - lx^3)$ give a wave with such S_{03} and S_{31} denoted in Fig. 4. In Fig. 4, E_3 as well as H_2 change in a space-time domain according as $sin(kx^0 - kx^1)$ whose space-time dependence are exactly the same as those of C_0 and C_1 derived from $\phi = \hat{\phi}sin(kx^0 - kx^1)$.

So, we may regard C_0 and C_1 as the polarization vector of plane-polarized "light" wave described by CP vortex dynamics. If we accept this interpretation, then we can say that the polarization vectors of conventional electromagnetic field perpendicular to the associated Poynting vector and those of a dual "electromagnetic" field described by CP vortex dynamics are complementary in the sense that they provide a complete orthogonal basis of 4-dimensional spacetime. It is also interesting to note that this complementarity is directly related to the classical wave-particle duality picture manifested in the energy momentum representation (17). Concerning the longitudinal modes in electromagnetic field, there have been many discussions: within the context of the classical Maxwellian theory, for instance, Lax et al. [59] discussed it in relation to paraxial optics and Cicchitelli et al. [60] further discussed their results and showed that the existence of longitudinal modes can be experimentally proven. Note also that the longitudinally polarized photons as virtual ones, similar to (C^0, C^1) mentioned above, are necessary physical ingredients in the perturbative calculations of quantum electromagnetic interaction theory [61] and one of the authors [62] discussed the physical relevance of the longitudinal mode in the formulation of manifestly covariant quantization of electromagnetic field.

4.4. Further remarks on the longitudinal modes

For the sake of a unified understanding of the longitudinal modes of electromagnetic field, we need clearly to treat both the relativistic and non-relativistic situations on the same footing. In the standard approach to this problem, however, the theoretical frameworks prepared are not along this way of thinking! For instance, in the so-called covariant quantization of gauge fields, it is common to focus upon the purely relativistic situation neglecting the presence of non-relativistic one, as a result what remains as physical modes in the physical Hilbert space are only the transverse modes with positive metric, with the longitudinal modes being confined as unphysical modes. To understand the mutual relations between such physical and unphysical modes, we need to unify both the relativistic microscopic level with high energies and the non-relativistic macroscopic level with low energies. Adopting such a wider formulation, we can observe that the longitudinal modes with negative metric hiding themselves from the high energy regions can show up themselves without the visible effects of negative metrics condensed into classical modes.

4.5. Extension to non-lightlike cases

The arguments developed so far are restricted to the dual vortex structure of the lightlike electromagnetic field whose energy-momentum tensor is given by (16) and that of the associated $S_{\mu\nu}$ in (17). In this section, we show that the newly introduced CP vortex formulation can be extended to the cases where U_μ is spacelike. Timelike U_μ is excluded because of (23). In terms of the vector symbols given in (7), the reduced CP flow vector originally defined in (4) can now be redefined as
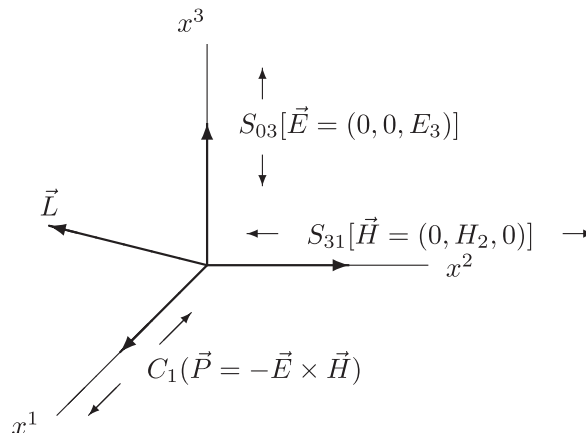
Fig. 4. Dual configuration of $[\vec{E},\ \vec{H},\ \vec{P}]$ and $[S_{03},\ S_{31},\ \vec{C}]$.

$$U_\mu = \frac{1}{2}\left(\lambda C_\mu - \phi L_\mu\right). \tag{25}$$

For electromagnetic field, we assume that U_μ satisfies the geodesic equation (1) which is rewritten as

$$S_{\mu\nu}U^\nu + \nabla_\mu V = 0, \tag{26}$$

where $V \equiv U^\nu U_\nu / 2$ and $S_{\mu\nu}$ remains to be the same as that given in (7). A natural extension from a lightlike to spacelike CP vortex formalism would be attained through replacing the d'Alembert equation (5) for ϕ by the Klein-Gordon Eq. (6) for λ, that is,

$$g^{\mu\nu}\nabla_\mu\nabla_\nu\psi - \kappa_0^2\psi = 0. \tag{27}$$

Namely, ϕ and λ satisfy the same equation. In the preceeding discussions on lightlike cases, we confine ourselves to real variables, but, in what follows, for mathematical simplicity let us consider a complex plane wave solution to (27) with the form of $\psi = \exp i(k_\sigma x^\sigma)$ which satisfies the following a couple of equations:

$$g^{\mu\nu}\nabla_\mu\nabla_\nu\psi = -k^\sigma k_\sigma \psi; \; g^{\mu\nu}\nabla_\mu\psi\nabla_\nu\psi = -k^\sigma k_\sigma \psi^2, \tag{28}$$

where $\kappa_0^2 = -k^\sigma k_\sigma$. Here, the second equation in (28) should not be confused with that in (6) since we now employ complex representations. Since ϕ and λ satisfy (28), using (7), we have

$$\nabla_\nu C^\nu - \kappa_0^2\phi = 0; \; C^\nu C_\nu - \kappa_0^2\phi^2 = 0, \tag{29}$$

$$\nabla_\nu L^\nu - \kappa_0^2\lambda = 0; \; L^\nu L_\nu - \kappa_0^2\lambda^2 = 0. \tag{30}$$

For the directional constraint between $\nabla_\mu\phi$ and $\nabla_\mu\lambda$, we can employ exactly the same conditions as (8 and 11). Note that using (8), (11) and the integrability conditions of $\nabla_\nu L_\mu = \nabla_\mu L_\nu = \nabla_\mu\nabla_\nu\lambda$ and the same for ϕ, we obtain

$$C^\nu\nabla_\nu L_\mu = 0; \; C^\nu L_\nu = 0, \Rightarrow L^\nu\nabla_\nu C_\mu = 0. \tag{31}$$

With this orthogonality condition, it can readily be shown that U^ν is a divergence free vector, namely, $\nabla_\nu U^\nu = 0$, which can be regarded as the Lorentz gauge in CP vortex formulation. In the use of the second equations in (29, 30) and of the orthogonality condition $C^\nu L_\nu = 0$ in (31), the quantity $V = U^\nu U_\nu / 2$ is reduced to

$$V = \left(\frac{1}{2}\right)^3 (\lambda C^\nu - \phi L^\nu)(\lambda C_\nu - \phi L_\nu) = \left(\frac{1}{4}\right)(\kappa_0)^2(\lambda\phi)^2. \tag{32}$$

Now, going back to (26), direct calculations of $S_{\mu\nu}U^\nu$ and $\nabla_\mu V$ yield

$$S_{\mu\nu}U^\nu + \nabla_\mu V = \frac{1}{4}(\lambda\phi)^2\nabla_\mu(\kappa_0)^2 = 0, \tag{33}$$

since κ_0 is not a variable but a constant. By similar simple calculations, we also get

$$U^\sigma\nabla_\sigma(\lambda\phi) = 0; \; \Omega \equiv S_{\mu\nu}S^{\mu\nu} = 2(\kappa_0)^4(\lambda\phi)^2, \tag{34}$$

from which we obtain an important advection equation:

$$U^\sigma\nabla_\sigma\Omega = 0. \tag{35}$$

In lightlike case, we have looked into the form of energy-momentum tensor given by (17) based on (16). For non-lightlike case, if we follow the conventional electromagnetic knowledge again, it is natural to start with the form:

$$\widehat{T}_\mu^\nu = -S_{\mu\sigma}S^{\nu\sigma} + \frac{1}{4}S_{\alpha\beta}S^{\alpha\beta}g_\mu^\nu. \tag{36}$$

Through the well-known manipulation in electromagnetic theory, we get

$$\nabla_\nu\widehat{T}_\mu^\nu = -S_{\mu\sigma}\nabla_\nu S^{\nu\sigma}. \tag{37}$$

By similar manipulations leading to (22), we have

$$\nabla_\nu S^{\nu\sigma} = \left[-C^\sigma(\nabla_\nu L^\nu) + L^\sigma(\nabla_\nu C^\nu)\right] + \left[C^\nu\nabla_\nu L^\sigma - L^\nu\nabla_\nu C^\sigma\right]. \tag{38}$$

We see that, by using (31), (38) reduces to a form similar to (22) and hence (37) becomes

4C

$$\nabla_\nu \widehat{T}_\mu^\nu = -S_{\mu\sigma}\big[-C^\sigma(\nabla_\nu L^\nu) + L^\sigma(\nabla_\nu C^\nu)\big]$$
$$= \kappa_0^2 S_{\mu\sigma}(\lambda C^\sigma - \phi L^\sigma) = 2\kappa_0^2 S_{\mu\sigma} U^\sigma. \tag{39}$$

By using (26), (32) and the second equation in (34), the above equation leads to

$$\nabla_\nu \widehat{T}_\mu^\nu = \nabla_\nu \left(-\frac{1}{4}\Omega g_\mu^\nu \right). \tag{40}$$

Combining (36) and (40), and introducing a new notation: $\widehat{S}_{\mu\nu\sigma\rho} = S_{\mu\nu}S_{\sigma\rho}$, we finally obtain

$$\nabla_\nu \widehat{G}_\mu^\nu = 0;\ \widehat{G}_\mu^\nu \equiv -\widehat{S}_{\mu\sigma}^{\nu\sigma} + \frac{1}{2}\widehat{S}_{\alpha\beta}^{\alpha\beta} g_\mu^\nu, \tag{41}$$

which is isomorphic to the following Einstein tensor G_μ^ν:

$$\nabla_\nu G_\mu^\nu = 0;\ G_\mu^\nu \equiv -R_{\mu\sigma}^{\nu\sigma} + \frac{1}{2}R_{\alpha\beta}^{\alpha\beta} g_\mu^\nu = T_\mu^\nu, \tag{42}$$

where $R_{\mu\nu\sigma\rho}$ denotes Riemann tensor and T_μ^ν is an energy-momentum tensor of non-gravitational origin. Since (41) is isomorphic to (42), tensor $\widehat{G}_\mu^\nu$ is well qualified for being an energy-momentum tensor of a new type of electromagnetic field. Recall that "space" and "time" as a couple of conceptual quantities in Newtonian physics were merged into a single notion of flat Minkowski spacetime by the theory of special relativity in which light plays a crucial role. CP vortex model for the new type of electromagnetic field has shown that not only flat but also curved spacetime structure can be regarded as an emergent feature of electromagnetic field with a "mass" term of $S_{\mu\nu}S^{\mu\nu}$. In order to check whether "mass" term Ω is positive or not, we first check the magnitude of V denoted by $\|V\|$ based on (32). Since U^μ is spacelike, $\|V\|$ must be negative, which can be verified by

$$\|V\| = \frac{1}{2^3}(\lambda C_\nu - \phi L_\nu)^*(\lambda C^\nu - \phi L^\nu) = -\frac{1}{4}(\kappa_0)^2 (\lambda^*\lambda)(\phi^*\phi), \tag{43}$$

where superscript * denotes the complex conjugate. Then, by combining (43) with the second equation in (34), we have

$$\|\Omega\| = 8(\kappa_0)^2 \|V\|, \tag{44}$$

from which we see that $\|\Omega\|$ is also negative.

In order to see the implication of (44), let us introduce a couple of constant dimensional and variable non-dimensional parameters $\widehat{V}_0$ and n with which the squared magnitude of U^μ given at one line below (26), namely, $V = U^\nu U_\nu/2$, is scaled as

$$V = \frac{1}{2}(\widehat{V}_0 n)^2 v^\nu v_\nu, \tag{45}$$

where v^ν denotes non-dimensional four velocity vector satisfying a spacelike condition of $\|v^\nu v_\nu\| = -1$. Since $-\|\Omega\|$ is a squared magnitude of the vorticity tensor in CP model, we can introduce ω which represents the magnitude of vorticity as $\omega^2 \equiv -\|\Omega\|$. Then, with this ω and (45), Eq. (44) is rewritten as

$$|\tilde{\omega}| = 2(\kappa_0)^2 n, \tag{46}$$

where $\tilde{\omega} \equiv \kappa_0 \omega/\widehat{V}_0$. Note that Eq. (46) is isomorphic to the linear relation known as Regge trajectories for resonance particles in the field of high energy particle physics. Actually, since the dimension of the r.h.s. of (46) is l^{-2} which is equal to M^2 in a natural units system, (46) says that the rotational measure defined as $\tilde{\omega}$ is proportional to the magnitude of squared "mass" field. In the case of Regge trajectories, the l.h.s. corresponds to the angular momentum of a resonance particle practice.

4.6. Physical interpretation of CP vortex as a model for off-shell photons

According to our discussion so far, there exist a couple of electromagnetic fields characterized respectively by (23) and (24), which may be called spacelike and timelike electromagnetic fields when we exclude lightlike modes in respective fields. Although both fields satisfy formally the same Lorentz gauge condition of the form: $\nabla_\nu A^\nu = 0$ and $\nabla_\nu U^\nu = 0$, their physical meanings are quite different. While the physical origin of $C_\mu = \nabla_\mu \phi$ in a lightlike mode is discussed in subsections 4.2 and 4.3, the fate of $L_\mu = \nabla_\mu \lambda$ has not been settled yet. Let us consider first the physical meaning of $S_{\mu\nu}$ expressed in a bivector representation in terms of C_μ and L_ν given in (7). Since C^μ can be regarded as the linear momentum vector field of a given current of "photons" as the classical particles, the vorticity tensor $S_{\mu\nu}$ may be formally regarded as the associated angular momentum tensor field if L^ν plays the role of the position vector field of the current, which is consistent with the fact that L^ν must be spacelike in CP vortex formulation. Note also that the physical dimension of U^μ becomes exactly

the same as that of A^μ, if $\phi = \nabla_\nu A^\nu$ and the physical dimension of L_μ is that of length! Clearly, in this reinterpretation, $S_{\mu\nu}$ becomes a so-called orbital angular momentum field. One of the striking features of photon missing in the classical electromagnetic theory is its intrinsic spin which is related to circularly polarized (right or left) classical electromagnetic field. So, in this sense, we may say that circularly polarized state is more fundamental than plane-polarized one. Notice that the circular motions of electric and magnetic vectors $\vec{E}$ and $\vec{M}$ in such a circularly polarized state naturally induce a current σ^μ whose mathematical expression is quite similar to that of the Poynting vector defined as the exterior product of those two vectors. In subsection 4.1, we referred to quantum-classical correspondence as an important guiding principle bridging the gap between the classical and quantum descriptions. From the viewpoint of quantum-classical correspondence, the introduction of a hypothetical σ^μ current as an intrinsic helicity vector field corresponding to the spin of photons seems to be a plausible component which smoothly connects the classical electromagnetic theory to quantum one and, from this viewpoint, the vector field $U_\mu = \lambda\nabla_\mu\phi$ given in (4) considered to be the vector potential for $S_{\mu\nu}$ can be physically interpreted as the above σ^μ current.

As we have shown in subsections 4.2 and 4.3, the difference between lightlike modes for (23) and (24) is the configuration of polarization vectors and the above argument on identifying circularly polarized state as the classical "photon" accompanying σ^μ current implies that such a state is a combined mode of (23) and (24) and is complete in the sense that its four polarization vectors provide orthogonal basis of the spacetime. When U^μ in (23) becomes spacelike, unlike the case of polaritons corresponding to timelike A^μ in (24), an excited state, when it interacts with a localized disturbance with timelike components in the Fourier-transformed space cannot remain to be a stable on-shell mode [63] even if it should elude the limitation arising from the uncertainty principle $\Delta E\Delta t > \hbar$. However, there exists an important exceptional case to this situation. Since any material field in a steady state is represented by spacelike vectors, the interactions with such fields does not lead to the instability of U^μ field. We think that the manifestation of DP around spatially fixed substances occurs as a result of such a stable interaction with steady state material fields and spacelike U^μ field excited at the characteristic length scale of $(\kappa_0)^{-1}$. A spherically symmetric solution to the Klein-Gordon equation (27) without a temporal differential term is known to yield Yukawa potential whose magnitude decreases exponentially in the radial direction. So far no theoretical attempt including ones referred to in section 2 can successfully reproduce such an experimentally verified damping feature of DP field in near vacuum environment. Thus, CP vortex model proposed in this article seems to be a promising approach to the undiscovered realm of DP.

5. Discussion and summary

For clarifying the essential line of main contents, it would be useful to make the following comments on the energy(-momentum) spectra of field operators and of state vector spaces. As mentioned in Introduction, there is a sharp difference in energy-momentum spectra of field operators between free and interacting fields, which cover a mass hyperboloid $p^2 = m^2$ to characterize the on-shell particles in the former case and the whole p-space in the latter. While the latter situation has been always neglected in the standard discussions in physics, it plays the crucial roles in describing all the interaction processes and also in the consistent formulation of DPs and of DPPs, which has been implemented in Section 4 by the help of $S_{\mu\nu}$ as the Clebsch dual of $F_{\mu\nu}$. Namely, the Clebsch duality relation between $F_{\mu\nu}$ and $S_{\mu\nu}$ can be seen from the viewpoint of duality between visible and invisible aspects, originating from the duality between positive and negative sides of the lightcone $p^2 = 0$.

The next remark to be given is the difference in the energy-momentum spectrum between field operators and state vector spaces, which is important though seldom noted nor mentioned explicitly: the presence of positive/negative energy spectra in field operators should easily be seen by the existence of creation and annihilation operators, which could not be distinguished without the sign difference of energies carried by these operators. In the state vector space, however, such a familiar condition on the vacuum vector $|0\rangle$ as $a|0\rangle = 0$ to characterize the Fock space structure is working as the selection of one-sided spectrum of energy at the level of state vector space. From this situation, such a blind belief seems to start that the energy spectra in quantum theory must always be positive, in combination with which the vacuum vector $|0\rangle$ generating all the state vectors (due to the cyclicity assumption) becomes such a mysterious object as creating everything in spite of its emptiness!! If we move from the vacuum situation to thermal ones, then the right/left symmetry of state vector space of Gibbs state or the modular inversion symmetry valid in the Tomita-Takesaki extension [64] of thermal equilibrium to infinite systems implies that energy spectrum in this situation is symmetric under the sign change of the energy. Actually, the positive energy spectrum is seen to be an exceptional condition to characterize the concept of vacua and it can be easily violated in almost all the physical situations. The scenario explained briefly in Introduction can naturally be understood, once the above two kinds of remarks are accepted: For instance, if you stick to the standard familiar concept of the usual (i.e., massless on-shell) photons, then the concept of off-shell photons or DPs may sound quite strange and unfamiliar. If you start to realize that any kinds of particles will experience their off-shell forms during the mutual interactions, then the existence of off-shell photons or DPs is seen to be quite natural in spite of their being invisible. As for the invisibility, you cannot observe any meaningful interaction processes causing changes on any seemingly "unchangeable" objects, without which this world become frozen!!

Therefore, it may be useful to add a comment on the parallelism of the above ubiquitous changes (of seemingly unchangeable objects via the duality between visible and invisible) with the essence of thermodynamics involving stability and instability! When we see any processes of working thermal engines, *e.g.*, Carnot cycles for instance, it is one of the universal features that the cycle contains the subprocesses in which heat and/or energy is absorbed and emitted. If we take the starting point of exerting the work as the origin of the energy levels, then the absorbing process is seen to correspond to the states with negative energy spectrum and the working one with energy emitted to those with positive energy spectrum. From this viewpoint, the usual formulation of the vacuum states in relativistic QFT can be seen to be quite unrealistic, where the existence of states with negative energy spectrum is denied and where the state with the zero energy is identified with the vacuum state. In this context, the usual $F_{\mu\nu}$ can be seen to correspond to the processes emitting heat

to the cooler reservoirs exerting the work onto the external world, and $S_{\mu\nu}$ to those absorbing heat from the hotter heat reservoirs. Similarly in the example of Mandelstam variables for scattering processes, the *s*-channel with incoming and outgoing particles can be put in analogy with the processes with energy emitted and *t*-channel with energy-momentum transfer caused by interaction potentials with those absorbing energy. If the former aspect is also put in correspondence with the branches of back and forth fluctuations in the steepest descent method, then the latter one with falling down slope, along which energy absorbing process let the working system climb up to the saddle point. These two kinds of examples can be unified actually into the context of large deviation principle [65,66], from the viewpoint of which the essence of DP will be well understood.

Acknowledgements

References

[1] R.F. Streater, A.S. Wightman, PCT, Spin and Statistics, and All That, Princeton University Press, 2000.
[2] I. Ojima, H. Saigo, Mathematics 3 (2015) 897.
[3] M. Ohtsu, Opt. Rev. 21 (2014) 905.
[4] D. Pines, Elementary Excitation in Solids, Perseus Books, Reading, 1999.
[5] M. Ohtsu, K. Kobayashi, Optical Near Fields, Springer, Heidelberg, 2004.
[6] M. Thomson, Modern Particle Physics, Cambridge Univ. Press, Cambridge, 2013, pp. 117–119.
[7] R.P. Feynman, The Theory of Fundamental Processes, W. A. Benjamin, New York, 1962, pp. 95–100.
[8] M. Ohtsu, H. Hori, Near-Field Nano-Optics, Kluwer Academic/Plenum Publishers, New York, 1999, pp. 29–31.
[9] K. Kobayashi, Surf. Sci. 30 (2009) 638.
[10] M. Ohtsu, Dressed Photons, Springer, Heidelberg, 2013, pp. 11–36.
[11] Y. Tanaka, Phys. E 40 (2007) 297.
[12] H. Hyuga, H. Ohtsubo, Nucl. Phys. A 294 (1978) 348.
[13] K. Kobayashi, M. Ohtsu, J. Microsc. 19 (1999) 2494.
[14] S. Sangu, K. Kobayashi, M. Ohtsu, J. Microsc. 202 (2001) 279.
[15] S. Sangu, K. Kobayashi, S. Shojiguchi, M. Ohtsu, Phys. Rev. B 69 (2004) 1153343.
[16] T. Kawazoe, K. Kobayashi, S. Sangu, M. Ohtsu, Appl. Phys. Lett. 82 (2003) 2957.
[17] W. Nomura, T. Yatsui, T. Kawazoe, M. Ohtsu, J. Nanophot. 1 (2007) 011591.
[18] T. Kawazoe, K. Kobayashi, M. Ohtsu, Appl. Phys. Lett. 86 (2005) 103102.
[19] T. Kawazoe, M. Ohtsu, S. Aso, Y. Sawado, Y. Hosoda, K. Yoshizawa, K. Akahane, N. Yamamoto, M. Naruse, Appl. Phys. B 103 (2011) 537.
[20] T. Yatsui, K. Hirata, W. Nomura, Y. Tabata, M. Ohtsu, Appl. Phys. B 93 (2008) 55.
[21] T. Yatsui, K. Hirata, Y. Tabata, W. Nomura, T. Kawazoe, M. Naruse, M. Ohtsu, Nanotechnol 21 (2001) 355303.
[22] W. Nomura, T. Yatsui, T. Kawazoe, N. Tate, M. Ohtsu, Appl. Phys. A 121 (2015) 1403.
[23] R. Teki, A.J. Kadaksham, M. House, J. Harris-Jones, A. Ma, S.V. Babu, A. Hariprasad, P. Dumas, R. Jenkins, J. Provine, A. Richmann, J. Stowers, S. Meyers, U. Dietze, T. Kusumoto, T. Yatsui, M. Ohtsu, in: Proc. SPIE 8322, 2012, p. 83220B.
[24] T. Yatsui, K. Hirata, Y. Tabata, Y. Miyake, Y. Akita, M. Yoshimoto, W. Nomura, T. Kawazoe, M. Naruse, M. Ohtsu, Appl. Phys. B 103 (2011) 527.
[25] T. Yatsui, W. Nomura, M. Ohtsu, Adv. Opt. Technol. 2015 (2015). Article ID 701802.
[26] T. Yatsui, W. Nomura, F. Stehlin, O. Soppera, M. Naruse, M. Ohtsu, Beilstein J. Nanotechnol. 4 (2013) 875.
[27] T. Yatsui, W. Nomura, M. Naruse, M. Ohtsu, J. Phys. D. 45 (2012) 475302.
[28] T. Kawazoe, H. Fujiwara, K. Kobayashi, M. Ohtsu, IEEE J. Select. Top. Quant. Electron 15 (2009) 1380.
[29] H. Fujiwara, T. Kawazoe, M. Ohtsu, Appl. Phys. B 98 (2010) 283.
[30] S. Yukutake, T. Kawazoe, T. Yatsui, W. Nomura, K. Kitamura, M. Ohtsu, Appl. Phys. B 99 (2010) 415.
[31] H. Tanaka, T. Kawazoe, M. Ohtsu, Appl. Phys. B 108 (2012) 51.
[32] T. Kawazoe, M.A. Mueed, M. Ohtsu, Appl. Phys. B 104 (2011) 747.
[33] M.A. Tran, T. Kawazoe, M. Ohtsu, Appl. Phys. A 115 (2014) 105.
[34] M. Yanaguchi, T. Kawazoe, T. Yatsui, M. Ohtsu, Appl. Phys. A 121 (2015) 1389.
[35] M. Ohtsu, Silicon Light-emitting Diodes and Lasers, Springer, Heidelberg, 2016, pp. 15–42.
[36] J.H. Kim, T. Kawazoe, M. Ohtsu, Adv. Opt. Technol. 2015 (2015). Article ID 236014.
[37] J.H. Kim, T. Kawazoe, M. Ohtsu, Appl. Phys. A 121 (2015) 1395.
[38] T. Kawazoe, M. Ohtsu, Appl. Phys. A 15 (2014) 127.
[39] Q.H. Vo, T. Kawazoe, M. Ohtsu, in: Extended Abstracts of the 61st Spring Meeting on Applied Physics and Related Societies, 2014, 18A–F12–10.
[40] T. Kawazoe, M. Ohtsu, in: Extended Abstracts of the 59st Spring Meeting on Applied Physics and Related Societies, 2012, 17p–B11–1.
[41] N. Wada, T. Kawazoe, M. Ohtsu, Appl. Phys. B 108 (2012) 25.
[42] T. Kawazoe, M. Ohtsu, K. Akahane, N. Yamamoto, Appl. Phys. B 107 (2012) 659.
[43] H. Tanaka, T. Kawazoe, M. Ohtsu, K. Akahane, Fluoresc. Mat. 1 (2015) 1.
[44] H. Tanaka, T. Kawazoe, M. Ohtsu, K. Akahane, N. Yamamoto, Appl. Phys. A 121 (2015) 1377.
[45] K. Kitamura, T. Kawazoe, M. Ohtsu, Appl. Phys. B 107 (2012) 293.
[46] N. Tate, T. Kawazoe, W. Nomura, M. Ohtsu, Sci. Rep. 5 (2015) 12762.
[47] N. Tate, T. Kawazoe, S. Nakashima, W. Nomura, M. Ohtsu, in: Proceedings the 22nd International Display Workshops (IDW15), 2015, p. 1066.
[48] T. Kawazoe, N. Tate, M. Ohtsu, in: Proceedings of the 22nd International Display Workshops (IDW15), 2015, p. 1081.
[49] H. Tanaka, T. Kawazoe, M. Ohtsu, in: Extended Abstracts of the 63rd Spring Meeting on Applied Physics and Related Societies, 2016, 19a–S622–8.
[50] T. Kawazoe, K. Hashimoto, S. Sugiura, in: Abstract of the EMN Nanocrystals Meeting, 2016, pp. 9–11.
[51] T. Kawazoe, K. Nishioka, M. Ohtsu, Appl. Phys. A 121 (2015) 1409.
[52] M. Ohtsu, T. Kawazoe, Silicon light emitting diodes and lasers using dressed photons, in: M. Ohtsu, T. Yatsui (Eds.), Progress in Nanophotonics, vol. 3, Springer, Heidelberg, 2015, pp. 1–56.
[53] I. Ojima, in: Proceedings of the International Conference of Stochastic Analysis, 2005. arXiv:math-ph/0502038.
[54] S. MacLane, Categories for the Working Mathematician, Springer, Heidelberg, 1971.
[55] I. Ojima, Micro-macro duality in quantum physics, in: T. Hida (Ed.), Stochastic Analysis: Classical and Quantum -Perspectives of White Noise Theory, World Scientific, 2005, pp. 143–161.
[56] S.H. Lamb, Hydrodynamics, sixth ed., Cambridge University Press, 1932.
[57] J. Marsden, A. Weinstein, Physica 7D (1983) 305–323.

[58] H. Sakuma, Note on a Novel Vortex Dynamics of Spacetime as a Heuristic Model of the Vacuum Energy, 2014 arXiv:1409.2607[gr-qc].
[59] M. Lax, W.H. Louisell, W.B. McKnight, Phys. Rev. A 11 (1975) 1365–1370.
[60] L. Cicchitelli, H. Hora, R. Postle, Phys. Rev. A 41 (1990) 3727–3732.
[61] I.J.R. Aitchison, A.J.G. Hey, Gauge Theories in Particle Physics, second ed., Adam Hilger, Bristol and Philadelphia, 1989.
[62] I. Ojima, Nakanishi-lautrup B field, crossed product and duality, in: RIMS Workshop: Research on Quantum Field Theory, 2006, pp. 29–37.
[63] Y. Aharonov, A. Komar, L. Susskind, Phys. Rev. 182 (1969) 1400–1403.
[64] O. Bratteli, D. Robinson, Operator Algebras and Statistical Mechanics, second ed., vol. 1, Springer-Verlag, 1987.
[65] R. Ellis, Entropy, Large Deviations, and Statistical Mechanics, Springer-Verlag, 1985.
[66] J. Deuschel, D. Stroock, Large Deviations, Academic Press, 1989.

複雑系としてのドレスト光子とその応用

大津 元一[1,2]，香取 眞理[3]

[1]東京大学大学院 工学系研究科（〒113-8656 東京都文京区弥生2-11-16）
[2]（任）ドレスト光子研究起点（〒221-0022 横浜市神奈川区守屋町3-13-19）
[3]中央大学 理工学部（〒112-8551 東京都文京区春日1-13-27）

Complex System of Dressed Photons and Applications

Motoichi OHTSU[1,2] and Makoto KATORI[3]

[1]*The University of Tokyo, 2-11-26 Yahoi, Bunkyo, Tokyo 113-8656*
[2]*Research Origin for Dressed Photon, 3-13-19 Moriya, Kanagawa, Yokohama 221-0022*
[3]*Chuo University, 1-13-27 Kasuga, Bunkyo, Tokyo 112-8551*

By noting that a dressed photon is a complex quasi-particle composed of photons, electrons, and phonons, creation of the dressed photon and its characteristics are reviewed from the viewpoint of the quantum field in an off-shell space. After applications to silicon light emitting diodes and lasers are presented, their fabrication and operating principle are analyzed by the stochastic model of a complex system.

Key Words: Dressed photon, Silicon, Light emitting diode, Laser, Complex system

1. はじめに

光の波長より大きな寸法の物質中を伝搬する光が電子・正孔対（励起子）と相互作用すると新しい定常状態が物質全体にわたり形成される．この定常状態は励起子ポラリトンと呼ばれる準粒子で記述することができる．その運動量とエネルギーの間の分散関係をグラフ化すると放物線となり，この曲線は量子場の理論でオンシェル（on shell）と呼ばれている[1,2]．一方この曲線から外れた広い領域はオフシェル（off shell）と呼ばれている．

ドレスト光子（DPと略記）はオフシェルの領域に発生する量子場であるが，本稿ではそれが光子，電子，フォノンからなる複合粒子であることに注目しDPの発生の原理，性質を解説する．応用例としてシリコン（Si）結晶を材料とする発光ダイオード（LED），レーザーを紹介する．これらの製作過程，発光の起源を複雑系として捉え，確率過程モデルを用いたシミュレーション結果を提示して今後の研究の方向を展望する．

2. オフシェル光子としてのドレスト光子

オフシェル領域に準粒子が存在するとすれば，それは次の2つの性質を持つ．

(1)運動量の取り得る範囲が広いので，運動量と位置に関する不確定性原理から決まる準粒子の局在寸法は光の波長以下である．この準粒子は物質中または表面にあるナノ構造の位置に発生するが，後者の場合に表面近傍の電磁場は「近接場光」と呼ばれている[3]．

(2)エネルギーの取り得る範囲は広いので，エネルギーと時間に関する不確定性原理から決まる準粒子の存在時間は短い．従ってこれは「仮想光子」と呼ばれている．

以上の2つの性質を持つ量子場がDPに対応する[4,5]．上記(1)のようにDPは物質のナノ構造の位置に発生するが，その発生のためには物質に光（オンシェルの光子）を照射するのがもっとも簡単である．このとき照射光がナノ物質中の励起子と相互作用する様子を記述するには系のエネルギーを量子化する必要がある．しかしDPのナノ寸法の局在性を表現しようとすると，そのような小さな空間では入射電磁場のモードを定義するために必要な共振器を構成することができない．そこで無限数のモードの場を考える．一方，(2)に記したようにエネルギー範囲が広いので，物質中の励起子のエネルギー準位も無限数考える．こうしてハミルトニアンを書き下すことができ，この相互作用を表す準粒子の生成・消滅演算子が導出される．これらの演算子は光子の演算子と励起子の演算子の和からなることから，光子は励起子の衣をまとうと考えられ，DPと呼ばれている[4,5]．これまでに明らかになっているDPの主な性質は次のとおりである．

(a)近接して置かれた複数のナノ物質の間でDPを授受す

る過程は湯川関数で表され，その空間的広がりはナノ寸法と同等である[6]．

(b) DPは励起子の局在性に起因して周囲の物質系のフォノンとも結合してその衣をまとい，DPフォノン（DPPと略記）と呼ばれる新たな準粒子を形成する[7]．このときDPが空間的に局在し，エネルギー範囲が広いことから，DPと結合するのは多モードのコヒーレントフォノンである．

(c) DPPは物質の突起部，物質中の不純物原子の位置に選択的に局在する[8]．

DPおよびDPPは光子，電子，フォノンを構成要素とする複合粒子である．従ってこれらが関わる現象を考察するとき，DPおよびDPPをその構成要素に分解・還元してしまうと意味を持たなくなる．すなわち扱う問題を素粒子に還元せず，メゾスコピックの系としてとらえるべきであり，ここに「複雑系」との接点がある．

3. 応 用

DPおよびDPPはこれまでに加工，デバイス，システムに広く応用されている[9]．ここでは前節の性質(c)のうち物質中の不純物原子の位置に局在するDPPの応用例としてSi結晶を材料とするLEDおよびレーザーを紹介する．

Siは間接遷移型半導体であり，帯間遷移のためには運動量の異なる電子と正孔とが再結合しなければならない．その際，運動量の保存則を満たすためには光子の他にフォノンも同時に放出する必要があるが，それを満たす確率は低い．しかしDPPはフォノンを含むので，これが伝導帯中の電子と相互作用すれば運動保存則が満たされ，発光デバイスが実現する．そのためには製作時，および動作時にDPPを使う．

3.1 製 作

ここでは近赤外光を発生するLEDを例にとり，その製作方法について概説する．まずn型Si結晶基板の表面にイオン注入法によりボロン(B)原子を注入しp型とする．これに順方向電流を流し，ジュール熱によりアニールする．これによりB原子は熱拡散するが，その際基板表面に波長約1.3 μmの近赤外光を照射する．この光の光子エネルギーはSiのバンドギャップエネルギーE_g(= 1.12 eV)にくらべ小さいので吸収されず，結晶内部に侵入し，前節(c)の性質によりB原子の位置にDPPが生成・局在する．

このDPPの付近にある伝導帯中の電子はDPP中のフォノンと運動量を授受し発光する．これはDPPにより駆動された誘導放出光であり，結晶外部に伝搬する．言い換えると，与えられたジュール熱は光エネルギーとなって外部へ散逸する．この散逸によりDPPの発生した位置ではSi結晶の過熱が局所的に抑えられ，B原子の拡散は制限される．

このようなDPPの発生，誘導放出，エネルギー散逸が各所で生じ，発光強度は次第に増加して定常値に達し製作が終了する．この製作方法はDPP援用アニールと呼ばれている[10]．なお，このアニールが効率よく進行する為の最適条件は，順方向電流および照射光によりpn接合部に毎秒注入される電子数と光子数の比がほぼ1：1であることが確認されている[11]．これは上記のジュール加熱と誘導放出による冷却のつり合いを表している．

3.2 動 作

製作されたLEDを動作させるには上記の照射光は不要である．また製作時の順方向電流にくらべ低電流を流せばよい．その際，結晶内部ではDPPが発生し，これが発光源となる．Fig. 1 中の曲線Aは30分間のDPP援用アニールにより作製されたLEDの発光スペクトルである[12]．このLEDの外部量子効率の値は15%，発光パワーは1.1 Wに達し，高効率・高パワー発光していることが確認されている．参考のためにアニール前の微弱な発光スペクトルを曲線Bに示す．

曲線Aの形は曲線Bと大きく異なっており，発光スペクトルはE_g以下の低エネルギー側に広がっている．E_gの位置に明瞭な発光ピークは存在せず，製作の際に照射した光の光子エネルギー(0.95 eV，波長1.30 μm)に相当する領域にピーク（下向き矢印）が現れている．すなわち発光は照射光の複製になっており，この現象は光子エネルギーに関する光子ブリーディング(PBと略記)と呼ばれている[13]．なお，二つの上向き矢印はDPPが各々一つの光学フォノン，二つの光学フォノンを放出することにより生じた側波帯である．

PBの起源を探るためにアトムプローブ法を用いB原子の空間分布が測定された[14]．ここでは一つのB原子とその近隣にあるもう一つのB原子に注目し，両者をB原子対とみなしてその長さと方向が評価された．なぜならば性質(c)に加え，不純物の対があるとフォノンはさらに局在しやすくなるため，この対はDPPを生成するためのフォノン局在中心として働くからである[15]．この性質に留意し，上記の測定結果を分析したところ，DPP援用アニール前にはB原子分布は不規則であるが，アニール後にはB原子対の長さdはSi結晶の格子定数aの3倍($d = 3a$)，かつその方向は入射光の伝搬方向と垂直面内（すなわち結晶基板表面内）となり，B原子の空間分布に
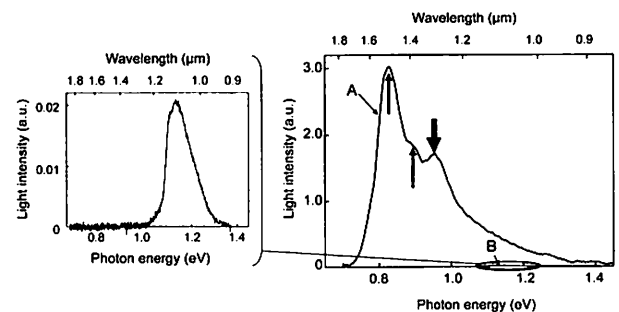
Fig. 1 Light emission spectra. Curve A is the spectrum of the fabricated device. Curve B is the spectrum acquired before the DPP-assisted annealing. Curve B is magnified and is displayed in the left part of this figure.

規則性が生じることが確認された[14]. これをSi結晶のエネルギー帯構造をもとに考察すると次のようになる.

近赤外光の発生に関わる電子の伝導帯の底はX点近傍にあり, 価電子帯の頂上はΓ点にある. この位置にある電子と正孔が再結合し発光するにはX点とΓ点の差に相当する運動量を電子とフォノンとの間で授受する必要がある. X点とΓ点の差に相当する運動量はh/a(hはプランク定数)であるが, $d = 3a$の場合, このB原子対に局在するフォノンの運動量は$h/3a$となり, 必要な値の1/3である. ここでDPPを構成するフォノンはコヒーレント状態であることから複数のフォノンを含み, 従ってフォノン三つ分の運動量を電子と授受することができる. その結果, 上記の要求に応えることができ電子は正孔と再結合して発光する. このとき発光の光子エネルギーはE_g-$3E_{phonon}$(E_{phonon}はフォノンのエネルギー)であり, これが製作の際に照射した光の光子エネルギーに相当する. これが光子エネルギーに関するPBである. 言い換えると, 製作の際にB原子は自律的にその空間分布を変え, 電子とフォノンとの運動量の授受, それによる発光, さらにはPBの効果を実現させているのである.

なお, DPP援用アニールの際に直線偏光を照射することにより, 製作されたLEDからの発光も同様に直線偏光していることが確認されている[14]. これは光子スピンに関するPBである. その起源としてアニール後のB原子対の長さ, 方向は上記と同等であり, さらに結晶基板表面内で直線偏光の方向と垂直に配列することが確認された. 製作の際にはDP中の横モードの光学フォノンがDPP援用アニールに寄与するが, このフォノンの格子振動の方向はDPP援用アニールの際の照射光の直線偏光の方向と平行である. 動作時にもこのフォノンが発光に寄与するので, 発光の偏光方向は照射光の偏光方向と一致するのである.

Si結晶に共振器構造を作りつけることにより, 上記LEDと同様の近赤外光を発するレーザーも同様のDPP援用アニールにより製作されている[16]. まず, 幅10 μm, 厚さ2 μm, 長さ550 μmのリッジ導波路を作りつけたデバイスが製作され, 室温でのレーザー発振のしきい値電流密度1.1 kA/cm², 注入電流60 mAのときの外部微分量子効率1%が得られた. これら直接遷移型半導体のInGaAsP/InPを用いた波長1.3 μmの二重ヘテロ構造のレーザーの値と同等の値である[17]. 発振しきい値以上(直流電流56 mA)で波長1.271 μm(DPP援用アニールの際の照射光波長と同等)における鋭い単一モード発振が実現したが, これはPBの証左である. 次に導波路内への光閉じ込め係数の増大化などの改良がなされ, しきい値電流密度は40 A/cm²まで減少した[18].

さらに赤外光に対する吸収損失が低いことに注目し, 高出力化を目的として狭ストライプ導波路を使わない長共振器(長さ1 mm)構造が採用された. その結果共振器両端面出力パワー200 mW, しきい値電流密度は12.5 A/cm²(上記の直接遷移型半導体の場合の約1/100)が得られた. 以上により上記のLEDと同様に高効率・高パワー発光が実現した[19].

4. 複雑系としての取り扱い

前節のPBの起源において重要な役割を演じたのはSi結晶に注入されたB原子であった. すなわちDPP援用アニールの結果B原子の配置に規則性が生じ, そこにLED製作時に照射した光の情報(光子エネルギーや偏光の情報)が埋め込まれるのである. すなわちB原子の空間分布と配置はPBにおいて, いわば遺伝子の役割を担っている.

ここで注意すべきことは, 「遺伝情報」であるB原子配置は, Si-LED製作者が材料内に意図的に定めたものではないという点である. 照射光の波長や偏光に応じてSi-B系が自律的に応答することにより, PBを可能とするB原子配置が形成され安定化するのである. 複雑系科学では多体系(大規模自由度系)が見せるこのような予定調和的な応答を自己組織化現象とよび, その表現の仕方が研究されている[20]. この方法に沿い最近では香取・小林によりLEDのPBを一つの自己組織化現象として捉えた数理的モデルが提案され, このモデルを数値シミュレーションした結果, LED製作と動作の実験結果が再現されている[21]. 本節では, この複雑系科学に基づくPBのモデル化について紹介する.

寸法3 mm×3 mm×625 μmのSi結晶基板に注入されたB原子は, 基板表面から1.5 μm-2.0 μmのごく薄い層内に分布する[14]. そこでこの層を2次元正方格子で表し, Si結晶中のB原子の熱拡散を, この正方格子上のN個の粒子のランダムウォークとしてモデル化する. ここで各粒子は熱活性状態($\alpha = +$)と不活性状態($\alpha = -$)の二状態をとり, $\alpha = +$状態のときにだけ最近接格子点へホッピングできる. またB原子の熱拡散は順方向電流によって与えられるジュール熱によって駆動されるので, 順方向電流の大きさを表す外部パラメータIを導入し, $\alpha = +$状態のランダムウォーカーのホッピング率をIの適当な単調増加関数で与える. また, 照射光の強度を表す外部パラメータをP^0と表す.

前節の後半で述べたように, B原子はPBが起こるように間隔$d = 3a$をもつ対構造を作る. この対構造ができるとそこでPBが起こり光の誘導放出によりエネルギー散逸が生じるため, B原子の拡散運動は抑えられ対構造は安定化する. この秩序化現象の原因を, 還元論的な考察に従って探ろうとすると, 「鶏が先か卵が先か」という循環論に陥ってしまう. そこで複雑系科学においては, そのような還元論的な原因追究は止め, 実現された機能を一つのサイクルとして捉え, それを単位として系全体の時間発展を議論することにするのである. この考え方にもとづくと数理モデルにおける基本サイクルは次のようになる[21].

① ランダムウォークの結果, 格子上に間隔$d = 3a$の対構造がいくつかできたとする. この条件の下, 各々の粒子対の位置において, 局所的にそれぞれ次のプロセスを考える.

② 順方向電流を表す外部パラメータIに比例する平均値をもつポアソン分布に従って, 乱数$X(\geq 0)$を生成さ

せる．この値をPBに関与する可能性のある仮想電子の数とする．

③ PBの結果新たに生成された光の強度P^{PB}（一つ前のサイクルの⑤で定義される）とP^0とを適当な重みで足し合わせ$P^{total} = c_1 P^0 + c_2 P^{PB}$とする．この値に比例した平均値をもつポアソン分布に従って②とは独立に乱数Y（$\geqq 0$）を発生させる．これに自然放出の分も加え$Y' = Y + 1$とし，この値をPBに関与する可能性のある仮想光子の数とする．

④ 3.1節の最後に述べた電子数と光子数のつり合い則[11]により，$Z = \min\{X, Y'\}$と定め，これが粒子対上で局所的に複製された光子の個数を与えるものとする．

⑤ ②～④のプロセスをすべての粒子対の上で行い，得られたZの値をすべて加えたものをP^{PB}とする．

⑥ 強度P^{PB}の複製された光は伝搬し，系の外にエネルギーを放出する．複製光子数Zが1以上であった粒子対においては，その粒子対を形成していたランダムウォーカーはエネルギーを失い不活性化するものとする（$\alpha = + \rightarrow -$）．

⑦ 依然として$\alpha = +$状態にあるランダムウォーカーをホッピングさせ，①に戻る．

このサイクルでは格子上の間隔$d = 3a$の粒子対構造の形成がフォノン生成を意味し，これが仮想電子（その個数はX）および仮想光子（その個数はY'）と相互作用した結果Z個の複製光子を生む過程を表現している．その意味でこのサイクルそのものがDPPであると言うこともできる．このサイクルが間隔$d = 3a$の粒子対という局所的な構造の上で巡回することが，（湯川関数で表される）DPの局所性に対応している．

DPが仮想的な複合粒子（すなわち，オフシェル粒子）であることに呼応し，上述のサイクルもまた一つのシナリオとして仮想されたものにすぎない．数理モデルを用いた複雑系研究においては，数値シミュレーションによってこのサイクルを何度も回したときに，実際にどのように機能するかを調べることがポイントになるのである．実際の数値シミュレーションでは格子寸法$L = 200$の系において，$N = 400$個のランダムウォーカーをランダムに初期配置した（Si結晶中のB原子数密度$\rho = N/L^2 = 0.01$に相当）[21]．上記①～⑦の基本サイクルに要する時間をシミュレーション時間tの単位と考えた．初期条件として，全粒子の活性状態αを $+$，外部パラメータ$I = 40$，$P^0 = 80$，$P^{PB}(0) = 0$とした．

数値シミュレーションの結果をFig.2 に示した．強度$P^{PB}(t)$は指数関数的に増大して（振動を伴いながら）大きな値をもつ平衡値に達し（図中の領域A），その後は平衡値の周りで揺動する様子が見られる（領域B）．また，活性状態$\alpha = +$にあるランダムウォーカーの個数の全粒子数Nに対する割合は指数関数的に減少した後，低い平衡値に達することが確認されている．このことは，間隔$d = 3a$の粒子対を多数もつ平衡状態が実現し，そこではPBが安定的に繰り返されていることを示している．（本稿では詳しく述べないが，実際に数値シミュレーションしたモデルでは，上記の基本サイクルの④で光子複製に
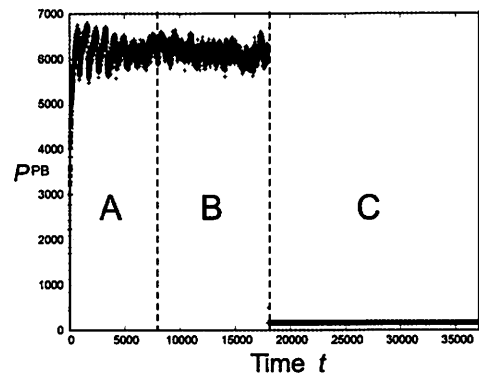
Fig. 2 Simulation results of the Si-LED model. Time dependence of the power of emitted light by PB, $P^{PB}(t)$, is shown. For the fabrication process ($0 \leqq t \leqq t_0 = 18000$), $P^0 = 80$, $I = 40$, and for the operation process ($t > t_0$), $P^0 = 0$, $I = 4$. The following three states were realized. A: $0 \leqq t < 8000$, transient state in the fabrication process. B: $8000 \leqq t \leqq t_0$, equilibrium in the fabrication process. C: $t > t_0$, stable state in the operation process.

寄与しなかった電子と光子の余剰エネルギーの蓄積が粒子の再活性化$\alpha = - \rightarrow +$を促すというプロセスも考慮した．これが上述の平衡状態での揺動に寄与している．）

次にLEDの動作時の条件の数値シミュレーションを行うため，系が平衡状態に達した後（時刻$t = t_0$，すなわちLED製作終了後），外部パラメータの値を$P^0 \rightarrow 0$，$I \rightarrow I/10$とした．つまり外部からの照射光をなくし，また順方向電流の値を極端に小さくした．その結果，Fig.2 の領域Cに示すように$P^{PB}(t)$の値は領域Bの値に比べ小さいものの，正の値を維持していることが示された．これは$t > t_0 (= 18000)$では順方向電流の値が小さいためランダムウォークが起こらず，その結果，間隔$d = 3a$の粒子対構造はいわば凍結され存在し続け，その上でPBの基本サイクル中の②～⑤が繰り返されることを意味する．

Fig.1 に示したように，実験ではPBの際にDPPが1，2個の光学フォノンを放出するプロセスが観測されている[12]．これは実際のDPP援用アニールにおいて間隔$d = 5a$や$d = 7a$をもったB原子対も形成され，その構造がPBによる複製光のスペクトルを豊富なものにしていることを示唆している[14]．数値シミュレーションモデルでは，間隔の異なる複数の粒子対を含むように基本サイクルを多様化することで，この効果も再現されている[21]．また，照射光の偏光状態もPBにおいて「遺伝」される実験結果[14]も基本サイクルの③で扱う仮想光子に縦偏光と横偏光の区別を考え，正方格子上の粒子対の配向に応じて別のポアソン分布を用いてそれぞれの仮想光子の発生個数を別々にカウントすることで再現されている[21]．

5. 今後の展望

本稿の冒頭で述べたように，DPはオフシェル領域の量子場であり，その定式化は未だ完成していない．他方，Si結晶を材料とするLEDとレーザーはこのメゾスコピックなオフシェル量子場の効果を利用して通常のマク

142

ロな伝搬光，すなわちオンシェルの光を複製することを実現している．ミクロな基礎理論が不在の中で，マクロな現象，それも自己組織的に時間発展する系を記述するために，ここでは複雑系科学の手法[20]を応用した結果を紹介した．この方法は現象論的モデル化といわれるものである．系の微細構造や原理が分からない研究段階において，コアと思われる仕組みを仮定し，それを単位とした粗視化モデルを提案する．そして，そのモデルを数値シミュレーションすることにより，系の総合的な振舞いを再現することを試みるという方法論である．本稿で紹介した香取・小林のモデル[21]をさらに改良することにより，LEDとレーザーの製作方法やその動作に対して，理論面から示唆を与えることが可能となるであろう．

ここで取り扱ったLEDはミクロな視点においても非平衡開放系である．流体力学系のようなマクロな非平衡ダイナミクスを，非平衡統計力学とよばれるミクロな視点に基づいた理論から導出する際には，局所平衡状態というメゾスコピックな概念が重要である[22]．しかし本稿で紹介したDPやB原子の対構造の空間的拡がりは原子スケールである．温度場や熱拡散といった既存の概念だけでPBを説明することには困難がある．また，順方向電流が供給するジュール熱を利用することによって照射光の情報をB原子配置としてSi結晶内に記憶させ，それに基づいて高能率・高パワーでエネルギーを系の外部に放出するLEDとレーザーのメカニズムを理解するには従来の熱力学の範囲を超えた情報理論的な視点も重要になるように思われる．DPの研究を進めることは，メゾスコピック領域におけるオフシェル量子場というミクロ科学だけでなく，複雑系科学や非平衡統計力学，さらには情報熱力学の研究に資するものと期待される．

6. むすび

ナノ寸法の空間において励起子のエネルギーの衣をまとった光子であるドレスト光子について，オフシェル領域に発生する量子場の観点から発生の原理，性質を紹介した．またドレスト光子は多モードのコヒーレントフォノンと結合し，ドレスト光子フォノンと呼ばれる新たな準粒子を形成して物質の突起部，物質中の不純物原子の位置に局在することを記した．

本稿ではシリコン結晶を材料とする発光ダイオード，レーザーを紹介した．これらのデバイスが発する光の光子エネルギーは製作時に照射する光の光子エネルギーの複製になっていること，すなわち光子ブリーディングと呼ばれる性質を示すことを指摘した．

その上で，発光ダイオードに対して，複雑系科学の手法を応用することにより提案されたモデル[21]を紹介した．この現象論的なモデル（粗視化モデル）は発光ダイオードの製作過程と動作特性を再現することに成功しており，将来的には，より高性能のデバイスを製作するための理論的指針を与えるものと期待される．

参考文献

1) R. P. Feynman: *The Theory of Fundamental Processes*（W. A. Benjamin, New York, 1962）p. 95.
2) 大津 元一: 応用物理 **85**（2016）1023.
3) M. Ohtsu: *Progress in Nanophotonics 4* ed. M. Ohtsu（Springer, Heidelberg, 2016）p. 1.
4) 大津 元一: ドレスト光子(朝倉書店，東京，2013)p. 10.
5) M. Ohtsu: *Dressed Photons*（Springer, Heidelberg, 2013）p. 11.
6) K. Kobayashi and M. Ohtsu: J. Microscopy **194**（1999）249.
7) Y. Tanaka and K. Kobayashi: Physica E **40**（2007）297.
8) Y. Tanaka and K. Kobayashi: J. Microscopy **229**（2008）228.
9) M. Ohtsu: *Progress in Nanophotonics 1* ed. M. Ohtsu（Springer, Heidelberg, 2011）p. 1.
10) M. Ohtsu: *Silicon light emitting diodes and lasers*（Springer, Heidelberg, 2016）p. 16.
11) J. H. Kim, T. Kawazoe, and M. Ohtsu: Appl. Phys. A **121**（2015）1395.
12) T. Kawazoe, M. A. Mueed, and M. Ohtsu: Appl. Phys. B **104**（2011）747.
13) M. Ohtsu: *Progress in Nanophotonics 4* ed. M. Ohtsu（Springer, Heidelberg, 2015）p. 10.
14) T. Kawazoe, K. Nishioka, and M. Ohtsu: Appl. Phys. A **9**（2015）1.
15) D. N. Payton and W. M. Visscher: Phys. Rev. **154**（1967）802.
16) T. Kawazoe, M. Ohtsu, K. Akahane, and N. Yamamoto: Appl. Phys. B **107**（2012）659.
17) Zh. I. Alferrov: Semiconductors **32**（1998）1.
18) H. Tanaka, T. Kawazoe, M. Ohtsu, and K. Akahane: Fluoresc. Mater. **1**（2015）1.
19) M. Ohtsu: *Silicon Light-Emitting Diodes and Lasers*（Springer, Heidelberg, 2016）p. 77.
20) 香取 眞理: 複雑系を解く確率モデル(講談社，東京，1997)p. 145.
21) M. Katori and H. Kobayashi: *Progress in Nanophotonics 4* ed. M. Ohtsu and T. Yatsui（Springer, Heidelberg, 2016）p. 19.
22) 香取 眞理: 非平衡統計力学(裳華房，東京，1999)p. 41.

[IV] OFF-SHELL ARCHIVE

Creation and Measurement of Dressed Photons: A Link to Novel Theories

M. Ohtsu[1,2] and H. Sakuma[2]

[1] Institute of Engineering Innovation, Graduate School of Engineering,

The University of Tokyo, 2-11-16 Yayoi, Bunkyo-ku, Tokyo, 113-8656, Japan

[2] Research Origin for Dressed Photon, c/o the University of Tokyo,

Bdg. Eng-9, 2-11-16 Yayoi, Bunkyo-ku, Tokyo, 113-8656, Japan

Abstract:

In order to identify the requirements in theoretical studies for analyzing the physical properties of dressed photons, this paper adopts a fiber probe developed for creating and measuring dressed photons. The principles and practices of using such a fiber probe in illumination and collection modes are reviewed. It is pointed out that the fiber probe can be replaced by a nano-particle and that multiple nano-particles exhibit a specific phenomenon of dressed photons, namely, autonomous energy transfer. A phase diagram is presented in order to identify the requirements in a novel theory for finding the optimum conditions for measuring dressed photons. It is pointed out that this theory should be able to describe the autonomy above and also the hierarchy that exists in the measurement. To meet these requirements, promising novel theoretical approaches are reviewed. One is the Clebsch dual field theory. The use of the quadrality scheme based on the category theory and a novel measurement theory are also suggested as promising approaches for analyzing the detailed physical properties of dressed photons, and this will open up a new field of off-shell science.

1 Introduction

A dressed photon (DP) is a form of photon created in a nanometer-sized material. It exists in an off-shell area that is displaced from the shell of the dispersion relation between energy and momentum [1]. To analyze its physical properties in detail, which will open up a new field of off-shell science, a novel theory that describes the micro-macro duality of quantum fields is essential. In order to develop such a theory, this paper reviews the requirements in theoretical studies, which have been identified from experimental results accumulated for more than a quarter of a century. For this review, a fiber probe is adopted as a representative device to create and measure the DP [2]. Since this device has a simple structure, it should be possible to analyze the

1

transformation of an electromagnetic (EM) field between micro- and macroscopic systems, which will open up a new field of off-shell science.

This fiber probe has been used at the heart of a novel microscope and spectrometer that exhibit ultrahigh spatial resolution beyond the diffraction limit of propagating light [3]. Conformations and structures of a variety of nanometric materials have been measured and analyzed with these instruments, which have been commercially available [4].

2. Experimental evaluation of the dressed photons

In order to identify requirements from an experimental viewpoint, this section reviews the principles of creation and measurement of DPs. The structures and performance levels of fiber probes are also reviewed. Also, it is pointed out that a fiber probe can be replaced by a nano-particle (NP). Finally, requirements for developing novel theories are presented.

2.1 Principles of creation and measurement of dressed photons

As schematically explained by Fig. 1, the DP is a quantum field that exists in an off-shell area that is displaced from the shell of the dispersion relation between energy and momentum [1,5]. Since the uncertainty Δp of the momentum p is large in this area $(\Delta p \gg p)$, the size a of the DP is much smaller than the wavelength λ of the propagating light $(a \ll \lambda)$ due to the Heisenberg uncertainty principle. In order to create such a small DP, a fiber probe has been used, as is schematically explained by Fig. 2(a). The operating mode of the fiber probe in this figure is called the illumination mode (I-mode) [6], in which the tail of the fiber probe is illuminated with propagating light (the EM field on shell) to create a DP at the nanometric tip of the probe.

Since the created DP is localized on the tip, it is measured by inserting a sonde into the DP for acquiring the response from the DP. That is, the DP is measured by acquiring its response to a stimulus applied from the outer system. A nano-particle (NP) has been used as such a sonde (Fig. 2(b)). By putting this NP in close proximity to the tip of the fiber probe, the DP energy is exchanged between the fiber probe tip and the NP, resulting in excitation of an electron in the NP. The excited electron can create a photon. Since this photon is a conventional scattered light field on shell, it can be

2

measured by a conventional photo-detecting device, and thus, the response can be acquired. In this I-mode, the fiber probe and NP respectively play the roles of a light source and a detector for creating and measuring the DP.
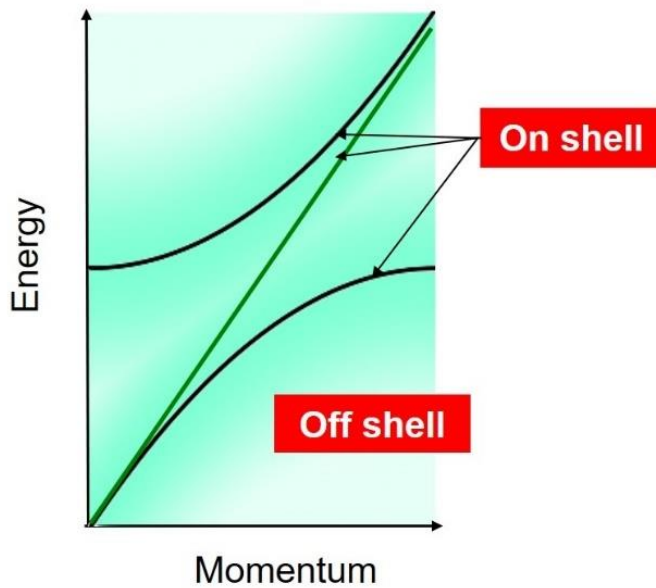
Fig.1   Dispersion relation between the momentum and energy of the electromagnetic field.

The green line and black curves are for the fields in vacuum and in a macroscopic material, respectively. They are the fields on shell. The green shaded rectangle is for the field off shell.

It is possible to exchange the roles of the fiber probe and the NP: First, the NP is illuminated by propagating light to create the DP. Next, a fiber probe, which is used as a sonde, is brought close to the NP (Fig. 3(b)). The DP energy is thus exchanged between the NP and fiber probe tip, resulting in excitation of an electron in the tip of the fiber probe. The excited electron can create a photon, i.e., scattered light. Since this scattered light is guided through the fiber probe and reaches its tail, it can be measured by a conventional photo-detecting device, and thus, the response can be acquired. The operating mode of the fiber probe in this figure is named the collection mode (C-mode) [6].

3
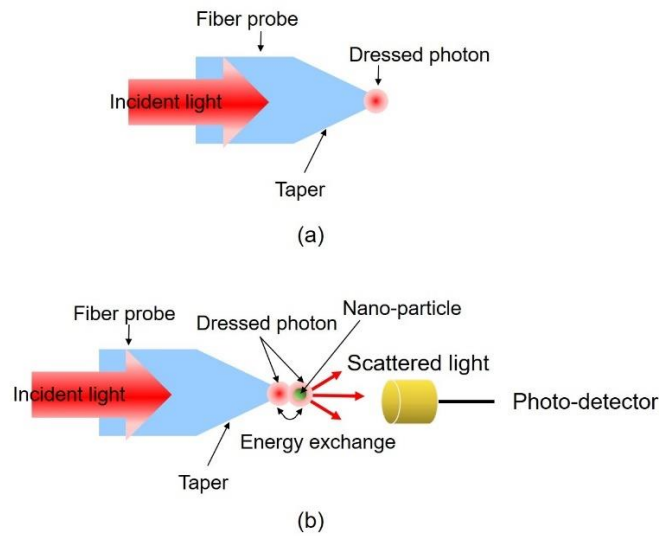
Fig.2　Illumination mode for the fiber probe operation.

(a) For creating the DP. (b) For measuring the DP.
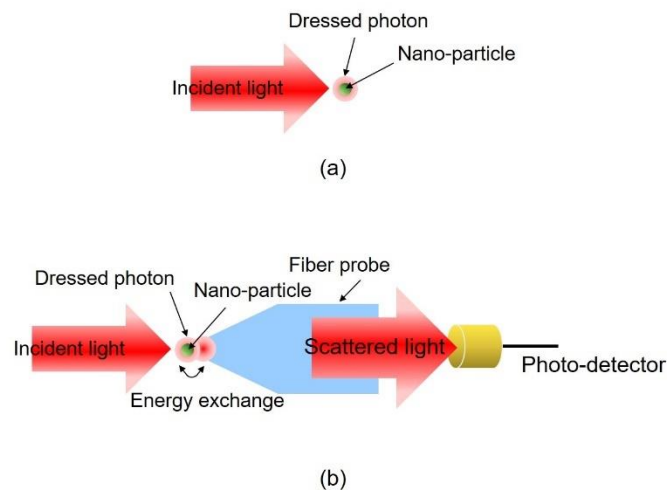
Fig.3　Collection mode of the fiber probe operation.

(a) For creating the DP. (b) For measuring the DP.

2.2 Performance of fiber probes

As is summarized in Fig. 4(a), a variety of fiber probes have been developed so far, some of which have been commercially available [2]. The size and conformation of the tip and taper of the fiber probe have been empirically controlled during the fabrication process, resulting in sufficiently high efficiencies for creating and measuring DPs for practical use. These high efficiencies are indispensable for reliable conversion of the EM field

4

from macro- to microscopic systems and also from micro- to macroscopic systems, respectively, in the case of the I- and C-modes.
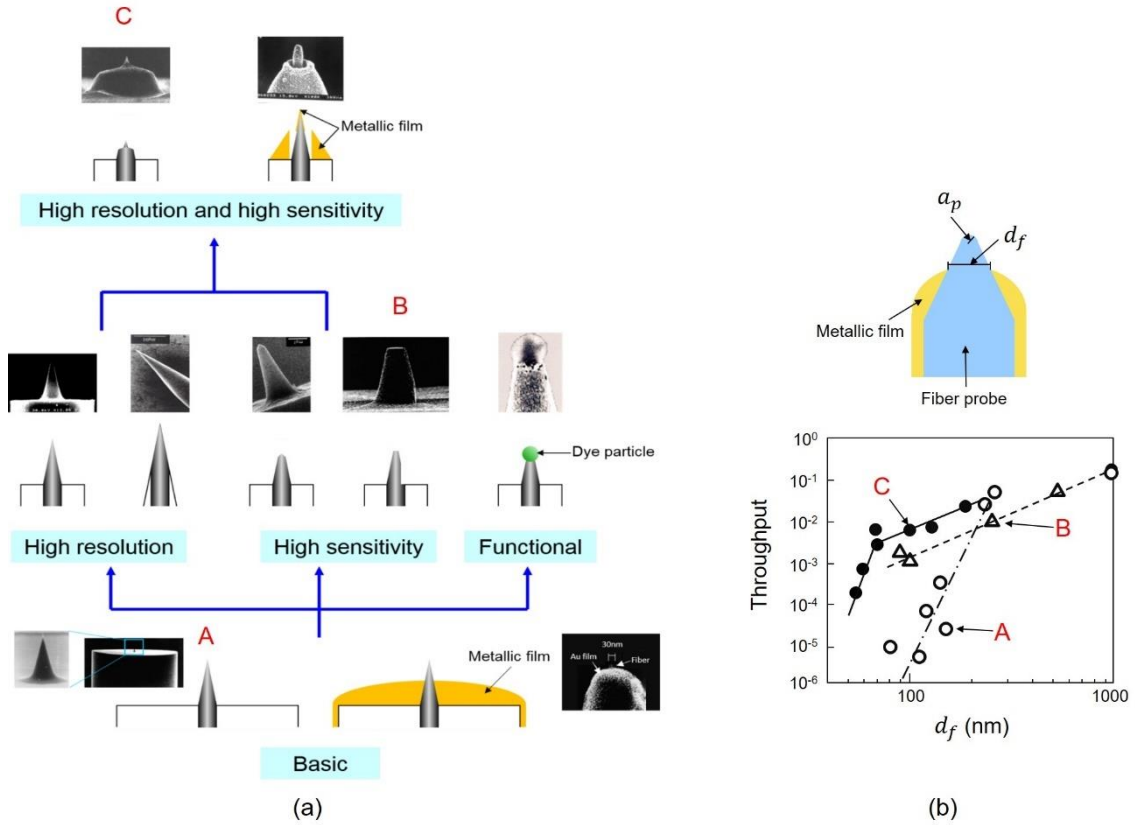
Fig. 4 Developed fiber probes.

(a) Cross-sectional profiles and scanning electron microscopic images. (b) The efficiency of measuring the DP. d_f is the foot diameter of the taper protruding from an opaque metallic film. Open circles, open triangles, and closed circles represent the experimental results measured for the fiber probes A, B, and C in (a), respectively.

Figure 4(b) represents the efficiency of measuring the DP acquired when the fiber probe was used in the I-mode [7]. This efficiency is expressed as the "throughput", which is the ratio between the measured optical power and the optical power incident at the tail of the fiber probe. The horizontal axis is the diameter d_f of the foot of the taper protruding from an opaque metallic film, which was deposited for blocking unwanted scattered light. In these old experimental results acquired more than 15 years ago, it should be pointed out that a certain amount of unwanted scattered photons was

5

measured simultaneously with the DP when d_f was larger than 100 nm. This signal mixing was due to insufficient shielding resulting from the immature metallic film coating technology available at the time.

It should be noted that the spatial resolution of this novel microscope and spectrometer are determined by the value of the tip radius, a_p. Detailed discussions of the special resolution, and also of the image contrast, are given in Appendix [8].

2.3 Using nano-particles

A novel method has been developed recently in order to replace the role of the fiber probe operating in the I-mode by an NP, as is schematically explained by Fig. 5(a). In this scheme, an NP is illuminated by propagating light to create a DP. One may worry that the creation efficiency will be very low because the interface between the macro- and microscopic systems, i.e., the taper of the fiber probe in Fig. 2, is missing in this configuration. However, novel interface devices, such as an optical nano-fountain and an optical energy transmitter [9], have been developed by using multiple NPs, enabling drastic increases in efficiency.
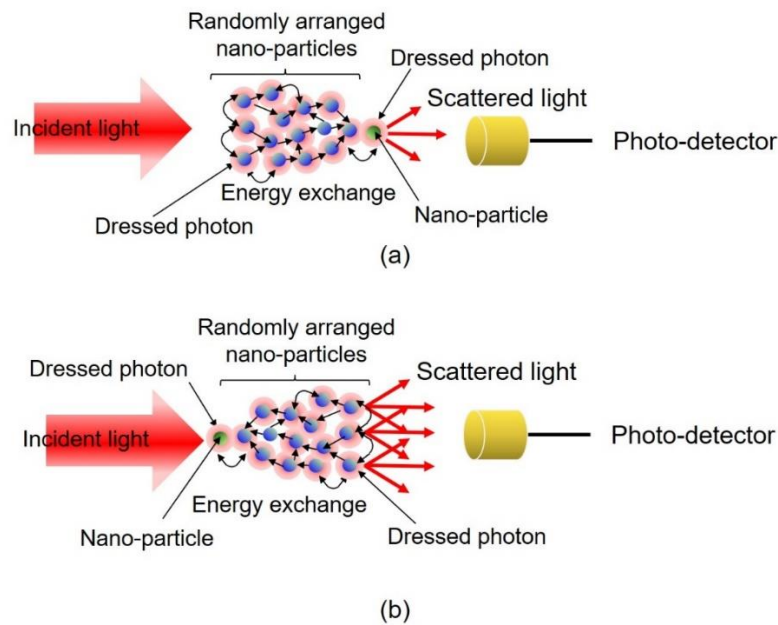
Fig. 5   Nano-particles for creation and measurement of the DP.

The multiple randomly arranged NPs correspond to the taper of the fiber probe.(a) For creating the DP.

(b) For measuring the DP.

6

The replacement mentioned above has been realized also for the C-mode: As is schematically explained by Fig. 5(b), in this scheme, multiple NPs are arranged around the NP on which the DP is originally created. As a result, the DP energy is exchanged between the center NP and the surrounding multiple NPs to excite an electron. The excited electron can subsequently create scattered light, which can be acquired by a conventional photo-detecting device.

It should be pointed out that a specific phenomenon of autonomous DP energy exchange has been observed among multiple randomly arranged NPs [9]. That is, it has been experimentally confirmed that the optimum route was autonomously selected for the DP energy transfer in the optical nano-fountain and optical energy transmitter devices above.

2.4 Requirements for novel theories

The gray cone in the phase diagram of Fig. 6 represents the area in which the DP measuring efficiency is high, which was empirically found through experimental work on fabricating and using an I-mode fiber probe. Here, a_p is the tip radius, a_s is the radius of the spherical NP, a_s / a_p is their ratio, and θ is the cone angle of the taper.

It should be pointed out that the efficiency is the highest when $a_s / a_p = 1$, which is due to the size-dependent resonance feature of the DP energy exchange [10]. A similar conical area can be derived also for the C-mode. A novel theory is required since one of the major requests from experimentalists is to find the optimum condition for realizing the highest efficiency of creation and measurement of DPs. It is expected that Fig. 6 will serve as a reference to find this condition.

To find the optimum condition, it should be also noted that the detailed profile of the tip and taper of the fiber probe are not smooth but have some roughness on their surfaces, as is schematically shown in Fig. 7. Specifically, Fig. 7(a) represents a conical surface profile with a smooth surface, which can be observed from a far field view point. However, the NP in Fig. 2(b), which is installed in the near field of the fiber probe surface, may see a magnified surface and find a lot of bumps (Fig. 7(b)), on which multiple DPs with a variety of sizes are created. That is, a hierarchy exists in the DP measurement, which depends on the position and size of the NP to be used as a sonde for the measurement. A novel theory that can describe this hierarchy, as well as the

7

autonomy mentioned in Section 2.3, is needed.
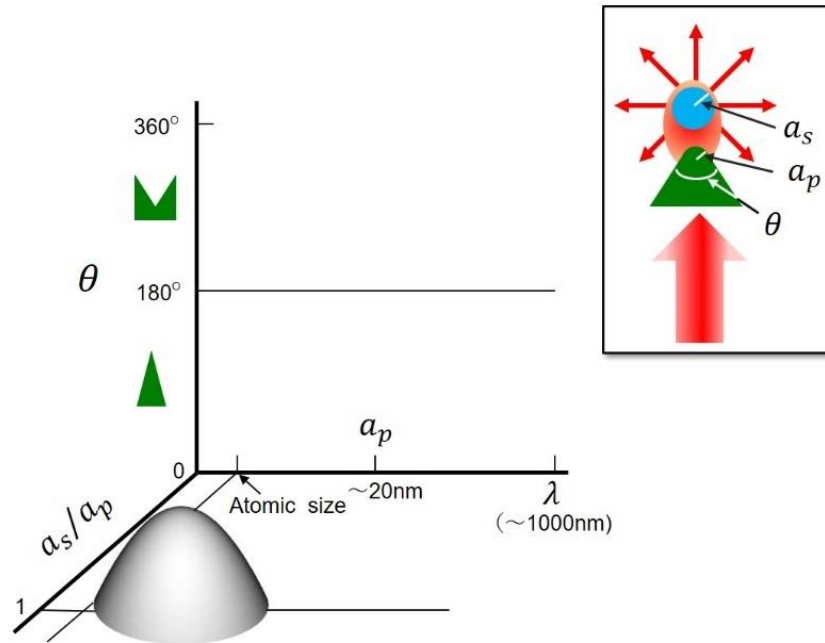
Fig. 6   Phase diagram for representing the area in which the efficiency of measuring the DP is high.

λ is the wavelength of the light incident on the fiber probe.
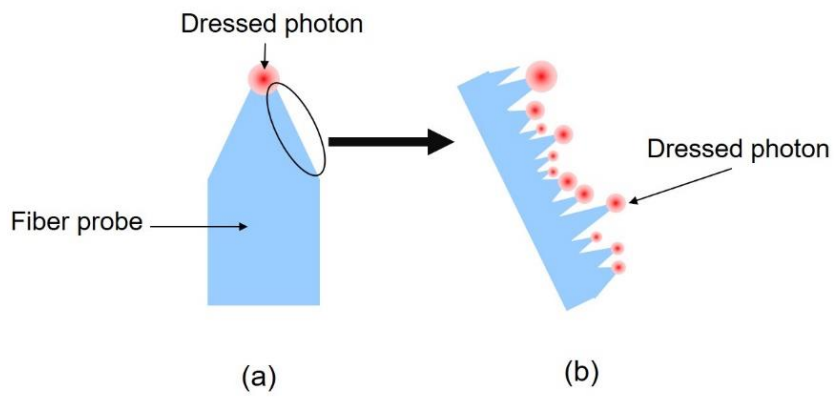
Fig. 7   Hierarchy of measuring the DP created on the tip and taper of the fiber probe.

(a) Cross-sectional profile of the tip and taper of the fiber probe.(b) Magnified profile of (a).

3 Strategies for novel theories

This section presents problems to be solved, which have been requested by experimentalists. Some promising novel theoretical methods for solving these problems are reviewed.

8

3.1 Problems to be solved

In the case where the I-mode is used by illuminating the tail of the fiber probe with propagating light, it is advantageous to create:

   (A) a small DP for achieving high-spatial-resolution measurement,
and
   (B) a high energy DP for achieving high-sensitivity measurement.

     In order to find the criteria for designing a fiber probe for creating these DPs, the following two-step theoretical calculation ought to be carried out (Fig. 8). That is, the problems to be solved are

(1) 1st step: Three kinds of EM fields in the taper have to be derived. They are

   a) Propagating light, which is guided through the taper (EM field on shell).

   b) Scattered light, which is dissipated via radiation from the taper (EM field on shell).

   c) A DP (EM field off shell), whose size is equivalent to the size of the taper because the spatial profile of the DP is expressed as a Yukawa function [10].

(2) 2nd step: The DP on the tip of the fiber probe has to be derived.
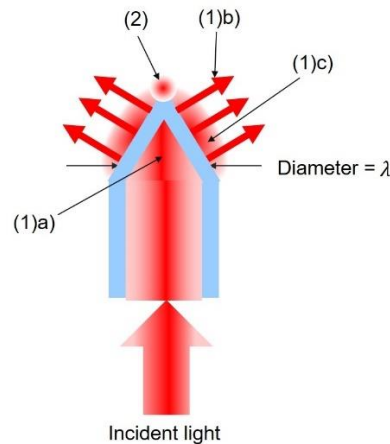
Fig. 8   Two-steps for theoretical calculation.

λ is the wavelength of the light incident on the fiber probe.

     The DP in (2) is created as a result of the DP energy transfer from the fields (1a) and (1c). It means that the conformation and structure of the taper play essential roles in creating the DP of (A) and (B) on the tip. In other words, it is essential to optimize the magnitude of the energy dissipated from the taper, which is the magnitude of the energy of the field (1b).

     It should be pointed out that this taper is the interface between micro- and macroscopic systems (i.e., between the tip and the tail of the fiber probe), and thus, it

9

plays an essential role in the micro–macro duality. However, EM fields in the taper have never been correctly described by the conventional EM field theories because these theories cannot be applied to the taper due to its sub-wavelength diameter. Namely, a method of numerical analysis based on Maxwell's equations (for example, the Finite Difference Time Domain (FDTD) method) is not suitable for deriving the EM field of (1b) and (1c) [11]. In particular, in the case of (1c), the use of the FDTD method is useless because it does not take into account the longitudinal component of the electric field [12].

3.2 Expected theoretical methods

Several novel theoretical methods have been proposed to solve the problems presented in Section 3.1. This section reviews these methods.

Figure 6 shows that the highest efficiency was obtained in the case of $a_s / a_p = 1$, due to the size-dependent resonance in the DP energy exchange between the fiber probe and the NP [10]. This case corresponds to the case where the magnitude of the energy dissipation from the taper (the scattered light energy of (1b) in Section 3.1) takes the minimum. Therefore, in order to find the creation methods (A) and (B) in Section 3.1, it is essential to explore the conformation and size of the fiber probe which maximize the difference between the energy of the DP localized at the tip and the energy lost due to dissipation at the taper. For this exploration, Fig. 9(a) was derived, in which the value of a_s / a_p in Fig. 6 was replaced by the magnitude of the energy loss E_d (magnitude of the light energy scattered from the taper). It should be noted that this figure uses the energy dissipation rate $\eta_d \left(= E_d / E_i \right)$, which is defined by the ratio between E_d and the energy E_i of the light incident on the tail of the fiber probe. For this replacement, a semi-quantitative relation between a_s / a_p and η_d was derived based on Fig. 2.6 of ref. [10], which is shown by Fig. 9(b).

Here, the problem is that the conventional EM field theories cannot be used to analyze the magnitude E_d of energy dissipation because the taper is of sub-wavelength size. To solve this problem, it would be advantageous to use the concept of effective mass of the EM field instead of using the conventional method. This may enable estimation of the magnitude of the energy dissipation by assuming that the energy

10

6C

dissipation takes place during the process of transforming the massless free photon on shell to the off-shell photon with a finite mass. The Clebsch dual field theory was developed for this estimation by noting the duality between the fields in the space-like and time-like areas in the Minkowski diagram [1,13].

(a)   (b)
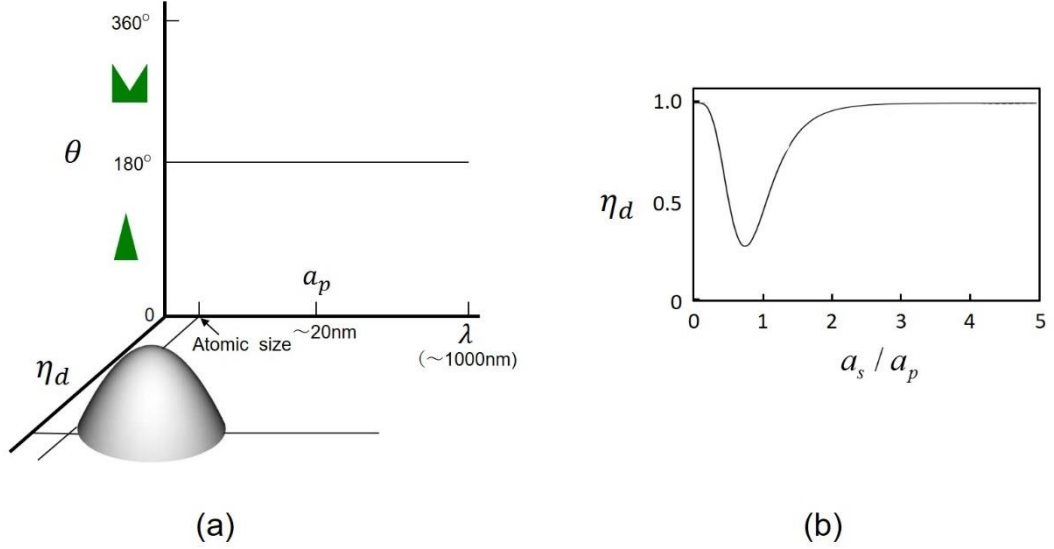
Fig.9   Phase diagram for representing the area in which the efficiency of measuring the DP is high.

(a) The ratio of the sizes a_s/a_p in Fig. 6 is replaced by the energy dissipation rate η_d. (b) The relation between a_s/a_p and η_d used for illustrating (a).

The energy–momentum tensor of the Clebsch dual field is isomorphic to the left-hand side of the Einstein field equation represented as a Ricci curvature tensor defined in terms of a contracting Riemann tensor, thus suggesting an interpretation wherein the energy–momentum tensor of a virtual photon field carries a part of the energy–momentum of "vacuum", as in classical space-time. It also suggests that it may represent a so-far unidentified energy field similar to the controversial dark energy in cosmology, since, corresponding to its space-like characteristics, the associated scalar curvature is negative. According to a quantum mechanical point of view, a vacuum is considered as a fluctuating energy field where creation and annihilation of a variety of virtual particles occur incessantly.

Mathematical analysis of the Clebsch dual field shows that a space-like Clebsch field is stable as long as it exists in wave-like modes extending uniformly in space–time. However, once local perturbations arising from the interactions of material fields are

11

given, the energy of the Clebsch field becomes unstable and is transformed into a spatially localized form having a Yukawa-potential distribution if its energy level exceeds a certain threshold value. In the case of Figs. 2(a) and 3(a), the Yukawa-potential means that the spatial extent of the DP field corresponds to the sizes of the tip of the fiber probe and that of the NP, respectively. The above unstable Clebsch field consists of amplifying and damping fields. When we consider the latter, we can interpret it as a rapidly decreasing time-like mode returning the excited energy back to the environmental material field in a manner consistent with the conventional explanation given in terms of the uncertainty principle since the damping rate is proportional to the magnitude of the excited energy.

Based on the discussions above, applying the Minkowski diagram to the I-mode reveals that the EM fields in the light-like, time-like, and space-like domains correspond to the propagating light incident on the tail of the fiber probe, the scattered light radiating from the taper of the fiber, and the DP created on the tip of the fiber probe, respectively, as is schematically explained by Fig. 10(a). In the case of the C-mode, this correspondence is also explained by Fig. 10(b). Since the light-like field produces a pair consisting of time-like and space-like fields, the creation rate of the space-like field can be maximized by minimizing the creation rate of the time-like field. As a result, the DPs in (A) and (B) in Section 3.1 can be efficiently created. It should be pointed out that the hierarchy explained in Fig. 7 can be described by including the nonlinear interaction in the theoretical approach described above.
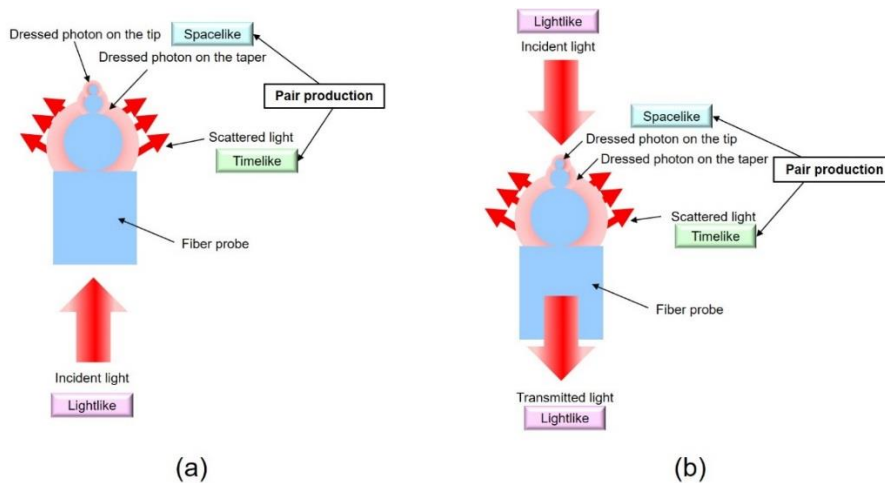
Fig.10   Electromagnetic fields in the light-like, time-like, and space-like domains.

(a) Illumination mode (transformation from macro- to microscopic systems). (b) Collection mode (transformation from micro- to macroscopic systems).

12

It should be noted that the gray cones in Figs. 6 and 9(a) have asymmetric profiles. This is because the DP is intrinsically created on the tip of the fiber probe, which has a translationally asymmetric profile. Theoretical models for the off-shell EM field should be developed based on this asymmetry. For this advanced theoretical model, use of the quadrality scheme [14] based on category theory is expected to be a promising approach for describing the transformation of the microscopic DP to the macroscopic system. Furthermore, a novel measurement theory should be constructed by noting that the fiber probe and NP in Figs. 2(b) and 3(b) form a composite system originating from the DP energy exchange. Tomita's decomposition theorem [15] is expected to be promising for this construction. Further advances in these theoretical studies are expected to lead to developments in the field of off-shell science.

4 Summary

This paper adopted a fiber probe to identify the requirements in theoretical studies for analyzing the physical properties of DPs. The principles of using this fiber probe in illumination and collection modes were reviewed. After the structures and performance of a variety of fiber probes were presented, it was pointed out that the fiber probe could be replaced by an NP, and that multiple NPs exhibited a specific phenomenon of autonomous energy transfer of the DP. A phase diagram was empirically derived through experiments in order to show the experimental condition for achieving high-efficiency measurements of the DP. Based on this diagram, requirements for a novel theory were identified to find the optimum condition giving the highest efficiency. Furthermore, it was required that this theory should be able to describe the intrinsic phenomena of the autonomy mentioned above, and also the hierarchy in the DP measurement.

It was pointed out that the conventional EM field theories cannot meet these requirements, as well as a description of the field in the taper of the fiber probe. To meet the requirements, some promising novel theoretical approaches were reviewed. One was an approach based on Clebsch dual field theory. The use of the quadrality scheme based on category theory and a novel measurement theory were also presented as promising approaches for analyzing the detailed physical properties of DPs, leading to the development of a new field of off-shell science.

The Appendix discusses the spatial resolution and the contrast of the image acquired by a microscope and spectrometer using such a fiber probe.

13

References

[1] H.Sakuma, I. Ojima, and M. Ohtsu: "Dressed photons in a new paradigm of off-shell quantum fields," Progress in Quantum Electronics, **55**, (2017) pp.74-87.

[2] M. Ohtsu (ed.): *Near-Field Nano/Atom Optics and Technology* (Springer, Tokyo, 1998) pp.15-100.

[3] Y. Narita, T. Tadokoro, T. Ikeda, T. Saiki, S. Mononobe, and M. Ohtsu: "Near-Field Raman Spectral Measurement of Polydiacetylene," Appl. Spectroscopy, **52** (1998) pp.1141-1144.

[4] M. Ohtsu (ed.): *Near-Field Nano/Atom Optics and Technology* (Springer, Tokyo, 1998) pp.133-192.

[5] M. Ohtsu: "New Routes to Studying the Dressed Photon," Offshell:1709R.001.v1.

[6] M. Ohtsu and K. Kobayashi: *Optical Near Fields* (Springer, Berlin, 2004) p.23.

[7] T. Yatsui and M. Ohtsu: "High-Throughput Probes for Near-Field Optics and Their Applications," *Prog. In Nano-Electro-Optics I* (ed. M. Ohtsu) (Springer, Berlin, 2003) p.12.

[8] M. Ohtsu and K. Kobayashi: *Optical Near Fields* (Springer, Berlin, 2004) pp.29-30.

[9] M. Ohtsu, T. Kawazoe, and H. Saigo: "Spatial and Temporal Evolutions of Dressed Photon Energy Transfer," Offshell:1710R.00.v1.

[10] M. Ohtsu: *Dressed Photons* (Springer, Heidelberg, 2014) pp.18-36.

[11] A. Taflove: *Computational Electrodynamics* (*The Finite-Difference Time-Domain Method*) (Artech House, Boston, 1995).

[12] I. Banno and M. Ohtsu, "Irrationality of the Permittivity in Non-resonant Near-field Optics," Abstract of the 11th Asia-Pacific Conference on Near-Field Optics, July 10-13, 2017, Tainan, Taiwan, p.35.

[13] H. Sakuma, I. Ojima, and M. Ohtsu: "Gauge symmetry breaking and emergence of Clebsch-dual electromagnetic field as a model of dressed photons," Appl. Phys. A (2017) 123:750.

[14] I. Ojima: "Micro-macro duality in quantum physics," *Statistic Analysis: Classical and Quantum – Perspectives of White Noise Theory* (ed. T. Hida) (World Scientific, Singapore, 2005) pp.143-161.

[15] O. Bratteli and D.W. Robinson: *Operator Algebras and Quantum Statistical Mechanics* (2nd ed.), vols.1 and 2 (Springer, Berlin, 1987,19977).

Appendix Spatial resolution and image contrast in measurements using a fiber probe

As was reviewed in Section 1, DPs have been used in a novel microscope and a spectrometer with ultrahigh spatial resolution beyond the diffraction limit of light. The NPs in Figs. 2(a) and 3(a) correspond to the specimens to be measured by these instruments. In the I-mode, the DP on the tip of the fiber probe serves as a light source to illuminate the specimen. In the C-mode, the light source is the DP on the NP, which is picked up by the fiber probe.

In order to analyze the spatial resolution and contrasts of the acquired microscopic and spectroscopic images, the cross-sectional profile of the fiber probe is shown in Fig. A(a), as was given in Fig. 4(b) [8]. Here, a_p is the tip radius, d_f is the diameter of the foot of the taper protruding from an opaque metallic film, which is deposited for blocking the propagating scattered light, and θ is the cone angle. The spatial resolution of the measurement is governed by the size of the DP created on the tip, which is equivalent to the tip radius a_p, because the spatial profile of the DP field is represented by the Yukawa function.

(a)   (b)   (c)
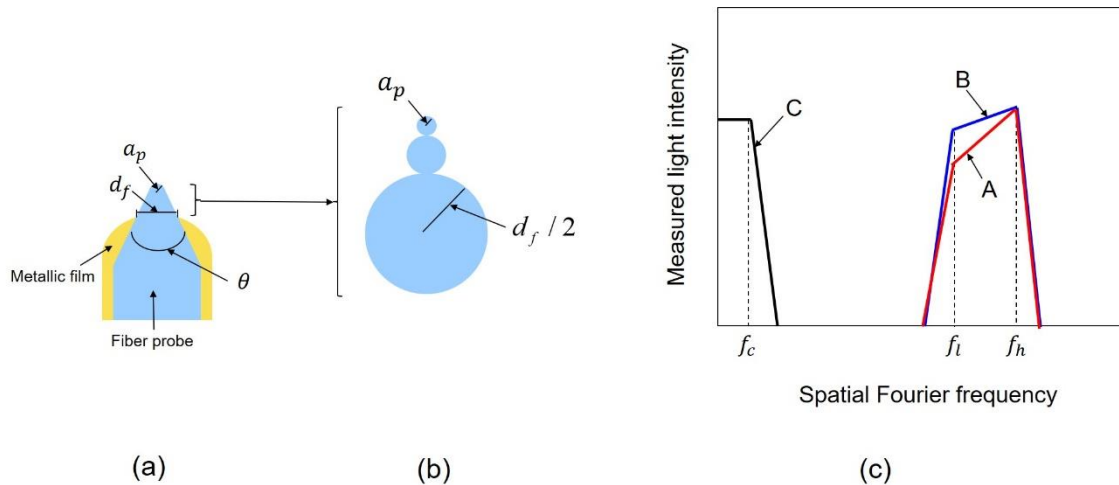
Fig. A   A fiber probe and spatial Fourier spectra of the acquired image.

(a) Cross-sectional profile of the fiber probe. (b) A taper approximated by a chain of spheres.(c) Spatial Fourier spectrum of the image acquired in the Collection mode. Lines A and B correspond to the fiber probe with small and large cone angles θ, respectively. Line C represents the spectrum acquired by a conventional optical microscope.

15

Here, the contributions from the DPs created on the taper have to be also considered for evaluating the contrast of the acquired image. For this consideration, Fig. A(b) schematically explains that the taper is approximated as a chain of small spheres which are connected in order to increase the radius, from a_p up to $d_f/2$, as shown in Fig. 10. These spheres receive the DP energy created on the NP in the case of the C-mode, whereas they create the DP on their surfaces in the case of the I-mode. Therefore, in the case of the C-mode, due to the size-dependent resonance feature of the DP energy exchange [10], high-efficiency measurement is achieved if the size of the DP on the NP falls between a_p and $d_f/2$. This means that this efficiency has the characteristics of a spatial band-pass filter. Its spatial Fourier spectra are shown by the lines A and B in Fig. A(c). They show that the C-mode can detect a DP whose size falls within the pass band of this spatial filter (i.e., between a_p and $d_f/2$). Its high-frequency cutoff f_h is proportional to a_p^{-1}, showing that the spatial resolution is determined by a_p. On the other hand, the low-frequency cutoff f_l is proportional to d_f^{-1}.

Figure A(c) shows that with a smaller θ (line A), a lower efficiency is exhibited at f_l than that with a larger θ (line B), because the sphere of radius $d_f/2$ is farther from the tip in the case of a smaller θ. This means that the sharper fiber probe can achieve higher selectivity in measuring the DP with a size as small as the tip radius a_p. In other words, the high-spatial-resolution component in the image is acquired with higher contrast. In the case of the I-mode, the lines A and B represent the size dependence of the DP energy created on the fiber probe; that is, a DP with a size ranging from a_p to $d_f/2$ is efficiently created.

A conventional optical microscope collects propagating light scattered from the specimen with convex lenses for acquiring an image of the specimen. The spatial Fourier spectrum of the acquired image is represented by the line C in Fig. A(c). Due to the diffraction limit of light, it has the characteristics of a low-pass filter, whose high-frequency cutoff f_c is determined by the wavelength λ of the light, i.e., is

16

proportional to λ^{-1}.

By comparing the lines A, B, and C, it is confirmed that the spatial resolution of the microscope using DPs is much higher than that of the conventional microscope because $a_p \ll \lambda$ ($f_h \gg f_c$), which is the origin of the name "ultrahigh spatial resolution microscope"

It should be noted here that the spatial Fourier spectral characteristics of the microscopic images acquired by this ultrahigh spatial resolution microscope and the conventional optical microscope do not have any strong correlation between each other. In other words, the images acquired by these microscopes are totally different from each other, in addition to the ultrahigh spatial resolution feature of the former. This is because their spatial filtering characteristics are different; i.e., band-pass filtering and low-pass filtering. By noting the size-dependent resonance feature of the DP energy exchange [10], it should be pointed out that the microscope using DPs acquires an image of the fiber probe tip itself instead of an image of the specimen NP.

17

Spatial and Temporal Evolutions of

Dressed Photon Energy Transfer

M. Ohtsu[1,2], T. Kawazoe[3], H. Saigo[4]

[1] Institute of Engineering Innovation, Graduate School of Engineering,

The University of Tokyo, 2-11-16 Yayoi, Bunkyo-ku, Tokyo, 113-8656, Japan

[2] Research Origin for Dressed Photon,

c/o The University of Tokyo, 2-11-16 Yayoi, Bunkyo-ku, Tokyo, 113-8656, Japan

[3] Tokyo Denki University,

Tokyo Senju Campus, Bldg.4-9F 906A, Senju-Asahi-cho, Adachi-ku, Tokyo 120-8551, Japan

[4] Nagahama Institute of Bio-Science and Technology,

1266 Tamura-cho, Nagahama-shi, Shiga, 526-0829, Japan

Abstract: It has been shown that dressed photon (DP) energy transfer exhibits unique autonomous spatial evolution features, and novel functional devices have been demonstrated as a first example of the practical application of this transfer. Temporal evolution features originating from nutating DP energy transfer followed by radiative relaxation have also been demonstrated. A novel film for highly efficient optical energy conversion is presented as a second example of the application of these features. It is suggested that these spatial and temporal evolution features can be analyzed based on theoretical models based on a quantum walk and a random walk. This film was placed on a silicon solar battery to convert UV light energy to visible light energy, resulting in an increased electrical power generation efficiency of 20.2%.

1 Introduction

The dressed photon (DP) is a novel form of quantum field, which is created in a nanometer-sized space [1]. It is also called an off-shell photon because it exists in the off-shell area that is displaced from the shell of the dispersion relation between energy and momentum. In drawing a physical picture of this quantum field, there have been some problems originating from the intrinsic nature of the DP; namely, its electromagnetic mode could not be defined do to its sub-wavelength size. However, recently developed novel

1

theories have succeeded in solving these problems, allowing the intrinsic properties of the DP to be suitably described. These properties are:

(a) A DP is created in or on the surface of a nano-particle (NP).

(b) The created DP localizes on the NP, and the extent of localization is equivalent to the size of the NP.

Two novel phenomena were predicted as a result of successfully describing these properties. They are:

(1) A transition that is normally electric dipole-forbidden becomes allowed.

(2) Size-dependent resonance occurs.

These phenomena, which originate from DP energy transfer between NPs, have been experimentally confirmed and applied to the development of a variety of novel application technologies. Progress in this area has been reviewed in a previous article in the Off-shell Archive [2].

Section 2 of the present paper reviews unique features of DP energy transfer between NPs, based on phenomena (1) and (2) above. Section 3 introduces the principles and practices of novel nanometric functional devices and an optical energy converter. Section 4 reviews the application of this DP energy transfer to optical energy conversion. In Sections 3 and 4, spatial and temporal evolutions of the DP energy transfer are demonstrated. A summary and conclusions are presented in Section 5.

2 Energy transfer of dressed photons

Novel devices that operate by using DPs are named DP devices. Some of these devices are introduced in Section 3. In order to examine the principle of operation of DP devices, two different-sized cubic semiconductor NPs are assumed, in which exciton energy is quantized, as schematically explained by Fig. 1. Small and large NPs (NP_S and NP_L, respectively) in this figure are used as input and output terminals, respectively. These NPs are irradiated with propagating light whose photon energy is resonant with the lowest quantized energy level (1,1,1) of the exciton in NP_S. This light corresponds to the input signal to the DP device. The propagating light emitted from the lowest energy level (1,1,1) in the large NP_L corresponds to the output signal.

Based on the localized nature of the DP (property (1) in Section 1), these NPs are installed in close proximity to each other, with a separation as short as their sizes. By assuming that the ratio between their side lengths is

$1 : \sqrt{2}$, one can readily find that the exciton energy of level $(1,1,1)$ in NP$_\text{S}$ is equal to that of level $(2,1,1)$ in NP$_\text{L}$; that is, these two energy levels are resonant with each other. It should be noted that level (2,1,1) in NP$_\text{L}$ is an electric-dipole forbidden level, whereas level (1,1,1) in NP$_\text{S}$ is an electric-dipole allowed level. Thus, the energy of the irradiated propagating light normally cannot be transferred from level (1,1,1) in NP$_\text{S}$ to level (2,1,1) in NP$_\text{L}$.
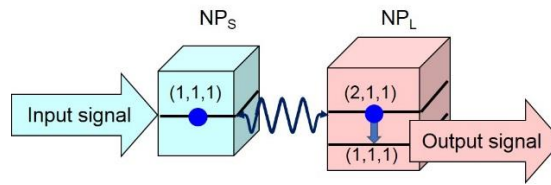
Fig. 1

DP energy transfer and dissipation in two cubic semiconductor NPs.

However, because of phenomena (1) mentioned above in Section 1, there is a way for the energy to be transferred from NP$_\text{S}$ to NP$_\text{L}$, as represented by the blue double-headed arrow in Fig. 1. The transfer process is:

(1) An exciton is excited to level (1,1,1) in NP$_\text{S}$ by the irradiated propagating light.

(2) A DP is created by this exciton and is localized on NP$_\text{S}$.

(3) The energy of this DP is transferred to NP$_\text{L}$.

(4) An exciton is excited to level (2,1,1) in NP$_\text{L}$ even though this level is electric-dipole forbidden.

After this process, the exciton promptly relaxes to the lower level (1,1,1) in the NP$_\text{L}$ and dissipates a small amount of energy, as shown by the downward blue arrow. Then, the relaxed exciton emits propagating light, to be used as the output signal.

3 Application to functional devices

The unique transfer and dissipation of the DP energy, reviewed in the previous section, have been applied to the development a variety of novel DP devices, such as AND and NOT logic gates, by integrating size-controlled

3

semiconductor NPs on a substrate. Figure 2 demonstrates the structure and operation of these devices [3]. In addition to these logic gate devices, a variety of other DP devices have been developed, including a nano-optical condenser [4], a digital-to-analog converter [5], an energy transmitter [6], a frequency up-converter [7], a delayed-feedback optical pulse generator [8], and so on. As representative examples of these devices, this section reviews a nano-optical condenser and an energy transmitter.

(a)

(b)

(c)

(d)
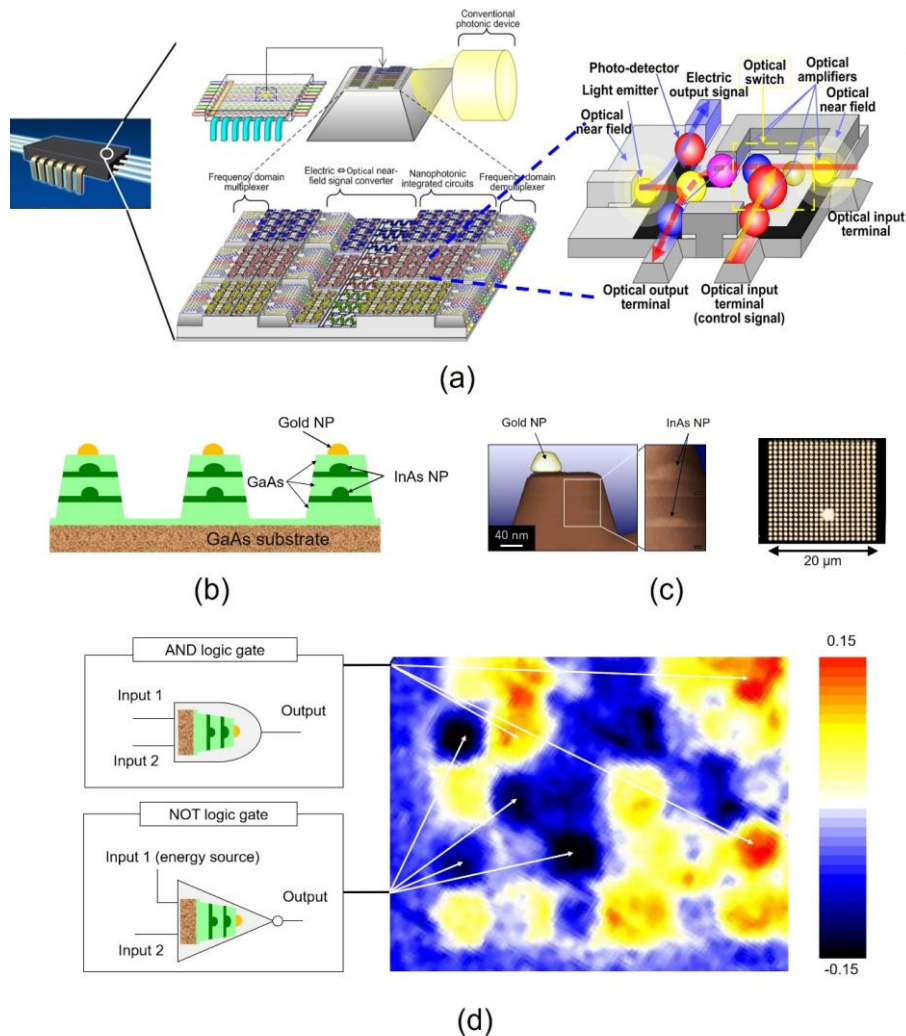
Fig. 2 Dressed photon devices.

(a) Prototype of integrated circuit composed of DP devices.

(b) Cross-sectional structure of mesa-shaped NOT logic gate composed of InAs NPs.

(c) Scanning transmission electron microscope image of structure in (b) (left) and optical microscope image of a two-dimensional array of structures in (b) (right).

(d) Measured spatial distribution of the output signal intensity from a two-dimensional array of fabricated devices composed of InAs NPs.

4

3.1 Nano-optical condenser

A nano-optical condenser that converts propagating light to DPs with high efficiency has been developed on the basis on the unique spatial evolution features of the DP energy transfer [4]. In order to construct this device, a large number of small nano-particles (NP_S) are used, and one large nano-particle (NP_L) is installed at the center, as shown in Fig. 3(a). Moreover, medium-sized nano-particles (NP_M) are installed in the intervening spaces. Since the sizes of these NPs are tuned so that the quantized exciton energy levels are resonant with each other, as was the case between the two NPs in Fig. 1, when an exciton is created in NP_S by irradiation with propagating light, the DP energy is transferred from NP_S to NP_M. After this transfer, relaxation promptly occurs in NP_M, and subsequently, the energy is transferred from NP_M to NP_L. After relaxation in NP_L, the output signal is generated from the exciton in the lowest energy level. Here, since the energy level $(1,1,1)$ in NP_S is tuned to the photon energy of the incident propagating light, almost all the incident propagating light energy can be absorbed by a large number of NP_Ss.

(a)   (b)   (c)
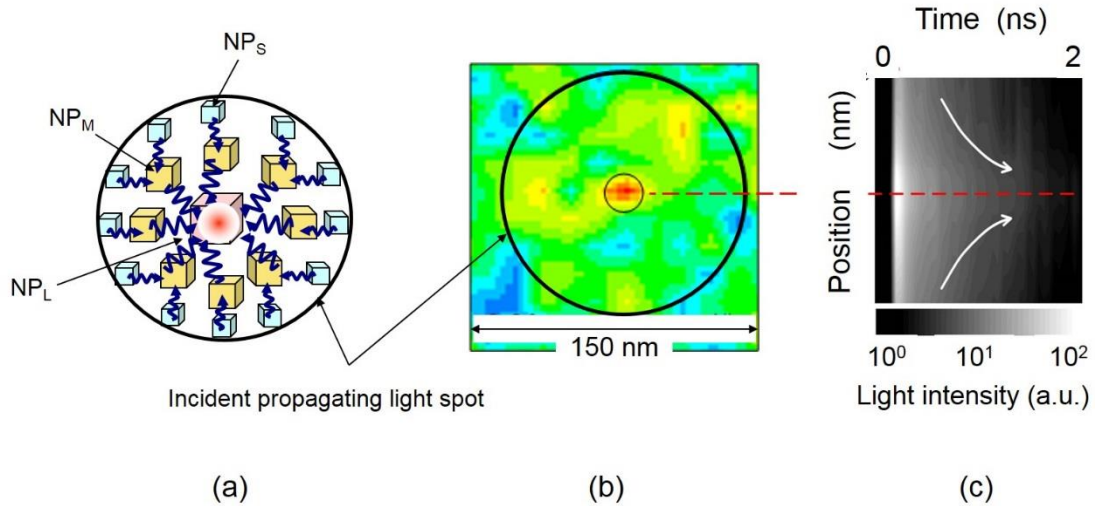
Fig. 3 Nano-optical condenser.
(a) Structure of the device. (b) and (c) show the spatial distribution and temporal evolution of the light intensity emitted from CuCl NPs, respectively.

Furthermore, since the energy dissipation in this system is due to the relaxation in NP_M and NP_L, its magnitude is very small. As a result, a high

5

efficiency is expected for concentrating the energy of the incident propagating light at NP_L.

Figure 3(b) shows an observed near field optical microscopic image of the spatial distribution of the DP energy by applying propagating light with a wavelength of 385 nm to cubic CuCl NPs in an NaCl host crystal. The bright spot at the center corresponds to the place at which the incident light energy was condensed at NP_L, which had a side length of 8 nm. Its diameter was about 20 nm, including the size of the probe apex used for the microscope, which governs the resolution of the measurement. The light power in this spot was more than five-times higher than that of the light power emitted from NP_L when it was isolated from the NPs. From these results, it is confirmed that this device worked as a high-efficiency optical condenser beyond the diffraction limit. This novel device has also been called an optical nano-fountain [4].

The high performance of this device can be confirmed by comparing it with a conventional convex lens. When propagating light is focused by a convex lens, the theoretical spot diameter at the focal plane is expressed as λ / NA, which corresponds to the diffraction limit of a focused light beam. Here, λ is the wavelength of the incident light, and NA is a parameter called the numerical aperture, which depends on the shape and material of the lens, being smaller than unity. By substituting the spot diameter in Fig. 3(b) into this formula, we fid that NA is more than 40, which is much larger than that of a conventional convex lens.

Figure 3(c) shows the measured spatial and temporal evolutions of the light intensity. The horizontal axis at the top of the figure represents time, and the vertical axis represents the radial position in polar coordinates centered at NP_L. The brightness gradation is proportional to the number of emitted photons, from which one can find that the energy is condensed at NP_L with a time constant as short as 2 ps.

Because of the extremely low energy dissipation due to the relaxation from the upper to lower energy levels in NP_M and NP_L, the efficiency of optical energy concentration can be higher than 0.9. The energy transfer process in the nano-optical condenser described above is similar to that in photosynthetic bacteria [9], whose high energy transfer efficiency is receiving attention as a novel system function inherent to such complex systems in a nano-scale space [10,11].

6

3.2 Energy transmitter

In addition to the nano-optical condenser described above, another example that uses the spatial evolution features of the DP energy transfer is an energy transmitter. This transmitter is used to transmit a signal from one DP device to another, corresponding to the function of a metallic wire in an electrical circuit or an optical waveguide in a conventional optical integrated circuit. It should meet the following two requirements:

(1) Signal reflection from the DP devices connected to the tail of this transmitter must be avoided to achieve stable uni-directional energy transmission.

(2) Transmission loss must be sufficiently low to realize a long transmission length.
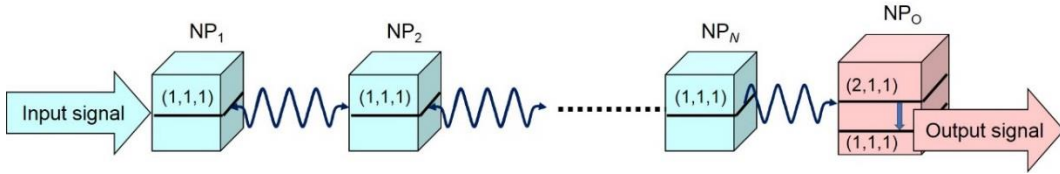
Fig. 4 Structure of energy transmitter.

Figure 4 shows the structure of an energy transmitter that was developed to meet these requirements. It is composed of an array of N NPs of the same size (NP$_1$ – NP$_N$), and a large NP (NP$_O$) installed at the end of this array. In the case of using cubic NPs, as an example, an exciton is created in energy level (1,1,1) in NP$_1$ by applying an input signal, i.e., by irradiating NP$_1$ with propagating light. This light is converted to a DP and is transferred to energy level (1,1,1) in NP$_N$, and nutation occurs among the N NPs. As a result, these NPs are coupled with each other. If the size of NP$_O$ is tuned so that its electric dipole-forbidden level (2,1,1) is resonant with the energy level of this coupled state of the N NPs, nutating energy is transferred to the upper energy level (2,1,1) in NP$_O$, and by subsequent relaxation to the lower energy level (1,1,1). Finally, the light is emitted from the exciton in level (1,1,1) and is used as the output signal.

The device in Fig. 4 meets requirement (1) above because the exciton cannot be excited to the upper energy level (2,1,1) in NP$_O$ even if the exciton is created in the lower energy level (1,1,1) in NP$_O$ by back-transfer of

7

the signal from the DP devices installed at the stage after NP_O. Thus, the energy is not back-transferred from NP_O to $NP_1 - NP_N$.

It can be easily found that requirement (2) is met because the magnitude of the energy dissipated during the relaxation from level $(2,1,1)$ to level $(1,1,1)$ in NP_O is as low as 20 meV, which is much lower than the photon energy of the light radiated onto the device.

For device fabrication, it is much easier to randomly disperse $NP_1 - NP_N$ and NP_O on a substrate than to arrange them accurately so as to maintain a constant separation. Figure 5(a) schematically explains this configuration [12], in which small NPs are randomly dispersed along the x-, y-, and z-axes, and are used as $NP_1 - NP_N$, whose numbers of rows are denoted by N_x, N_y, and N_z, respectively. NP_O is installed among the dispersed small NPs. NP_1 and NP_O are respectively denoted by NP_{in} and NP_{out} in this figure.

(a) (b)
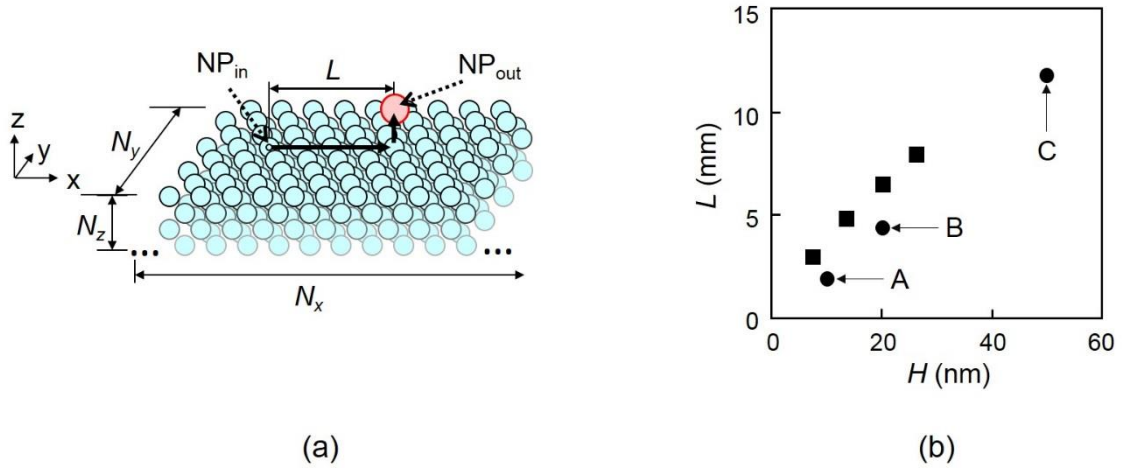
Fig. 5 Calculated results for NPs dispersed on a planar substrate.

(a) Arrangement of multiple small NPs (NP_S) and one larger NP (NP_L).

(b) Dependence of the energy transfer length L on the thickness H of the small NP layers.

For experiments, spherical CdSe NPs were used for simplicity of material preparation. The diameters of $NP_1 - NP_N$ were maintained at 2.8 nm, whereas that of NP_O was 4.1 nm in order to satisfy the resonance condition of the exciton energy levels. These spherical CdSe NPs were dispersed on a SiO_2 substrate, and the average separation between the

8

adjacent NPs was arranged to be close to 7.3 nm in order allow efficient DP energy transfer (refer to property (b) in Section 1). Moreover, the thickness of the NP layers, H in Fig. 5(a), was fixed to 10 nm, 20 nm, and 50 nm, which is proportional to the number of rows N_z of $NP_1 - NP_N$ along the z-axis. These devices are denoted by A, B, and C, respectively.

By applying propagating light with a wavelength of 473 nm, the energy transfer length L was measured as a function of H. The results are shown in Fig. 5(b), from which the values of L for devices A, B, and C were found to be 1.92 µm, 4.40 µm, and 11.8 µm, respectively. These are much longer than the wavelength of the incident light, which also meets requirement (2) above. This figure shows that these measured values agree with the values calculated by using the rate equations representing DP energy transfer between two adjacent NPs. It also shows that L increases with increasing H, i.e., with increasing N_z.

3.3 Autonomy in dressed photon energy transfer

The DP devices reviewed in the previous subsections exhibit novel characteristics which are superior to those of conventional photonic devices. They are: single-photon operation [13], low energy dissipation [14], low energy consumption [15], tamper resistance [16], and skew resistance [17]. Furthermore, an outstanding advantage conferred by the spatial evolution features is autonomy in the DP energy transfer [18], which is reviewed in this subsection.

As is schematically explained by Fig. 6(a), the present model contains N small NPs (NP_S) and one large NP (NP_L). By assuming that each NP_S is initially occupied by an exciton, quantum master equations for the density matrix are solved to derive the occupation probability of the exciton in the lower energy level in NP_L. The time-integrated value of this probability corresponds to the output signal intensity.

This intensity is calculated as a function of the number N of CuSe NP_S. The calculated results are indicated by closed circles in Fig. 6(b) and show that the efficiency in energy transfer is highest when $N \cong 4$. Since the radiative relaxation rate from the lower energy level in NP_L takes a finite value, the DP energy is not transferred to NP_L until the exciton in the lower energy level is annihilated, and as a result, the energy is dissipated from

9

NP$_S$ if N is too large. Therefore, the output signal intensity does not increase if too many NP$_S$ are installed around an NP$_L$, and as a result, the efficiency of the energy transfer to NP$_L$ decreases when N is larger than 4.

(a)   (b)
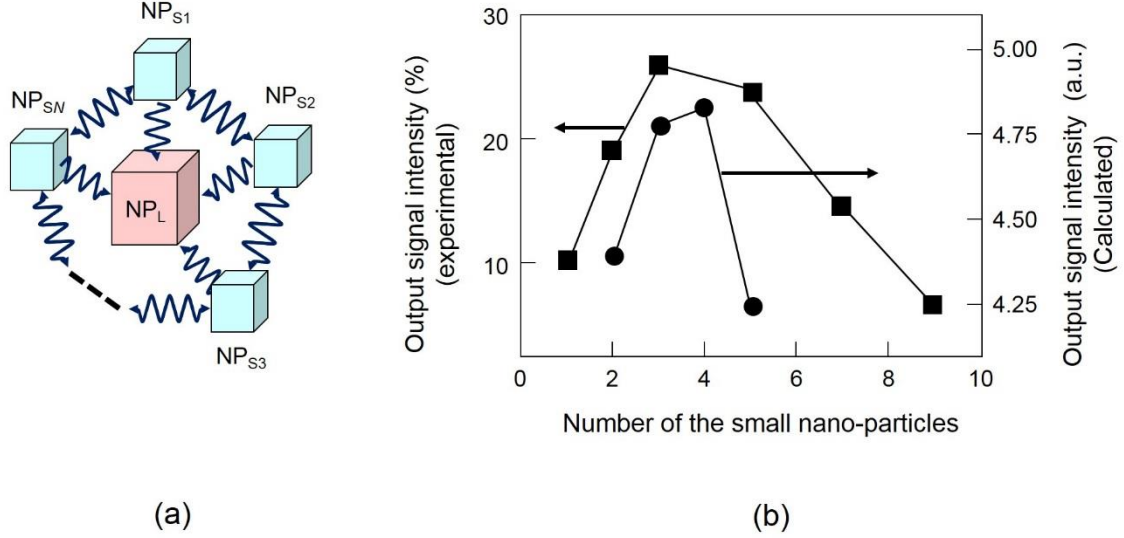
Fig. 6 Autonomy of the DP energy transfer.
(a) Layout of NPs. (b) Dependences of the output signal intensities emitted from CuSe NPs on the ratio of the number of NP$_S$s to that of NP$_L$.

Small and large spherical CdSe NPs (2.0 nm and 2.8 nm diameters, respectively) were used, as was the case described in Subsection 3.2, to experimentally measure the magnitude of the energy transferred from NP$_S$ to NP$_L$. The results are represented by the closed squares in Fig. 6(b), which show that the output signal intensity takes the maximum at $N \cong 4$.

The dependence of the energy transfer on the number N of the NPs suggests that the output signal intensity can be controlled by designing the positions of the NPs. Let us assume that interactions between some NP$_S$s and NP$_L$ may be degraded or lost because their resonant conditions are not satisfied due to, for example, size-detuning of NPs, fluctuations in the separations between NPs, and deterioration of the NP materials. In the case of a pentagonal layout, as shown in Fig. 7(a), there can be eight degraded configurations: By referring to system E0 without any degradations, system E1 represents the layout in which the interaction between one NP$_S$ and NP$_L$ is degraded or lost (represented by the mark $\times$ between NP$_{S1}$ and NP$_L$ in this figure). Systems E2 and E2' have two degraded interactions.

10
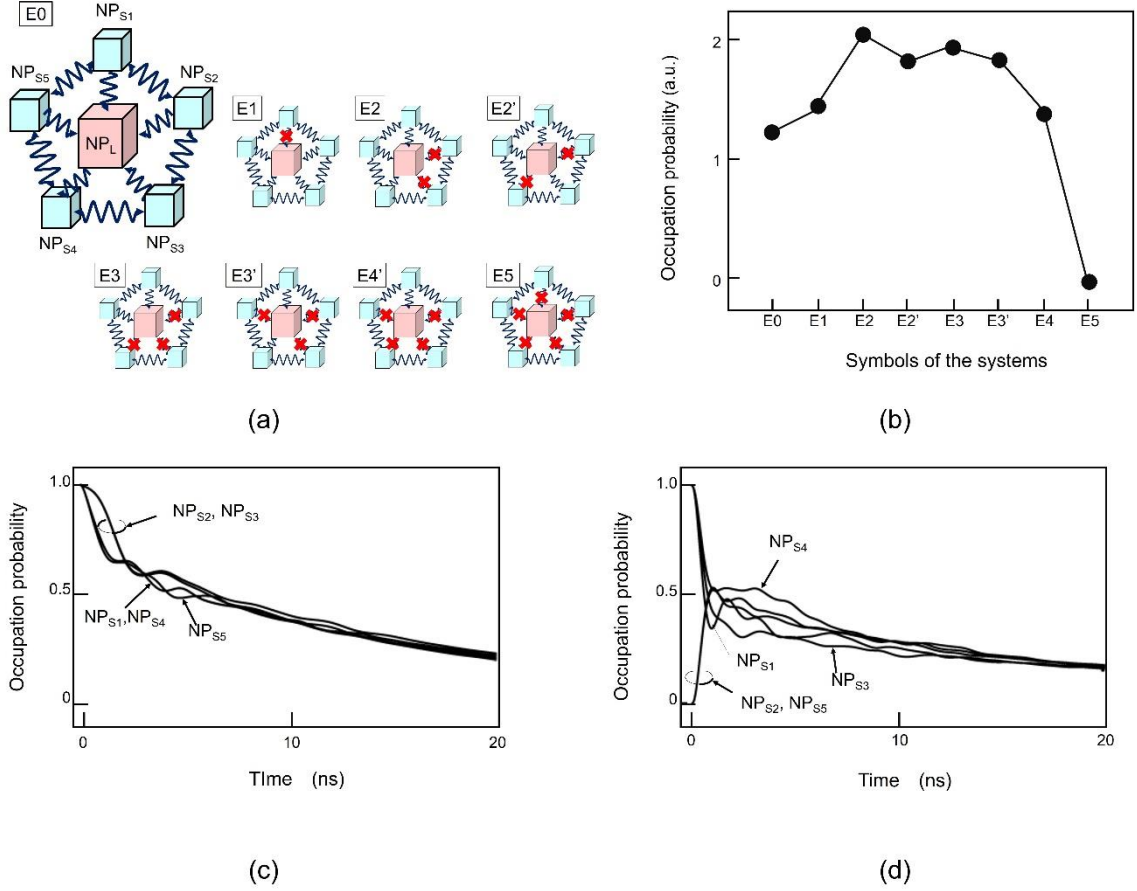
Fig. 7 Degraded or lost interaction between NP$_S$s and NP$_L$.

(a) Layout of NPs. (b) Time-integrated values of the occupation probabilities for systems E0 to E5. (c) and (d) are temporal evolutions of the occupation probabilities of the exciton in the energy levels in five NP$_S$s in systems E2 and E0, respectively.

Figure 7(b) shows the relation between the systems (E0–E5) and the time-integrated values of the occupation probability of the exciton in NP$_L$. This figure shows that system E5 does not generate any output signals because the interaction between NP$_S$ and NP$_L$ is completely lost. In contrast, the output signal intensities from systems E1–E4 with degraded interactions are larger than that from system E0. In particular, the value of the output signal intensity from system E2 is 1.64-times that from system E0, which is consistent with the fact that the signal intensity takes the maximum at $N \cong$ 4 in Fig. 6(b).

Moreover, the autonomy in energy transfer can be understood from Fig. 7(c). This figure shows the temporal evolutions of the occupation

11

probabilities of excitons in the energy levels in five NP_S in system E2, in which two interactions are degraded (NP_{S2}–NP_L and NP_{S3}–NP_L), as was shown in Fig. 7(a). The energy levels in all the NP_S are initially occupied by excitons, and afterward for several ns, the occupation probabilities in NP_{S2} and NP_{S3} remain high, which means that the energy is efficiently stored in NP_{S2} and NP_{S3} until it is transferred to NP_L. On the other hand, Fig. 7(d) shows the time evolutions of the occupation probabilities in the case of system E0, in which the energy levels in three NP_S (NP_{S1}, NP_{S3}, and NP_{S4}) are initially occupied by excitons. It is found from this figure that the occupation probabilities for NP_{S2} and NP_{S5} increased within 2 ns even though they were initially zero. This means that, in a sense, the transferred energy autonomously searches for unoccupied NP_Ss in the system.

It was demonstrated that a single energy transfer process is about 10^4-times more efficient compared with the single bit-flip energy required in conventional electronic devices [14]. On the other hand, energy transfer in light harvesting antennas exhibits superior efficiency [19], and these structures have similarities to nanostructures networked via interactions by DP energy transfer. In summary, these studies will be extremely helpful for developing advanced DP devices with higher performance.

3.4 Temporal evolution of dressed photon energy transfer

In addition to the spatial evolutions shown in Subsections 3.2 and 3.3, Fig. 8 (a) shows the temporal evolution of the output signal from the DP device, i.e., the light intensity from NP_L, emitted when a propagating light pulse (pulse width: 10 ps) is applied to NP_S. Red circles are the measured values acquired for $0 \leq t \leq 4$ ns. The optical intensity increases rapidly with a rise time τ_r of 90 ps, which depends on the magnitude of the transferred DP energy. After the applied signal pulse decays, the output signal also decays with small amplitude oscillation. This oscillation originates from the nutation of the DP energy transfer between NP_S and NP_L. The period of oscillation is found to be about 400 ps from this figure. The decay time, i.e., the fall time τ_f, is about

4 ns, which depends on the value of the radiative relaxation rate from the low energy level in NP_L. The solid curve represents the result calculated by using quantum master equations for the density matrix [20], which agrees

12

well with the experimental results.

For more detailed analyses of the temporal evolution of the DP energy transfer, the optical intensity was acquired in the time range $0 \leq t \leq 10$ ns, which is longer than that in Fig. 8(a). Black squares in Fig. 8(b) are the acquired values. The blue curve represents the temporal evolution expressed as $\exp\left(-t/\tau_{f1}\right)$, where τ_{f1} is the fall time, depending on the magnitude of the transferred DP energy. This curve agrees with the black squares only for an initial stage as short as $0 \leq t \leq 2$ ns. On the other hand, the red curve represents the temporal evolution expressed as $\exp\left(-\sqrt{t/\tau_{f2}}\right)$, where the fall time τ_{f2} is the radiative relaxation rate from the low energy level in NP_L. This agrees with the black squares for a wide range of time periods up to 10 ns. For more detailed analyses of the DP energy transfer dynamics, it will be advantageous to suppress the component expressed as $\exp\left(-\sqrt{t/\tau_{f2}}\right)$, which can be realized by decreasing the device temperature.
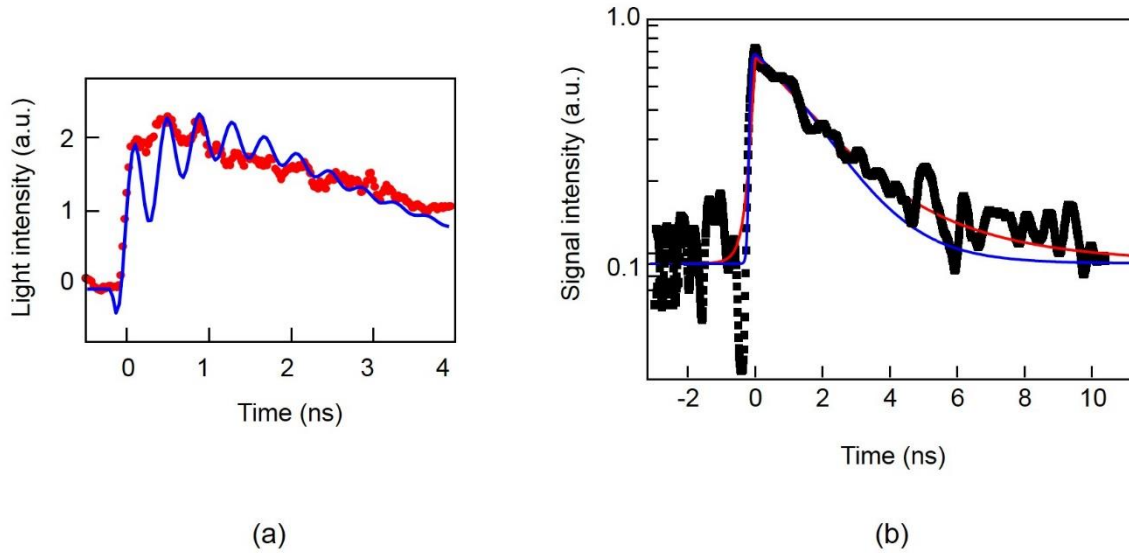
Fig. 8 Temporal evolution of the light intensity emitted from the CuCl NP_L.
(a) and (b) are the optical intensities, acquired for $0 \leq t \leq 4$ ns and for $0 \leq t \leq 10$ns, respectively.

4 Application to optical energy conversion

A novel thin film was invented recently, which efficiently converts ultraviolet (UV) photon energy to visible photon energy by means of DP energy transfer and dissipation. It has been used to drastically improve the electrical power generation efficiency of a solar cell battery. This section reviews the principle and operation of this film.

4.1 Principle

Transparent silicone or ethylene-vinyl acetate (EVA) was used as the film material, with a thickness of $10\,\mu$m. ZnO semiconductor NPs (average size and number density are 3–5 nm and 10^{17} to 10^{18} /cm^3, respectively) and DCM dye NPs (weight density 3–5 mg/cm^3) were dispersed in this film. It is required that the separation between the ZnO and DCM NPs be as close as possible to their sizes in order to transfer the DP energy between them (refer to (b) in Section 1). The number density and weight density above meet this requirement [21,22].

The roles of the ZnO and DCM NPs in this film are to absorb UV light and emit visible light, respectively. They correspond respectively to NP$_S$ and NP$_L$ in Fig. 1. That is, UV light absorption excites an electron in the ZnO NP to create the DP. Then, the DP energy is transferred to the DCM NP, resulting in excitation of the electron in the DCM NP. This electron dissipates a small amount of its energy by relaxing to a lower energy level, emitting visible light.

For the DP energy transfer, an electronic dipole-forbidden transition is utilized (refer to (1) in Section 1). Furthermore, since the magnitude of the energy dissipation above is very low, very high-efficiency optical energy conversion can be realized.

Figures 9(a) and (b) show the electronic energy levels in the ZnP and DCM NPs for UV light absorption and visible light emission, respectively. They are:

[In ZnO NP]

$|a_{\mathrm{ZnO}}\rangle$: An energy level of the electron in the conduction band. Since it is an electric dipole-allowed level, the electron is excited to this level by UV light absorption.

14

$|a'_{\mathrm{ZnO}}\rangle$: An electric dipole-allowed energy level in the conduction band. Its

energy is slightly lower than that of $|a_{\mathrm{ZnO}}\rangle$.

$|b_{\mathrm{ZnO}}\rangle$: Several energy levels in the bandgap, which originate from impurity

atoms in the ZnO NP. They consist of electric dipole-allowed and -forbidden
energy levels.

$|c_{\mathrm{ZnO}}\rangle$: An electric dipole-allowed level of the energy levels $|b_{\mathrm{ZnO}}\rangle$ above,

which is a defect level originating from the oxygen atoms in the ZnO NP. The
electron in this level emits blue light.

$|e_{\mathrm{ZnO}}\rangle$: An electric dipole-forbidden level of the energy levels $|b_{\mathrm{ZnO}}\rangle$ above.

However, it can emit light because it is the lowest energy level of $|b_{\mathrm{ZnO}}\rangle$.
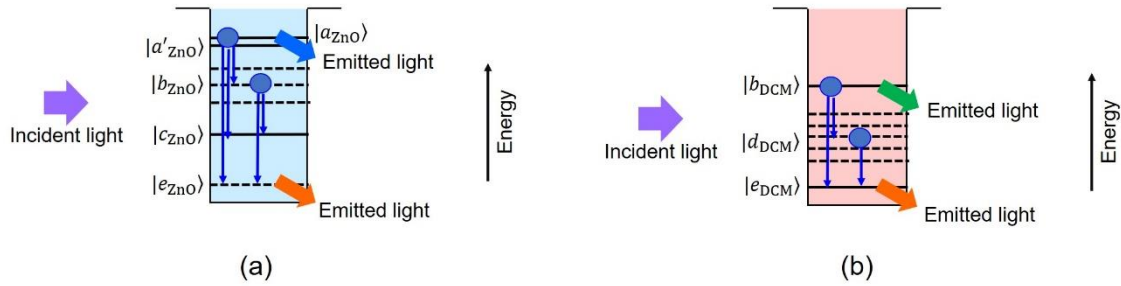
Fig. 9 Electronic energy levels in a ZnO NP (a) and a DCM NP (b).

[In DCM NP]

$|b_{\mathrm{DCM}}\rangle$: An electric dipole-allowed level. Thus, the electron in this level can

emit light. It is resonant with the energy level $|b_{\mathrm{ZnO}}\rangle$ in the ZnO NP.

$|d_{\mathrm{DCM}}\rangle$: Electric dipole-forbidden energy levels, which originate from the

impurity atoms in the DCM NP. Some of them are resonant with the energy

level $|c_{\mathrm{ZnO}}\rangle$ in the ZnO NP.

15

$|e_{DCM}\rangle$: An electric dipole-allowed level of the energy levels $|d_{DCM}\rangle$. Thus, the electron in this level can emit light. It is resonant with the energy level $|e_{ZnO}\rangle$ in the ZnO NP.

The UV light absorption and visible light emission processes in the ZnO NP and DCM NP, are:
[In ZnO NP (Fig. 9(a))]

An electron in the ZnO NP is excited to the energy level $|a_{ZnO}\rangle$ by UV light absorption. This excited electron has a higher probability of UV light emission than that of relaxation to a lower energy level. Thus, the conversion efficiency from UV light to visible light is low.
[In DCM NP (Fig. 9(b))].
After an electron in the DCM NP is excited to a higher energy level by UV light absorption, it relaxes to an electric dipole-forbidden energy level, which is a triplet energy level. Thus, the conversion efficiency from UV light to visible light is low.

However, in the case where both the ZnO and DCM NPs are dispersed in the film, the light absorption and emission processes are remarkably different from those above. They are (Fig. 10): An electron in the ZnO NP is excited to the energy level $|a_{ZnO}\rangle$ by UV light absorption. It subsequently relaxes to the lower energy levels $|b_{ZnO}\rangle$, $|c_{ZnO}\rangle$, or $|e_{ZnO}\rangle$. Then, a DP is created, and its energy is transferred to the resonant energy levels $|b_{DCM}\rangle$, $|d_{DCM}\rangle$, or $|e_{DCM}\rangle$ in the DCM NP. As a result, an electron is excited to these levels and emits visible light. This visible light emission realizes a high efficiency of energy conversion from UV light to visible light. It should be noted that the DP energy can be transferred back from the DCM to the ZnO particles even though the electron in the DCM particles relaxes to the triplet energy level. This back transfer contributes to further increases in the energy conversion efficiency.

16
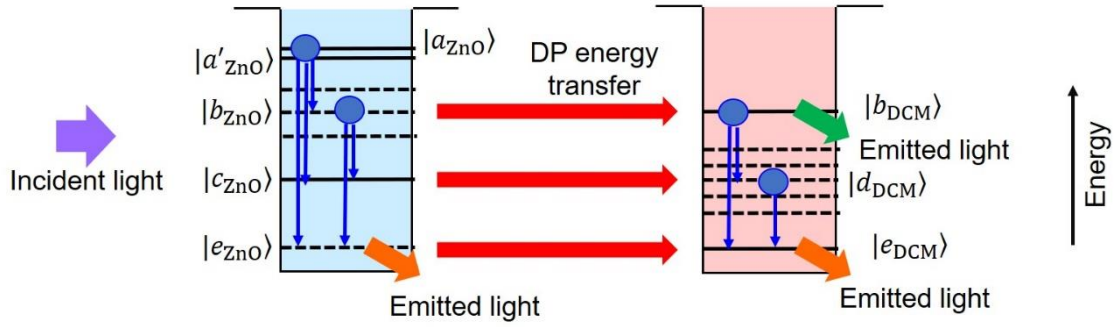
Fig. 10 Light absorption and emission of a film in which ZnO and DCM NPs are dispersed.

4.2 Operating characteristics

Figure 11 shows measured excitation spectra, in which the horizontal axis represents the wavelength of the light incident on the film, and the vertical axis is the intensity of the visible light (wavelength 560 nm) emitted from the electron in the energy level $|e_{\mathrm{DCM}}\rangle$ of the DCM NP. Figures 11(a) and (b) show the results acquired when only the ZnO and DCM NPs are dispersed in the film, respectively. Figure 11(c) shows those when both ZnO and DCM NPs are dispersed. Comparing the areas below the curves in these figures, the efficiency of the conversion from UV light to visible light (wavelength 560 nm) energy in Fig. 11(c) is estimated to be at least 10-times higher than that in Fig. 11(a) or (b).

Furthermore, a bump A on the curve in Fig. 11(c) represents that the efficiency of the visible light emission is selectively enhanced when the incident UV light is resonant with the energy level $|a_{\mathrm{ZnO}}\rangle$ of the ZnO NP. Furthermore, the bumps B and C also represent that the efficiency is selectively enhanced when the incident light is resonant with the energy level $|b_{\mathrm{ZnO}}\rangle$ or $|c_{\mathrm{ZnO}}\rangle$ of the ZnO NP. These selective enhances are due to the DP energy transfer to the energy levels $|b_{\mathrm{DCM}}\rangle$ or $|d_{\mathrm{DCM}}\rangle$ of the DCM NPs, and subsequent relaxation to the energy level $|e_{\mathrm{DCM}}\rangle$.

17
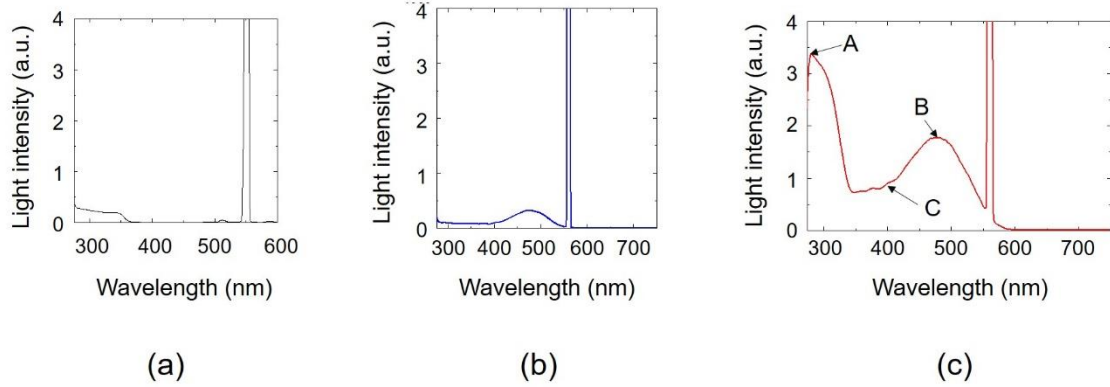
Fig. 11 Excitation spectra.

(a) and (b) The results acquired when only the ZnO and DCM particles are dispersed in the film, respectively. (c) The result when both ZnO and DCM particles are dispersed.

Figure 12 shows the measured relation between the incident UV light intensity (wavelength 325 nm) and the efficiency of the energy conversion to visible light (wavelength 560 nm). It shows that the measured efficiency is proportional to the square of the incident UV light intensity[*]. This is because the conversion efficiency is proportional to the product of the numbers of DPs created in the ZnO and DCM NPs.

---

[*] Figure 12 shows that the efficiency saturates when the UV light intensity is higher than 0.2 W/m². Since the UV light component in sunlight is higher than 0.2 W/cm², this saturation is advantageous for the solar cell battery application to be reviewed in Section 4.3 because the conversion efficiency is maintained constant even if the incident sunlight intensity may vary from hour to hour during daytime.

Figure 13 shows the temporal evolution of the light intensity emitted from the film when a propagating light pulse (pulse width: 2 ps) was applied to the NPs. Figures 13(a) and (b) were acquired when only the ZnO and DCM NPs were respectively dispersed in the film. They are nothing more than the intensities of the light emitted from the ZnO and DCM NPs, respectively, as a result of conventional fluorescence.

The rise time τ_r of the light intensity is as short as 10 ps in Fig. 13(a) and (b). On the other hand, the fall time τ_f is as long as 15 ns and 1.4 ns, respectively, which corresponds to the radiative relaxation rate.

18
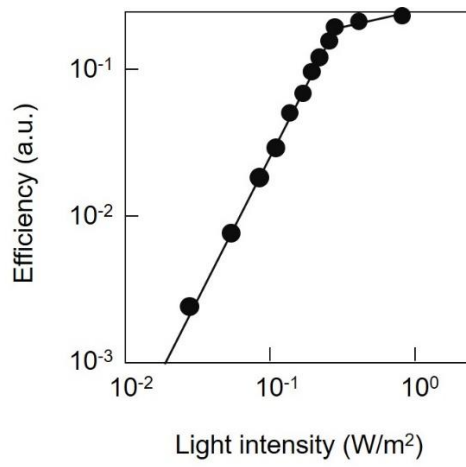
Fig. 12 Measured relation between the incident UV light intensity (wavelength 325 nm) and the efficiency of the energy conversion.

(a)

(b)

(c)

(d)
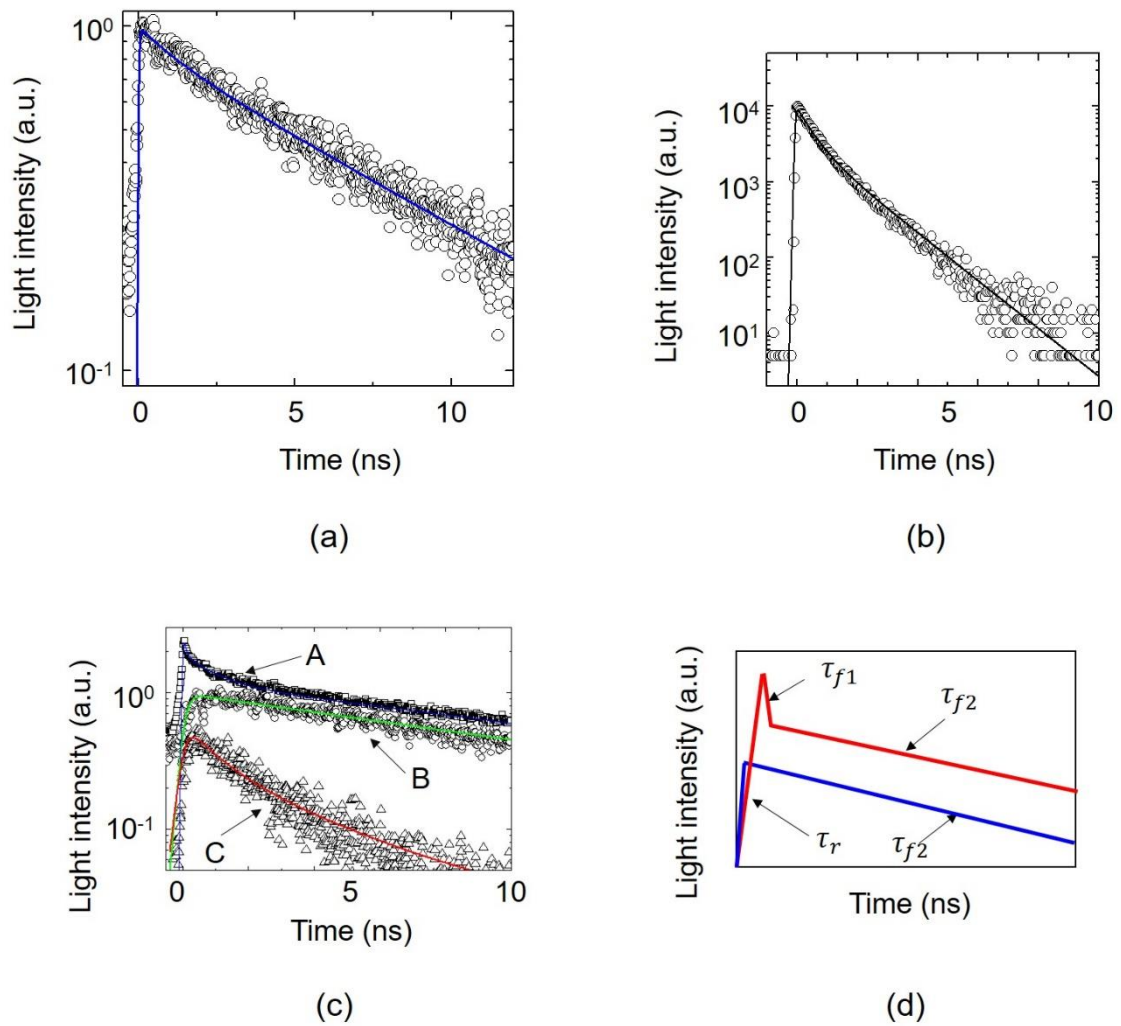
Fig. 13 Temporal evolutions of the light intensity emitted from the film.

19

(a) The result acquired when only the ZnO NPs are dispersed in the film. The vertical axis represents the light intensity (wavelength 350 nm) emitted from the electron in the lower energy level $\left| a'_{ZnO} \right\rangle$ of the ZnO by illuminating the film with light (wavelength 340 nm), which is resonant with the higher energy level $\left| a_{ZnO} \right\rangle$.

(b) The result acquired when only the DCM NPs are dispersed in the film. The vertical axis represents the light intensity (wavelength 560 nm) emitted from the electron in the energy level $\left| e_{DCM} \right\rangle$ of the DCM by illuminating the film with light (wavelength 340 nm).

(c) The result acquired when both the ZnO and DCM NPs are dispersed in the film. Curve A represents the light intensity (wavelength 350 nm) emitted from the electron in the lower energy level $\left| a'_{ZnO} \right\rangle$ of the ZnO by illuminating the film with light (wavelength 340 nm), which is resonant with the energy level $\left| a_{ZnO} \right\rangle$.

Curve B represents the light intensity (wavelength 560 nm) emitted from the electron in the energy level $\left| e_{DCM} \right\rangle$ of the DCM by illuminating the film with light (wavelength 340 nm), which is resonant with the energy level $\left| a_{ZnO} \right\rangle$ in the ZnO.

Curve C represents the light intensity (wavelength 420 nm) emitted from the electron in the energy levels $\left| b_{ZnO} \right\rangle$ and $\left| d_{DCM} \right\rangle$ of the ZnO and DCM, respectively, by illuminating the film with light (wavelength 420 nm), which is resonant with the energy level $\left| c_{ZnO} \right\rangle$ in the ZnO. (d) Schematic explanation of the curves in (c).

Figure 13(c) shows the results acquired when both ZnO and DCM NPs are dispersed in the film. Figure 13(d) is a schematic explanation of the curves in Fig. 13(c). The time constant τ_r in this figure represents the rise time. Two constants τ_{f1} and τ_{f2} represent two different fall times. Figure 13(c) shows that the values of τ_r and τ_{f1} are 100–150 ps. These correspond to the DP energy transfer times from the ZnO to DCM NPs, which are much

20

longer than the fluorescence rise times in Figs. 13(a) and (b).

Similar to the fall time of the curves in Figs. 13(a) and (b), the fall time τ_{f2} is 15 ns, which is much longer than τ_{f1}. This fall time τ_{f2} corresponds to the value of the radiative relaxation rate. It means that, after the DP energy transfer, conventional florescence occurs in the case where both the ZnO and DCM NPs are dispersed in the film. It should be noted that Figs. 13(a) and (b) do not have the temporal behaviors represented by the time constants τ_r and τ_{f1}.

The temporal evolutions shown in Figs. 8 and 13(c) have several common features even though the materials used are different:

(1) The temporal evolution expressed as $\exp\left(-t/\tau_{f1}\right)$ and the nutation behavior in Fig. 8 have the same origin as that of the time evolution represented by τ_{f1} in Fig. 13(c), namely, the DP energy transfer between NPs. The rise time τ_r also originates from this transfer.

(2) The temporal evolution expressed as $\exp\left(-\sqrt{t/\tau_{f2}}\right)$ in Fig. 8 has the same origin as that of the time evolution represented by τ_{f2} in Fig. 13(c), namely, the radiative relaxation in each NP.

Features (1) and (2) above represent unique phenomena which are different from each other. The former is exactly the novel off-shell scientific phenomenon [2]. The latter is no more than a conventional on-shell phenomenon. The fact that these temporal evolutions are respectively expressed as $\exp\left(-t/\tau_{f1}\right)$ and $\exp\left(-\sqrt{t/\tau_{f2}}\right)$ suggests that they correspond to the quantum walk [23] and the relaxation processes, respectively. As for the former process, it should not be considered as a mere random walk because its energy transportation is linearly dependent on time, not on the square root of time. It is expected that the unique autonomous spatial evolution feature described in Subsection 3.3 can be also analyzed in terms of a quantum walk, one fundamental feature of which is a linear dependence on time.

21

4.3 Evaluation of the optical energy conversion efficiency

It is expected that the optical energy conversion efficiency of the film is as high as 90%–95% by referring to the large difference between the DP energy transfer time (τ_r, τ_{f1} = 100–150 ps) and the lifetime (τ_{f2} = 15 ns) for fluorescent light emission from the DCM NP. Based on this expectation, a novel film was fabricated for converting UV light energy (wavelength 300–350 nm) to visible light energy (wavelength 560 nm) by dispersing ZnO and DCM NPs (Fig. 14(a)) [24]. By putting this film on the surface of a commercially available Si solar cell battery (surface area 156 mm × 156 mm, nominal electrical power generation efficiency 18.1 %), the electrical power generation efficiency was measured to be as high as 20.0 %, which is an increase of 1.9 % compared with the nominal efficiency mentioned above.

(a)　　　　　　　　　　　(b)
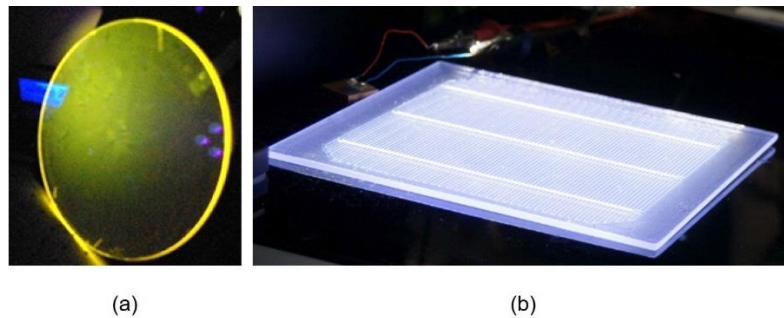
Fig. 14 Photographic images of the film.

The film is 10 μ m thick and is coated on the front surface of a glass substrate. After an index-matching oil is coated on the rear surface, it is placed on a solar cell battery surface.

(a) ZnO and DCM NPs are dispersed in the film. (b) ZnO and BBQ NPs are dispersed in the film.

To realize an even higher increase, another type of film was recently developed by replacing the DCM NPs with BBQ dye NPs (Fig. 14(b)), which allowed UV light in the wavelength range 300–350 nm to be efficiently converted to visible light with a wavelength of 450 nm [25]. By putting this film on the surface of the Si solar battery above, the electrical power generation efficiency was measured to be as high as 20.2 %, which is an increase of 2.1 % compared with the nominal efficiency mentioned above.

It should be pointed out that the efficiencies higher than 20% realized by these films have never been achieved with conventional solitary Si solar batteries. The technical details of the method of fabricating these films will be published elsewhere.

5. Summary

The introduction of this paper reviewed the intrinsic nature of the DP, which is a novel form of quantum field created in a nanometer-sized space. Next, a unique DP energy transfer process between semiconductor nanoparticles was described. As a first application of this transfer, novel functional devices were demonstrated by focusing on a nano-optical condenser and an energy transmitter. It was shown that the DP energy transfer in these devices exhibited an autonomous spatial evolution feature. A temporal evolution feature was also demonstrated, which originated from nutating DP energy transfer followed by radiative relaxation.

As a second application, a highly efficient optical energy conversion film was demonstrated. By evaluating the temporal evolution feature of the converted optical energy, the origin of this feature was confirmed to be equivalent to that of the functional devices described above. It was suggested that the spatial and temporal evolutions above can be analyzed based on theoretical models involving a quantum walk and a random walk. As an application of this film, it was placed on a silicon solar battery to convert UV light energy to visible light energy, resulting in an increased electrical power generation efficiency of 20.2%.

References

[1] M. Ohtsu: *Dressed Photons* (Springer, Heidelberg, 2014) pp.11-37.

[2] M. Ohtsu, Offshell: 1709R.001.v1 (2019).

[3] T. Kawazoe, M. Ohtsu, S. Aso, Y. Sawado, Y. Hosoda, K. Yoshizawa, K. Akahane, N. Yamamoto, M. Naruse, Appl. Phys. B **103**, 537 (2011).

[4] T. Kawazoe, K. Kobayashi, M. Ohtsu, Appl. Phys. Lett. **86**, 103102 (2005).

[5] M. Naruse, T. Miyazaki, F. Kubota, T. Kawazoe, K. Kobayashi, S. Sangu, and M. Ohtsu, Opt. Lett. **30**, 201 (2005).

[6] W. Nomura, T. Yatsui, T. Kawazoe, M. Ohtsu, J. Nanophotonics **1**, 011591 (2007).

[7] T. Yatsui, S. Sangu, K. Kobayashi, T. Kawazoe, M. Ohtsu, J. Yoo, G.-C. Yi, Appl. Phys.

23

Lett. **94**, 083113(2009).

[8] M. Naruse, H. Hori, K. Kobayashi, T. Kawazoe, M. Ohtsu, Appl. Phys.B **102**, 717(2011).

[9] H. Imahori, J. Phys. Chem. B **108**,6130 (2004).

[10] M. Naruse, T. Kawazoe, R. Ohta, W. Nomura, M. Ohtsu, Phys. Rev. B **80**, 125325 (2009).

[11] N. Johnson, *Simply Complexity*, (Oneworld Publications, Oxford, 2007).

[12] W. Nomura, T. Yatsui, T. Kawazoe, M. Naruse, M. Ohtsu, Appl. Phys.B **100**, 181 (2010).

[13] T. Kawazoe, S. Tanaka, M. Ohtsu, J. Nanophotonics **2**, 029502 (2008).

[14] L.B. Kish, IEE Proc. Circ. Dev. Syst. **151**, 190 (2004).

[15] M. Naruse, P. Holmstrom, T. Kawazoe, K. Akahane, N. Yamamoto, L. Thylen, M. Ohtsu, Appl. Phys. Lett. **100**, 241102 (2012).

[16] M. Naruse, H. Hori, K. Kobayashi, M. Ohtsu, Opt. Lett. **32**,1761 (2007).

[17] M. Naruse, F. Pepper, K. Akahane, N. Yamamoto, T. Kawazoe, N. Tate, M. Ohtsu, ACM J. on Emerging Technol. in Computing Systems **8**, 4-1 (2012).

[18] M. Naruse, K. Leibnitz, F. Peper, N. Tate, W. Nomura, T. Kawazoe, M. Murata, M. Ohtsu, Nano Commun. Networks **2**,189 (2011).

[19] A. Olaya-Castro, C.F. Lee, F.F. Olsen, N.F. Johnson, Phys. Rev. B **78**, 085115 (2008).

[20] S. Sangu, K. Kobayashi, T. Kawazoe, A. Shojiguchi, M. Ohtsu, Trans. Materials Res. Soc. Jpn. **28**, 1035 (2003).

[21] T. Kawazoe, A. Mizushima, K. Matsue, and M. Ohtsu: "A wavelength conversion film using energy transfer via dressed photon," Abstract of the 60th JSAP Spring Meeting, March 2013, Atsugi, Japan, paper number 28p-A1-11.

[22] T. Kawazoe, K. Matsue, and M. Ohtsu: "Fabrication of ZnO-QDs for wavelength conversion film using a dressed photon," Abstract of the 74th JSAP Autumn Meeting, September 2013, Kyoto, Japan, paper number 18p-C14-16.

[23] N. Konno, *Quantum Walk*, Chapter 8, Quantum Potential Theory, ed. by U. Franz and M. Schürmann, (Springer, Heidelberg, 2008) pp.309-452.

[24] T. Kawazoe, K. Matsue, and M. Ohtsu: "Size control of ZnO quantum dots in a wavelength conversion film using a dressed photon for a solar cell," Abstract of the 61st JSAP Spring Meeting, March 2014, Sagamihara, Japan, paper number 18a-F12-6.

[25] T. Kawazoe, C. Amagai, and M. Ohtsu: "High-effectiveness of crystalline silicon solar cell by a wavelength conversion film using a dressed photon," Abstract of the 62th JSAP Spring Meeting, March 2015, Hiratsuka, Japan, paper number 11p-A12-7.

24

New Routes to Studying the Dressed Photon

M. Ohtsu[1,2]

[1] Institute of Engineering Innovation, Graduate School of Engineering,

The University of Tokyo, 2-11-16 Yayoi, Bunkyo-ku, Tokyo, 113-8656, Japan

[2] Research Origin for Dressed Photon, c/o the University of Tokyo,

Bdg. Eng-9, 2-11-16 Yayoi, Bunkyo-ku, Tokyo, 113-8656, Japan

Abstract: First, this paper reviews the history of studies on the dressed photon (DP) by classifying them into older and modern times, between which there exists a great difference in the concepts, principles, and methods involved. Quantum field theories, developed more recently, have succeeded in solving three problems originating from the intrinsic features of the light–matter interactions occurring in nanometric spaces. First, a variety of applications of these theoretical studies, which have resulted in the development of generic technology, are introduced. Second, the present status of experimental studies is reviewed. Among them, the fabrication and operation of novel light emitting devices using crystalline silicon (Si) are demonstrated. In these devices, the DP enabled high-power light emission even though Si is an indirect-transition-type semiconductor. Furthermore, it is shown that these devices exhibit a unique feature, named photon breeding. Third, a future outlook of DP research is presented, where it is pointed out that novel theoretical studies are required in order to support the rapid progress made in recent experimental studies and to develop further novel application technologies. As a route to such novel theoretical studies, three steps are presented, and several results derived from these steps are reviewed. Furthermore, a theory of micro–macro duality in the quantum field is presented as a powerful tool that will enable future progress in theoretical studies. Finally, a variety of phenomena in nano-systems, macro-systems, inorganic materials, and organic materials, which have similar features to those of the DP, are introduced. By referring to this similarity, it is pointed out that studies on the DP are connected to a more generic and broader science that is expected to produce a novel generic science, named off-shell science, in the near future.

1 Introduction

The dressed photon (DP), a novel form of photon created in a nanometer-sized space, has been referred to as an optical near field, and the science for dealing with this type of photon has been called near field optics. The history of near field optics is long and can be classified into older and modern times, based on the great differences in the concepts, principles, and methods of studying the DP. The older time started with a simple proposal to use light falling on a sub-wavelength sized aperture for high-resolution microscopy [1]. After a long time during which this proposal was ignored, theoretical analyses were carried out on the diffraction and radiation of electromagnetic waves through a small aperture [2,3]. Afterward, these analyses were experimentally demonstrated by using microwaves [4].

Demonstrations using light were finally carried out using a novel methodology, named near-field optical microscopy, by several scientists in several countries, including Japan (M.O.), almost simultaneously [5]. Among them, this author (M.O.) developed high-quality optical fiber probes for generating and detecting optical near fields with high resolution and high sensitivity (Fig. 1) [6]. These fiber probes have been used to assemble novel spectrometers, and microscopic and spectroscopic images of specimens, e.g., a single strand of DNA, were successfully acquired with a high resolution beyond the diffraction limit [7]. They have since become commercially available and have been exported to many countries around the world [8].

Based on the successful experimental demonstrations above, the Near-Field Optics Workshop has held in order to promote basic studies and applications of optical near fields [5]. In this workshop, a physical picture of the optical near field was drawn using a conventional optical method, i.e., by using the dispersion relation between the momentum and energy of the photon. After this workshop, the International Near-Field Optics Conference was organized, and the most recent 14th conference was held in 2016 [9]. In order to promote near field optics in the Asia-Pacific area, the author organized the Asia-Pacific Workshop on Near-Field Optics in 1996 [10]. After this workshop, the Asia-Pacific Near-Field Optics Conference was also organized, and the most recent 11th conference was held in 2017 [11].

It should be pointed out that the older time mentioned above has already ended. The reason for this is that conventional optical microscopy is

based on the methodology of nondestructive measurement of the specimen's conformation and/or structure, which is described by conventional optics. Unlike this conventional microscopy, near-field optical microscopy is based on destructive measurement because it acquires an image of the specimen through optical near field interactions between the probe tip and the specimen. Even though a high resolution beyond the diffraction limit of light could be realized by this microscopy, a fatal problem was that electronic energy levels in the specimen were disturbed as a result of these interactions, which resulted in the acquired image profile being different from and uncorrelated with the conventional optical microscope images.
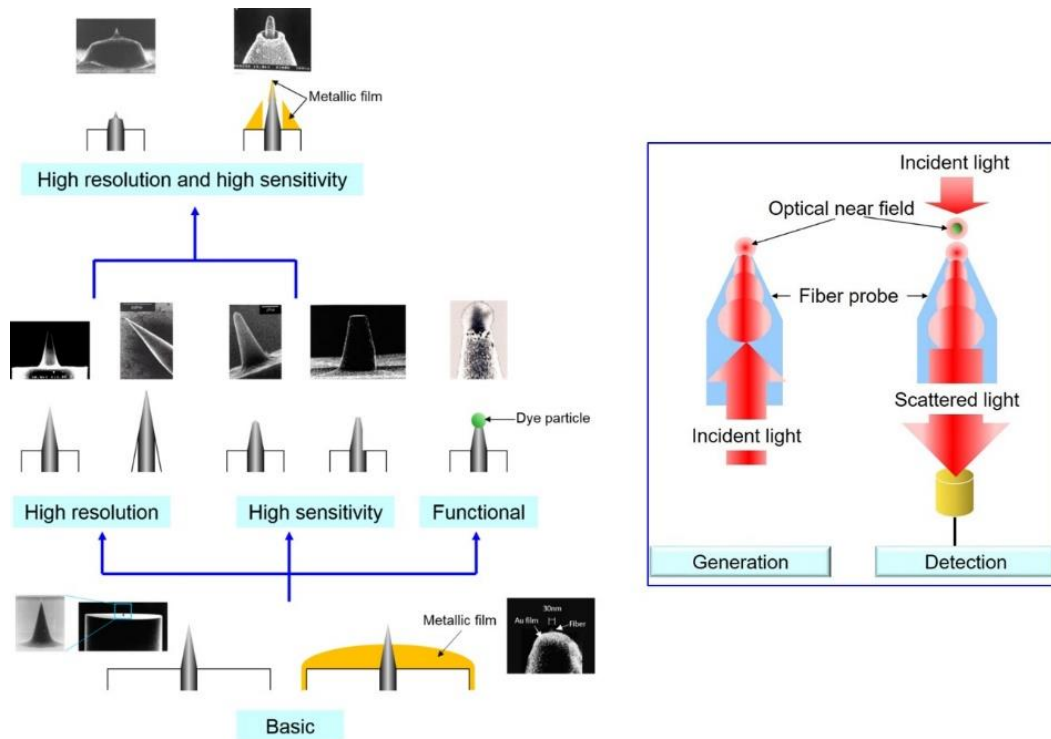
Fig. 1 High-quality fiber probes.

Noting this difference, the application of the optical near field to microscopy ended, and the modern time started. In the modern time, enormous efforts were devoted to studying the above-mentioned optical near field interactions, i.e., light–matter interactions that take place via the optical near field.

This paper reviews a brief history of the modern time and describes the present status of studies on the DP [12]. A future outlook on theoretical

studies is also presented, followed by some concluding remarks.

2 History of the modern time

As was pointed out in the previous section, there were great differences between studies on the DP in the older and modern times in terms of their concepts, principles, and methods. That is, the studies promoted in the modern time are essentially incompatible with those in the older time. They are called off-shell and on-shell sciences, respectively, as will be reviewed in Section 4. In the modern time, extensive experimental studies were carried out by using two kinds of materials. The first kind was metals, in which plasmonic oscillation of the free electrons was utilized. Although the ease of fabricating nanometer-sized metallic particles or metallic thin films was high, these materials had two intrinsic features; a short conversion time from the optical energy to the plasmonic oscillation energy of the electrons, and a short phase-relaxation time of the electrons. Due to these short time constants, the quantum nature of the incident light was not maintained in the metal. Therefore, quantum field theory was not required for describing the light–matter interactions in the metal,; instead, the conventional optical theory was sufficient, and conventional parameters, including the optical refractive index, the wave-number, and the mode, were used. This means that the dispersion relation was valid for describing the interactions, as has been used since the Near-Field Optics Workshop a quarter of a century ago. This situation means that studies using the first kind of material were left behind by the modern time.

Productive experimental studies in the modern time were promoted by using the second kind of materials, including semiconductors, organic materials, and gaseous molecules, in which their discrete electronic energy levels were utilized. Although fabrication of nanometer-sized particles or thin films was not straightforward in the beginning, technological advances enabled fabrication of suitable devices, which promoted further studies. As a result, a variety of applications were developed to establish a generic technology, as illustrated in Fig. 2 [13]. They include: lithography [14] and information storage [15] at densities beyond the diffraction limit, polishing of material surfaces to atomic-level flatness [16], photon breeding devices [17], logic gate devices [18], optical router systems [19], optical pulse shape

measurement systems [20], optical security systems [21], energy conversion systems [22,23], and so on.
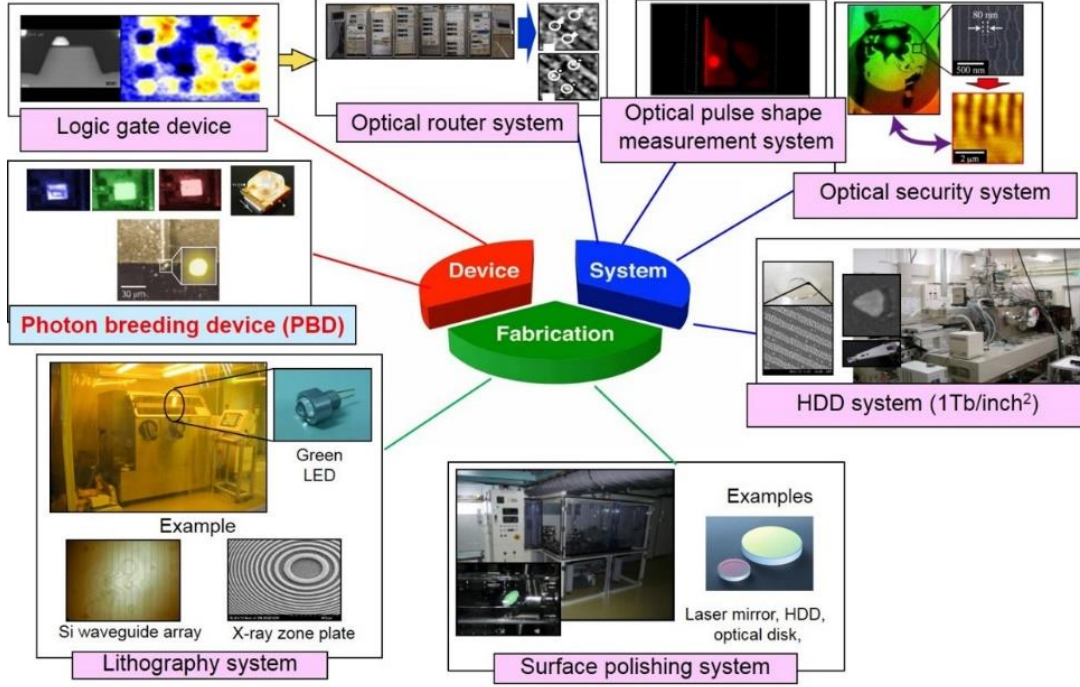
Fig. 2 A variety of applications.

To promote experimental studies in the modern time, three theoretical problems had to be solved:

[1] **Problem 1**: Quantum field theory for photons and electron–hole pairs was required to describe the light–matter interactions taking place in a nanometric space. However, the problem was that a virtual cavity, for deriving the Hamiltonian operator, could not be defined because the sub-wavelength-sized optical near field existed in a nanometric space. In other words, the electromagnetic mode could not be defined. It should be noted that the optical near field was regarded neither as a collection of corpuscles nor as a free photon, proposed by Newton and Einstein, respectively.

To solve this problem, a novel physical picture of the optical near field was drawn by representing the Hamiltonian operator $\hat{H}$ under illumination with propagating light having photon energy $\hbar W_o$:

$$\hat{H} = \sum_{k\lambda} \hbar\omega_k \hat{a}_{k\lambda}^{\dagger} \hat{a}_{k\lambda} + \sum_{\alpha>F,\beta<F} \left(E_\alpha - E_\beta \right) \hat{b}_{\alpha\beta}^{\dagger} \hat{b}_{\alpha\beta} + \hat{H}_{\text{int}} . \tag{1}$$

The first term represents the photon energy created in the nanometric space,

which is given by the sum of an infinite number of photon modes with angular frequency W_k, polarization state λ, and energy $\hbar\omega_k$. Here, the subscript k represents the wave-vector, and $\hat{a}_{k\lambda}$ and $\hat{a}^\dagger_{k\lambda}$ are annihilation and creation operators, respectively. They satisfy the commutation relation

$$\left[\hat{a}_{k\lambda},\hat{a}^\dagger_{k'\lambda'}\right]=\delta_{kk'}\delta_{\lambda\lambda'}, \tag{2}$$

where $\delta_{kk'}$ and $\delta_{\lambda\lambda'}$ are Kronecker deltas. The second term represents the energy of the electron–hole pair, which is also given by the sum of the energies of the electron–hole pairs of the infinite number of energy levels, identified by the subscripts a and b. The energy difference $E_a - E_b$ represents the bandgap energy in the case of a semiconductor, and F represents the Fermi energy level. The operators $\hat{b}_{\alpha\beta}$ and $\hat{b}^\dagger_{\alpha\beta}$ respectively represent the simultaneous annihilation and creation of the electron and hole, i.e., the annihilation and creation operators of the electron–hole pair. They satisfy the commutation relation

$$\left[\hat{b}_{\alpha\beta},\hat{b}^\dagger_{\alpha'\beta'}\right]=\delta_{\alpha\alpha'}\delta_{\beta\beta'}. \tag{3}$$

The third term represents the energy of the interaction between the photon and the electron–hole pair, which is given by

$$\hat{H}_{\text{int}}=-\int\hat{\psi}^\dagger(r)p(r)\hat{\psi}(r)\cdot\hat{D}^\perp(r)dv, \tag{4}$$

where $p(r)$ is an electric dipole moment, $\hat{\psi}(r)$ and $\hat{\psi}^\dagger(r)$ are respectively annihilation and creation operators for the field of the electron–hole pair, and $\hat{D}^\perp(r)$ is the transverse component of the electric displacement operator of the incident propagating light, which is perpendicular to the wave-vector k. This operator $\hat{D}^\perp(r)$ is expressed as

$$\hat{D}^\perp(r)=i\sum_k\sum_{\lambda=1}^2 N_k e_{k\lambda}(k)\left\{\hat{a}_{k\lambda}(k)e^{ik\cdot r}-\hat{a}^\dagger_{k\lambda}(k)e^{ik\cdot r}\right\}, \tag{5}$$

where plane waves are used for the mode functions. Here, N_k and $\boldsymbol{e}_{k\lambda}(\boldsymbol{k})$ are a proportionality constant and the unit vector along the direction of polarization, respectively.

By diagonalizing the Hamiltonian operator of eq. (1), annihilation and creation operators ($\tilde{a}$ and $\tilde{a}^\dagger$, respectively) of the novel quasi-particle were derived, which represented the quantum state of the coupled photon and electron–hole pairs as a result of their interaction in the nanometric space:

$$\tilde{a} = \sum_{\boldsymbol{k}\lambda}\left\{\hat{a}_{\boldsymbol{k}\lambda} - iN_k \sum_{\alpha>F,\beta<F}\left(\rho^*_{\alpha\beta\lambda}(\boldsymbol{k})\hat{b}_{\alpha\beta} + \rho^*_{\beta\alpha\lambda}(\boldsymbol{k})b^\dagger_{\alpha\beta}\right)\right\}, \qquad (6)$$

and

$$\tilde{a}^\dagger = \sum_{\boldsymbol{k}\lambda}\left\{\hat{a}^\dagger_{\boldsymbol{k}\lambda} + iN_k \sum_{\alpha>F,\beta<F}\left(\rho_{\alpha\beta\lambda}(\boldsymbol{k})\hat{b}^\dagger_{\alpha\beta} + \rho_{\beta\alpha\lambda}(\boldsymbol{k})b_{\alpha\beta}\right)\right\}, \qquad (7)$$

where $\rho_{\alpha\beta\lambda}(\boldsymbol{k})$ is the spatial Fourier transform of the electric dipole moment. These operators are represented by the sum of the operators for the photons of the infinite number of modes and for the electron–hole pairs of the infinite number of energy levels. Because of this summation, this quasi-particle was named the dressed photon (DP), i.e., a photon dressed by the material excitation energy (Fig. 3)[24].

Photon　　　Material excitation energy　　　Dressed photon
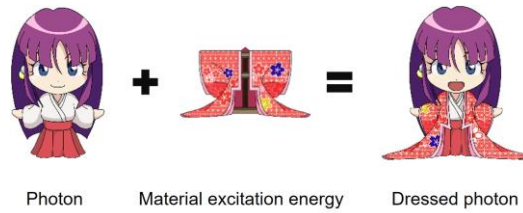
Fig.3 Illustrative explanation of the dressed photon.

[2] Problem 2: Since the DP is non-propagating and localized on a nanomaterial, another nanomaterial was required for its detection; in other words, another material had to be placed in close proximity to convert the DP to propagating light via multiple scattering of the DP. Here, the problem was

how to describe this scattering, because the two nanomaterials, i.e., the source and detector for the DP, are not independent of each other but are coupled via the DP. However, this problem was solved by using the solution to problem 1. That is, scattering was described by using the annihilation and creation operators of DPs on the two nanomaterials.

[3] Problem 3: Since the actual nanomaterials and DP are always surrounded by a macroscopic system composed of macroscopic materials and macroscopic optical fields, the problem was how to take into account the contribution from the macroscopic energy in order to derive the magnitude of the DP interaction energy between nanomaterials. To solve this problem, the contributions from the macroscopic system were renormalized by the projection operator method. As a result, the magnitude of the DP interaction energy was derived and represented by a Yukawa function:

$$Y(r) = \frac{\exp(-r/a)}{r}, \tag{8}$$

where r is the distance from the center of the nanomaterial, and a represents the extent of localization, which is equivalent to the size of the nanomaterial [25].

In the solution to problem 3 above, it should be noted that a is independent of the wavelength λ of the incident propagating light. Furthermore, the DP is strongly localized in the sub-wavelength-sized space because $a \ll \lambda$. Due to this localization, the following two novel phenomena were found: The first one is with respect to the electronic transition. For explaining this transition, an atom with a simple two-energy level electron is considered by assuming that the state functions of these levels have the same parity. In this case, the electric dipole transition is forbidden under irradiation with propagating light incident on the atom. This is because the state functions have the same parity and, more essentially, the long-wavelength approximation is valid. However, this electric dipole-forbidden transition turns out be allowed in the case where the DP is involved. This is because the long-wavelength approximation is not valid any more since $a \ll \lambda$. The second phenomenon was named size-dependent resonance; in this phenomenon, the magnitude of the DP energy transferred between the two nanomaterials takes a maximum when the sizes of these

nanomaterials are equal [26]. This corresponds to the momentum conservation law for the DP. It is different from diffraction, which is a typical phenomenon in classical optics, where the cross-sectional size of the light beam on a screen after being transmitted through an aperture is inversely proportional to the aperture size. By utilizing these two phenomena, a variety of applications were developed, some of which are shown in Fig. 2. To realize more developments, further theoretical studies were carried out.

(a)

(b)
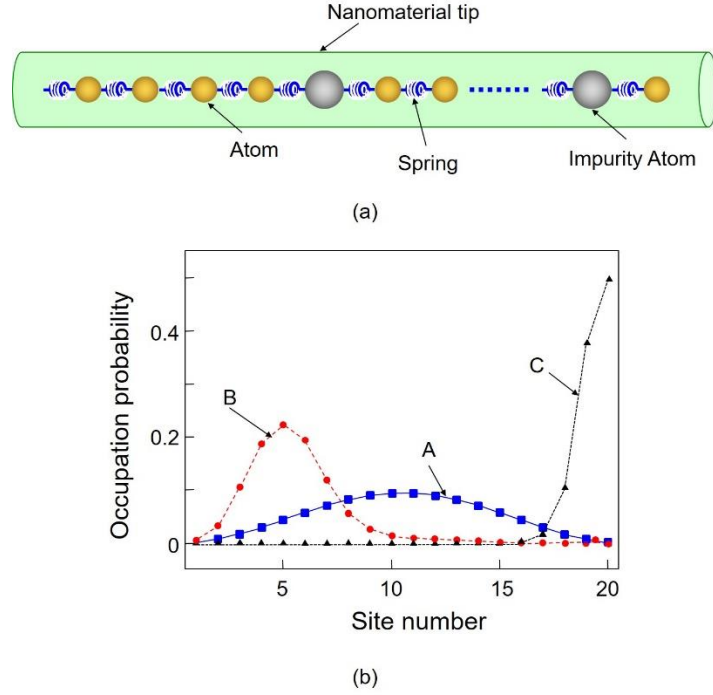
Fig. 4 Occupation probability of the dressed photon.

(a) One-dimensional model for calculation. The number of atoms is 20. The impurity atoms are at sites 4, 6, 13, and 19. (b) Calculated results. The mass of the impurity atoms is 0.2-times that of the other atoms. $\hbar\omega = 1.81$ eV and $\hbar J = 0.5$ eV. Curves A, B, and C represent the results for $\chi = 0$, 40.0, and 54.0 fs^{-1}nm^{-1}, respectively.

One successful result of these studies was the further possibility of dressing, i.e., the possibility of coupling DPs and phonons [27]. In order to describe this coupling, for simplicity a nanomaterial tip is assumed, in which a one-dimensional crystal lattice is provided (Fig. 4(a)). When the tip is illuminated with light, a DP can be created on a lattice site and hops to an adjacent site. During the hopping, the DP can excite lattice vibrations to create phonons, and then the DP couples with these phonons.

For a theoretical formulation of this coupling, the Hamiltonian

operator $\hat{H}$ is given by

$$\hat{H} = \sum_{i=1}^{N} \hbar \omega \tilde{a}_i^\dagger \tilde{a}_i + \sum_{p=1}^{N} \hbar \Omega_p \hat{c}_p^\dagger \hat{c}_p + \sum_{i=1}^{N} \sum_{p=1}^{N} \hbar \chi_{ip} \tilde{a}_i^\dagger \tilde{a}_i \left(\hat{c}_p^\dagger + \hat{c}_p \right) + \sum_{i=1}^{N-1} \hbar J \left(\tilde{a}_i^\dagger \tilde{a}_{i+1} + \tilde{a}_{i+1}^\dagger \tilde{a}_i \right).$$

(9)

In the first term, $\tilde{a}_i$ and $\tilde{a}_i^\dagger$ respectively denote the annihilation and creation operators of a DP with energy $\hbar W$ at site i in the lattice. In the second term, $\hat{c}_p$ and $\hat{c}_p^\dagger$ are respectively the annihilation and creation operators of the phonon of mode p, which satisfies the boson commutation relation:

$$\left[\hat{c}_p, \hat{c}_q^\dagger \right] \equiv \hat{c}_p \hat{c}_q^\dagger - \hat{c}_q^\dagger \hat{c}_p = \delta_{pq}.$$

(10)

The phonon energy is represented by $\hbar \Omega_p$. The third and fourth terms stand

for the DP–phonon interaction with the interaction energy $\hbar \chi_{ip}$ and DP

hopping with hopping energy $\hbar J$, respectively.

By diagonalizing $\hat{H}$ of eq. (9), annihilation and creation operators of the novel quasi-particle are derived and expressed as

$$\hat{\alpha}_i = \tilde{a}_i \exp \left\{ \sum_{p=1}^{N} \frac{\chi_{ip}}{\Omega_p} \left(\hat{c}_p^\dagger - \hat{c}_p \right) \right\},$$

(11)

$$\hat{\alpha}_i^\dagger = \tilde{a}_i^\dagger \exp \left\{ -\sum_{p=1}^{N} \frac{\chi_{ip}}{\Omega_p} \left(\hat{c}_p^\dagger - \hat{c}_p \right) \right\},$$

(12)

which is the product of the DP operator of eqs. (6) and (7) and the displacement operator function for the phonon. It should be noted that this function creates a multi-mode phonon with a coherent state. In other words, the DP excites a multi-mode coherent phonon, and they coupled to form a novel quasi-particle named a dressed-photon–phonon (DPP). Further theoretical studies found that the created DPP localized on an impurity atom in a lattice site or on the edge of the nanomaterial tip when the DP–phonon

interaction energy was sufficiently high (curve B or C in Fig. 4(b), respectively).

(a)

(b)
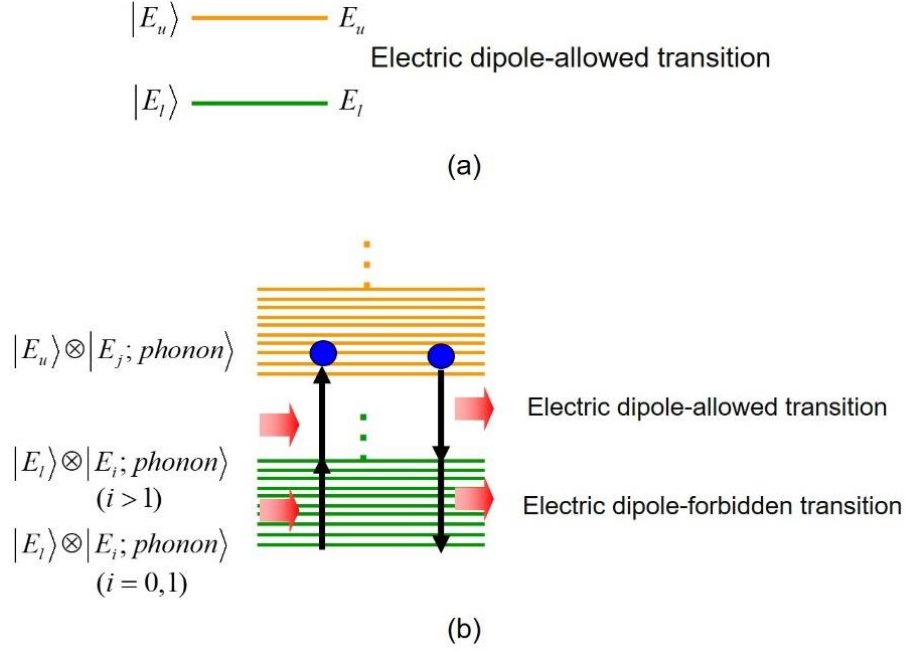
Fig. 5 Energy levels of electron and phonon.

(a) Assumed two electronic energy levels, between which the electric dipole transition is allowed. (b) Energy levels, represented by the direct product of electron and phonon energy levels. Two arrows at the left and right represent two-step excitation and de-excitation, respectively.

As a result of the theoretical studies on the DPP above, a novel light–matter interaction, named a DPP-assisted light–matter interaction, was found [28]: For simplicity, two electronic energy levels ($|E_u\rangle$ and $|E_l\rangle$) are assumed in the two nanomaterials, and an electric dipole transition is allowed between these levels (Fig. 5). It is also assumed that the photon energy $h\nu_{in}$ of the incident light is lower than the energy difference

$E_d = E_u - E_l$ between the energies of these two levels. Here, by irradiating a nanomaterial 1 with incident light, the DPP is created. When another nanomaterial 2 is installed in close proximity to nanomaterial 1, the DPP energy is transferred to nanomaterial 2. Here, to describe the novel light–matter interaction between the nanomaterials 1 and 2, not only the two

electronic energy levels but also infinite numbers of phonon energy levels have to be considered. This is because the DPP is a quasi-particle in which the DP is accompanied by multi-mode coherent phonons. That is, for describing the light–matter interaction induced in nanomaterial 2 by the DPP energy transfer, the electronic energy levels in nanomaterial 2 are accompanied by an infinite number of phonon energy levels. Thus, the energy levels in nanomaterial 2 are represented by $|E_l\rangle \otimes |E_i; phonon\rangle$ and

$|E_u\rangle \otimes |E_i; phonon\rangle$ $(i = 1, 2, 3, \cdots)$, where $\otimes$ is the direct product. Thus, even though $h\nu_{in} < E_d$, nanomaterial 2 can be excited to a high phonon energy level

$|E_l\rangle \otimes |E_i; phonon\rangle$ $(i > 1)$ by the first arriving incident photon. Here, it should be noted that this is an electric dipole-forbidden transition because it is a transition in the electronic energy state $|E_l\rangle$. In the case where $h\nu_{in} > E_d / 2$,

nanomaterial 2 is subsequently excited from $|E_l\rangle \otimes |E_i; phonon\rangle$ $(i > 1)$ to one of the phonon energy levels in the excited electronic energy level $|E_u\rangle \otimes |E_j; phonon\rangle$ by the second arriving incident photon. This transition is

an electric dipole-allowed transition because it is the transition from $|E_l\rangle$ to

$|E_u\rangle$. As a result of this two-step transition, a free electron is created in nanomaterial 2. The opposite transition is possible; i.e., the electron in level

$|E_u\rangle \otimes |E_j; phonon\rangle$ is de-excited to $|E_l\rangle \otimes |E_i; phonon\rangle$ $(i = 0, 1)$ by the

subsequent electric dipole-allowed and -forbidden transitions, and two photons are emitted. This novel DPP-assisted light–matter interaction has contributed considerably to the development of a variety of applications, as shown in Fig. 2.

3. Present status of studies on dressed photons

Recently, there have been a large number of extensive experimental studies on DPs. This section reviews the principles and practices of photon breeding (PB) devices in particular, and examples of the rapidly developing applications of these studies.

Crystalline silicon (Si) has long been a key material supporting the development of technology for more than half a century because of its numerous advantages: Si is an abundant material in the earth's crust, and is the most widely used material for modern electronics. However, because Si is an indirect-transition-type semiconductor, it has been considered to be unsuitable for light-emitting devices: Since the bottom of the conduction band and the top of the valence band in Si are at different positions in reciprocal lattice space, the momentum conservation law requires an interaction between an electron–hole pair and phonons for radiative recombination. However, the probability of this interaction is very low.

This problem has been solved by using a DPP because the phonons in the DPP can provide momentum to the conduction band electron to meet the requirement for the momentum conservation law [29]. However, the technical problem was how to fabricate such a light emitting device. To solve this problem, a novel fabrication method named DPP-assisted annealing was invented. For this annealing, an n-type Si substrate is used, in which As atoms or Sb atoms are doped. By implanting B atoms, the substrate surface is transformed to a p-type material, forming a p-n homojunction. After metallic films are coated to serve as electrodes, a forward current is injected. The principle of the DPP-assisted annealing is: By this current injection, Joule heat is generated to diffuse the B atoms. During this Joule-annealing, the substrate surface is irradiated with infrared light (for example, light with a wavelength of 1.3 μm). Because its photon energy $h\nu_{anneal}$ (=0.95eV) is sufficiently lower than the bandgap energy E_g (=1.12eV) of Si, the light can penetrate into the Si substrate without suffering absorption. Then, the light reaches the p-n homojunction to create the DPP on the B atom. The created DPP localizes at this impurity atom, as explained by curve B in Fig. 4. Then, phonons in the created DPP can provide momenta to the electron nearby to satisfy the momentum conservation law, resulting in emission of a photon. This is stimulated emission triggered by the irradiated infrared light.

The emitted light propagates away from the crystal to the outside, which means that part of the Joule energy to be used for diffusing B atoms is dissipated in the form of optical energy, resulting in local cooling that decreases the diffusion rate. As a result, by the balance between the heating by the Joule energy and the cooling by the stimulated emission, the spatial distribution of B atoms varies and reaches a stationary state autonomously.

It is expected that this DPP-assisted annealing will form the optimum spatial distribution of B atoms for efficient generation of DPPs, resulting in efficient device operation for light emission. Figure 6 shows the temporal evolution of the temperature of the device surface as the DPP-assisted annealing progressed. After the temperature rapidly rose, it fell and asymptotically approached a constant value. The features of this temporal evolution are consistent with those of the principle of the DPP-assisted annealing described above.
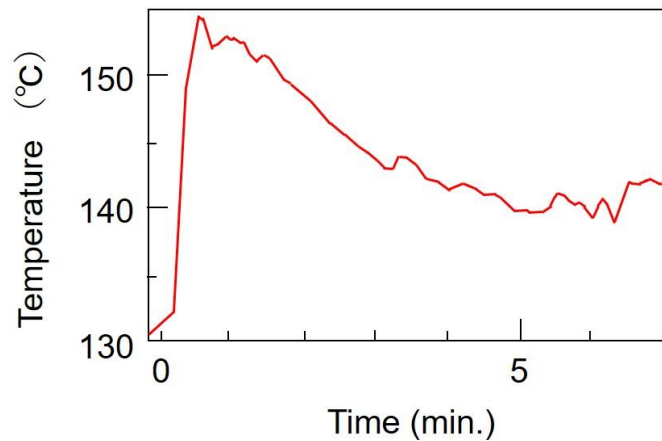
Fig. 6 Temporal evolution of the temperature of the device surface as the DPP-assisted annealing progressed.

Figure 7(a) shows a photograph of a prototype Si light emitting diode (LED) fabricated by this DPP-assisted annealing. It had an area as large as 12 mm^2. By injecting a forward current, the device emitted infrared light with a wavelength of 1.3 μm (Fig. 7(b)). The emitted optical power and the external quantum efficiency were as high as 1 W and 15% (at wavelengths in the range 1.32±0.15 μm), respectively, at room temperature. Figures 7(c) and (d) respectively show the configuration and a photograph of a recently fabricated high-power device. Its area was as small as 1 mm^2 [30]. The output power was as high 200 mW, which means that the areal power

density was three times that of the device in Figs. 7(a) and (b).
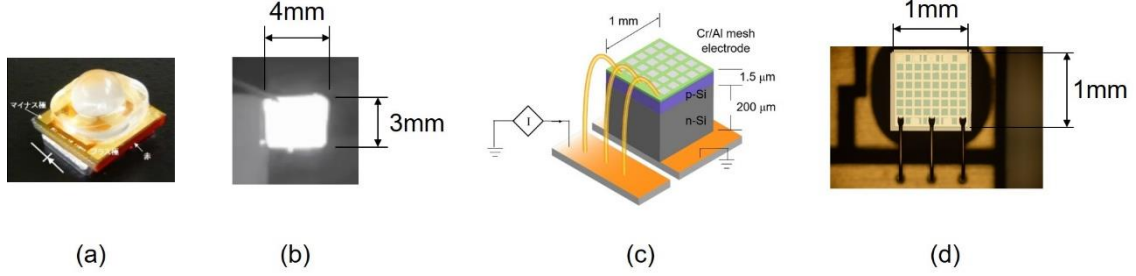
Fig. 7 Photograph of prototype Si-LED.
(a) External appearance of the fabricated device after packaging. (b) Emitted light profile. (c) and (d) show the configuration and a photograph, respectively, of the high-power device.

Figure 8 shows the light emission spectra of the fabricated Si-LED. Curves A–C are the spectra of devices fabricated by DPP-assisted annealing for 1, 7, and 30 min., respectively. They clearly show that the emitted light intensity increases with increasing DPP-assisted annealing time. The essential feature of these curves is the differences in their profiles: Although curve A has a peak around E_g, curve B shows a new peak at around 0.83 eV.

In the case of curve C, no peaks were seen around E_g. Instead, a new peak appeared, identified by a downward thick arrow, at an energy that corresponds to the photon energy $h\nu_{anneal}$ of the light radiated in the DPP-assisted annealing process. This peak is evidence that DPPs were created by the light irradiation, and that the B diffusion was controlled. Other evidence is that the photon energy of the emitted light, $h\nu_{em}$, was identical to that of the irradiated light, $h\nu_{anneal}$. That is, the irradiated light served as a breeder that created a photon with energy $h\nu_{em} = h\nu_{anneal}$. For this reason, this phenomenon is named photon breeding (PB) with respect to photon energy.

Here, the separations between the energies identified by two upward thin arrows (0.83 eV and 0.89 eV) on curve C, and by the downward thick arrow (0.95 eV) were 0.06 eV, which is equal to the energy of an optical

phonon in Si. This means that the two upward thin arrows show that the DPP with an energy of 0.95 eV was converted to a free photon after emitting one and two optical phonons. This conversion process demonstrates that the light emission described here used the phonon energy levels as an intermediate state.
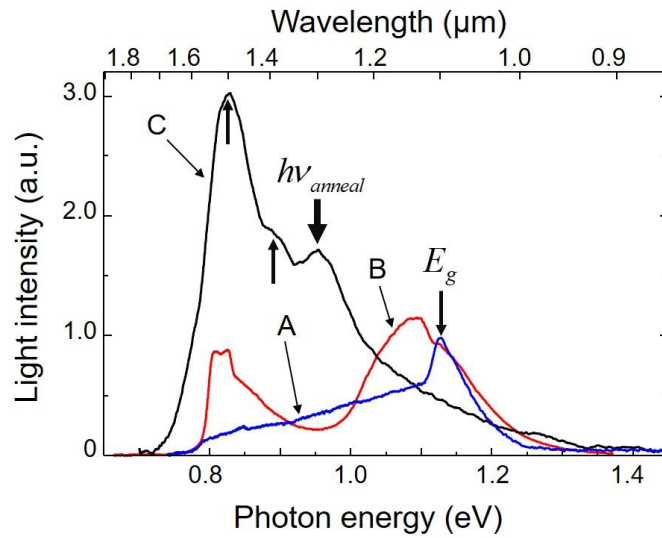
Fig. 8 Light emission spectra.

Curves A–C are the spectra of the devices fabricated by DPP-assisted annealing for 1, 7, and 30 min, respectively.
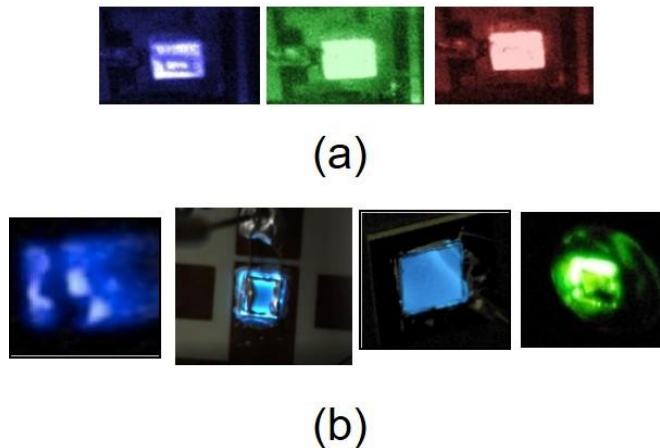
Fig. 9 Light emitted from a variety of LEDs emitting visible light.

(a) (Left to right) Blue, green, and red light emitted from Si-LEDs.

(b) (Left to right) UV-violet, bluish-white, blue, and green light emitted from SiC-LEDs.

By using the novel PB phenomenon, a variety of LEDs have been fabricated by using crystalline Si. Specifically, blue, green, and red light emitting LEDs were fabricated by radiating blue, green, and red light, respectively, during the DPP-assisted annealing (Fig. 9(a))[31]. In order to increase the efficiency of extracting this visible light, a lateral p-n homojunction structure was developed [32]. Crystalline SiC is also a known typical indirect transition-type semiconductor. A variety of visible LEDs have been fabricated even using this material. They were fabricated by irradiating them with UV-violet, bluish-white, blue, and green light during the DPP-assisted annealing, and respectively emitted UV-violet, bluish-white, blue, and green light (Fig. 9(b))[33-36].

PB was observed not only with respect to photon energy but also with respect to photon spin. That is, the polarization of the emitted light was equivalent to that of the light irradiated during the DPP-assisted annealing (Fig. 10)[37].
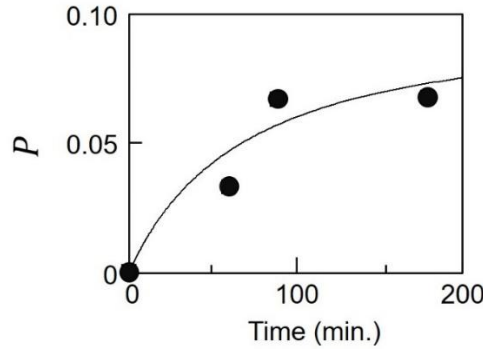
Fig. 10 Relation between the DPP-assisted annealing time and the degree of polarization $P = \left(I_\parallel - I_\perp \right) / \left(I_\parallel + I_\perp \right)$ of the light emitted from the Si-LED. $I_\parallel$ and $I_\perp$ are the light intensities emitted from the Si-LED whose polarizations are parallel and perpendicular to that of the light irradiated during the DPP-assisted annealing, respectively.

The origin of the PB was attributed to the spatial distribution of B atoms, which was controlled autonomously during the DPP-assisted annealing. By analyzing the three-dimensional spatial distribution of B atoms at the p-n homojunction, acquired by atom probe field ion microscopy with sub-nanometer resolution, it was found that the B atoms were apt to orient along a plane parallel to the top surface of the Si crystal and to form

pairs with a length $d = 3a$, where a (=0.54 nm) is the lattice constant of the Si crystal.

As a preliminary discussion on this origin, Fig. 11 shows the calculated vibration amplitudes of the crystal lattice of Si atoms, where a one-dimensional lattice was assumed for simplicity [27]. The curve A shows the amplitude of the lattice vibration in the case where the lattice is formed only by the Si atoms, which corresponds to a non-localized phonon mode. On the other hand, when some of the Si atoms are replaced by impurity B atoms, the amplitude profile of the lattice vibration changes greatly. As represented by curves B and C, the vibration amplitude is localized at the B atom-pair, because the B atom-pair serves as a cavity resonator to confine the lattice vibration. The confined lattice vibration corresponds to the localized phonon mode. As a result, impurity B atom-pairs serve as phonon localization centers, at which the DPPs can be created and localized efficiently.
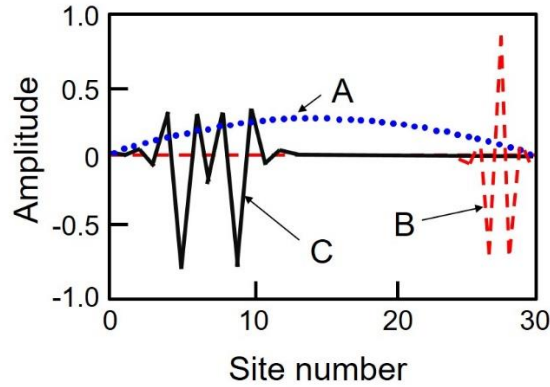
Fig. 11 Vibration amplitudes of the crystal lattice of Si atoms.
The number of lattice sites is 30. Curve A represents the non-localized mode. Curves B and C represent the first and second localized modes, respectively, where impurity atoms were assumed to be at sites 5, 9, 18, 25, 26, and 27.

The main discussion below follows from the preliminary discussion above: If d is equal to the lattice constant a, the B atom-pair can orient in a direction parallel to the [1,0,0], [0,1,0], or [0,0,1] orientation because the Si crystal is composed of multiple cubic lattices. As a result, the momentum of the localized phonon points in this direction, which corresponds to the $\Gamma - X$ direction in reciprocal space (Fig. 12(a)). Thus, a photon is efficiently emitted because this $\Gamma - X$ direction is the same as the direction of the momentum of the phonon required for recombination between an electron at

the bottom of the conduction band at the X-point and a hole at the top of the valence band at the Γ-point. Here, it should be noted that the value of the momentum of the phonon has to be h/a for this electron–hole recombination to take place. Furthermore, it should also be noted that the value of the momentum of the mode localized at the B atom-pair with $d = 3a$ is $h/3a$. By comparing these two values, it is found that the DPP at this B atom-pair has to create three phonons for recombination. In the other words, the B atom-pairs with $d = 3a$ most efficiently create three phonons for light emission. As a result, as is schematically shown in Fig. 12(b), the emitted photon energy $h\nu_{em}$ is expressed as $h\nu_{em} = E_g - 3E_{phonon}$. By substituting the values of E_g (= 1.12eV) and the relevant optical mode phonon energy E_{phonon} (=65meV) into this equation, the value of $h\nu_{em}$ is derived to be 0.93 eV, which is nearly equal to the photon energy $h\nu_{anneal}$ (=0.95eV) irradiated during the DPP-assisted annealing. This numerical relation confirms that PB with respect to photon energy occurs.

In the case where the Si crystal surface is irradiated with linearly polarized light during the DPP-assisted annealing, analyses of the spatial distribution of B atoms confirmed that B atom-pairs with $d = 3a$ were also apt to be formed, and the direction of the B atom-pairs was normal to the polarization direction of the irradiated light. A possible origin of the induced polarization of the emitted light is as follows: First, when the Si-LED is fabricated by the DPP-assisted annealing, transverse optical phonons are created at the B atom-pairs and couple with the DPs. The vibration direction of these phonons is parallel to that of the electric field of the polarized light irradiated during the DPP-assisted annealing. Next, when the fabricated LED is operated, since these phonons are created again, the direction of the electric field vector of the emitted light becomes also parallel to the vibration direction of these phonons. Therefore, the polarization direction of the emitted light becomes identical to that of the light irradiated during the DPP-assisted annealing.

In summary, the spatial distribution of B atoms was controlled autonomously by the DPP-assisted annealing to satisfy the momentum

conservation law and to realize PB with respect to photon energy and to photon spin.
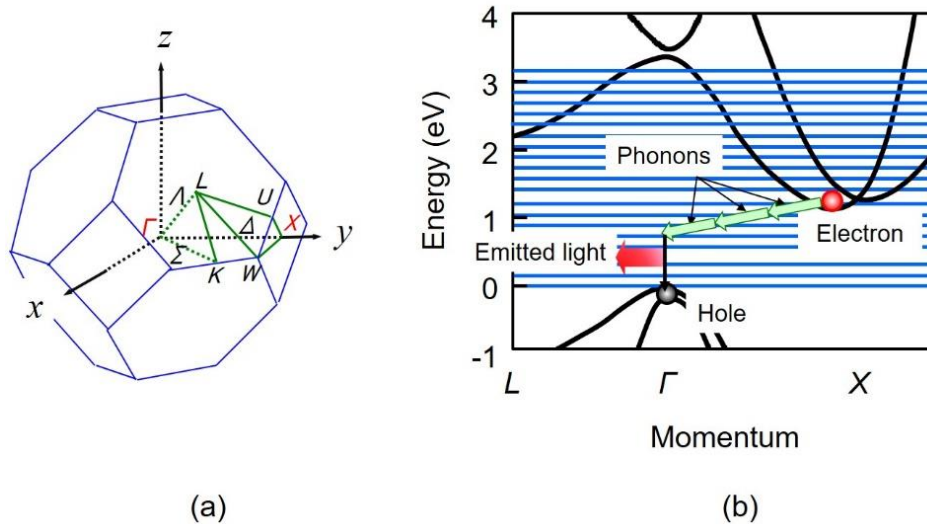
Fig. 12 Energy band structure of Si.

(a) A unit cell of the Si crystal in reciprocal lattice space. (b) Energy band structure and schematic illustration of light emission. Blue horizontal lines represent phonon energy levels involved in the light emission.

Si-lasers were also fabricated by using the DPP-assisted annealing. Figure 13(a) shows the device structure and a scanning electron microscopic image of the fabricated device [38]. A simple ridge waveguide was incorporated into the structure, and the cleaved facets were used as mirrors of a Fabry-Perot cavity. DPP-assisted annealing was then carried out by injecting 1.3 μm-wavelength light into the cavity through one of the end facets. Figures 13(b) and (c) show the light emission spectra of the fabricated Si-laser. Above the threshold, a sharp lasing spectrum was observed (Fig. 13(b)), which demonstrates single-mode oscillation at room temperature even though the cavity length was as long as 550 μm. The origin of this single-mode oscillation is that the low infrared absorption by the Si provides a low threshold for the principal longitudinal mode at the optical amplification gain spectral peak and, as a result, the gains for other modes are depleted by this principal mode due to nonlinear mode competition [39,40]. The spectral profile below the threshold (Fig.13(c)) does not show any ASE spectra, which is evidence of the gain depletion due to the mode

112

competition above.
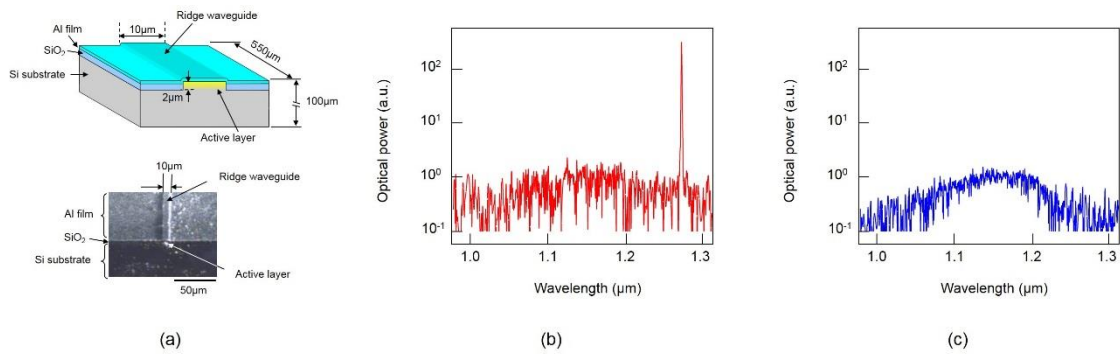
Fig. 13 Structure of Si laser and the light emission spectra.
(a) Structure and a scanning electron microscopic image of the device. (b),(c) Spectral profiles above and below the threshold, respectively.
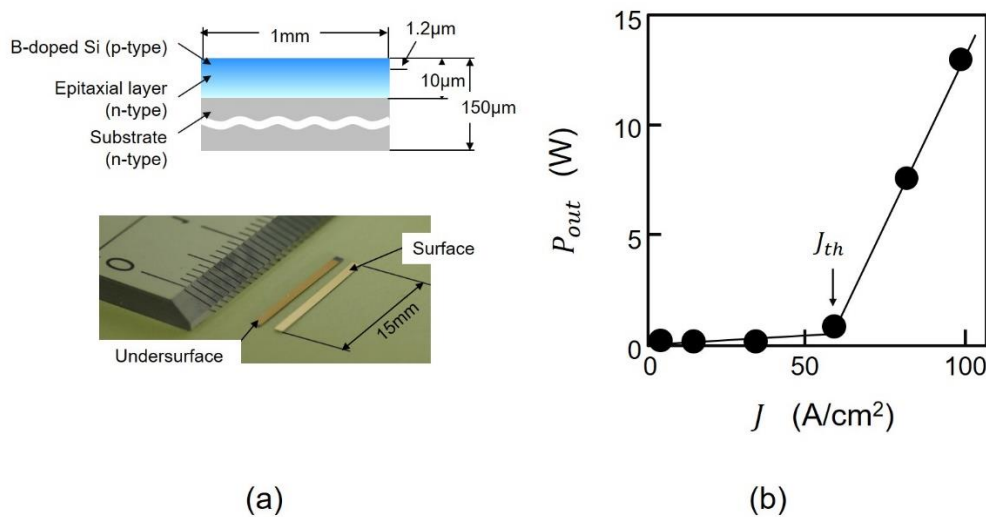
Fig. 14 Structure of a high-power Si laser and the output power.
(a) Structure and a photograph of the device. (b) Relation between the injected current density and the output optical power.

By modifying the device structure in Fig. 13(a), a high-power infrared laser device was successfully fabricated by utilizing the very low infrared absorption of crystalline Si. Figure 14(a) shows a photograph of the device [41]. A cross-sectional profile is also shown, in which the ridge waveguide was not built-in because very efficient optical confinement was not expected by this waveguide as long as the device had a p-n homojunction. Instead, the cavity length was increased to 15 mm to realize high power. After the

DPP-assisted annealing, the relation between the injected current density J and the output power P_{out} of the fabricated laser device was measured. As shown in Fig. 14(b), an output power as high as 13 W was obtained. This value was more than 10^3-times that of a conventional double heterojunction-structured InGaAsP/InP laser (10 mW at 1.3 μ m wavelength: SLT1130 series manufactured by Sumitomo Electric). The threshold current density J_{th} was as low as 60 A/cm^2.

Since crystalline Si was used without a built-in waveguide, the structure of the present device is more similar to those of solid-state and gas lasers than those of conventional double heterojunction-structured semiconductor lasers [42,43]. Further similarities can be found by referring to the magnitude of the absorption loss: In the case of solid-state and gas lasers, electronic transitions in electronically isolated ions, atoms, and molecules are used for lasing. Therefore, even though direct electric current injection to these laser media is difficult, the absorption loss per unit volume is very low. Thus, a high optical output power can be obtained by increasing the size of the laser medium even though the photon density of the lasing light was low

Since the DPPs used in the present Si laser were electronically isolated, as in the case of ions in the solid-state and gas lasers above, the absorption loss per unit volume was maintained very low. Thus, the threshold current density was very low. Furthermore, the optical output power was greatly increased by increasing the size of the Si crystal even though the photon density of the lasing light was low. An additional advantage was that electrons could be easily supplied by direct electric current injection, due to the low recombination loss in the crystalline Si.

For comparison, in the case of conventional semiconductor lasers, coupled electrons and holes in the conduction and valence bands, respectively, have been used for lasing. Therefore, direct electric current injection to the laser medium is easy. An additional advantage is that the laser medium can be very small. However, the problem was that the absorption loss per unit volume was large, making it impossible to achieve high optical output power and low threshold current density even though the photon density of the lasing light was high.

It has been believed for a long time that indirect transition-type semiconductors are unsuitable for use as laser media. Instead, direct transition-type semiconductors have been widely used until now [44]. However, thanks to the advent of DP science and technology, DPPs have resulted in the manifestation of large optical amplification gain in indirect transition-type semiconductors, which was the secret to the dramatically high optical output power and low threshold current density realized by using crystalline Si.

4. Future outlook

After extensive experimental and theoretical studies on DPs in the last three decades, the main effort in recent years has focused on experimental studies, and the development of generic technologies. To achieve further advances, now is a good opportunity to promote novel theoretical studies.

It should be pointed out that the theoretical studies carried out so far relied on nanomaterial structures, i.e., on the structures of electron energy levels and phonon energy levels. In order to draw more generic physical pictures, new routes to future theoretical studies should not strongly rely on such detailed material structures. Such routes are expected to be developed by the following three steps:

Step 1: To draw a more generic and basic physical picture of the DP.

Step 2: To draw a picture that allows us to treat multiple DPs created in a macroscopic material.

Step 3: To draw a picture for demonstrating how to take out the DP from a nano-system to a macro-system.

A hint to achieving step 1 can be found in the photon dispersion relation, i.e., the relation between the momentum and energy of a photon, as shown in Fig. 15. Since conventional optics deals with propagating light (free photons with a definite electromagnetic mode), its dispersion relation is represented by the black curve in this figure when the photon exists in a macroscopic material. The three-dimensional profile of this curve is a shell. The profile in vacuum is represented by the blue line, whose three-dimensional profile is a so-called light cone, which is a special case of the shell. That is, a free photon exists on the shell, and because of this, conventional optics can be called *on-shell science*.

In the case of a DP, on the contrary, it should be noted that its electromagnetic mode cannot be defined because of its nanometric nature, which makes the use of the dispersion relation invalid. This means that the DP does not exist on the shell. Instead, it exists off the shell, a situation that is represented by the shaded green rectangle in this figure. Intrinsic features of the off-shell photon are: Since the momentum uncertainty Δp, represented by the horizontal double-headed arrow in this figure, is large, the size of the field Δx is small, which is a consequence of the uncertainty principle $\Delta p \cdot \Delta x \geq \hbar$. Because of this feature, the DP has been called an optical near field. Furthermore, since the energy uncertainty ΔE, represented by the vertical double-headed arrow in this figure, is also large, the duration of the created photon Δt is short, which is also a consequence of the uncertainty principle $\Delta E \cdot \Delta t \geq \hbar$. A photon with this feature has been called a virtual photon. From these two intrinsic features, it is found that the off-shell photon is an optical near field and a virtual photon, which is the physical picture of the DP.
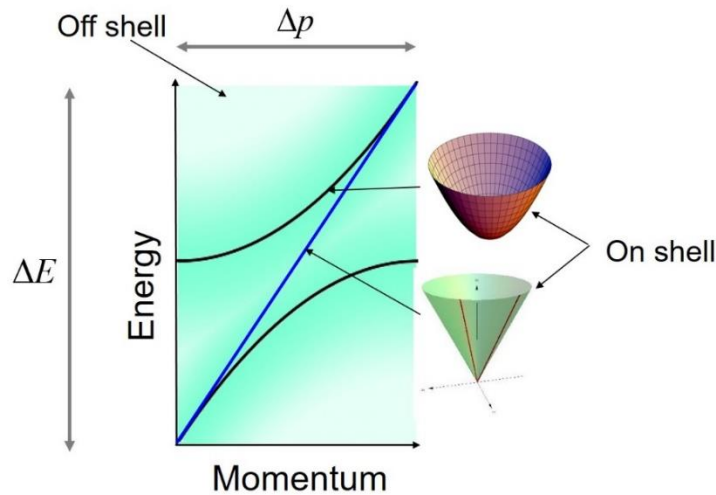
Fig. 15 Dispersion relation.

Two black curves represent the relation of a photon in a macroscopic material. The blue line is for a photon in free space. The green shaded rectangle represents that for the dressed photon. The brown and green three-dimensional forms represent a shell and a light cone, respectively.

With the help of this hint, realization of step 1 was promoted by novel theoretical analysis of the Clebsch-dual electromagnetic field, for which a

notion of a space-time vortex field was used [45,46]. The main results of this analysis are: (1) It was found that the DP exists in a spacelike domain of the Riemannian manifold. (2) The spatial profile of the DP is represented by the Yukawa function, which is equivalent to eq. (8). Furthermore, it was found that the effective mass m_{eff} of the DP field, being inversely proportional to the size a of localization (a consequence of the Klein-Gordon's equation), is expressed as $m_{eff} = \sqrt{E^2 - \chi^2}$. Here, E and χ are the instantaneous energy spent to create the DP and a characteristic scale of the nanomaterial, respectively. It suggests that the DP can be transferred from the spacelike to the timelike domain if $E > \chi$, and that the DP can be transformed to be observable, however, within the very short duration Δt above. (3) It was found that the energy-momentum tensor of the DP became isomorphic to Einstein's equation, which implies that the DP is closely related to the vacuum energy.

The reasons why step 2 is indispensable are: As was reviewed in the previous section describing the DPP-assisted annealing of crystalline Si, there were too many Si atoms, electrons, B atoms, DPs, and DPPs in the crystal. Since it is difficult to treat these multiple quasi-particles and elementary particles by the conventional deterministic method of theoretical analysis, a method of avoiding this difficulty was proposed by considering a system composed of these mutually interacting particles as a complex system [47].

Based on this consideration, computer simulations were carried out by using a stochastic model. Here, an interactive random-walk process on a crystal lattice and phenomenological coupled-Poisson process were assumed to describe the diffusive motion of doped B atoms and electron–phonon coupling, respectively. As a result, the main experimental results were successfully reproduced, such as the temporal behaviors of the crystal temperature and the emitted light intensity observed during the DPP-assisted annealing.

Step 3 is indispensable, especially for connecting the theoretical and experimental studies. In the experiment, it is essential to create or detect the DP in the most efficient manner; that is to say, the most efficient micro–macro conversion is required. To meet this requirement, high-quality fiber

probe tips (Fig. 1) have been developed [6] in order to create or detect DPs with high spatial resolution or high sensitivity. The concept of micro–macro duality in the quantum field has been found to be a powerful and promising theoretical tool for drawing a picture of the micro–macro conversion [48], and detailed studies have commenced [49].

In order to support further progress in achieving steps 1-3 above, another route to future theoretical studies is also under development, based on the classical electromagnetic field theory [50,51]. These studies recently found that the longitudinal electric field, which has been ignored in conventional optics, induced a non-resonant light–matter interaction in a nanometric space, as has been previously observed in several experiments [52].

Figure 16 represents a variety of phenomena occurring in nature, which have similar features to those of the DP. They have been found in nano-systems and in macro-systems, as well as in organic materials and in inorganic materials. In an inorganic nano-system, a representative example is a meson, which connects two nucleons. Some features of the meson are similar to those of the DP, which connects nanomaterials by means of DP energy exchange. It has been known that the potential profile of the meson is expressed by the Yukawa function, shown in eq. (8).

In an organic nano-system, an example is a light-harvesting photosynthetic system, whose light trapping operation is similar to the operation of logic gate devices based on DP energy transfer [53]. In an organic macro-system, an example is the natural computing observed in single-celled amoeboid organisms [54], whose signal transmission features are similar to those of DP energy transfer. Some features of this computing have been demonstrated by using the logic gate devices described above [55].

Finally, one example of an inorganic macro-system is the photochemical reaction in the weathering of rocks. Some features of this reaction are similar to the photochemical reaction induced by a DP, which has been used for polishing material surfaces to atomic-level flatness [56]. Another example is a binary pulsar [57]. Some of the features of the gravitational wave radiation from a binary pulsar are similar to the propagating light radiation from two nanomaterials as a result of DP energy exchange and relaxation.

By referring to Fig. 16, it can be understood that the DP is not a

special topic of a narrow field of science but is connected to more general and broader scientific fields.
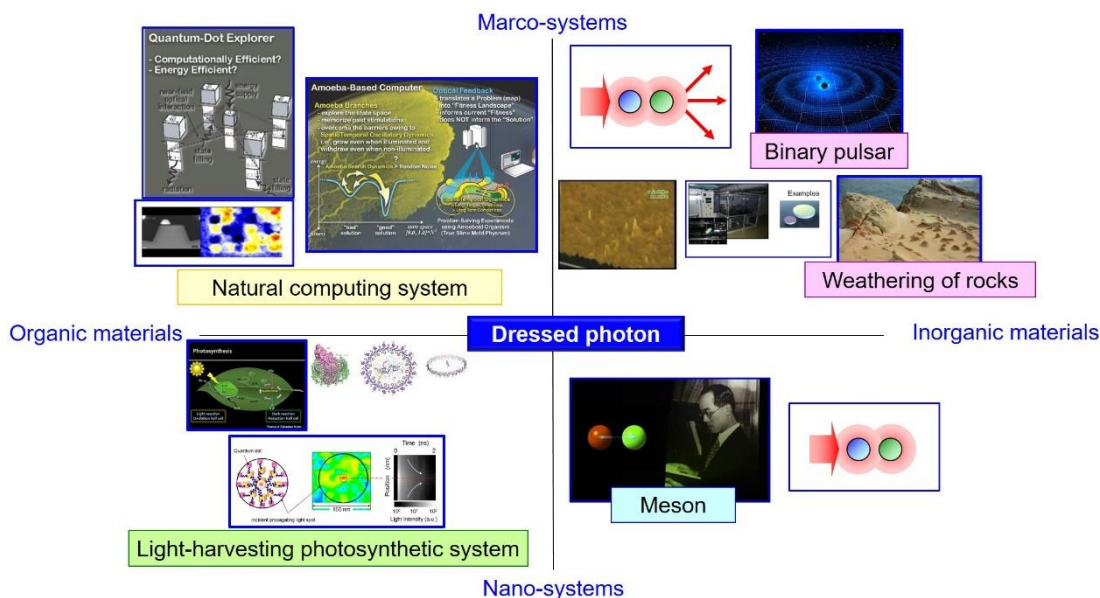
Fig. 16 A variety of phenomena occurring in nature that have similar features to those of the dressed photon.

5. Conclusion

The present paper reviewed some of the experimental and theoretical studies on DPs carried out in the last three decades. It was pointed out that the main effort in recent years has focused on experimental studies, resulting in the development of generic technologies for supporting modern society. By referring to these drastic experimental advances, it was also pointed out that further effort should be devoted to finding new routes to theoretical studies from now on, by which a more detailed and precise physical picture of the DP can be drawn, and also to establish criteria for novel application systems. That is, now comes a good opportunity to take a step toward a novel generic science by promoting theoretical studies on DPs.

The routes to this novel science can be developed by following the three steps reviewed in the last section. It is expected that a novel process for creating or detecting DPs will be found by using these developed theories as criteria for designing novel experimental systems, resulting in further advances in DP science and establishing a generic off-shell science in the

near future. Future advances in these studies are expected to be reported in forthcoming papers to be published in this Off-shell archive in the near future.

Acknowledgements

References

[1] E.H.Synge: "A Suggested Method for Extending Microscopic Resolution into the Ultra-Microscopic Region," Phil. Mag., **6** (1928) pp.356-362.

[2] H. Bethe: "Theory of diffractin by small holes," Phys. Rev., **66** (1944) pp.163-182.

[3] C.J. Bouwkamp: " On the Diffraction of Electro-Magnetic Waves by Small Circular Discs and Holes," Philips Res. Rep., **5** (1950) pp.401-422.

[4] E. A. Ash and G. Nicholls:" Super-Resolution Aperture Scanning Microscope," Nature, **237** (1972) pp.510-516.

[5] D.W. Pohl and D.Courjon (ed.): *Near Field Optics* (Kluwer, Dordrecht, 1993) pp.1-324.

[6] M. Ohtsu(ed.): *Near-Field Nano/Atom Optics and Technol.* (Springer, Tokyo, 1998) pp.31-100.

[7] M. Ohtsu(ed.): *Near-Field Nano/Atom Optics and Technol.* (Springer, Tokyo, 1998) pp.101-152.

[8] For example, JASCO catalogue for Scanning Near-Field Optical Microspectrometer (NFS series), (JASCO, Tokyo, 2003).

[9] Optical Society of Japan (organizer): *The 14th International Conference on Near-Field Optics, Nanophotonics, and Related Technologies*, Shizuoka, Japan, Sept.4-8, 2016.

[10] Condensed Matter Res. Inst., Seoul National Univ. (organizer): *The First Asia-Pacific Workshop on Near Field Optics*, Seoul, Korea, Aug. 17-18, 1996.

[11] National Chung-Kung Univ.(organizer): *The 11th Asia-Pacific Conference on Near-Field Optics*, Tainan, Taiwan, July 10-13, 2017.

[12] M. Ohtsu: *Dressed Photons* (Springer, Heidelberg, 2014) pp.1-324.

[13] M. Ohtsu: *Dressed Photons* (Springer, Heidelberg, 2014) pp.89-214.

[14] T. Kawazoe, T. Takahashi, and M. Ohtsu: "Evaluation of the dynamic range and spatial

resolution of nonadiabatic optical near-field lithography through fabrication of Fresnel zone plates," Appl. Phys.B, **98** (2010) pp.5-11.

[15] T. Matsumoto, K. Nakamura, T. Nishida, H. Hieda, A. Kikitsu, K. Naito, and T. Koda: "Thermally assisted magnetic recording on a bit-patterned magnetic medium using a near-field optical head with a beaked metallic plate," Proc. ISOM'07 (2007) pp.90-91.

[16] T. Yatsui, W. Nomura, M. Naruse, and M. Ohtsu: "Realization of an atomically flat surface of diamond using dressed photon-phonon etching," J. Phys.D, **45** (2012) 475302.

[17] M. Ohtsu: "Silicon Light Emitting Diodes and Lasers Using Dressed Photons," Prog. in Nanophotonics 3 (ed. M. Ohtsu) (Springer, Heidelberg, 2015) pp.1-56.

[18] M. Ohtsu: *Dressed Photons* (Springer, Heidelberg, 2014) pp.89-136.

[19] M. Naruse, T. Miyazaki, T. Kawazoe, K. Kobayashi, S. Sangu, F. Kubota, and M. Ohtsu: "Nanophotonic computing based on optical near-field interactions between quantum dots," IEICE Trans. Electron., **E88-C** (2005) p.1817-1823.

[20] H. Fujiwara, T. Kawazoe, and M. Ohtsu: "Nonadiabatic nongenerated excitation by optical near-field and its application to optical pulse-shape measurement," Appl. Phys.B, **100** (2010) pp.85-91.

[21] M. Naruse, M. Aono, S.-J. Kim, T. Kawazoe, W. Nomura, H. Hori, M. Hara, and M. Ohtsu: "Spatiotemporal dynamics in optical energy transfer on the nanoscale and its application to constraint satisfaction problems," Phys. Rev. B, **86** (2012) 125407.

[22] T. Kawazoe, H. Fujiwara, K. Kobayashi, M. Ohtsu: "Visible light emission from dye molecular grains via infrared excitation based on the nonadiabatic transision induced by the optical near field," IEEE J. Select. Top. on Quantum Electron., **15** (2009)pp.1380-1386.

[23] N. Tate, Y. Liu, T. Kawazoe, M. Naruse, T. Yatsui, and M. Ohtsu: "Fixed-distance coupling and encapsulation heterogeneous quantum dots using phonon-assisted photo-curing,"Appl. Phys.B, **110** (2013) pp.39-45.

[24] M. Ohtsu: *Dressed Photons* (Springer, Heidelberg, 2014) p.3.

[25] M. Ohtsu: *Dressed Photons* (Springer, Heidelberg, 2014) p.31.

[26] M. Ohtsu: *Dressed Photons* (Springer, Heidelberg, 2014) pp.33-36.

[27] K. Kobayashi, Y. Tanaka, T. Kawazoe, and M. Ohtsu: "Localized Photon Inducing Phonons' Degrees of Freedom," Prog. in Nano-Electro-Optics VI (ed. M. Ohtsu) (Springer, Heidelberg, 2008) pp.41-66.

[28] K. Kobayashi, S. Sangu, H. Ito, and M. Ohtsu: "Near-field optical potential for a neural atom," Phys. Rev.A, **63** (2001) 013806.

[29] T. Kawazoe, M.A. Mueed, and M. Ohtsu: "Highly efficient and broadband Si homojunction structured near-infrared light emitting diodes based on the phonon-assisted optical near-field process," Appl. Phys.B, 104 (2011) pp.747-754.

[30] B. Thubthimthong, T. Kawazoe, and M. Ohtsu: "*Spectral Analysis of a High-Power Infrared Silicon Light Emitting Diode of Dressed Photons*," Abstracts of the OSA Laser Congress, October 1-5, 2017, Nagoya, Japan, paper number JTh2A.10.

[31] M. A. Tran, T. Kawazoe, and M. Ohtsu: "Fabrication of a bulk silicon p-n homojunction-structured light emitting diode showing visible electroluminescence at room temperature," Appl. Phys. A, **115** (2014) pp.105-111.

[32] M. Yamaguchi, T. Kawazoe, T. Yatsui, and M. Ohtsu: "Spectral properties of a lateral p-n homojunction-structured visible silicon light-emitting diode fabricated by dressed-photon—phonon-assisted annealing," Appl. Phys.A, **121** (2015) 1389-1394.

[33] T. Kawazoe, M. Ohtsu: "Bulk crystal SiC blue LED with p-n homojunction structure fabricated by dressed-photon—phonon-assisted annealing," Appl. Phys. **A 115** (2014) pp.127-133.

[34] K. Suzuki, K. Chieda, T. Kawazoe, T. Yatsui, and M. Ohtsu : "*Control of emission spectrum from a green SiC-LED using dressed-photon—phonon annealing,*" Abstract of the 61st JSAP Spring Meeting, March 2014, Sagamihara, Japan, paper number 18a-F12-11.

[35] Q.H. Vo, T. Kawazoe, and M. Ohtsu: "*Fabrication of SiC-LED using d dressed-photon—phonon annealing with two light sources,*" Abstract of the 61st JSAP Spring Meeting, March 2014, Sagamihara, Japan, paper number 18a-F12-10.

[36] T.Kawazoe, K. Nishioka, M. Ohtsu : "SiC light emitting diode and its polarization control using dressed photons," Abstract of the International Display Workshop 2014, (Niigata, Japan, Dec., 2014) pp.1061-1063.

[37] T. Kawazoe, K. Nishioka, and M. Ohtsu: "Polarization control of an infrared silicon light-emitting diode by dressed photons and analyses of spatial distribution of doped boron atoms," Appl. Phys. A, 121 (2015) pp.1409-1415.

[38] T. Kawazoe, M. Ohtsu, K. Akahane, and N. Yamamoto: "Si homojunction structured near-infrared laser based on a phonon-assisted process," Appl. Phys. B, 107 (2012) pp.659-663.

[39] M. Ohtsu, Y. Teramachi, and T. Miyazaki: "Mode Stability Analysis of Nearly Single-Longitudinal-Mode Semiconductor Lasers," IEEE J. Quantum Electron., 24 (1988) pp.716-723.

[40] M. Ohtsu and Y. Teramachi: "Analyses of Mode Partition and Mode Hopping in Semiconductor Lasers," IEEE J. Quantum Electron., **25** (1989) pp.31-38.

[41] T. Kawazoe, K. Hashimoto, and S. Sugiura: "High-power current-injection type Silicon Laser using nanophotonics," Abstract of the EMN Nanocrystals Meeting, Oct. 2016, X'ian, China, pp.9-11.

[42] M. Ohtsu, *Coherent Quanatum Optics and Technology*, Tokyo, Dordrecht, Boston,

London: KTK Scientific and Kluwer Academic, 1992, pp.49-81.

[43] M. Ohtsu, *Highly Coherent Semiconductor Lasers*, Boston, London: Artech House, 1992, pp.7-60.

[44] W.P. Dumke: "*Interband Transitions and Maser Action*," Phys. Rev., **127** (1962) 1559-1563.

[45] H. Sakuma, I. Ojima, and M. Ohtsu: "Dressed Photons in a New Paradigm of Off-shell Quantum Fields," J. Quantum Electron., in press.

[46] H. Sakuma, I. Ojima, and M. Ohtsu: "Novel View Towards Gauge Condition as a Conceptual Basis of Dressed Photons," Abstracts of the 11th Asia-Pacific Conference on Near-Field Optics, July, 2017 , Tainan, Taiwan, p.32.

[47] M. Katori and H. Kobayashi: "Nonequilibrium Statistical Mechanical Models for Photon Breeding Processes Assisted by Dressed-Photon-Phonons," *Prog. in Nanophotonics* 4 (ed. M. Ohtsu and T. Yatsui) (Springer, Heidelberg, 2017) pp.19-55.

[48] I. Ojima: "Micro-macro duality in quantum physics,"
in *Stochastic Analysis: Classical and Quantum Perspective of White Noise*
Theory, T. Hida (ed.) (World Scientific, 2005) pp. 143-161.

[49] M. Ohtsu, I. Ojima, and H. Saigo: "Who Has Seen A Free Photon? ⋯From Mathematical Physics to Light-Matter Fusion Technologies⋯," Abstracts of the 11th Asia-Pacific Conference on Near-Field Optics, July 10-13, 2017, Tainan, Taiwan, p.54.

[50] I. Banno and M. Ohtsu, "Irrationality of the Permittivity in Non-resonant Near-field Optics", Abstracts of the 11th Asia-Pacific Conference on Near-Field Optics, July 10-13, 2017, Tainan, Taiwan, p.35.

[51] I. Banno and M. Ohtsu, "The Nonlinear Response Theory for Near-field Optics and Application to Non-resonant Effect", Abstracts of the 11th Asia-Pacific Conference on Near-Field Optics, July 10-13, 2017, Tainan, Taiwan, p.62.

[52] M. Ohtsu: *Dressed Photons* (Springer, Heidelberg, 2014) pp.137-214.

[53] M. Ohtsu: T. Kawazoe, K. Kobayashi, and M. Ohtsu, "Optical nanofountain: A biomimetic device that concentrates optical energy in a nanometric region," Appl. Phys. Lett., **86** (2005) 103102.

[54] M. Aono, S.-J. Kim, M. Naruse, M. Wakabayashi, H. Hori, M. Ohtsu, and M. Hara: "Amoeba-Inspired Nanoarchtectonic Computing: Solving Intractable Computational Problems Using Nanoscale Photoexcitation Transfer Dynamics," Langmuir, **29** (2013) pp.7557-7564.

[55] M. Naruse, W. Nomura, M. Aono, M. Ohtsu, Y. Sonnenfraud, A. Drezet, S. Huant, and S.-J. Kim: "Decision making based on optical excitation transfer via near-field interactions between quantum dots," J. Appl. Phys., **116** (2014) 154303.

[56] M. Ohtsu: *Dressed Photons* (Springer, Heidelberg, 2014) pp.160-169.

[57] R.W. Hilditch: *An Introduction to Close Binary Stars* (Cambridge University Press, 2001).

[V] PUBLISHED BOOKS
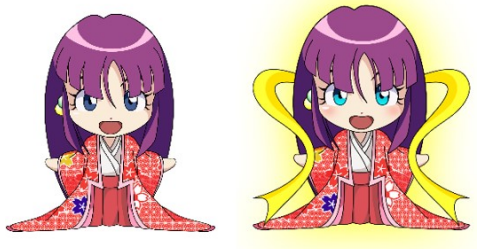
これからの光学

光学

古典論・量子論・
物質との相互作用・新しい光

大津元一

[著]

朝倉書店

目　　次

126

Motoichi Ohtsu · Takashi Yatsui
Editors

Progress in Nanophotonics 4

ohtsu@nanophotonics.t.u-tokyo.ac.jp

Contents

ohtsu@nanophotonics.t.u-tokyo.ac.jp

[VI] PRESENTATIONS
IN DOMESTIC CONFERENCES

Spectral Analysis of High-Power Infrared Silicon Light Emitting Diodes by Dressed Photons : Contribution of Phonons

The Univ. of Tokyo[1], Tokyo Denki Univ.[2], Nanophoton. Eng. Org.[3], Res. Origin of DP[4],

°Borriboon Thubthimthong[1], Tadashi Kawazoe[2,3], Motoichi Ohtsu[1,3,4]

E-mail: borriboon@nanophotonis.tu-tokyo.ac.jp

We studied the phonon-assisted radiative recombination process in the high-power infrared Si light-emitting diodes fabricated using the dressed-photon-phonon-assisted annealing. A photoluminescence study conducted by using an exciting wavelength of 532 nm indicated that one and three optical phonons were responsible for the efficient light emission of the device. The device exhibited a high external quantum efficiency of 14 % and a total output optical power of 200 mW.

1. Introduction

Recent dressed photon research has spurred new developments of efficient high-power Si light-emitting diodes (LEDs) [1]. The key to achieve the Si LED is the dressed-photon-phonon (DPP)-assisted annealing technique at the p-n junction that causes the implanted B atoms redistribution. At the DPP-rich site at the diffused B atoms, momentum exchanges between conduction-band electrons and DPPs occur, leading to radiative electron relaxations [2]. We have previously reported that the Si LED after the annealing showed the photon breeding effect where emitted photon energy is equal to that constituting the DPP [2]. Here, we present the emission mechanism of the infrared Si LED obtained from a photoluminescence (PL) study using a fabricated Si LED.

2. The emission mechanism of the Si LED

The Si LED consists of a p-n junction, formed by B implantation into an As-doped Si substrate, and a Cr/Al mesh electrodes (Fig. 1(a)). After the fabrication, a DPP-assisted annealing was performed by irradiating the implanted area with a 1 W laser of a wavelength of 1314 nm for 1 hour. During this time, conduction-band electrons were simultaneously injected into the p-n junction using a time-dependent electrical current of a triangular waveform of an amplitude of 1 A and a frequency of 1 Hz. The fabricated Si LED had a total output optical power characteristics depending upon the injected current as shown in Fig. 1b. When the injected current amplitude is below 1.0 A, the total output optical power (P) versus the injected current amplitude (I) follows a quadratic relationship as shown in Fig. 1b. When $I > 1.0$ A, P varies with I exponentially, leading to the maximum total output optical power of 200 mW, or, an external quantum efficiency of 14%.

To understand the Si LED's emission mechanism, we conducted a PL study using a 120 mW excitation laser of a photon energy of 2.33 eV (532 nm). We measured the PL spectrum of the Si LED shown in Fig. 1(c). We observed two emission peaks at 1.047 eV (1184 nm) and 0.9432 eV (1314 nm), which had lower energies than the Si band gap. This indicates the phonon-assisted radiative processes (Fig. 1(d)). Furthermore, the observed emission peak at 0.9432 eV (1314 nm) confirmed the photon breeding effect in the device. We believe that the radiative recombination process in the Si LED was assisted by optical phonons since the differences in the peak energies were of integer multiples of that of the phonons (63 meV [3]) as illustrated in Fig. 1(d).

3. Conclusions

We studied the electroluminescence mechanism in the Si LED. PL study showed that the photon breeding effect occurred after the DPP-assisted annealing. The emission mechanism could be explained by the radiative recombination processes assisted by either one- or three-phonon coupling.
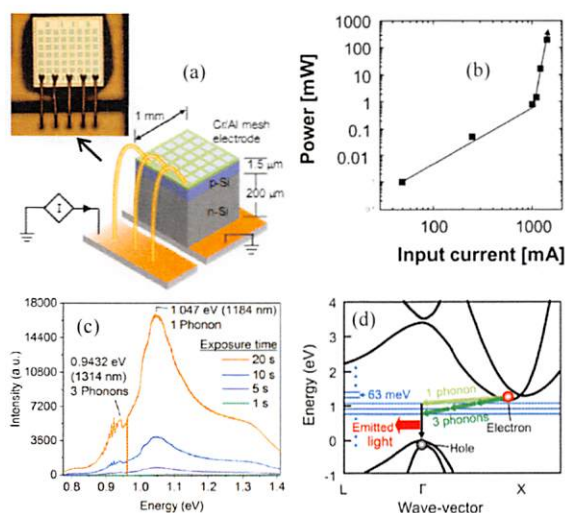

Fig. 1. (a) The Si LED. (b) The total output optical power vs input current. (c) The PL spectrum. (d) The band diagram of the Si LED.

References

[1] M. Ohtsu, Silicon Light-Emitting Diodes and Lasers (Springer, 2016).

[2] T. Kawazoe, M. A. Mueed, and M. Ohtsu. "Highly efficient and broadband Si homojunction structured near-infrared light emitting diodes based on the phonon-assisted optical near-field process." Applied Physics B: Lasers and Optics 104.4 (2011): 747-754.

[3] P.M. Amirtharaj and D.G. Seiler, "Optical Properties of Semiconductors" in Handbook of optics, M. Bass et al, eds. Handbook of Optics (McGraw-Hill, New York, 2001).

高出力ホモ接合シリコンレーザーの作製 (2)
Fabrication of a High power Homojunction Silicon Laser (2)

電機大 [1], NPEO[2], 東大工 [3] ○川添 忠[1]、橋本和信 [2]、杉浦聡 [2]、大津 元一 [3]
TDU[1], NPEO[2], Univ. Tokyo[3] ○T. Kawazoe[1], S. Sugiura[2], K. Hashimoto[2], and Motoichi Ohtsu[3]
E-mail: kawazoe@mail.dendai.ac.jp

これまでにドレスト光子フォノン援用アニールによって間接遷移型半導体を用いた LED, レーザーなど受発光素子の作製及び動作検証報告行っている[1-3]。間接遷移型半導体は直接遷移過程半導体とは異なる発光遷移過程に従い、ドレスト光子フォノンと呼ばれる中間状態を介して起こる。

通常の pn 接合 Si 基板に電流を注入しても発光せず、注入された電子と正孔のエネルギーは熱を発生させる。これは Si の伝導体の底と価電子帯の頂上の波数が大きく異なり、光子放出ために必要な波数保存則を満たすためのフォノンに散乱される確率が極めて小さいからである。次にある規則性を持つドーパント対が Si 結晶中に存在すると仮定する。ドーパント原子は Si と質量数が大きく異なれば何でもよい。周囲の Si 原子と質量の異なるドーパント原子は原子振動すなわちフォノンの反射境界となる。その結果、2つのドーパント対の間には特定のモードのフォノンが集中し、そのフォノン密度は均一な Si 結晶の 10^4 も大きくなるという結果も報告されている[4]。このフォノンの波数が Si の伝導体の底と価電子帯の頂上の波数の差と一致する場合、注入された電子と正孔は速やかにフォノン散乱され光子を放出して対消滅すると予想される。我々はこのような特異なドーパント対配列を作り出す方法（DPP アニール法）を開発した[1-3]。

DPP アニールされた Si の pn 接合部はレーザーの活性層としても機能する。前回の報告では、大きな導波路構造 (1mm×100μm×15mm) をもつ Si レーザー素子を作製し、赤外領域にて光出力高強度は 10W 以上を得たことを報告した (Fig.1) [5]。今回、この DPP アニールの効果を大きくするためにこれまで用いていたドーパント種を変更し、原子の質量数の Si との違いがより大きな新しいドーパントを用いて Si レーザーを作製した。その結果、これまでよりも低い電圧において、DPP アニールの進捗を示す負性抵抗特性が現れることが分かった。(Fig.2)。発表では新しく作製した素子の
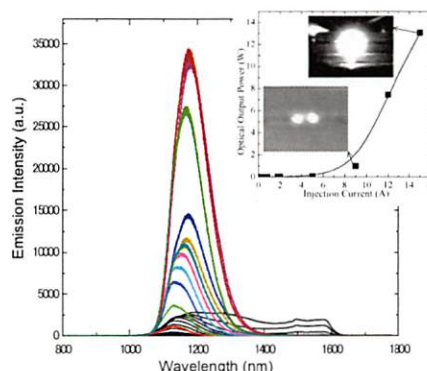
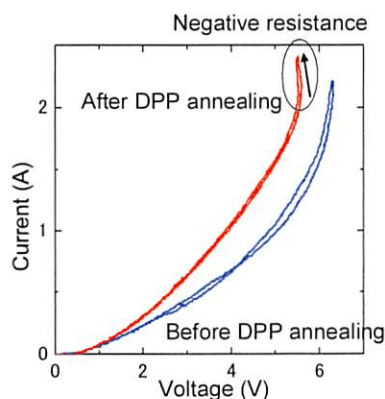光出力特性等に関して報告を行う。

Fig.1 Si laser emission spectra.

Fig.2 IV characteristics of Si laser after and before DPP annealing.

参考文献
[1] T. Kawazoe & M. Ohtsu, Appl. Phys. A, **115**, 127-133, (2014).
[2] T. Kawazoe, et al., Appl. Phys. B-Lasers and Optics, **98**, 5-11 (2010). also **107**, 659-663 (2012).
[3] H. Tanaka, et al., Appl. Phys. B-Lasers and Optics, **108**, 51-56 (2012).
[4]Y. Tanaka, K. Kobayashi, J. Microscopy **229** 228-232(2008).
[5] 川添忠、杉浦聡、大津 元一、2017 年第 64 回春季応用物理学会、パシフィコ横浜公園番号 15a-F202-9.

近接場光学における非共鳴効果の理論 II:
非線形応答理論によるドレスト光子の基礎づけの試み
Theory of Non-resonant Effect in Near-filed Optics II:
Approach to a Base of Dressed Photon employing Non-linear Response Theory

○ 坂野　斎 [1], 大津元一 [2,3]
(**1. 山梨大院医学工学総合, 2. 東大院工, 3. ドレスト光子研究起点**)
○**I. Banno[1], M. Ohtsu[2,3]**
(**1. Univ. of Yamanashi, 2. Univ. of Tokyo, 3. Research Origin of Dressed Photon**)
E-mail: banno@yamanashi.ac.jp

私たちは光源であるナノ構造近傍の多電子系という近接場光学（NFO）系に相応しい線形・非線形応答関数を第1原理から定式化してきた [1]. その応答関数は, 近接場光学系に共存するスカラー・ベクトルポテンシャル（SP ϕ・VP $\mathbf{A}$）を応答の原因として対等に扱い, 結果である誘導電荷・電流密度と関係づける. n 次の非線形応答関数は作用積分の ϕ・$\mathbf{A}$ による $(n+1)$ 階の汎関数微分として Heisenberg 演算子の形式で得られ, 電荷保存則とゲージ不変性を保証する. 本発表では, n 次と $(n+1)$ 次の非線形応答関数の漸化式を議論する. 例えば, $n=2$ の場合, 次のようになる:

$$\hat{\chi}^\mu_{\mu_1\mu_2\mu_3}(x,x_1,x_2,x_3) = \frac{1}{3}\frac{-q}{mc^2}\left\{ \delta^4(x_2-x_3)\,\bar{\delta}_{\mu_2\mu_3}\,\hat{\chi}^\mu_{\mu_1 0}(x,x_1,x_2) + \begin{pmatrix}1\,2\,3\\2\,3\,1\end{pmatrix} + \begin{pmatrix}1\,2\,3\\3\,1\,2\end{pmatrix} \right\}$$

$$+ \frac{1}{3}\frac{1}{ihc^2}\left\{ \theta(ct_2-ct_3)\left[\hat{\chi}^\mu_{\mu_1\mu_2}(x,x_1,x_2),\hat{\jmath}^{(in0)}_{\mu_3}(x_3)\right] + \begin{pmatrix}1\,2\,3\\2\,3\,1\end{pmatrix} + \begin{pmatrix}1\,2\,3\\3\,1\,2\end{pmatrix} \right\}. \qquad (1)$$

非相対論だが電荷保存則とゲージ不変性の可視化のため4元表示を使い $\bar{\delta}^\mu{}_{\mu'}$ は $\mu=\mu'=1,2,3$ に対し $\bar{\delta}^\mu{}_{\mu'}=1$, そうでない場合, $\bar{\delta}^\mu{}_{\mu'}=0$, また, $\begin{pmatrix}1\,2\,3\\2\,3\,1\end{pmatrix}+\begin{pmatrix}1\,2\,3\\3\,1\,2\end{pmatrix}$ は示数を輪環順で置換した項である. 前回の発表で線形応答関数に非共鳴条件下の NFO 系で $\mathbf{A}$ により強調される寄与があり, 誘電率による記述が破綻することを述べた [2]. Eq.(1) にも同様の構造があり, 第1項によって $\mathbf{A}$ を伴う光学フォノンが NFO 系の非共鳴非線形過程に強く寄与できる. 川添・大津らは非共鳴条件下での様々な実験 [3,4] でドレスト光子を利用して NFO 特有の現象を発見, 実用に供してきた. 理論的に多フォノンが関わるモデルで説明され [5], 特に光学フォノンが関わる実験的証拠が得られている [6]. このようなドレスト光子とフォノンの関わりについて第1原理から基礎付けを試みる.

　NFO は縦電場（ϕ 自由度）を介して多電子問題と関係する；非摂動状態の基底状態, 励起状態を束縛状態（分子や固体）に保っているのは交換・相関相互作用という量子論的多電子効果である. 通常の方法と異なり ϕ を電子間相互作用に転化しない本理論では密度汎関数法の考えを用い, 多電子系に内在する ϕ と入射される ϕ を切り分け, 後者を入射される $\mathbf{A}$ と対等に扱う処方をとっている. これにより NFO の非線形過程の系統的な解析が可能となる.

[1] 論文投稿予定；坂野　斎,"ナノ構造と非放射場の理論,"応物講演会 (2013 秋 17p-D2-2);"非放射場と放射場を対等に扱う単一感受率による光学の理論 I,II, III,IV,V",応物講演会 (2013 秋 18p-C13-1,2014 春 17p-F6-5, 秋 18p-C1-1,2015 春 12a-A12-1,2016 春 19a-S622-13).
[2] 坂野　斎,"近接場光学における非共鳴効果の理論 I"応物講演会 (2017 春 15a-F202-12); I. Banno.,"Response Theory in Near-field Optics: Two Distinct Dipole Transitions",14th International Conference on Near-field Optics, Nanophotonics, and Related Technics,(浜松市, 2016 年 9 月 We-10A-5);坂野　斎,"近接場光学における 2 種の双極子遷移", Optics and Photonics Japan 2016(2016 秋 1PC3).
[3] 川添 忠, 杉浦聡, 大津 元一, "高出力ホモ接合シリコンレーザーの作製", 応物講演会 (2017 春 15a-F202-9); T. Kawazoe and M. Ohtsu,"Bulk crystal SiC blue LED with p-n homojunction structure fabricated by dressed-photon-phonon-assisted annealing", Appl. Phys. A, **115**, 127-133, (2014); M. A. Tran, T. Kawazoe, M. Ohtsu, "Fabrication of a bulk silicon p-n homojunction-structured light-emitting diode showing visible electroluminescence at room temperature", Appl Phys A **115**,105-111(2014).
[4] For review articles: M. Ohtsu, "Progress in Dressed Photon Technology and the Future", *in Progress in Nanophotonics 4* eds. by M. Ohtsu and T. Yatsui (Springer, 2017) Chap. 1; M. Ohtsu, "Dressed photon technology", Nanophotonics **1** 83-97 (2012).
[5] T. Kawazoe, K. Kobayashi, S. Takubo, and M. Ohtsu, "Nonadiabatic photodissociation process using an optical near field", J. Chem. Phys. **122**, 024715 (2005); K. Kobayashi, T. Kawazoe, and M. Ohtsu, "Importance of Multiple-Phonon Interactions in Molecular Dissociation and Nanofabrication Using Optical Near Fields", IEEE Trans. Nanotech. **4(5)** 517-522 (2005).
[6] T. Kawazoe, K. Nishioka, and M. Ohtsu, "Polarization control of an infrared silicon light-emitting diode by dressed photons and analyses of the spatial distribution of doped boron atoms", Appl. Phys. A **121**, 1409-1415 (2015); M. Yamaguchi, T. Kawazoe, and M. Ohtsu, "Evaluating the coupling strength of electron-hole pairs and phonons in a 0.9 μ m-wavelength silicon light emitting diode using dressed-photon-phonons", Appl Phys A **115**, 119-125 (2014); N. Wada, M. A. Tran, T. Kawazoe, and Motoichi Ohtsu, "Measurement of multimode coherent phonons in nanometric spaces in a homojunction-structured silicon light emitting diode", Appl. Phys. A **115**, 113-118 (2014).
[7] P. Hohenberg and W. Kohn, Phys. Rev. **136**, 3864 (1964); W. Kohn and L. J. Sham, Phys Rev **140**, A1133 (1965).

仮想光子としてのドレスト光子理解に向けての新たな試み
New initiative of understanding the dynamics of dressed photons as virtual ones

○佐久間弘文 [1]，小嶋泉 [1]，大津元一 [1,2]

○Hirofumi Sakuma [1] , Izumi Ojima [1], Motoichi Ohtsu [1,2]

1:ドレスト光子研究起点、2:東京大学大学院工学系研究科総合研究機構

E-mail: sakuma@rodrep.ro.jp

1980 年代に始まった近接場光学の研究は、量子論的アプローチを取り入れドレスト光子科学技術として大きく前進し、「入射伝搬光の波長よりも"小さな粒状の光の出現"」のメカニズムの解明が続いている[1]。その過程で、従来のではその現象を解明できなかった理由を、既存の電磁理論が量子論の用語で言うところの on-shell 的であるのに対して、ここで対象とする現象が off-shell 的であることに注目して研究が急進展している。

一般的に量子場の相互作用に伴う off-shell 的な場の表現は、通常の timelike な領域に起こる自由場的な現象と異なり、その energy-momentum support は spacelike 領域を含む非常に複雑なものである。Sakuma *et al.* [2] は、光が関わるその様な off-shell 的な場を研究する為に必要な、足掛かり的一歩となる timelike と spacelike 領域の対比という意味における電磁場の新たな双対構造の存在を示した。その導出に際しては、これまでにも知られていながら専門分野間の縦割り構造の為に、その知見が物理学界に広く共有されていない重要な二つのテーマを絡めて議論した。その一つは電磁波の縦波の存在である。標準的な物理の教科書には、電磁波は横波と明記してあるのに対して、Cicchitelli *et al.* により理論的にも実験的にも真空中における縦波の存在が報告されている [3]。これは、どう理解されるべきなのか？実は、共変的電磁場の量子化という問題に絡め、この問題は Ojima [4] により、ミクロ・マクロ双対性の観点から既に矛盾なく解決されている。

本発表では、これらの知見に加え、ゲージ不変性の破れに伴い、Goldstone mode として機能する 4 元電磁ポテンシャルの発散量を核として、時空構造を随伴する双対電磁場が創発される概要を説明し、更にその双対場がどの様にして仮想光子としてのドレスト光子を記述する理論となり得るのかを議論する。
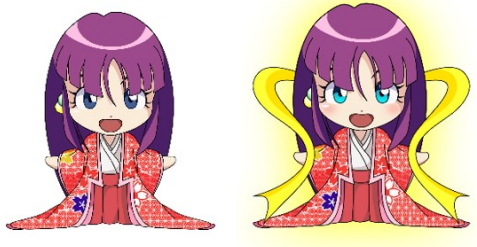
[1] M. Ohtsu, *Dressed Photons* (Springer, Heidelberg, 2014).

[2] H. Sakuma, I. Ojima and M. Ohtsu, Dressed Photons in a New Paradigm of Off-shell Quantum Fields to appear in Prog. in Quantum Electron., 2017.

[3] L. Cicchitelli, H. Hora, R. Postle, Longitudinal field components for laser beams in vacuum, Physical Review A **41** (1990) 3727-3732.

[4] I. Ojima, Nakanishi-Lautrup B-Field, Crossed Product & Duality, RIMS, Kyoto University departmental bulletin paper, (2006), **1524**, 29-37.

[VII] APPENDIX

H-7-01 (Invited)

High power Silicon laser based on the dressed photon technology

Tadashi Kawazoe

Tokyo Denki University.
Tokyo Senju Campus, Bldg.4-9F 906A
5 Senju-Asahi-cho, Adachi-kuChiyoda-ku, Tokyo 120-8551, Japan
Phone: +81-3-5284-5981 E-mail: kawazoe@mail.dendai.ac.jp

Abstract

A Silicon laser based on the dressed photon technology is reviewed. A dressed photon generated at around a dopant-atom pair is easily coupled with phonon which is satisfied the conservation low of wavenumber for the radiative recombination of Silicon. The silicon laser operates via the dressed photon state couple with phonons.

1. Introduction

Radiative recombination life time of electrons and holes in the indirect-transition-type semiconductor is very long. Due to this physical property, usually, indirect-transition-type semiconductors including with Silicon (Si) are not suitable materials for light-emitting devices, for example, light emitting diode (LED), a laser diode (LD), and so on. In spite of this disadvantage, the light emitters using Si have been studied due to many other advantages, for example, compatibility with electronics, low-cost, an abundant supply, and so on[1-3]. The realization of Si laser also has been studied. In recent years, Si Raman lasers [2] and a stimulated emission of a Si quantum wells are reported. In these previous studies, the physical mechanisms are based on a conventional semiclassical solid-state physics of optical properties.

We have also reported a unique radiative recombination mechanism in the indirect-transition-type semiconductor based on the dressed photon and Si laser has been also developed by using this mechanism [5,6]. We have achieved the laser output power of more than 10 W so far. In the presentation, I review the dressed-photon-phonon annealing for fabrication of the light-emttable Si pn junction, first. Second, we demonstrate current injection type high power Si laser with a unique design. Its lasing threshold current density decreased to 60A/cm^2 and the output power of the laser increased to 13W at the wavelength of 1.34μm for the current density of 100A/cm^2. Finally, I demonstrate Si lasers with the reflection layers fabricated at the both end of the laser chip. Its threshold current was decreased to 40% (he current density of 22 A/cm^2). The lasing wavelength was 1190 nm due to the spectral properties of the reflection layers.

2. DPP annealing and Dressed-Photon-Phonon Emission

The fabrication methods of the Si light emitting device with the p-n junction have already reported [7-13]. First, the p-n homojunction was fabricated by the ion-implanting of a p-dopant (Boron:B) into an n-type Si substrate which was As-doped n-type Si wafer with an electrical resistivity of 10 Ω·cm. The energy of the ion-implantation for the B doping was 700 keV, and the dose density was 5×10^{13} cm^{-2}. Second, in order to optical activation of the Si p-n junction, the fabricated p-n homojunction is annealed by Joule heating causing the foreword injection current. During this annealing process, the p-n homojunction is irradiated by the infrared light. This annealing process has been named DPP (dressed photon-phonon) annealing.

The dressed photon-phonon (DPP) is a quasi-particle formed by the coupling of photon and phonon via an electron-hole pair in the materials [14]. For creation of DPP, the dopant pair is very important. Generally, the interaction between a photon and a phonon is more than 10^{-3} smaller than that between a photon and electron, which is nearly equal to the mass ratio between an electron and a nucleus. Beside, when B dopant pair in the Si crystal acts as the confinement boundaries for phonons causing the difference of mass between Si and B atoms, the phonon density drastically increases, which is satisfying confinement boundary condition. In the previously theoretical calculation [14], the phonon density in the B dopant pair becomes more than 10^4 times higher than that in the pure Si crystal. In the experiment, the Huang–Rhys factor of 4.08 using DPP annealed Si p-n junction, giving the coupling strength between electrons and optical mode phonons has been obtained [13]. This value is 10^3 times larger than that in bulk Si crystals. Thus, if B dopant pair in the Si crystal well acts as the confinement boundaries for phonons, the total interaction strength between a photon and a phonon become as same as that between a photon and an electron. When the wavenumber of a confined phonon in B pair is equal to the wavenumber difference between an electron at the bottom in the conduction band and a hole at the top in the valence band of a Si crystal, the radiative recombination rate increases and the radiation efficiency of the Si becomes as same as the direct transition type semiconductors..

3. 10W Si laser

An Sb-doped n-type Si wafer with an As-doped n-type epitaxially formed layer was used as a device substrate. The thickness and the electrical resistivity were 10 μm and 10 Ω·cm, respectively. Boron (B) was induced in this epitaxial layer as a p type dopant by ion implantation. The implantation energy and dose density were 700 keV and 5×10^{13} cm^{-2}, respectively. After the implantation, the external shape of the laser cavity was formed by a polishing and a cleaving. The size of the cavity was 15 mm × 1 mm × 150 μm (length × width × thickness).

(a)
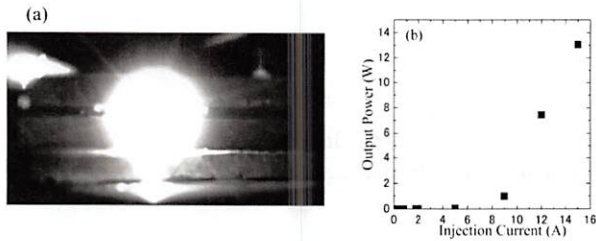
Fig1. (a) infrared photograph of the operating Si laser. (b) The injection current dependence of the laser output power.

Figure 1(a) shows the photograph of the front view of the Si laser device in operation taken by the infrared camera. Figure 1(b) shows a injection current dependence of the laser output power. Its lasing threshold current density decreased to $60 A/cm^2$ and the output power of the laser increased to 13W at the wavelength of 1.34μm for the current density of $100 A/cm^2$. The obtained threshold current density is very low comparing with the conventional semiconductor lasers and the output power was more than 10^5 times larger than previous Si lasers that we fabricated. The lasing spectral line width was more than 100 nm, because the device was a multimode broad area laser. The external power efficiency was about 20 %, and the external quantum efficiency was 80 %. We consider the high quantum efficiency comes from the multi-step transition via dressed-photon state.

4. Si Laser with Reflective layers

After deposition of a gold (Au) film as electrodes, the reflective coating layers were was deposited on both end-side of the Si laser cavity. Finally, the laser chip was mounted on the Cupper mounting plate. After the mounting, the laser device was DPP-annealined. Here, we used the annealing laser with a wavelength of 1342 nm and a power of 4W. The applying a forward-bias current was 4.5 A.
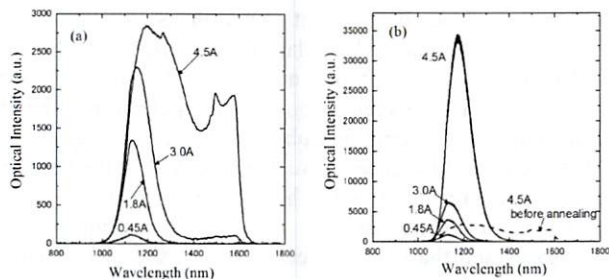
Fig.2. Emission spectra from the Si lasers (a) before DPP annealing (b) after DPP annealing.

Figure 2 (a) shows EL spectra from the Si laser chip for the currents of 0.45 A, 1.8A, 3.0A, and 4.5A before DPP annealing. The spectral peak appeared at the wavelength of 1140nm corresponds to the Si indirect band gap energy for the lower current and it shifted to longer wavelength with the increase in the injection current. Additionally, another emission band appeared in the wavelength region of 1400-1600 nm. The solid curves in Fig.2(b) show EL spectra from the Si laser chip for the currents of 0.45 A, 1.8A, 3.0A, and 4.5A after DPP annealing. The peak emission wavelength appeared at 1180 nm. The emission intensity increased and single emission peak appeared. The

broken curve in Fig.2 (b) shows a emission spectrum before DPP annealing for the injection current of 4.5 A. The spectra for injection current of 4.5 A had fine oscillatory structures. We consider this structure indicates the lasing of the Si chip.
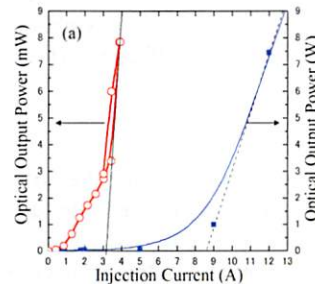
Fig.3. Optical output power VS Injection current.

Figure 3 shows a current dependency of output optical power from the Si laser chip with the reflection layer (open circles) and without reflection layer (closed squares). The laser oscillation threshold current of the fabricated Si laser with the reflection layers was 3.3 A, which corresponds to the current density of 22 A/cm². This is about 40% for the threshold current of Si laser without reflection layers.

5. Conclusions

I have explained the dressed-photon-phonon annealing for fabrication of the light-emttable Si pn junction. We demonstrate current injection type high power Si laser with a unique design. Its lasing threshold current density decreased to $60 A/cm^2$ and the output power of the laser increased to 13W at the wavelength of 1.34μm for the current density of $100 A/cm^2$. Finally, I demonstrate Si lasers with the reflection layers fabricated at the both end of the laser chip. Its threshold current was decreased to 40% (he current density of 22 A/cm²). The lasing wavelength was 1190 nm due to the spectral properties of the reflection layers.

References

[1]. D. Liang, and J. E. Bowers, Nat. Photonics **4**, 511 (2010).
[2]. H. Rong, R. Jones, A. Liu, O. Cohen, D. Hak, A. Fang, and M. Paniccia, Nature **433**, 725 (2005).
[3]. S. Saito, Y. Suwa, H. Arimoto, N. Sakuma, D. Hisamoto, H. Uchiyama, J. Yamamoto, T. Sakamizu, T. Mine, S. Kimura, T. Sugawara, and M. Aoki, Appl. Phys. Lett. **95**, 241101 (2009).
[4]. Russelld .D Upuis, IEEE J. Quant. Electoron. Vol. **23**, NO. 6, 651(1987). "An Introduction to the Development of the Semiconductor Laser"
[5]. T. Kawazoe, M. Ohtsu, K. Akahane, N. Yamamoto, Appl. Phys. B, **107**, 659 (2012).
[6]. H. Tanaka, T. Kawazoe, M. Ohtsu, K. Akahane, Fluorescent Materials. **1**, 1 (2015).
[7]. T. Kawazoe, M. A. Mueed, M. Ohtsu, Appl. Phys. B, **104**, 747–54 (2011).
[8]. N. Wada, T. Kawazoe, M. Ohtsu, Appl. Phys. B, **108**, 25–29 (2012).
[9]. H. Tanaka, T. Kawazoe, M. Ohtsu, Appl. Phys. B, **108**, 51–56 (2012).
[10]. M. A. Tran, T. Kawazoe, M. Ohtsu, Appl. Phys. A, **115**, 105–111(2014).
[12]. N. Wada, M. A. Tran., T. Kawazoe, M. Ohtsu, Appl. Phys. A, **115**, 113–118 (2014).
[13]. M. Yamaguchi, T. Kawazoe, M. Ohtsu, Appl. Phys. A, **115**, 119–125 (2014).
[14]. Y. Tanaka, K. Kobayashi, Physica E **40**, 297 (2007).

High Power Silicon Lasers via Dressed Photon

Tadashi Kawazoe and Satoshi Sugiura

Tokyo Denki University, (NPO)Nanophotonics Engineering Organization
kawazoe@npeo.or.jp

Abstract: the Si broad area lasers with the optical output power of 10 W are demonstrated. The external power and quantum efficiency achieved at 20 % and 80 %, respectively.

1. Introduction

Formerly, the potentials of the indirect-transition type semiconductor Silicon (Si) had been discussed as a laser medium [1]. The long recombination life time of the indirect-transition type semiconductor easily realizes a population inversion of carriers, which is necessary for the lasing. Even now, Si Raman lasers and a stimulated emission of a Si quantum wells are reported. Namely, if there is a radiable relaxation pass, which is even low probability like a Raman scattering, Si is able to act as a laser medium. Recently, we have reported a unique radiative recombination mechanism in the indirect-transition type semiconductor via dressed photon. Its probability is much higher than the Raman scattering process. Thus, Si light emitting diodes and diode lasers have been demonstrated so far [2-5]. The developed Si laser diode shows low absorption loss but small optical gain compared with the conventional semiconductor laser diode. These features indicate that the Si laser medium is suitable for a large sized and high power laser. In this presentation, the Si broad area lasers with the optical output power of 10 W are demonstrated. The external power and quantum efficiency achieved at 20 % and 80 %, respectively.

2. Device properties of the Silicon Broad Area Laser

The thin rectangular Si laser chip (15 mm × 1 mm × 0.1 mm) had large output window (1 mm × 0.1 mm) and long cavity (15mm). The p-n homojunction was formed by the ion implantation method. Before the dressed photon phonon (DPP) annealing, the junction emits a very weak light at a wavelength of 1.1 μm by the current injection. After the DPP annealing, the emission power increased drastically and the Si p-n junction lasing finally. Figure 1 shows the emission spectra from the Si laser for the different injection currents. Figure 2 shows the injection current dependency of the output power from the Si laser. The threshold currents of the lasing was 6A. The spectral shape changed as shown in Fig.1 for more than 10A and spectral peak also shifted from the Si band edge (1.1 μm) to the laser wavelength used in the DPP annealing process (1.34 μm). For small current than the threshold, the emission power linearly increased for the injection current as shown by the blue line in Fig.2. For large current more than the threshold, the output laser power increased rapidly as shown by the red arrow in Fig.2. The external power and quantum efficiency was 20 % and 80 % for the injection current of 14 A, respectively.
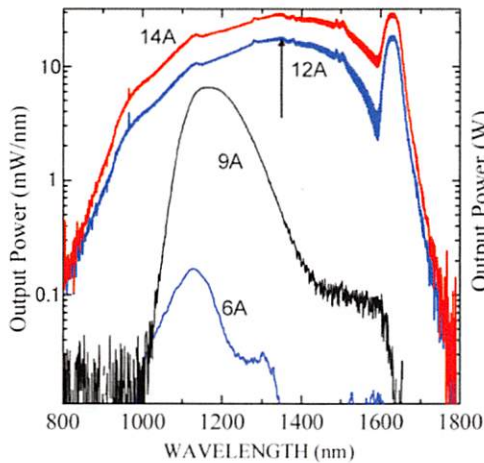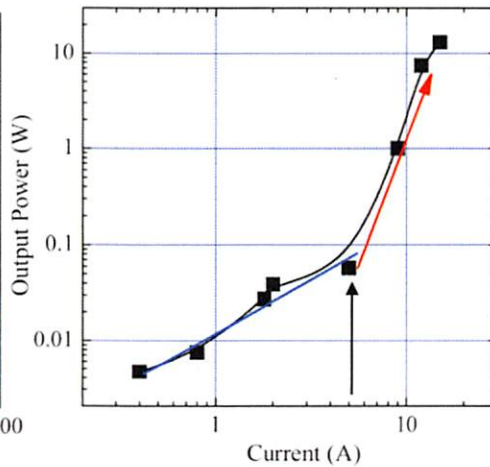

Fig.1. Output Spectra from the Si Laser. Fig.2. Laser Output Power vs Injection Current

[1] Russelld .D Upuis, IEEE J. Quant. Electoron. Vol. **23**, NO. 6, 651(1987). "An Introduction to the Development of the Semiconductor Laser".
[2] T. Kawazoe, M. A. Mueed, M. Ohtsu, Appl. Phys. B, **104**, 747–54 (2011).
[3]. H. Tanaka, T. Kawazoe, M. Ohtsu, Appl. Phys. B, **108**, 51–56 (2012).
[4]. M. A. Tran, T. Kawazoe, M. Ohtsu, Appl. Phys. A, **115**, 105–111(2014).
[5]. N. Wada, M. A. Tran., T. Kawazoe, M. Ohtsu, Appl. Phys. A, **115**, 113–118 (2014).